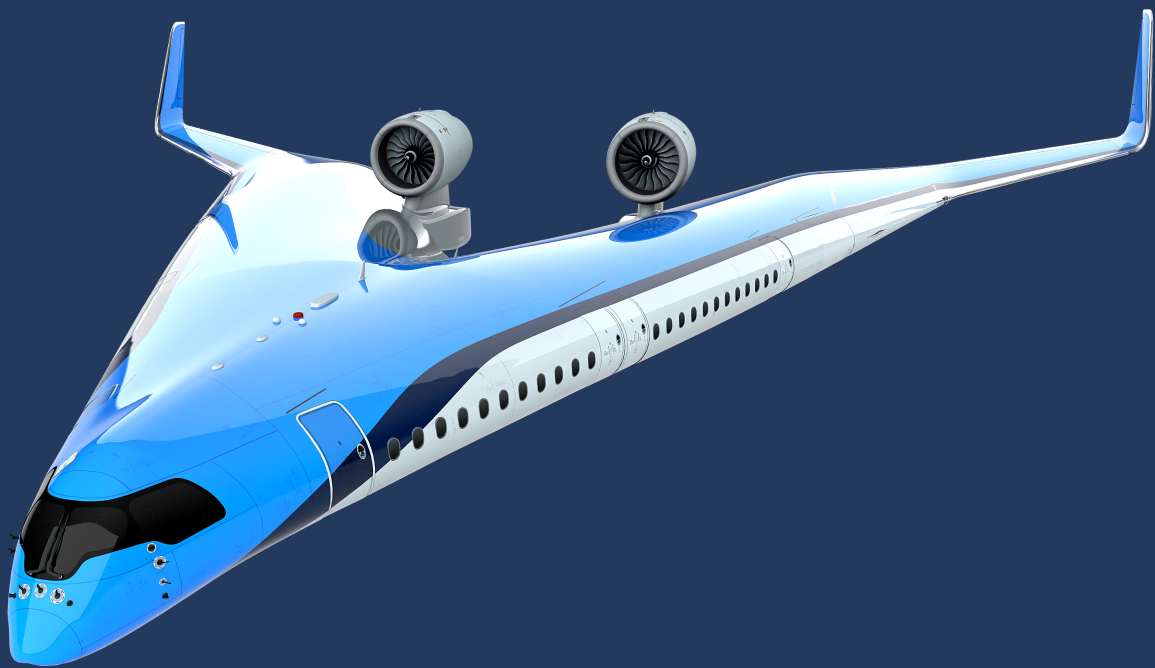


Robust Flight Control for the Flying-V

Mixed μ -optimal Incremental Dynamic
Inversion-based Flight Control

Ramzi Shahin



Robust Flight Control for the Flying-V

Mixed μ -optimal Incremental Dynamic Inversion-based
Flight Control

Master of Science Thesis

by

Ramzi Shahin

To obtain the degree of Master of Science
at the Delft University of Technology
to be defended publicly on November 6, 2024 at 14:00

Thesis committee:

Chair:	Dr. ir. Coen de Visser, CS-CO
Supervisor:	Dr. ir. Erik-Jan van Kampen, CS-CO
External examiner:	Dr. Steven Hulshoff, FPT
Additional Members:	Dr. Eng. Spilios Theodoulis, CS-CO Dr. ir. Tijmen Pollack, ASM
Place:	Faculty of Aerospace Engineering, Delft
Project Duration:	January, 2023 - November, 2024
Student number:	4559037



Copyright © Ramzi Shahin, 2024
All rights reserved.

Preface

I proudly present this thesis report.

This thesis presents a robust control approach to inversion-based flight control. I sincerely want to thank my supervisors Erik-Jan and Tijmen for their guidance and patience. Moreover, I want to thank Spilios, who was somewhat of an unofficial advisor to me and helped deepen my interest in robust control. In having to navigate and comprehend two branches of Control Theory, I was lucky to have access to all of you. A special thanks to Tijmen, who was always available to help me, provided me with invaluable feedback and forced me to think critically. I thoroughly enjoyed the conversations we had and the rabbit holes we went down, both on topic and off topic. I also want to thank Tim, Bea, Leo and the boys at Simona, you guys have made the last few months a more enjoyable journey.

Moreover, I would like to express my gratitude to my family, friends and the boys at Combat Brothers, who have all provided me with continuous support along the way. A special thanks to my lovely parents, who have always backed me in all of my pursuits and provided me with the opportunity to pursue a MSc degree in the first place.

Lastly, a special thanks to my grandfather Opa Tom, who first introduced me to control theory and the concept of feedback many years ago. You might say you fed forward the concept of feedback to me, and now I'm just closing the loop.

Enough talking, time for some Robust Flight Control.

"Uncertainty is the only certainty there is, and knowing how to live with insecurity is the only security."

- John Allen Paulos

Ramzi Shahin
Rotterdam, September 2024

Abstract

The Flying-V is a tailless, V-shaped flying-wing type aircraft that promises to offer significant increases in aerodynamic efficiency. Due to its configuration, the Flying-V faces some control and stability related issues. These include limited control authority, pitch break tendencies and non-ideal handling qualities.

To enhance the handling qualities of the Flying-V, Incremental Nonlinear Dynamic Inversion (INDI)-based flight control systems have been proposed. INDI, a sensor-based alternative to conventional Nonlinear Dynamic Inversion (NDI), is rooted in the principle of feedback linearization. Unlike NDI, INDI does not depend heavily on accurate on-board models (OBM), thereby offering increased robustness to aerodynamic uncertainties. However, singular perturbations—such as time delays, aeroelastic effects, and additional unmodeled or unknown dynamics—have been identified as challenges for INDI-based control laws. Various strategies have been explored to improve the overall robustness of INDI-based flight control systems, including outer-loop tuning and inversion loop augmentation strategies.

In this research a multi-loop μ -optimal approach for designing robust inversion-based flight control laws is explored for the design of an explicit model-following pitch-rate control system for a short-period approximation of the Flying-V's longitudinal dynamics. The design problem takes into account both regular and singular perturbations.

To assess the robust stability and performance of the proposed control systems, a structured singular value analysis was performed. It was concluded that a multi-loop synthesis approach is capable of achieving better robust stability and performance levels when compared to either strictly inner-loop or outer-loop synthesis. As such, it can be concluded that multi-loop synthesis approaches are best capable of leveraging the robustness functionalities of multi-loop inversion-based control systems.

Contents

List of Figures	vi
List of Tables	viii
1 Introduction	1
1.1 The Flying-V	3
1.2 Research objective & research questions	5
1.3 Research Scope	5
1.4 Structure of the Report	6
I Scientific Article	7
II Literature Study	29
2 State-of-the-Art Research Flying V	30
2.1 Historical overview of the development of the Flying-V	30
2.2 Simulation model of the Flying-V	33
2.3 Stability & Handling quality assessment.	41
2.4 Stability & Control augmentation systems for the Flying-V	45
2.5 State-of-the-art INDI	47
2.6 Conclusions.	52
3 Robust Control methods for Flight Control applications	55
3.1 Introduction to multivariate linear control analysis	55
3.2 Practical robust control design methods.	63
3.3 Robustness properties of (I)NDI based control laws	68
3.4 Multi-loop robust design of (I)NDI-based control laws	71
3.5 Conclusions.	72
4 Longitudinal Handling Quality, Performance & Stability Criteria for the Flying V	75
4.1 Flying Quality requirements	75
4.2 Stability requirements	81
4.3 Performance requirements.	82
4.4 Conclusions.	83
III Preliminary Analysis	85
5 Preliminary Analysis	86
5.1 Short-period model of the Flying-V	86
5.2 Design Requirements	87
5.3 Controller Synthesis	89
5.4 Results	91
IV Closure	100
6 Conclusions	101
7 Recommendations	108
7.1 The Flying-V	108

- 7.2 The flight control law clearance process 108
- 7.3 Inversion-based control law design 109
- 7.4 The use of \mathcal{H}_∞ -tools in inversion-based flight control design. 109
- References** **120**
- A D,G-K iterations** **120**

List of Figures

1.1	The BW-17 and the BWB-450, from [6]	1
1.2	side-by-side view of a BWB and a pure flying-wing, from [11]	2
1.3	Artist rendition of the Flying-V, from [12]	3
1.4	Initial sketch and configuration of the Flying-V, from [16]	3
2.1	Flight test with glider model of the Flying-V, adopted from [13]	30
2.2	Flight test with powered model of the Flying-V, adopted from [13]	30
2.3	Flying V and Airbus A350-900 side by side, adopted from [13]	31
2.4	Optimized Flying-V wing shape for cruise flight with mach contours, adopted from [17]	31
2.5	2020 iteration of the Flying-V enabling family design, adopted from [14]	32
2.6	Control surface layout of the Flying-V, adopted from [12]	32
2.7	Reference frames of the Flying-V, from [21]	34
2.8	Comparison of aerodynamic coefficients from VLM model and WTT, from [20]	35
2.9	Convex estimation hulls, α versus airspeed (left), α versus elevator deflection (right), taken from [44]	36
2.10	The TU Delft Flying-V on the runway during its maiden Flight, taken from [45]	37
2.11	Comparison between the lift and drag coefficients obtained from the maiden flight test and those from wind tunnel tests, taken from [44]	37
2.12	Comparison between the lift and pitching moment coefficients obtained from the test flight campaign and those from wind tunnel experiments, obtained from [46]	38
2.13	Control surface layout differences between the model used in the VLM and the 4.6 % half-wingspan model used in the WTE, obtained from [21]	38
2.14	Comparison of aerodynamic coefficients from WTE model and VLM model, obtained from [21]	39
2.15	Aerodynamic coefficients of the combined model displaying pitch break tendency at $\alpha = 20^\circ$, from [21]	39
2.16	Sensor dynamics model, as seen in [24]	41
2.17	Eigenvalues of the Flying-V during approach, considering both the forward and aft CG configuration. [21]	42
2.18	Eigenvalues of the Flying-V during cruise, considering both the forward and aft CG configuration, obtained from [21]	43
2.19	Damping ratios and natural frequencies of the Flying-V's eigenmodes, taken from [21]	43
2.20	Flight control system design process, taken from [58]	45
2.21	Modular structure of NDI, obtained from [35]	47
2.22	NDI control law with linear outer control loop, adopted from [34]	48
2.23	INDI control law with linear outer control loop, adopted from [34]	50
3.1	Standard closed-loop LFT interconnection, from [93]	57
3.2	General control configuration with perturbations, from [36]	59
3.3	$N\Delta$ -structure, from [36]	59
3.4	$M\Delta$ -structure, from [36]	60
3.5	Loop shape specification, adopted from [35]	64
3.6	S/KS mixed-sensitivity minimization in its standard form [36]	65
3.7	General two-DOF control system, taken from [127]	67
3.8	Typical signal based \mathcal{H}_∞ control system, obtained from [36]	68
3.9	INDI-based EMF control system interconnection structure, from [35]	72
4.1	Levels of handling qualities, as defined in [144]	76
4.2	Alternative short-term pitch response criteria seen in WL-TR-94-3162 [86]	78

4.3	Road map for the use of alternative short-term pitch response criteria [86]	78
4.4	CAP boundaries for category B flight phases, from [86]	79
4.5	Dropback Criterion from [86]	80
4.6	Bandwidth criteria from [132]	80
4.7	Gain and phase margin requirements from [150]	81
5.1	Comparison of responses to 1° elevator step input	87
5.2	Short period dynamic requirements for category B flight phases	88
5.3	Desired pitch rate response alongside bare air-frame response	89
5.4	Control system interconnection structure with unstructured μ -controller	91
5.5	Closed-loop transfer functions	92
5.6	Disk-based stability margins of closed-loop system	94
5.7	Robust Stability breakdown	95
5.8	Robust Performance breakdown	95
5.9	Pitch rate response of unstructured controller	96
5.10	Elevator deflection	97
5.11	Elevator deflection rate	97
5.12	CAP criteria assessment	98
5.13	Gibson drop-back criterion assessment	99
5.14	Flight Path angle simulation	99

List of Tables

2.1	Design parameters Flying-V, adopted from [20]	33
2.2	Moments of Inertia of the Flying-V around the principle axes, sourced from [20]	34
2.3	Verified operational range of the aerodynamic model, sourced from [21]	40
2.4	Control surface deflection limits of scale model, adopted from [21]	40
2.5	Baseline sensor values, adopted from [32]	41
2.6	Two flight Conditions of the Flying-V defined by van Overeem [47]	41
2.7	Trim results seen in [47]	42
2.8	Flying quality assessment at approach condition, adopted from [47]	44
2.9	Flying quality assessment at cruise condition, adopted from [47]	44
2.10	CAP parameters of the Flying-V, as seen in [47]	44
4.1	Flight phase categories, adopted from [144]	76
4.2	Phugoid damping requirements from [56]	77
5.1	Short period poles, damping and natural frequency	87
5.2	Short period handling quality requirements during cruise	88
5.3	Short period design parameters for preliminary analysis, based on MIL-STD-1797A [132]	88
5.4	Non-weighted transfer functions	89
5.5	Classical and disk-based stability margins	93
5.6	Gibson criteria values of the nominal closed-loop system	98

Introduction

Growing concerns about emissions from the aviation sector has led industry and academia alike towards exploring various strategies aimed at improving sustainability. In a systematic review by Afonso et al. [1], key battleground were identified and the various strategies were categorized as follows: aircraft operations, energy storage, propulsion systems, aerodynamics, structures, materials and manufacturing processes [1]. In order to improve aerodynamic efficiency specifically, designers aim for drag minimization and lift-to-drag ratio optimisation. These include the use of passive and/or active flow control, various surface treatments and even morphing wings and various bio-inspired design features aimed at improving aerodynamic characteristics.

A more drastic approach is the redesign of the overall aircraft configuration. Over a decade ago, Abbas et al. [2] identified this as a necessary innovation for achieving sustainable aviation. According to Abbas et al., conventional concepts have been optimized over the last decades and have reached a point where further advancements are highly costly and offer only marginal improvements. Amongst the proposed configurations are High Aspect-Ratio Wings (HARWs), non-planar wings, various braced wing aircraft and various hybrid (HWB) and blended wing-body aircraft (BWB) [1]. The latter aims to replace the conventional tube and wing configuration with a blended fuselage. As the name suggests, the BWB does not have a distinct fuselage with wings attached. Rather, the wings are blended into the main body to generate something resembling a flying wing [3].

The BWB aircraft in its current form was first conceptualised by Robert Liebeck in 1988 at the McDonnell Douglas Corporation (MDC), now part of Boeing. The BWB design offers increased aerodynamic efficiency by merging the wings and fuselage together into one single lifting surface [4]. Several years later, a technical and commercial feasibility study on the BWB concept was conducted by a team of researchers from NASA, MDC and Stanford [5]. The researchers built a 17 ft span radio-controlled model aircraft, known as the BWB-17, to demonstrate the flying capabilities of BWBs. Following the success of the BWB-17, NASA further explored the feasibility of the BWB-design for commercial aviation purposes. Eventually culminating into the BWB-450, a conceptual 450 passenger commercial aircraft [6].

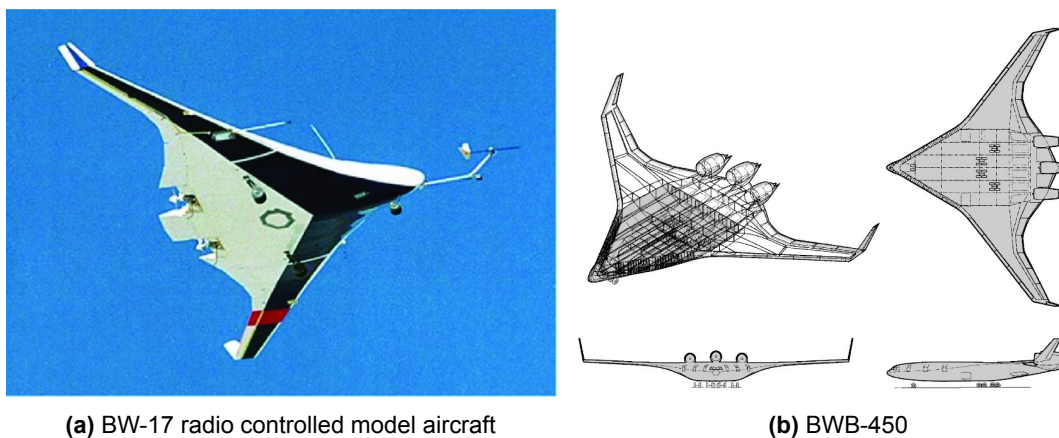


Figure 1.1: The BW-17 and the BWB-450, from [6]

The aforementioned study was the first of many and sparked the interest in BWB aircraft in academia and industry alike. Over the years, numerous BWB designs have been proposed by researchers worldwide [7].

In a 2019 review paper by Chen et al. [8], the authors provided a historical overview of the research on BWB and an assessment of the state-of-the-art at the time. Moreover, the authors provide an overview of the advantages of the BWB design, alongside the remaining design challenges. The main benefit of the BWB design pertains to its increased aerodynamic efficiency, resulting in increased fuel efficiency over the entire flight envelope, as well as reduced noise levels during take-off and landing [9]. The integration of the fuselage and the wings results in a lower wetted surface area to volume ratio, lower frictional drag and reduced interference drag. As a result, BWB aircraft display greater lift-to-drag ratios compared to conventional tube-and-wing aircraft [7]. Large scale implementation of BWB aircraft could thus offer a significant decrease in both environmental and noise pollution and would usher in a new era in commercial aviation.

Adjacent to the BWB design, the concept of a flying-wing type aircraft has been explored. This concept differs from the BWB in that a pure flying-wing has straight leading and trailing edges with no definite fuselage [7], as shown in figure 1.2. Amongst the proposed designs of flying-wings is the Flying-V, a concept which began its development well over a decade ago [10].

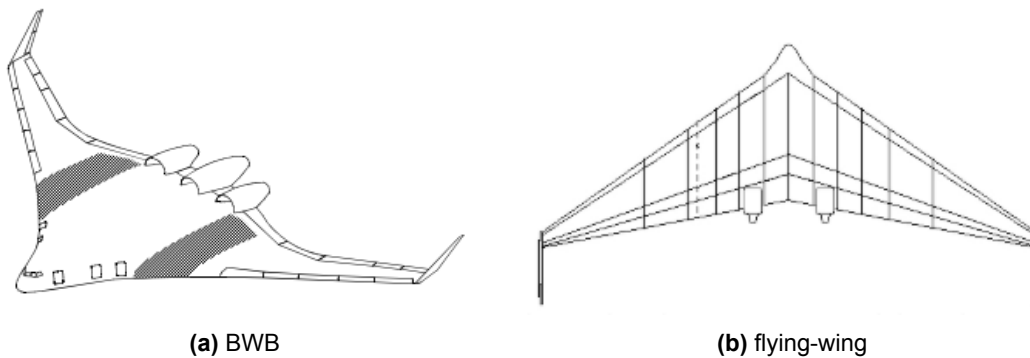


Figure 1.2: side-by-side view of a BWB and a pure flying-wing, from [11]

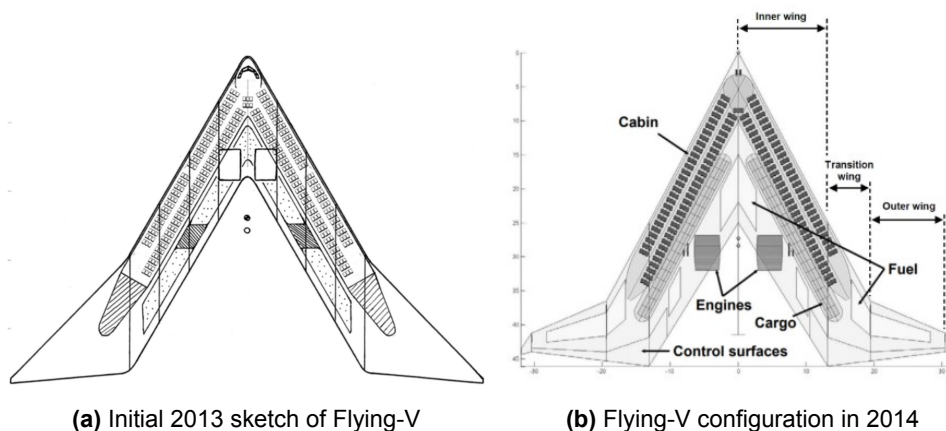
1.1. The Flying-V



Figure 1.3: Artist rendition of the Flying-V, from [12]

2013 marked the start of the development of the Flying-V at the Airbus Future Projects office in Hamburg. As the name suggests, the Flying-V concept is based on a design featuring two fuselage barrels arranged in a V-shape, consisting of a highly swept inner wing and an outer wing with a reduced sweep angle [13]. The rationale behind the design was to place an efficient, pressurized cabin structure within an aerodynamically favorable wing shape.

Between 2013 and 2015, various design features were added to the initial design. As can be seen in figure 1.4, the highly swept inner wing trunk transitions into an outer wing trunk with a lower sweep angle. The transition section has the same leading edge sweep as the inner wing and the outer wing trunk possesses the same trailing edge sweep as the transition wing trunk [10]. This multi-element wing design allows the Flying V to be stretched or shrunk by simply adding or removing constant-section wing plugs, thus offering the possibility for family design [14]. This was identified as one of the major hurdles in the commercialization of BWB aircraft years earlier by Liebeck, who claimed that achieving commonality amongst BWB aircraft may provide the incentive and courage for manufacturers to further develop these aircraft [15].



(a) Initial 2013 sketch of Flying-V

(b) Flying-V configuration in 2014

Figure 1.4: Initial sketch and configuration of the Flying-V, from [16]

In order to demonstrate the flight characteristics of the initial design proposed by Benad, a radio controlled model was built and flown in 2014. Both non-powered glider flights and powered flights with engines mounted on the aircraft were performed, demonstrating good handling qualities [13].

2016 also saw the start of a collaboration between Airbus, KLM and the TU Delft resulting in sustained research & development on the Flying-V. Ever since, research efforts have been dedicated to the improvement of the design on various aspects. A 2017 study by Faggiano et al. [17] claimed that the aerodynamic L/D ratio of the Flying-V could amount to 23.5, signifying a 25% increase w.r.t. the NASA common research model.

In the following years, several aerodynamic parameter estimation efforts have culminated in a variety of models. These include a Vortex Lattice Method (VLM) model, a model based on extensive Wind Tunnel Experiments (WTE) on a half-wing sub-scale model of the Flying-V and a model obtained from a series of flight tests with a subscale flight-test model.

Some key findings from these studies include a pitch-break tendency of the Flying-V at angles of attack larger than $\alpha = 19^\circ$ [17]. Moreover, nonlinear effects as a result of vortex formation were seen to occur at angles of attack greater than $\alpha = 10^\circ$ [18]. These findings were later confirmed by Benad in 2022 [19]. Van Overeem developed a dynamic model of the Flying-V based on the results obtained by Cappuyns earlier in 2019 and simulations performed by Airbus GmbH [20, 21]. Van Overeem concluded that in the majority of its flight envelope, the bare airframe displays Level 1 predicted handling qualities. Piloted simulations later confirmed these findings, although concerns about the lack of control authority at certain control allocation configurations were raised [22]. Joosten et al. suggested that the Flying-V's lateral eigenmodes are similar to that of a conventional aircraft [23]. However, it was observed that at certain approach conditions, the Flying-V in its current configuration lacks control authority to comply with certification regulations. These conclusions were based on control derivatives obtained from an inviscid model, which did not take into account the complex vortex formations observed independently by Viet and Benad, suggesting a considerable contribution of these flow phenomena at larger angles of attack [18, 19].

In an attempt to further enhance the Flying-V's handling qualities, stability and control augmentation systems have been proposed. Van Overeem proposed an INDI-based flight control system [21]. Subsequently, Stougie proposed an INDI-based controller including flight envelope protection (FEP) [24].

INDI, short for Incremental Nonlinear Dynamic Inversion, is a sensor-based alternative to Nonlinear Dynamic Inversion (NDI) and was first introduced by Smith in 1998 [25]. INDI relies on the availability of sensor measurements to estimate state derivatives. Contrary to NDI, which relies on model based estimates of the state derivatives. As such, INDI is less reliant on the presence of an accurate on-board model (OBM), as it only requires knowledge of the control effectiveness. This in turn, leads to an increased robustness to aerodynamic uncertainty when compared to its model-based counterpart, NDI. However, this comes at the cost of an increased sensitivity to time delays, which has been observed both in simulation and in flight tests [26, 27, 28, 29, 30].

Stougie studied the robustness of the proposed controller by varying the values of certain aerodynamic parameters and concluded that this has a negligible effect on the tracking performance of the controller [24]. Moreover, the gain and phase margin of the control system were assessed and were shown to decrease with increased uncertainty. Stougie concluded that additional effects such as time delays and aero-elasticity must be considered to gain a better understanding of the robustness properties of the INDI-based controller. Stougie's findings are consistent with existing literature on INDI, which demonstrate INDI's robustness to aerodynamic uncertainty, yet an increased sensitivity to time delays [31, 26, 29, 32, 30, 33].

Time delays are considered to be a part of a wider class of perturbations known as singular perturbations. Up until recently, formal robustness analyses of INDI-based control laws were limited to regular perturbations [34]. Pollacks convincingly argues that to gain deeper insight into the robustness properties of INDI-based control laws, these singular perturbations must be considered [35]. Subsequently, Pollack established the necessary tools to assess the robustness of INDI-based control laws in the presence of both regular and singular perturbations. The framework presented by Pollack is rooted in multivariate linear control analysis [36]. This framework provides powerful formal robustness analysis tools, such as μ -analysis. Moreover, well established \mathcal{H}_∞ -synthesis tools can be utilized, enabling the design of robust multi-objective control laws.

This research contributes to the ongoing research on the Flying-V in the following manner. A multi-loop mixed μ -optimal synthesis approach is applied to the design of a INDI-based pitch rate controller for a short period model of the Flying-V. This case study sheds a light on the multi-loop robustness functionality of

I(N)DI-based controller. Moreover, the case study demonstrates how classical handling quality requirements can be included in the \mathcal{H}_∞ -framework. The results provide fundamental insight into the possibilities and limitations of inversion-based controllers in the presence of both regular and singular perturbations.

1.2. Research objective & research questions

Research Objective

The goal of this research is to assess the capability of \mathcal{H}_∞ -based tools to improve the robust performance of IDI-based flight control laws for the Flying-V in the presence of regular and singular perturbations.

Research Questions

In pursuit of attaining the research objective, the following main research question is formulated.

How can \mathcal{H}_∞ -based tools aid in the design of robust IDI-based pitch-rate control laws to satisfy longitudinal handling quality requirements for the Flying-V?

The main research question is split into the following sub-questions.

1. What is the state-of-the-art research on the Flying-V?
 - (a) Which elements make up the simulation model of the Flying-V?
 - (b) What are the stability and handling quality characteristics of the bare airframe?
 - (c) Which stability & control augmentations systems have been applied to the Flying-V?
 - (d) What is the state-of-the-art on INDI-based flight control design?
2. How can \mathcal{H}_∞ tools be used to establish robust flight control systems?
 - (a) How is the \mathcal{H}_∞ framework defined?
 - (b) How can \mathcal{H}_∞ -based tools be applied to flight control system design?
 - (c) What are the robustness properties of (I)NDI based control laws?
3. Which longitudinal handling quality, stability and performance criteria must the Flying-V satisfy?
 - (a) Which requirements are useful for assessing the Flying-V's longitudinal handling qualities
 - (b) Which stability requirements must the FCS on the Flying-V adhere to?
 - (c) Which performance metrics does the Flying-V have to adhere to and how can these be incorporated into design requirements?
4. How can \mathcal{H}_∞ tools be applied to INDI-based flight control law design to improve the longitudinal handling qualities of the Flying-V?
 - (a) How can the design criteria be included in the formulation of a structured \mathcal{H}_∞ -synthesis problem?
 - (b) How can IDI-based control systems be included in the formulation of a structured \mathcal{H}_∞ -synthesis problem?
 - (c) What are the robust stability & performance characteristics of robust IDI-based control systems on the Flying-V?

1.3. Research Scope

Scope of simulation model

The simulations and controller designs presented in this work are based on an LTI model of the short-period approximation of the longitudinal dynamics of the Flying-V at a single cruise condition. Moreover, no pilot-in-the-loop simulation component is included, nor are sensor dynamics. All of the components of the flight control system are assumed to operate in continuous time. Uncertainty is added to the simulation model in the form of structured and unstructured uncertainty.

Scope of stability, performance and handling requirements

As the simulation model is limited to the short-period approximation of the Flying-V, so are the requirements. Specifically, it was decided to limit the scope of this research to a subset of the requirements discussed in chapter 4.

Scope of flight control system design

The flight control system design presented in I are variations of hybrid IDI-based pitch-rate controllers. These are designed with the use of mixed μ -synthesis tools embedded in the Matlab Robust Control Toolbox™ [37]. The design case study is centered around a LTI short-period model of the Flying-V containing both parametric and non-parametric uncertainty.

Scope of robust stability & performance analysis

The robust stability & performance analysis provided in part I is done in various ways. Firstly, classical SISO margins are evaluated for the nominal plant descriptions, alongside classical margins for the worst-case perturbed plant. Moreover, a closed-loop frequency-domain analysis is provided. Moreover, robust stability and performance are assessed through a structured singular value (μ)-analysis. Finally, linear simulations are performed.

1.4. Structure of the Report

This report is structured as follows: in part I, the main findings of this research are presented in the form of a scientific article. In part III, the findings of the literature review and a preliminary analysis are provided. Readers who are unfamiliar with the framework used in robust control are strongly advised to read part III. Finally, the conclusions and recommendations are provided in part IV.

Part I

Scientific Article

Robust Multi-loop Mixed μ -optimal Inversion-based pitch rate control for the Flying-V

R. Shahin*

The Flying-V is a tailless, V-shaped flying wing that was conceptualized over a decade ago. Its aerodynamically favorable shape promises significant reductions in emissions and noise pollution. However, its configuration also presents a number of stability and control related challenges. These result in unfavorable handling qualities throughout parts of its flight envelope. To enhance the handling qualities of the Flying-V, Incremental Nonlinear Dynamic Inversion (INDI)-based flight control systems have been proposed. INDI, a sensor-based alternative to conventional Nonlinear Dynamic Inversion (NDI), is rooted in the principle of feedback linearization. Unlike NDI, INDI does not depend heavily on accurate on-board models (OBM), thereby offering increased robustness to aerodynamic uncertainties. However, singular perturbations—such as time delays, aeroelastic effects, and additional unmodeled or unknown dynamics—have been identified as challenges for INDI-based control laws. Various strategies have been explored to improve the overall robustness of INDI-based flight control systems, including outer-loop tuning and inversion loop augmentation strategies. In this article, we adopt a multi-loop, DGK-iteration based, mixed μ -synthesis approach to the design of robust inversion-based control laws for a LTI short-period model of the Flying-V. Subsequently, a robust stability and performance analysis of the synthesized controllers is provided.

I. Introduction

GROWING concerns about emissions from the aviation sector has led industry and academia alike towards exploring various strategies for improving sustainability [1]. One promising strategy is the redesign of the overall aircraft configuration. To that extent, a revived interest in the blended-wing-body (BWB) for commercial transport aircraft has emerged. These promise to offer reductions in the wetted surface area to volume ratio, reduced frictional drag and reduced interference drag, all contributing to an increased lift-to-drag ratio, in turn increasing aerodynamic efficiency. This promises a reduction in emissions and reduced noise levels during take-off and landing. The Flying-V, first introduced in 2015 by Benad, is a tailless, V-shaped flying-wing type aircraft consisting of two pressurized cylindrical cabins housed in the leading edge of the aircraft [2]. Previous research has demonstrated that the Flying-V may offer a 25% increase in aerodynamic efficiency compared to the NASA common research model [3]. In line with earlier observations on BWB and wing-shaped aircraft, it has been observed that the Flying-V exhibits challenges with respect to its stability and control characteristics. It was concluded that the Flying-V suffers from pitch break-up for angles of attack greater than 20 degrees [3–5]. Moreover, it was observed that the Dutch roll mode of the Flying-V is unstable and that its lateral-directional controllability is limited [6, 7].

To stabilize the unstable mode and to improve the handling qualities of the Flying-V, various stability and control augmentation systems have been proposed. In [8], a INDI-based flight control system (FCS) is proposed, rendering all of the eigenmodes stable and resulting in Level 1 handling qualities. In [9], a C^* outer-loop in combination with a INDI-based inner-loop rate control system is proposed. Moreover, flight envelope protection (FEP) was added to prevent the Flying-V from reaching angles of attack where the pitch-break results in open-loop instability. The performance of the proposed FCS was assessed in the presence of aerodynamic uncertainty, discretization effects and time-delays. It was observed that the aerodynamic uncertainty had negligible impact on the tracking performance and that the aircraft could be tuned to Level 1 handling qualities for an angular rate sensor sampling frequency of 100 Hz. Moreover, the effect of time-delays on the closed-loop system was briefly assessed. It was concluded that for delays up to 0.05s, the aircraft remains tunable to Level 1 handling qualities. It was observed that for greater time-delays, this was no longer possible [9]. The latter sheds a light on well-known limitations of INDI-based control laws. That is, the fundamental trade-off between the robustness to low-frequency perturbations and an increased sensitivity to high-frequency perturbations. This trade-off can be traced back to the "fundamental costs of feedback", a phrase coined by Horowitz back in 1963

*Graduate student, Control and Simulation Research Group, Delft University of Technology, Kluyverweg 1, 2629HS Delft, The Netherlands, rshahin@student.tudelft.nl

[10]. These findings align with previous research on INDI-based control laws, which have demonstrated robustness to aerodynamic uncertainties in both simulations and flight tests [11–15]. Moreover, analytical proofs of the nominal and robust stability properties in the presence of external disturbances and regular perturbation have been established [16]. However, it has also been observed that compared to conventional NDI, INDI displays relatively small stability robustness margins in the presence of time-delays affecting the feedback path [13, 16–18]. These belong to a wider category of disturbances known as singular perturbations. The importance of singular perturbations and their impact on sensor-based INDI flight control laws has become increasingly recognized in the literature [17, 19–21]. However, many of the research is limited to robustness analyses that make use of fixed-structure state-space representations, such as in [19–21]. This implies that all of the considered model uncertainty and singular perturbations can be parameterized in known form. This is a fundamentally flawed assumption, as it is well known that for physical systems, this is not the case [22]. Examples include the bare airframe dynamics of an aircraft at high frequencies, which are often difficult to model due to badly understood or unknown structural dynamics and unsteady aerodynamic effects. Similarly, these complex effects are often also present in the actuator dynamics [23–25]. These high-frequency uncertainties belong to the category of singular perturbations, which are described as a category of perturbations stemming from unmodeled dynamics [26]. These arise from either unknown dynamics, as presented earlier, or from deliberate model simplifications. Singular perturbations are non-parametric by nature and can be captured adequately by norm-bounded uncertainty descriptions [22]. In order to adequately assess the robust stability and performance properties of INDI-based control laws, singular perturbations must be taken into account. In [27], Pollack first establishes the fundamental robustness properties of (I)NDI-based control laws in the presence of both regular and singular perturbations. It is demonstrated that the inversion residual, which represents the residual closed-loop dynamics stemming from non-ideal inversion in the presence of regular and singular perturbations, has an upper bound for model-based NDI control laws. On the contrary, it is shown that for INDI-based control laws, the upper bound on the inversion residual can not always be found. Pollack demonstrated that to ensure the boundedness, hence stability, of INDI-based control laws, additional inversion augmentation is required. Subsequently, Pollack presents a robust stability and performance assessment of (I)NDI-based flight control laws in terms of their linear counterparts, referred to as (I)DI. This allows for \mathcal{H}_∞ -based robustness assessments and enables the use of \mathcal{H}_∞ -synthesis tools [22, 28]. Examples of the application of these tools to inversion-based control design include the \mathcal{H}_∞ mixed sensitivity approach in [29] and the multi-objective optimization approaches in [30, 31]. However, these studies do not optimize for the inner inversion loop itself. Therefore, the resulting robustness properties of these laws are thus inherited from the specific inversion strategy. In later work by Pollack [32], it is demonstrated how multi-loop synthesis of an explicit model-following (EMF) (I)NDI design can be leveraged to establish adequate robust stability and performance in the presence of mixed parametric and dynamic uncertainty. Moreover, a structured \mathcal{H}_∞ synthesis algorithm is established to optimize the design parameters of the various inversion architectures. In addition, a robustness analysis is provided based on the Integral Quadratic Constraint (IQC) framework, which extends the robustness analysis to include Linear Time-Varying (LTV) uncertainties. The primary contribution of this paper is a case study that employs a multi-loop mixed μ -synthesis method for hybrid INDI-based pitch rate control design for the Flying-V. This work builds on the findings of [32], adapting the techniques presented in chapters 2 and 3 with specific modifications. This approach uncovers important insights into the essential robustness characteristics of inversion-based control design. This article is organized as follows: Section II provides background on (I)NDI-based control laws, along with key insights into their robustness and performance characteristics. These insights lay the groundwork for the design methodology discussed in section III, which focuses on a case study involving the design of a pitch-rate control law for a short-period approximation of the Flying-V under mixed perturbations. The results of this case study are presented in section IV. Finally, section V offers concluding remarks.

II. (I)NDI-based control law design

This section offers a brief overview of (I)NDI-based control law design, highlighting key insights into their robust stability and performance characteristics. These insights serve as the foundation for the design strategy presented in section III. The insights discussed in section II.B are derived from the work of Pollack in [32], readers are encouraged to consult that source for more detailed derivations.

A. Inversion-based control law design

Inversion-based control law design is rooted in the principle of feedback linearization. Consider some input-affine nonlinear system in its state-space form.

$$\Sigma : \begin{cases} \dot{\mathbf{x}} = \mathbf{f}(\mathbf{x}) + \mathbf{G}(\mathbf{x})\mathbf{u} \\ \mathbf{y} = \mathbf{h}(\mathbf{x}) \end{cases} \quad (1)$$

Which is characterized by the state vector $\mathbf{x} \in \mathcal{R}^n$, the input vector $\mathbf{u} \in \mathcal{R}^m$, the controlled variable $\mathbf{y} \in \mathcal{R}^p$ and where \mathbf{f} , \mathbf{G} and \mathbf{h} represent smooth mappings. To accomplish feedback linearization, Lie derivatives of the controlled variable \mathbf{y} are repeatedly taken until the input vector \mathbf{u} appears explicitly in the expression of \mathbf{y} [33]. The number of times the Lie derivative has to be taken before \mathbf{u} appears is known as the relative degree ρ . As such, the output dynamics can be formulated as follows [16]:

$$\begin{aligned} \mathbf{y}^{(\rho)} &= L_f^\rho \mathbf{h}(\mathbf{x}) + L_g L_f^{\rho-1} \mathbf{h}(\mathbf{x})\mathbf{u} \\ &\triangleq \boldsymbol{\alpha}(\mathbf{x}) + \boldsymbol{\beta}(\mathbf{x})\mathbf{u} \end{aligned} \quad (2)$$

Where $L_f^k h_i(\mathbf{x})$ and $L_{g_i} L_f^k h_i(\mathbf{x})$ represent repeated Lie derivatives of h_i along the vector field \mathbf{f} and column vectors \mathbf{g}_i of matrix \mathbf{G} . This expression can be rearranged such that a control law \mathbf{u} emerges that reduces these nonlinear dynamics to a set of integrators [33].

$$\mathbf{u} = \hat{\boldsymbol{\beta}}^{-1}(\mathbf{x})[\boldsymbol{\nu} - \hat{\boldsymbol{\alpha}}(\mathbf{x})] \quad (3)$$

Here, $\hat{\boldsymbol{\alpha}}(\mathbf{x})$ and $\hat{\boldsymbol{\beta}}(\mathbf{x})$ represents the estimates of the state derivative $\boldsymbol{\alpha}(\mathbf{x})$ and the control effectiveness matrix $\boldsymbol{\beta}(\mathbf{x})$, which is assumed to be invertible. The source of the state derivative depends on the inversion strategy. $\boldsymbol{\nu} \in \mathcal{R}^m$ represents the virtual control law stemming from the outer-loop controller, which is responsible for stabilizing the external dynamics as well as providing improved performance and robustness. Note that the internal dynamics are unobservable from the controlled variable $\mathbf{y}^{(\rho)}$. If the virtual control law includes feedback of the internal dynamics, the control law in equation 3 is capable of stabilizing these internal dynamics. If the virtual control law is solely dependant on external dynamics, the control law in equation 3 is not capable of stabilizing the internal dynamics. The choice of the controlled variable, and by extension the virtual control law, must therefore be made diligently, such that it exhibits stable zero dynamics [34].

1. Model based-NDI

As stated, the source of the control derivative estimate $\hat{\boldsymbol{\alpha}}(\mathbf{x})$ depends on the inversion strategy. In the case of standard model-based (MB) NDI, the control derivative estimate directly follows from the on-board model (OBM) estimate $\hat{\boldsymbol{\xi}} = \hat{\boldsymbol{\alpha}}(\mathbf{x})$. Considering the short-period dynamics of an aircraft $\hat{\boldsymbol{\xi}} \rightarrow \boldsymbol{\xi} \triangleq \dot{q} - M_{\delta_e} \delta_e$ refers to an (uncertain) mapping of the bare airframe state and exogenous disturbances. Which in the model-based case, results in the following inversion scheme.

$$\hat{\boldsymbol{\xi}}^{(MB)}(s) = \hat{M}_\alpha \alpha + \hat{M}_q q \quad (4)$$

Where α and q refer to the angle-of-attack and pitch rate measurements, which are assumed to be available in this study. Moreover, \hat{M}_α and \hat{M}_q refer to the OBM representations of the short-period stability and control derivatives associated with the unperturbed airframe dynamics.

2. Sensor based-INDI

An incremental form of the control law in equation 3 can be obtained by performing a Taylor expansion of the output dynamics $\mathbf{y}^{(\rho)}$ around the state at time $t - \Delta t$, where Δt represents the sampling time. Performing the Taylor expansion, the following expression arises.

$$\mathbf{y}^{(\rho)} = \mathbf{y}_0^{(\rho)} + \left. \frac{\partial [\boldsymbol{\alpha}(\mathbf{x}) + \boldsymbol{\beta}(\mathbf{x})\mathbf{u}]}{\partial \mathbf{x}} \right|_0 (\mathbf{x} - \mathbf{x}_0) + \boldsymbol{\beta}(\mathbf{x}_0)(\mathbf{u} - \mathbf{u}_0) + \mathbf{R}_1 \quad (5)$$

Where \mathbf{R}_1 represents the expansion remainder. By applying the time-scale separation principle, the incremental control input $\Delta \mathbf{u} = \mathbf{u} - \mathbf{u}_0$ is derived under the assumption that state-dependent and residual terms can be neglected [13, 17].

This assumption is typically considered valid with sufficiently high sampling rates and the presence of high-bandwidth actuators. As such, the incremental control law can be described as follows:

$$\mathbf{u} = \mathbf{u}_0 + \hat{\beta}^{-1}(\mathbf{x}_0) \left[\mathbf{v} - \mathbf{y}_0^{(\rho)} \right] \quad (6)$$

Where $\mathbf{y}_0^{(\rho)}$ and \mathbf{u}_0 , in the case of sensor-based INDI, are sourced directly from the previous control variable derivative and the previous control vector through sensor measurements. A discrepancy in the time of arrival of these measurements has a profound effect on the closed-loop dynamics. This has repeatedly been observed in the literature [12, 13, 17] and is known as the *synchronization effect* and arises due to the presence of actuator dynamics. The inversion scheme for sensor-based INDI can be represented as follows:

$$\hat{\xi}^{(SB)}(s) = \dot{q} - M_{\delta_e} \delta_e \quad (7)$$

Direct implementation of SB-INDI is considered problematic due to its sensitivity to high-frequency uncertainty [27]. As such, augmentation filters are required to guarantee adequate roll-off of the incremental feedback loop beyond a certain frequency. Moreover, the angular acceleration and control input feedback signals must be synchronized in time (recall the synchronization effect). Introducing a lag to the control input feedback signal, aligning it with the sensed angular acceleration, has been shown to effectively address this issue [12]. Consequently, the sensor-based inversion scheme can be modified as follows:

$$\hat{\xi}^{(SB)}(s) = H_c(s) \left[\hat{q}(s) - G_s(s) \hat{M}_{\delta_e} u_s(s) \right] \quad (8)$$

Here, $\hat{q} \triangleq G \dot{q}$ represents a measurement of \dot{q} which is possibly contaminated by a bounded operator G . H_c represent a compensation filter, G_s represents the synchronization filter and u_s represents the control input feedback signal. A typical choice for H_c is a second-order low-pass filter [12, 13, 30], which alongside filtering, also provides the time-derivative of q .

3. Hybrid INDI

Alternatively, different inversion schemes can be combined into what is known as Hybrid-INDI. The existence of Hybrid-INDI schemes builds on the following equality, which holds only in the absence of OBM uncertainty and disturbances [32].

$$\underbrace{M_\alpha \alpha + M_q q}_{\xi^{(MB)}} = \dot{q} - \underbrace{M_{\delta_e} \delta_e}_{\xi^{(SB)}} \quad (9)$$

Various versions of Hybrid-INDI have been developed, including a constant compensation gain approach [31] and a complementary-filter-based method [35]. Additionally, a Scaled Complementary Filter (SCF) was proposed in [32], which integrates both blending strategies. This leads to the following inversion scheme

$$\hat{\xi}^{HB}(s) = (1 - K_c H_c(s)) \left[\hat{M}_\alpha \alpha(s) + \hat{M}_q q(s) \right] + K_c H_c(s) \left[\dot{q}(s) - \hat{M}_{\delta_e} u_s \right] \quad (10)$$

Where $K_c \in [0, 1]$ represent the compensation gain and H_c represents the compensation filter, corresponding to that seen in the sensor-based approach. Note that in this study, it is assumed that the pitch acceleration measurement is not contaminated by some dynamic operator, as seen in equation 8, hence \hat{q} reduces to \dot{q} . Equation 10 can be rewritten as follows [32]:

$$\begin{aligned} \hat{\xi}^{HB}(s) &= \hat{\xi}^{MB}(s) + K_c H_c(s) \left[\dot{q}(s) - \hat{\xi}^{MB}(s) - \hat{M}_{\delta_e} u_s(s) \right] \\ &\triangleq \hat{\xi}^{MB}(s) + K_c H_c(s) e_\xi(s) \end{aligned} \quad (11)$$

This equivalence demonstrates that Hybrid INDI can be viewed as the standard model-based approach with an additional model error compensation term. Moreover, it can be concluded that if $K_c = 0$, the hybrid scheme reduces to the model-based approach. Similarly, if $K_c = 1$, the hybrid scheme reduces to the form presented in [35]. In addition, it follows that $\hat{\xi}^{HB}(s) \rightarrow \hat{\xi}^{SB}(s)$ if $K_c = 1$ and the bandwidth of the compensation filter H_c is sufficiently large [32].

The control input feedback signal u_s can be retrieved in different ways. This presents a design choice that must be viewed in the context of control law complexity, robustness implications and hardware availability. Assuming that no dynamics occur between the actuator and the control surface position, three options are available. One option is

to use direct sensor measurements of the actuator position (AS). With this approach, the synchronization effect is circumvented. A second approach is to make use of internal control command (CC) feedback. This approach does not require additional sensors, yet it does not resolve the synchronization effect. Another option is to make use of the control command feedback and to pass it through an on-board actuator model (AM) [12, 27].

B. Robust Stability & Performance Insights

In [27], the robustness properties of (I)NDI-based control laws in the presence of mixed perturbations are established. It is shown that for model-based NDI control laws, the residual term ϵ_{NDI} , associated with the closed-loop residual dynamics emerging as a consequence of non-ideal inversion in the presence of mixed perturbations, has an upper bound $\bar{\epsilon}$ under bounded virtual control input \mathbf{v} . Yet the upper bound can be relatively large, indicating poor robustness properties [16]. For INDI-based control laws, it is demonstrated that the upper-bound on the inversion residual can not always be found. To ensure boundedness, hence stability for INDI-based control systems, additional inversion augmentation is required. One possible augmentation strategy is known as the matching strategy seen in [12, 13, 27]. The robustness ramifications of the various (I)NDI architectures can be better understood by examining their local characteristics in the frequency domain [32]. To that extent, Pollack establishes several important equivalences and distinctions in the properties of the various architectures.

One of the key insights is provided by the broken-loop shapes of the distinct inversion laws. Pollack [32] establishes an equivalence for the nominal loop gain of model-based inversion at the plant input (location C) in figure 2 and the all-loops broken (location B) transfer function in the case of hybrid INDI.

$$L_i^{(MB)}(s) = L_s^{(HB)}(s) = L_s^{(MB)}(s) = L_s(s) \triangleq \bar{G}_q(s) [C_{OL}(s) + C_{INV}(s)] \quad (12)$$

Where $\bar{G}_q(s) \triangleq M_{\delta_e}^{-1} q(s)/\delta(s)$. The series interconnection of the open-loop plant dynamics and the inversion controller highlights that the overall loop-shape and the resulting robustness properties remains plant-dependant. In the augmented sensor-based case, that is $H_c \neq 1$, the compensation filter results in the distortion of the inversion loop dynamics $\bar{C}_{INV}(s)$. In turn, this results in a distorted broken loop-shape $L_s^{(SB)} \triangleq \bar{G}_q(s) [C_{OL}(s) + \bar{C}_{INV}(s)]$.

The broken loop shape L_s refers to a transfer function that is embedded internally in the control law itself, therefore it does not provide any information of the robustness and performance at the bare airframe level [27]. By closing the control input feedback loop, the broken-loop response at the airframe input can be obtained [32]:

$$L_i^{(\cdot)}(s) = C_c(s) \left(L_s^{(\cdot)}(s) + K_c H_c(s) \right) \quad (13)$$

Where $C_c(s) \triangleq (1 - K_c H_c(s))^{-1}$. This result highlights the importance of adequate design of H_c and K_c , as these play a significant role in shaping of the broken-loop response at the airframe input.

Similarly, disturbance rejection properties at the plant input can be traced back to the input sensitivity $S_i \triangleq (1 + L_i)^{-1}$, which can be written as a function of the synchronization sensitivity as follows [32]:

$$S_i^{(\cdot)}(s) = [1 - K_c H_c(s)] S_s^{(\cdot)}(s) \quad (14)$$

The additional control action stemming from the incremental inversion loop is directly visible in equation 14. Moreover, it illustrates the difference in disturbance rejection properties of MB and SB-INDI. Note that disturbance rejection is often also addressed with adequate virtual control law design, highlighting the redundancy of multi-loop design to an extent. In the context of designing for robust flying qualities, explicit model following (EMF) architectures are a popular choice. It can be shown that for inversion-based controllers, ideal inversion results in ideal model following performance, regardless of the virtual control law design [32]. The quality of the inversion and the resulting model-following mismatch is captured by the synchronization sensitivity function $S_s(s)$. Performance degradation due to on-board model mismatches and the synchronization effect are therefore directly visible through $S_s(s)$. As such, the shaping of $S_s(s)$ - and by extension $L_s(s)$ - plays a crucial role in guaranteeing adequate model following performance. This also highlights that adequate model-following performance can also be addressed by adequate virtual control law design. Once again, highlighting the redundant functionality in multi-loop, inversion-based control law design. For a detailed explanation and derivation of these results, the reader is referred to [32].

III. Design case study

In this section, a design case study is presented which explores the capability of multi-loop, structured μ -synthesis to establish robust inversion-based control law designs. First off, the simulation model of the Flying-V and its constituents

are introduced in section III.A. Next, the FCS design requirements are discussed in section III.B. This is followed by the formulation of the structured μ -synthesis problem in section III.C.

A. Simulation model

The simulation model of the Flying-V used in this research is based on the configuration established in [36]. Cap-puyns presents two different centre of gravity configurations on the Flying-V. The model used in this research is based on the forward centre of gravity configuration, located at 29.4m behind the nose of the aircraft. In addition, the analysis in this research is based on a single cruise condition, at an altitude of 13km, at Mach 0.85. The mass of the aircraft is set to 240.000 kg. The control surface configuration, alongside some important design parameters are shown in figure 1 and table 1.

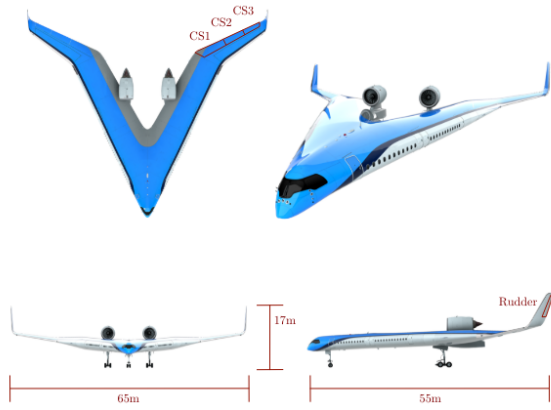


Fig. 1 Control surface layout of the Flying-V [36]

Parameter	Value	Unit
Length	55	[m]
Wingspan	65	[m]
Height	17	[m]
Pax	314	[-]
Fuel Capacity	140.000	[l]
Cargo Capacity	160	[m ³]
Design Mach number	0.85	[-]
Cruise altitude	43.000	[ft]

Table 1 Design parameters of the Flying-V [36]

1. Bare Airframe model

The bare airframe model used in this paper is based on the short-period approximation of the Flying-V's longitudinal dynamics. To obtain the short period model, the nonlinear equations of motion are trimmed and linearized at the aforementioned cruise condition. This results in the following nominal two-state, state-space model:

$$\begin{bmatrix} \dot{\alpha} \\ \dot{q} \end{bmatrix} = \begin{bmatrix} Z_{\alpha} & 1 \\ M_{\alpha} & M_q \end{bmatrix} \begin{bmatrix} \alpha \\ q \end{bmatrix} + \begin{bmatrix} Z_{\delta_e} \\ M_{\delta_e} \end{bmatrix} \delta_e \quad (15)$$

Here, δ_e represents the effective elevator deflection, as a result of slaving these together. Note that in this case study, as merely the longitudinal axis is considered, the elevators effectively function as purely elevons. The aerodynamic stability derivatives are based on aerodynamic data that has been obtained from a Vortex Lattice Method (VLM) model [36].

Atmospheric turbulence and gust disturbances are included in the model in the form of α -gusts, these are included by way of expanding the input matrix. Moreover, it is assumed that measurements of the pitch rate, the pitch acceleration, the angle of attack and the effective elevator deflection are all available. The resulting system is described by the following state-space system.

$$\begin{bmatrix} \dot{\alpha} \\ \dot{q} \end{bmatrix} = \begin{bmatrix} Z_{\alpha} & 1 \\ M_{\alpha} & M_q \end{bmatrix} \begin{bmatrix} \alpha \\ q \end{bmatrix} + \begin{bmatrix} Z_{\delta_e} & -Z_{\alpha} \\ M_{\delta_e} & -M_{\alpha} \end{bmatrix} \begin{bmatrix} \delta_e \\ \alpha_g \end{bmatrix} \\ \begin{bmatrix} \alpha_s \\ q_s \\ \dot{q}_s \end{bmatrix} = \begin{bmatrix} 1 & 0 \\ 0 & 1 \\ M_{\alpha} & M_q \end{bmatrix} \begin{bmatrix} \alpha \\ q \end{bmatrix} + \begin{bmatrix} 0 & -1 \\ 0 & 0 \\ M_{\delta_e} & -M_{\alpha} \end{bmatrix} \begin{bmatrix} \delta_e \\ \alpha_g \end{bmatrix} \quad (16)$$

Where α_g represents external changes in the angle of attack due to wind gusts. These are shaped by a first-order approximation of the Dryden gust model, defined as follows [25]:

$$W_g(s) = \left(\frac{180}{\pi} \frac{1}{V_{t0}} \right) \frac{4}{s + 0.2} \quad (17)$$

2. Actuator Model

In addition to the aerodynamic model of the aircraft, a FCS hardware model has been proposed in [9] in the form of a second-order actuator model, which is based on the following model presented in [37]:

$$G_{act}(s) = \frac{\omega_{act}^2}{s^2 + 2\zeta_{act}\omega_{act}s + \omega_{act}^2} \quad (18)$$

Where $\omega_{act} = 20 \text{ rad/s}$ and $\zeta_{act} = 0.71$, which are typical values for electro-mechanical servos seen on large transport aircraft [38, 39].

3. Uncertainty definition

In practice, the actual bare airframe dynamics differ from the dynamics described in 16. This model mismatch is due to a variety of reasons, often stemming from physical uncertainties and/or modelling error. Uncertainty entering the plant is typically categorized into parametric and non-parametric uncertainty. The former do not change the order of the system, whereas the latter do [22]. Non parametric uncertainties represent unmodelled and/or neglected dynamics, hence introducing new state variables, ultimately increasing the order of the system.

Parametric uncertainties arise in various forms, such as uncertainties in mass, inertia, airframe configuration settings, and aerodynamic stability derivatives. This is particularly relevant for aircraft in the early design stages, where designers often depend on preliminary data, as is the case with the Flying-V. Consequently, parametric uncertainty is modeled as multiplicative uncertainty applied to the stability and control derivatives, as shown below:

$$\tilde{M}_{(\cdot)} = (1 + w_{M_{(\cdot)}} \delta_{M_{(\cdot)}}) M_{(\cdot)} \quad (19)$$

Where $M_{(\cdot)}$ refers to the respective control derivatives M_α , M_q and M_{δ_e} . The lumped uncertainty bounds on these parameters equate to $w_{M_\alpha} = 0.75$ and $w_{M_q} = w_{M_{\delta_e}} = 0.25$, corresponding to 75% and 25% uncertainty in the parameters respectively. These bounds are not the actual uncertainty bounds of the aerodynamic data of the Flying-V, as these have not been established, yet are in line with typical parametric uncertainty ranges [22, 27, 40].

The bare airframe dynamics and actuator model, as described in equations 16 and 18 are often considered valid within the low-to-medium frequency range up to 10-20 rad/s [25]. Outside of this range, these models are generally considered invalid. This is twofold, as on one end, dynamics at high frequencies are often unknown and uncertain. In addition, designers often prefer to simplify models by deliberately excluding high-order dynamics, even if their presence is known. This is commonly done to reduce development costs and computational costs associated with high-fidelity modeling. This makes the presence of high-frequency dynamic uncertainty unavoidable [22]. Common sources of dynamic uncertainty include unknown structural dynamics, aeroelastic behavior and unmodeled complex aerodynamic effects [25]. Furthermore, the short period dynamics of an aircraft may be substantially altered by the aircraft configuration and flight conditions [24]. To that extent, dynamic uncertainty is assumed to enter the bare airframe in the form of multiplicative input uncertainty, described as follows:

$$\tilde{G}_p(s) = G_{nom}(s)(1 + W_{(\cdot)}(s)\Delta(s)) \quad (20)$$

Where $W_{(\cdot)}(s)$ pertains to an uncertainty weighting filter. For the bare airframe uncertainty, the weighting filter takes on the form of a cascaded first-order and second-order lead-lag filter, similar to that established in [32].

$$W_{ba}(s) = K_{ba} \frac{(s + \tau_{nba})}{(s + r_{ba}\tau_{d_{ba}})} \frac{(s^2 + 2\zeta_{nba}\omega_{nba} + \omega_{nba}^2)}{(s^2 + 2\zeta_{d_{ba}}\omega_{d_{ba}} + \omega_{d_{ba}}^2)} \quad (21)$$

It is assumed that the uncertainty on the airframe input channel exceeds 100% beyond 25 rad/s. The upper break frequency ω_{nba} corresponds to the frequency at which the uncertainty approaches its peak gain, corresponding to

almost 50 rad/s in this case. An additional scaling factor r_{ba} is applied to the first-order lag term to introduce a plateau to the uncertainty. Similarly, the actuator model is subjected to dynamic uncertainty, the weighting filter of the actuator uncertainty takes on the form of first-order lead-lag filter.

$$W_{act}(s) = K_{act} \frac{(s + \tau_{n_{act}})}{(s + \tau_{d_{act}})} \quad (22)$$

Where the weighting filter is defined such that it introduces 100% of uncertainty beyond a frequency of 25 rad/s. An overview of numerical values of the parameters of W_{ba} and W_{act} is provided in table 2. In addition, multiplicative uncertainty is added to the feedback channel of the control input signal u_0 in the form of a time-delay filter. This filter introduces uncertainty in the time of arrival of u_0 and is represented as follows [41]:

$$W_{del}(s) = \frac{\delta_\theta s}{(\delta_\theta/3.465)s + 1} \quad (23)$$

Here, δ_θ corresponds to the time-delay uncertainty. This value is chosen to be equal to one sampling period of the flight control computer, given by $T_s = \frac{1}{80}$ s, a representative value [40].

Table 2 Weighting filter parameters

Parameter values			
$K_{ba} = 79.4$	$\tau_{n_{ba}} = 1.16$ s	$\zeta_{n_{ba}} = 0.5$	$\omega_{n_{ba}} = 1.16$ rad/s
$r_{ba} = 10$	$\tau_{d_{ba}} = 49.8$ s	$\zeta_{d_{ba}} = 0.5$	$\omega_{d_{ba}} = 49.7$ rad/s
$K_{act} = 2$	$\tau_{n_{act}} = 2.176$ s	$\tau_{d_{act}} = 43.52$ s	

B. Design requirements

A typical design objective for a FCS is to guarantee an appropriate level of flying qualities throughout the flight envelope. Within the broader context of the FCS design cycle, these design objectives form the backbone of the iterative process [42]. Choosing the appropriate handling quality criteria hinges on the correct identification of the response type of the aircraft, a topic that has seen some discussion historically [43–45].

For the design task at hand, the Control Anticipation Parameter (CAP) criterion is used as the primary design goal. The CAP criterion is widely used throughout FCS design and is defined as the amount of instantaneous pitch acceleration \dot{q} per unit of steady state normal acceleration $\Delta n_{z,ss}$ following a step input. The following approximation of the CAP has been established [46].

$$CAP = \frac{\dot{q}}{\Delta n_{z,ss}} \approx \frac{\omega_{sp}^2 W}{L_\alpha} \approx \frac{\omega_{sp}^2}{(n/\alpha)} \quad (24)$$

$$\text{Where } L_\alpha \approx \frac{1}{T_{\theta_2}}$$

Where W refers to the weight of the aircraft and (n/α) represents the normal acceleration per radian angle of attack. Moreover, ω_{sp} and L_α follow from the assumption that the pitch-rate response can be captured by a reduced order model, as defined in [44]. Which, assuming that the short-period and phugoid modes are sufficiently disjoint from one another, can be captured as follows [44]:

$$\frac{q(s)}{\delta_s(s)} = \frac{K_q (s + T_{\theta_2}^{-1}) e^{-\tau_e s}}{(s^2 + 2\zeta_{sp}\omega_{sp}s + \omega_{sp}^2)} \quad (25)$$

This transfer function is subsequently used as a command filter for the stick input. The parameters of equation 25 are chosen such that the reference model corresponds to Level 1 handling qualities according to the CAP criterion for Class III aircraft in Category B flight phases [44].

To enforce that the closed loop system tracks the reference model, a weighting filter is introduced on the model following error $e_{MF} = q_{ref} - q$. The weighting filter $W_{MF}(s)$ is shaped such that it penalizes the model following error in the piloted bandwidth to a greater extent and takes on the following lead-lag form.

$$W_{MF}(s) = K_{MF} \frac{s + \tau_{n_{MF}}}{s + \tau_{d_{MF}}} \quad (26)$$

C. Structured mixed μ -synthesis

The closed-loop design problem is captured in the interconnection diagram shown in figure 2. The closed-loop system consists of two distinct feedback loops, the inversion loop and the virtual control loop.

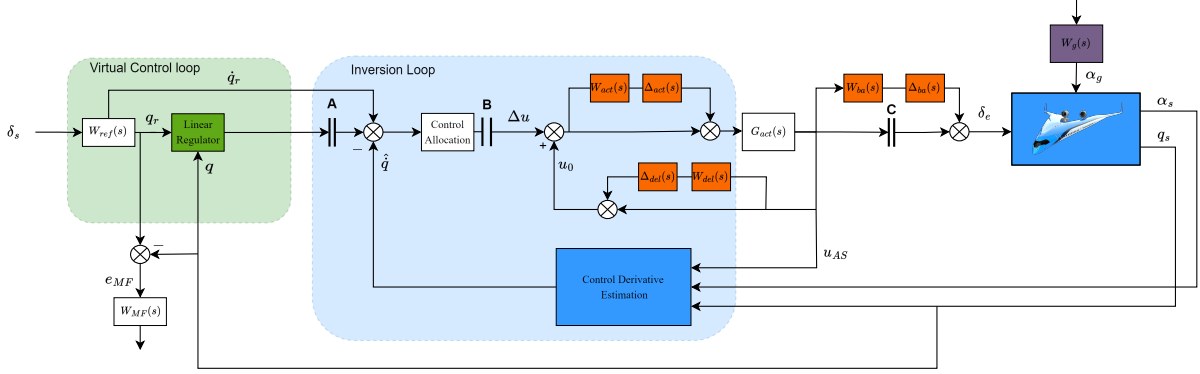


Fig. 2 Control system interconnection structure

As mentioned in section II.B, virtual control law design plays an important role in the design of an inversion-based FCS. Inversion errors, caused by OBM errors and higher-order dynamics can be compensated for by adequate outer-loop design [30]. In the design case at hand, the virtual control loop is based on an explicit model-following (EMF) PI-structure, which is a commonly seen choice for (I)NDI-based flight control [13, 25, 47]. Moreover, a feed-forward term is added to improve model-following performance. This results in the following virtual control law.

$$v_q = \dot{q}_{ref} + \left(K_p + \frac{K_i}{s} \right) [q_{ref} - q] \quad (27)$$

Where q_{ref} follows from the desired pitch rate response established in equation 25. This EMF architecture decouples the piloted response task from the disturbance rejection task. As the pilot response is shaped by the command filter in the stick path and disturbance rejection is handled separately by the feedback gains. The PI-gains of the virtual control law are selected based on the suggestion in [25], which relates these to the desired virtual control loop bandwidth as follows:

$$K_p = K_b, K_i = \frac{K_b^2}{4} \quad (28)$$

Where $K_b = \omega_{bw}$, this particular form of the virtual control law is chosen to provide adequate phase margin at the crossover frequency ω_{bw} . It may be argued that additional integrator gain in the outer-loop is unnecessary given the integration produced by the inversion loop. However, in practice, the ability to achieve perfect inversion - and by extension pure integration - is limited due to model errors, actuator dynamics, time-delays and uncertainty. Therefore, the additional integrator is necessary to account for these effects. A typical value for the desired outer-loop bandwidth for large, heavy transport aircraft lies around $\omega_{bw} = 1 - 3$ rad/s. Although this specification is highly airframe specific [48].

Note that the source of the control input feedback signal u_s is an actuator sensor (AS) for all of the considered architectures in this paper. Various inversion schemes are explored, including a SCF-hybrid IDI setup. In which case the pitch acceleration estimate \hat{q} is defined as follows:

$$\hat{q} = K_c H_c s q_s + (1 - K_c H_c) \dot{q}_m \quad (29)$$

Where K_c pertains to the scaling gain, taking on a value between [0,1] and H_c represents the complementary filter, defined as a second order filter with a tunable natural frequency ω_c in the range [0,100]. Note that the derivative of q_s is obtained through the SCF filter. \dot{q}_m refers to the undisturbed onboard model (OBM) estimate of the pitch acceleration, which is defined as:

$$\dot{q}_m = M_\alpha \alpha + M_q q + M_{\delta_e} \hat{\delta}_e \quad (30)$$

The aerodynamic stability derivatives take on their nominal value in the OBM. The closed-loop interconnection structure depicted in figure 2 captures the structured \mathcal{H}_∞ -based problem formulation. The to be optimized parameters are

the virtual control law gain K_b , the complementary filter bandwidth ω_c and the scaling gain K_c . As mentioned, various inversion schemes are explored to gain insight into the robust stability and performance characteristics of each of these. This includes the standard MB approach, the standard SB approach, a sensor-based complementary filtered multi-loop (HB-CF-ML) approach and two SCF hybrid approaches. The two SCF approaches differ in that, in the first approach, only the inner-loop is tuned, while the outer-loop gains are pre-determined, using the value obtained from the MB approach via optimization. This method is referred to as the hybrid-SCF-inner-loop (HB-SCF-IL) approach. In the second approach, both the inner-loop and outer-loop parameters are tunable, which is why it is referred to as the hybrid-SCF-multi-loop (HB-SCF-ML) approach. Table 3 offers an overview of these architectures and summarizes their key characteristics.

Table 3 Overview of the tunable parameters for the different inversion methods (All entries denoted with an asterisk are fixed a-priori)

Inversion Method	K_b [-]	K_c [-]	ω_c [rad/s]
MB	$[0, \infty]$	–	–
SB	$[0, \infty]$	1*	5000*
HB-CF-ML	$[0, \infty]$	1*	$[0, 100]$
HB-SCF-IL	$K_b^{(MB)*}$	$[0, 1]$	$[0, 100]$
HB-SCF-ML	$[0, \infty]$	$[0, 1]$	$[0, 100]$

The problem is formulated as a *mixed parametric control problem*, which can be cast as the following semi-infinite minmax optimization problem within the \mathcal{H}_∞ -framework [49].

$$\min_{\kappa \in \mathbb{R}^n} \max_{\Delta \in \Delta} \|T_{w \rightarrow z}(\Delta, \kappa)\|_\infty \quad (31)$$

Where $T_{w \rightarrow z}$ is defined as the closed-loop system that maps the exogenous inputs w to the exogenous outputs z . κ represents a structured control law, while $\Delta = \text{diag}(\Delta_p, \Delta_d)$ denotes the set of mixed uncertainty scenarios. In this paper, the optimization problem is solved using mixed μ -synthesis in the form of the DGK-iteration algorithm embedded in the MATLAB Robust Control Toolbox™ [50]. For a detailed explanation of the theoretical foundations behind these tools, the reader is referred to [22, 28, 50, 51].

IV. Results

This section presents the results of the synthesized μ -optimal controllers. A summary of the optimization outcomes is given in section IV.A. This is followed by a broken- μ analysis in section IV.B and a closed-loop analysis in section IV.C. Finally, section IV.D offers a discussion of the results.

A. Optimization results

The parameters returned by the DGK-iteration process are summarized in table 4. To mitigate the risk of encountering local minima, 50 independent runs were performed, starting at randomly selected parameter values within the prescribed bounds. Again, the entries denoted with an asterisk in table 4 correspond to values that were fixed prior to the optimization.

Table 4 Returned optimization parameters and resulting robust stability & robust performance measures ($\bar{\mu}_{RS}$ and $\bar{\mu}_{RP}$)

Inversion method	$\bar{\mu}_{RS}$ [-]	$\bar{\mu}_{RP}$ [-]	K_b [-]	K_c [-]	ω_c [rad/s]
MB	0.95	0.98	8.69	–	–
SB	0.98	0.98	5.71	1*	5000*
HB-CF	0.77	0.84	7.24	1*	3.07
HB-SCF-IL	0.96	0.97	8.69*	0.19	0.48
HB-SCF-ML	0.78	0.84	7.33	1.00	2.28

A few things stand out from these results. First off, it can be seen that the best RP is achieved by the HB-CF and HB-SCF-ML approaches. These are rounded off to $\bar{\mu}_{RP} = 0.84$, although the HB-SCF-ML approach resulted in a marginally lower value, only captured in the third significant number. It can also be seen that the value of K_c in the HB-SCF-ML approach converged to a value of $K_c = 1$, equivalent to the HB-CF approach. Both these approaches seem to prefer to limit the value of ω_c , as to keep the bandwidth of the incremental inversion loop low. Another interesting observation can be made when comparing the MB approach with the HB-SCF-IL approach. The latter takes on the value of $K_b = 8.69$ as returned by the optimization for the MB approach. It can be observed that the HB-SCF-IL approach limits the amount of additional sensor-based incremental control input, as the value of K_c and ω_c are very low. This does very little for the robust stability and performance of the HB-SCF-IL approach when compared to the standard MB approach.

B. Broken-loop analysis

Both the nominal and worst-case broken-loop shapes at the virtual control input L_v , and at the airframe input L_i are depicted in figures 3 and 4. Examining the loop-shapes at the plant input L_i , it can be observed that most of the approaches result in loop-shapes that closely resemble one another in the crossover region. The SB approach being the exception, displaying an overall elevated loop-shape, as well as a noticeably higher crossover frequency. In the lower frequency range, it can be seen that the SB, the HB-CF and the HB-SCF-ML approaches have a steeper slope when compared to the MB and the HB-SCF-IL approaches. When examining the high frequency range, it can be seen that the MB, the CF-HB and the SCF-HB approaches all provide similar roll-off, whereas the SB approach does not. These results are a manifestation of the fundamental trade-off in feedback design [10, 24]. When examining the loop-shape at the virtual control input L_v , it can be seen that these are very similar. The crossover frequency there being determined by the optimized value of K_b . Judging by the shape of L_v , one could imagine that each of the approaches have very similar robustness properties. This is however not the case, as clearly reflected in the shapes of L_i . As such, an assessment of the robustness of inversion-based controllers based on the loop shape at the outer-loop (the virtual control loop) is not sufficient, confirming findings in [32]. This is further confirmed by a closed-loop analysis and a μ -analysis, as will be presented in the following sections.

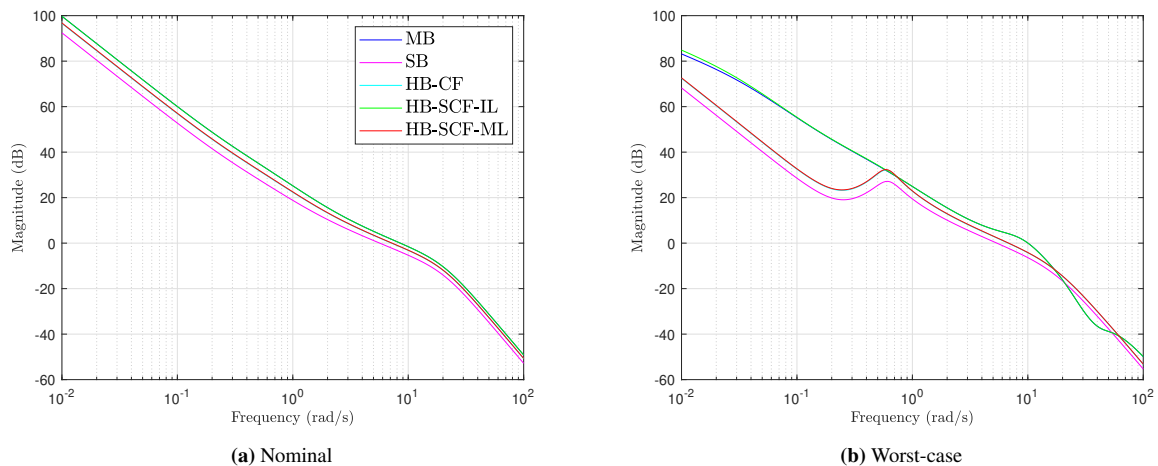


Fig. 3 Loop shape at virtual control L_v

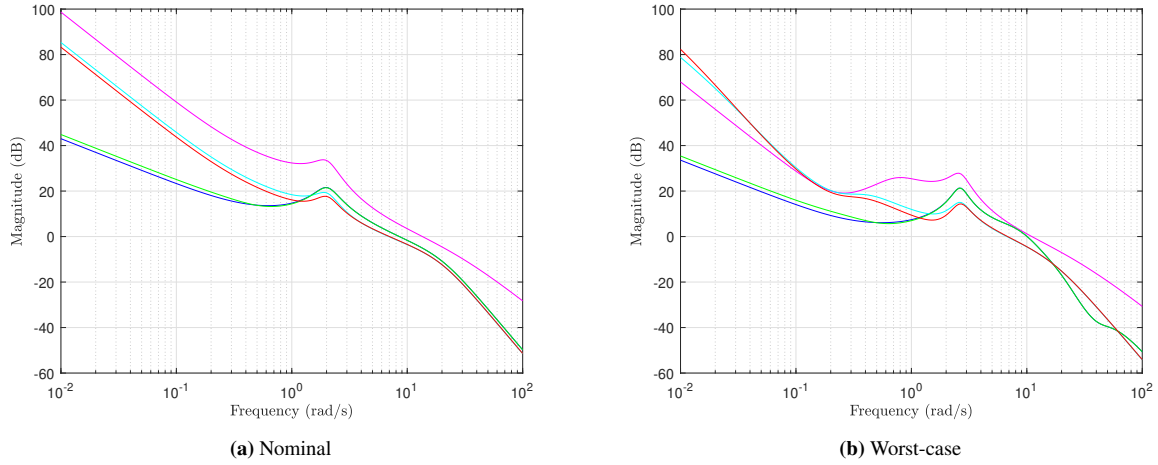


Fig. 4 Loop shape at plant input L_i

C. Closed-loop analysis

1. Closed-loop transfer function analysis

A deeper insight into the robust stability & performance characteristics of the resulting closed-loop systems is provided by studying the closed-loop transfer functions. To that extent, the singular values of both the nominal and worst-case perturbed closed-loop transfer functions are shown in figure 5. Looking at these figures, it can be seen that the model-following error e_{MF} is very similar for all of the presented approach. It can be observed that the standard MB approach, despite its model dependency, performs very well. This is expected to be a result of the sufficiently high PI-gains returned by the synthesis algorithm. Moreover, it can be seen that the standard SB approach does not actually result in improved model-following performance. In fact, the model-following performance is decreased as a result of inversion distortion, as shown in equation 14. The additional integral action introduced by the input feedback loop reduces the need for outer-loop integration. This is reflected in the lower value of K_b . However, the outer loop control is still required to compensate for the inversion distortion, in line with the findings in [32]. When examining the model-following error of the various HB architectures, it can be seen that these result in smaller nominal inversion distortions when compared to the SB approach, as shown in [32]. It can also be seen that as the HB-SCF-IL converged to a solution approximating the MB approach, hence it does not offer any significant robust performance benefit. Examining the input complementary sensitivity function T_i provides an indication of the robust stability with respect to input disturbances. Which, as depicted, is bounded by the bare airframe input uncertainty weighting filter W_{ba}^{-1} . Examining the worst case T_i , it can be seen that all of the designs stay below this bound. As also reflected in L_i , the lack of high-frequency roll off in the SB approach demonstrates that this can result in stability issues in the high-frequency region, as $T_i^{(SB)}$ can be seen to come very close to the upper bound. Similarly, it can be seen that the MB and the HB-SCF-IL approaches display a significant peak at 10 rad/s, although achieving adequate high frequency roll-off. The HB-CF and HB-SCF-ML approaches achieve the best robust stability, reflected in table 4 as well. According to Pollack [32], the combination of frequency-based weighting achieved by H_c and phase margin reduction mitigation through K_c effectively results in lead-lag action. This essentially adds a degree-of-freedom which allows these designs to maneuver around the robust stability restrictions which are encountered by the standard MB and SB approach.

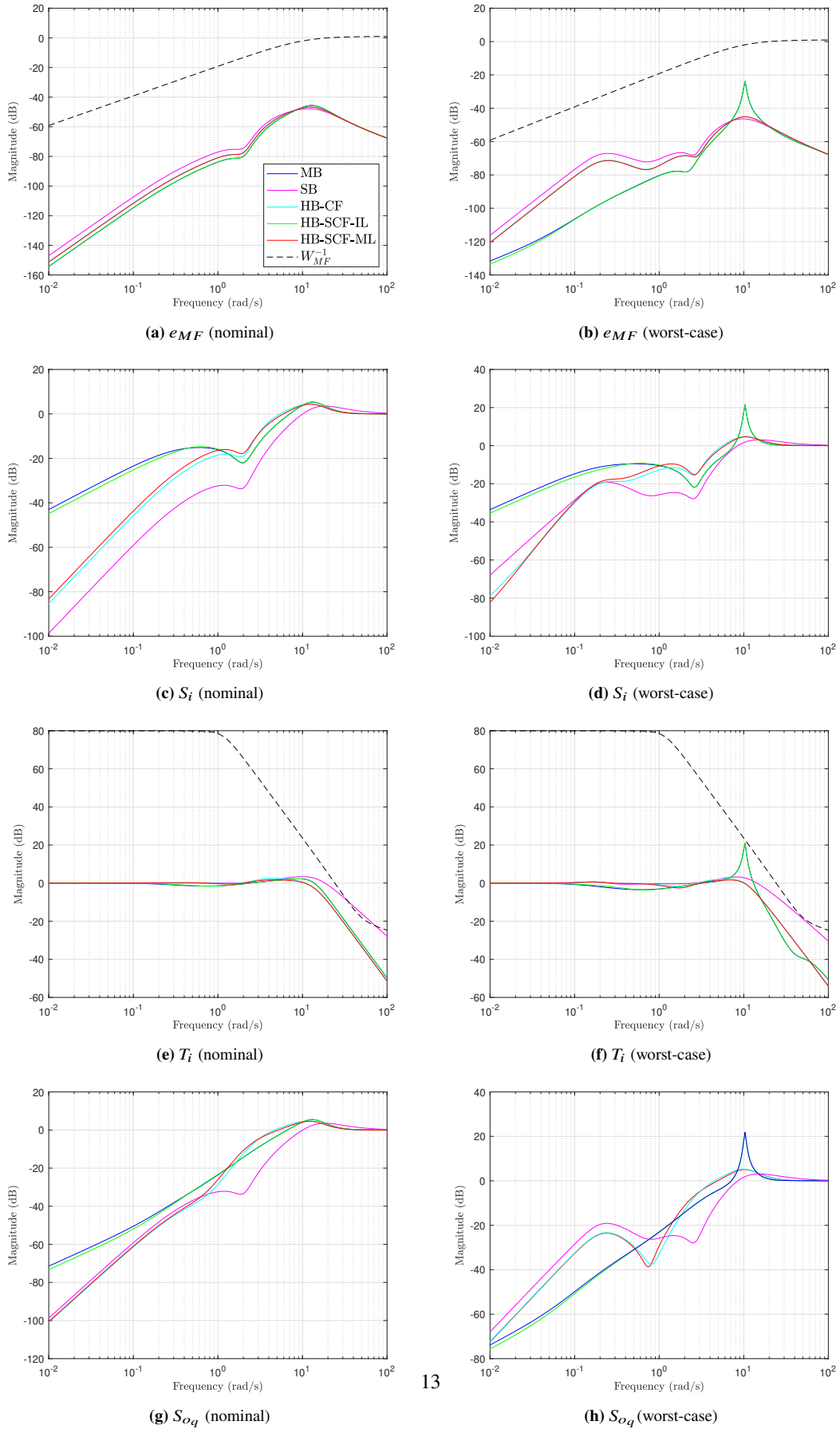


Fig. 5 Closed-loop transfer function

2. μ -analysis

Figure 6 displays the upper bounds of the robust stability measure μ_{RS} and the robust performance measure μ_{RP} associated with the different architectures. Again, it can be seen that μ_{RS} of the MB approach and the SB approach take on a larger value than those of the HB-CF and HB-ML approaches. Moreover, it can also be seen that these peak at different frequencies, confirming the observations made on the basis of T_i . Again, it can be observed that the HB-CF and HB-ML approaches achieve the greatest robust stability. It can also be seen that the robust stability profile of these two approaches closely resembles the profile of the standard MB approach, albeit scaled down. This demonstrates the similarity between the two [32]. Similar observations can be made based on μ_{RP} .

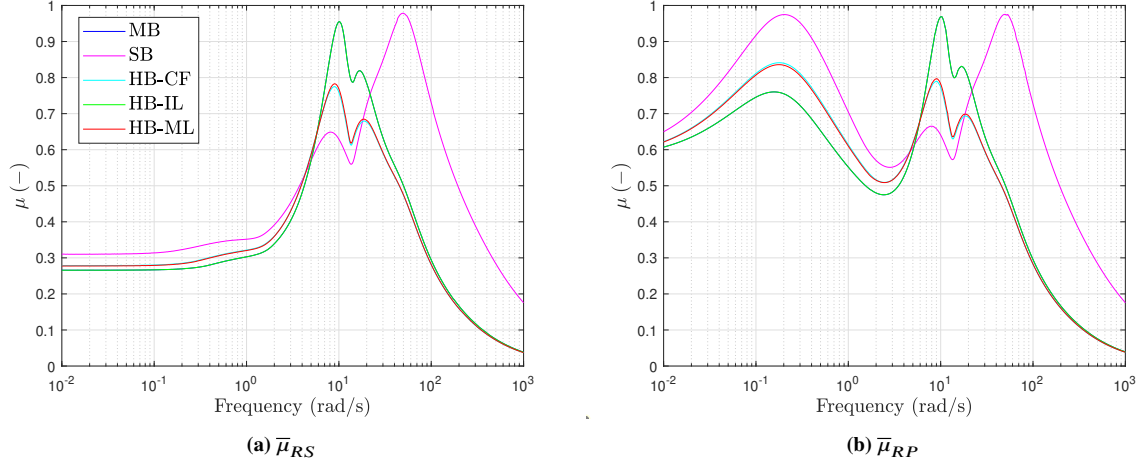


Fig. 6 Upper bounds on $\bar{\mu}_{RS}$ and $\bar{\mu}_{RP}$ of the various closed-loop systems

A further breakdown of $\bar{\mu}_{RP}$ is provided in figure 7, this sheds a light on the relative contribution of each of the uncertainties. Although the contributions of each of the uncertainties are similar for all of the different inversion strategies, subtle differences can be found. One that jumps out is the contribution of Δ_{act} . In the standard MB approach, thus also in the HB-SCF-IL approach, it can be seen that its peak is relatively large compared to the other architectures. This can be explained due to the lack of feedback action in the inner-loop, which provides additional robustness to uncertainty in the actuator.

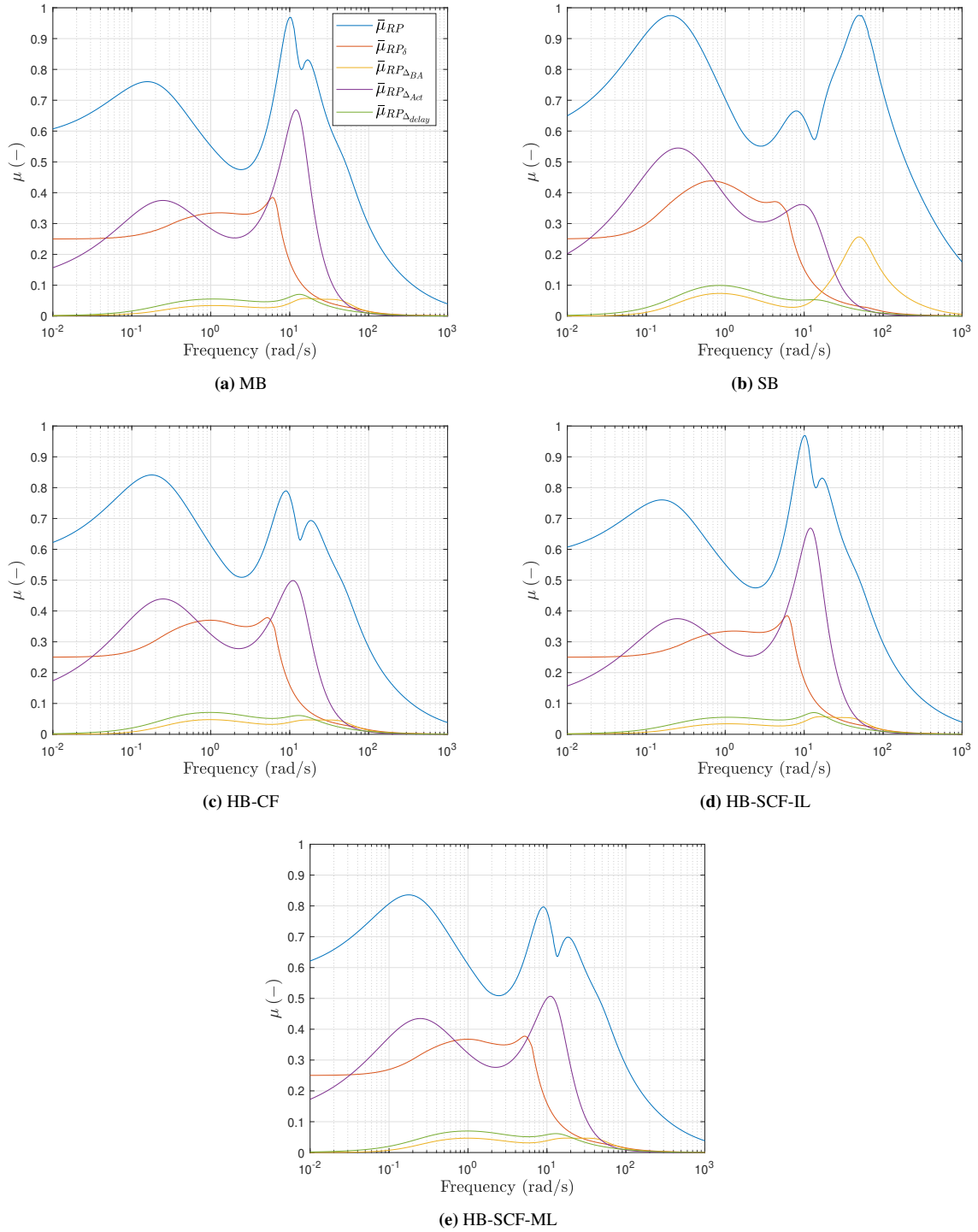


Fig. 7 Breakdown of $\bar{\mu}_{RP}$

3. Linear simulations

Linear simulations of the resulting closed-loop systems were performed. In addition, Monte-Carlo simulations were performed with $n = 500$ random samples of the perturbed plant within the prescribed uncertainty bounds. For the sake of brevity, only the responses of the standard MB, the HB-CF and the HB-SCF-ML architecture are shown. As the hybrid approaches closely resemble the model-based approach, the result of the HB architectures are best understood in comparison to the results of the MB approach. To that extent, only the step responses of the aforementioned inversion architectures are shown in figure 8. Specifically, the response to a 1° step input on the stick is depicted for the pitch rate q , the angle of attack α and the elevator deflection rate $\dot{\delta}_e$.

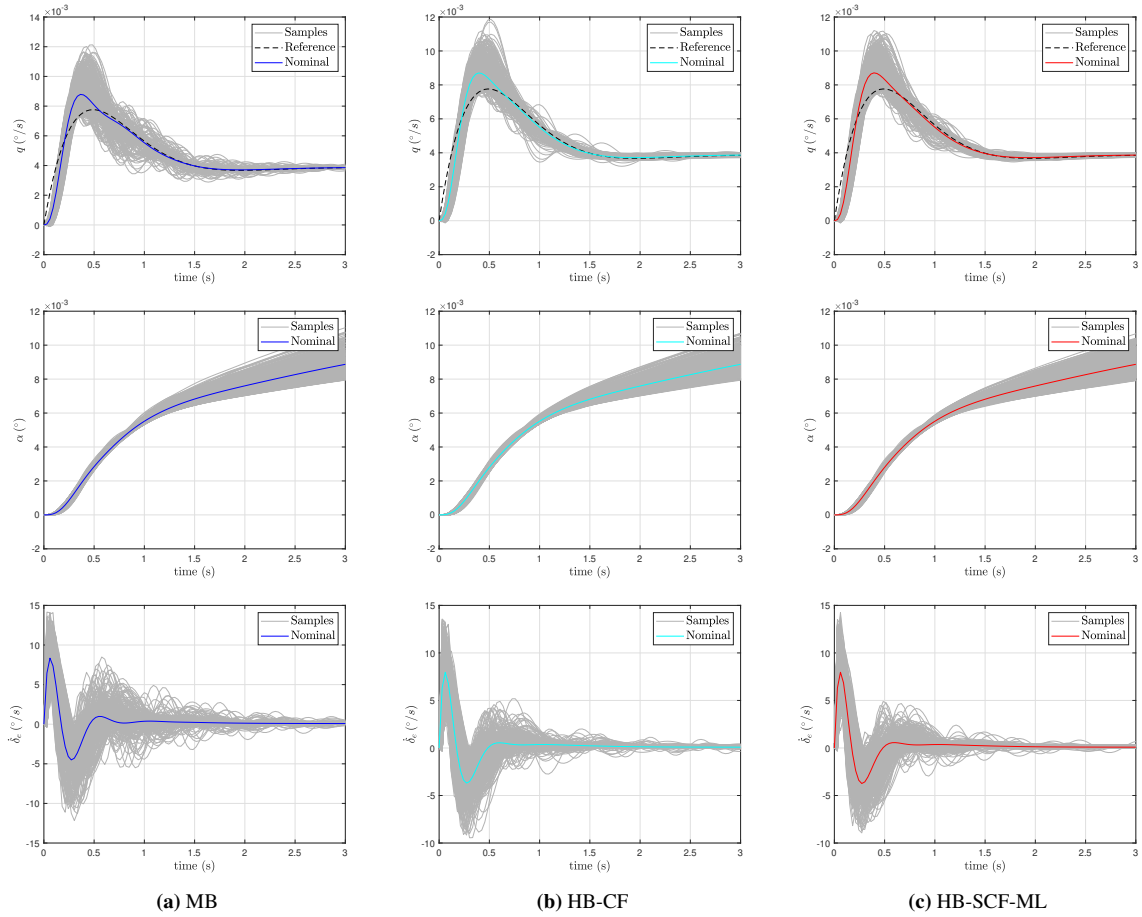


Fig. 8 Step responses to 1° stick input

Note how the pitch rate responses of the various architectures display very similar tracking performance with respect to the reference signal, in accordance with the shape of e_{MF} seen in figure 5. It can be seen that for both HB approaches, the perturbed samples converge to the steady state value quicker. More so, the samples of the HB-SCF-ML approach seem to converge quicker than those of the HB-CF approach. This is expected to be a result of the additional integral action added by the incremental loop of the HB approaches.

D. Discussion

The results presented in this paper shed a light on some fundamental robustness properties of the various inversion-based controller architectures. Although it must be stated that the outcomes of this study are representative of the specific numerical example used in this research. This is particularly important to keep in mind when judging the robust stability & performance characteristics mentioned previously, as these are a result of the combination of the described model, the prescribed uncertainty set and the defined robust stability and performance bounds. Nonetheless, the observations that were made regarding the implications of inversion-based designs can be extrapolated and provide insight into the applicability of various inversion-based controllers for the Flying-V. It must also be noted that both the synthesis and the analysis are based on LTI descriptions of the plant and the uncertainties. In reality, the airframe, actuators and uncertainties might behave in a nonlinear and time-varying fashion. In [32], the scope of the class of uncertainty was extended to include LTV uncertainty. It was demonstrated that similar trends to those observed in this paper hold in the LTV case, with infinitely fast variations that is, hence extending the depth of the insights provided in this paper [32]. To extend the robustness analysis to a class of LTV uncertainties, Pollack made use of the Integral Quadratic Constraints (IQCs) framework described in [52–54]. It must also be stated that the case study in this paper is centered around a highly simplified model of the Flying-V, not taking into account the full three-axis coupled dynamics, nor considering any form of control allocation. The former having significant implications for the use of \mathcal{H}_∞ -synthesis tools in the first place, as this becomes increasingly difficult for larger systems, particularly in the presence of mixed uncertainty and fixed controller structures. Structured \mathcal{H}_∞ -synthesis is non-convex by nature [49, 55], as opposed to unstructured \mathcal{H}_∞ -synthesis, for which linear matrix inequalities (LMIs) can be used to find globally optimal solutions through semi-definite programming [56, 57]. Imposing a controller structure turns the LMIs into bilinear matrix inequalities (BMIs), which are much more costly to solve computationally. Hence, imposing a structured controller, such as INDI for instance, inherently requires the use of non-convex optimization methods [49, 55]. Moreover, if the plant and the uncertainties contain nonlinearity in the form of a LPV plant formulation and LTV uncertainties, it would be desirable to account for this in the synthesis. To that extent, the IQC-based synthesis approaches presented in [52, 53] could be used. Although practical IQC-based synthesis algorithms for structured controllers have been proposed [54, 58], these are not widely used yet due to their computational shortcomings. Pollack proposes a IQC-based synthesis algorithm that effectively combines the DK-iteration approach of classical μ -synthesis with the multi-model, multi-objective \mathcal{H}_∞ -synthesis approach of *MATLABTM* *systune* [50]. This approach allows for the incorporation of robust disk stability margin constraints. This opens up the opportunity for the use of μ -tools for control law clearance, as described in [59].

A promising alternative to classical μ -analysis has emerged in the form of the so called probabilistic μ analysis, which offers a middle-of-the-road solution between classical μ -analysis - relevant for detecting extreme events - on the one hand and Monte Carlo simulations - useful for quantifying the probability of sufficiently frequent events - on the other. Probabilistic μ has been around for two decades, although the computational tools have significantly improved recently, making it a viable practical tool [60]. Utilizing these tools may result in less conservativeness compared to classical μ -analysis.

Aside from the discussion about the use of various μ -based tools for the synthesis of robust control design, its utility could be questioned in the first place. Although μ -analysis provides great insight into the specific robust stability and performance characteristics of a given closed-loop system, the use of μ -synthesis tools can be rather tedious. In the authors experience, the synthesis outcomes are highly dependent on the combination of uncertainty weighting filters, plant description and synthesis settings. From a practical perspective, this is perhaps not very desirable. Ultimately, the goal of the μ -synthesis machinery is to establish a design with adequate robust stability and performance. This is ultimately reflected in the shape of L_i . As such, simpler tools, such as \mathcal{H}_∞ -loop shaping, might be capable of yielding very similar results in terms of robustness, without the need for explicit uncertainty descriptions. This is however a design trade-off, as on the other hand μ -based tools provide machinery that is capable of establishing optimal or slightly suboptimal designs. In the context of inversion-based control design, these tools have their place. Specifically, these tools are best capable of utilizing the multi-loop architecture to achieve the greatest robust stability and performance.

V. Conclusions

In this article a multi-loop, structured, mixed μ -synthesis approach was applied to the design of a dynamic inversion-based controller for a short-period approximation of the Flying-V. Various inversion architectures and synthesis approaches were considered, including the standard MB and SB architectures and various hybrid schemes. It was observed that the model-based approach can be tuned to relatively good robust performance levels with adequate outer-loop de-

sign. Moreover, it was shown that the hybrid approach is capable of adding slight robust performance improvements with respect to the model-based approach, in accordance with the findings in [32]. The findings shed a light on the fundamental trade-off between robust performance and robust stability encountered in feedback control, which is reflected in the loop shape at the plant input L_i . A greater crossover frequency of L_i , often a result of incremental input from sensor-based inversion, typically results in greater (low-frequency) robust performance. This comes at the cost of (high-frequency) robust stability. Alternatively, robust stability and performance can be improved by increasing outer-loop gains, which highlights the multi-loop robustness properties of inversion-based designs. Therefore, in order to fully leverage the robustness functionality of inversion-based control designs, a multi-loop approach must be considered. This approach effectively makes use of all the degrees-of-freedom in a multi-loop control system. Moreover, it highlights the fact that a robustness analysis of inversion-based control systems must always be viewed in a multi-loop context. These findings emphasize that future inversion-based control design for the Flying-V must take these fundamental properties into account. Besides the awareness of the robustness implications of the various inversion strategies, the choice of inversion strategy is of course dependent on the availability of adequate models and/or sensor measurements. Therefore, the choice for either MB, SB or HB design is not only guided by robustness insights, but also by design limitations. If a specific design choice is made, \mathcal{H}_∞ -synthesis tools offer a means to achieve more robust designs. Either by outer-loop tuning in the standard MB approach, or by multi-loop tuning in the filtered SB and HB approaches. Keeping in mind the design uncertainty surrounding the Flying-V, in terms of modeling uncertainty, design choice uncertainty (i.e. availability of certain sensors) and singular perturbations, the use of these tools is advised. As these can result in more robust controller designs, irrespective of the underlying control law architecture. Therefore, it is recommended that these tools are further explored for robust control design for the Flying-V. If μ -synthesis is to be used specifically, it is recommended that the uncertainty descriptions be further substantiated. Moreover, it is highly recommended that the IQC-based synthesis approach described in [32] is explored, as it is capable of dealing with multi-objective \mathcal{H}_∞ problems, which allows for the incorporation of robust disk margin constraints. The latter being of great importance for the purpose of flight control law clearance.

References

- [1] Afonso, F., Sohst, M., Diogo, C. M., Rodrigues, S. S., Ferreira, A., Ribeiro, I., Marques, R., Rego, F. F., Sohoul, A., Portugal-Pereira, J., Policarpo, H., Soares, B., Ferreira, B., Fernandes, E. C., Lau, F., and Suleman, A., "Strategies towards a more sustainable aviation: A systematic review," *Progress in Aerospace Sciences*, Vol. 137, 2023, p. 100878. <https://doi.org/https://doi.org/10.1016/j.paerosci.2022.100878>.
- [2] Benad, J., "The Flying V - A new Aircraft Configuration for Commercial Passenger Transport," *Deutscher Luft- und Raumfahrtkongress 2015, Rostock ; Conference date: 22-09-2015 Through 24-09-2015*, 2015, pp. 1–8. <https://doi.org/10.25967/370094>.
- [3] Faggiano, F., Vos, R., Baan, M., and van Dijk, R., "Aerodynamic Design of a Flying V Aircraft," *17th AIAA Aviation Technology, Integration, and Operations Conference*, American Institute of Aeronautics and Astronautics Inc. (AIAA), United States, 2017. <https://doi.org/10.2514/6.2017-3589>, 17th AIAA Aviation Technology, Integration, and Operations Conference ; Conference date: 05-06-2017 Through 09-06-2017.
- [4] R., V., "Analysis of the flight characteristics of a highly swept cranked flying wing by means of an experimental test," Master's thesis, Delft University of Technology, 2019.
- [5] Benad, J., "Development of a numerical flow channel with the Lattice Boltzmann method and application to highly swept wings at high angles of attack," Ph.D. thesis, TU Berlin, 2022.
- [6] van Overeem, S., Wang, X., and Kampen, E.-J. V., *Handling Quality Improvements for the Flying-V Aircraft using Incremental Nonlinear Dynamic Inversion*, AIAA, 2023. <https://doi.org/10.2514/6.2023-0105>.
- [7] Joosten, S., "Piloted Assessment of the Lateral-Directional Handling Qualities of the Flying-V," Master's thesis, Delft University of Technology, 2022.
- [8] van Overeem, S., "Modelling, Control, and Handling Quality Analysis of the Flying-V," Master's thesis, Delft University of Technology, 2022.
- [9] Stougie, J., Pollack, T., and Kampen, E.-J. V., *Incremental Nonlinear Dynamic Inversion control with Flight Envelope Protection for the Flying-V*, AIAA, 2024. <https://doi.org/10.2514/6.2024-2565>.
- [10] Horowitz, I. M., *Synthesis of Feedback Systems*, Academic Press, 1963.

- [11] Simplício, P., Pavel, M., van Kampen, E., and Chu, Q., “An acceleration measurements-based approach for helicopter nonlinear flight control using Incremental Nonlinear Dynamic Inversion,” *Control Engineering Practice*, Vol. 21, No. 8, 2013, pp. 1065–1077. <https://doi.org/https://doi.org/10.1016/j.conengprac.2013.03.009>.
- [12] Smeur, E. J. J., Chu, Q., and de Croon, G. C. H. E., “Adaptive Incremental Nonlinear Dynamic Inversion for Attitude Control of Micro Air Vehicles,” *Journal of Guidance, Control, and Dynamics*, Vol. 39, No. 3, 2016, pp. 450–461. <https://doi.org/10.2514/1.G001490>.
- [13] Grondman, F., Looye, G. H., Kuchar, R. O., Chu, Q. P., and van Kampen, E. J., “Design and flight testing of incremental nonlinear dynamic inversion based control laws for a passenger aircraft,” *AIAA Guidance, Navigation, and Control*, American Institute of Aeronautics and Astronautics Inc. (AIAA), United States, 2018. <https://doi.org/10.2514/6.2018-0385>, aIAA Guidance, Navigation, and Control Conference, 2018 ; Conference date: 08-01-2018 Through 12-01-2018.
- [14] Keijzer, T., Looye, G., Chu, Q. P., and Kampen, E.-J. V., *Design and Flight Testing of Incremental Backstepping based Control Laws with Angular Accelerometer Feedback*, AIAA, 2019. <https://doi.org/10.2514/6.2019-0129>.
- [15] Ekeren, W., Looye, G., Kuchar, R., Chu, Q., and Van Kampen, E.-J., “Design, Implementation and Flight-Tests of Incremental Nonlinear Flight Control Methods,” *AIAA 2018-0384*, 2018. <https://doi.org/10.2514/6.2018-0384>.
- [16] Wang, X., van Kampen, E.-J., Chu, Q., and Lu, P., “Stability Analysis for Incremental Nonlinear Dynamic Inversion Control,” *Journal of Guidance, Control, and Dynamics*, Vol. 42, No. 5, 2019, p. 1116–1129. <https://doi.org/10.2514/1.g003791>.
- [17] van ’t Veld, R., Kampen, E.-J. V., and Chu, Q. P., *Stability and Robustness Analysis and Improvements for Incremental Non-linear Dynamic Inversion Control*, AIAA, 2018. <https://doi.org/10.2514/6.2018-1127>.
- [18] Linden, F., Looye, G., and Pollack, T., “Aircraft control using actuator current,” *International Conference on Recent Advances in Aerospace Actuation Systems and Components*, 2018.
- [19] Huang, Y., Zhang, Y., Pool, D. M., Stroosma, O., and Chu, Q., “Time-Delay Margin and Robustness of Incremental Nonlinear Dynamic Inversion Control,” *Journal of Guidance, Control, and Dynamics*, Vol. 45, No. 2, 2022, pp. 394–404. <https://doi.org/10.2514/1.G006024>.
- [20] Cordeiro, R. A., Marton, A. S., Azinheira, J. R., Carvalho, J. R. H., and Moutinho, A., “Increased Robustness to Delay in Incremental Controllers Using Input Scaling Gain,” *IEEE Transactions on Aerospace and Electronic Systems*, Vol. 58, No. 2, 2022, pp. 1199–1210. <https://doi.org/10.1109/TAES.2021.3123215>.
- [21] Chang, J., Breuker, R. D., and Wang, X., *Discrete-time Design and Stability Analysis for Nonlinear Incremental Fault-tolerant Flight Control*, AIAA, 2022. <https://doi.org/10.2514/6.2022-2034>.
- [22] Skogestad, S., and Postlethwaite, I., *Multivariable Feedback Control: Analysis and Design*, John Wiley and Sons, 2005, Vol. 2.
- [23] Stevens, B., Lewis, F., and Johnson, E., *Aircraft Control and Simulation: Dynamics, Controls Design, and Autonomous Systems*, Wiley, 2015, Chap. 2 and 6.
- [24] Stein, G., “Respect the unstable,” *IEEE Control Systems Magazine*, Vol. 23, No. 4, 2003, pp. 12–25. <https://doi.org/10.1109/MCS.2003.1213600>.
- [25] Unknown, “Application of Multivariable Control Theory to Aircraft Control Laws - Multivariable Control Design Guidelines,” Tech. rep., Honeywell Technology Center, Lockheed Martin Skunk Works. Lockheed Martin Tactical Aircraft Systems, 1996.
- [26] Khalil, H., *Nonlinear Systems*, Pearson Education, Prentice Hall, 2002. URL https://books.google.nl/books?id=t_d1QgAACAAJ.
- [27] Pollack, T., and van Kampen, E.-J., “Robust Stability and Performance Analysis of Incremental Dynamic-Inversion-Based Flight Control Laws,” *Journal of Guidance, Control, and Dynamics*, Vol. 46, No. 9, 2023, pp. 1785–1798. <https://doi.org/10.2514/1.G006576>.
- [28] Zhou, K., Doyle, J., and Glover, K., *Robust and Optimal Control*, Feher/Prentice Hall Digital and, Prentice Hall, 1996. URL <https://books.google.nl/books?id=RPSOQgAACAAJ>.
- [29] Pineau, S., Theodoulis, S., Zasadzinski, M., and Boutayeb, M., “Terminal Phase Nonlinear Attitude Autopilot Design For Dual-Spin Guided Projectiles,” *Proceedings of the 2022 CEAS EuroGNC conference*, Berlin, Germany, 2022. CEAS-GNC-2022-073.

- [30] Gong, A., Hess, R. K., and Tischler, M., “Deterministic Reconfiguration of Flight Control Systems for Multirotor UAV Package Delivery,” *Proceedings of the Vertical Flight Society 77th Annual Forum*, 2021. URL <https://api.semanticscholar.org/CorpusID:250042525>.
- [31] Kim, C.-S., Ji, C.-H., Koh, G.-O., and Kim, B. S., “Stability Margin and Structural Coupling Analysis of a Hybrid INDI Control for the Fighter Aircraft,” *International Journal of Aeronautical and Space Sciences*, Vol. 22, No. 5, 2021, p. 1154–1169. <https://doi.org/10.1007/s42405-021-00394-8>.
- [32] Pollack, T., “Advances in Dynamic Inversion-based Flight Control Law Design: Multivariable Analysis and Synthesis of Robust and Multi-Objective Design Solutions,” Ph.D. thesis, Delft University of Technology, 2024. <https://doi.org/10.4233/uuid:28617ba0-461d-48ef-8437-de2aa41034ea>.
- [33] Slotine, J., and Li, W., *Applied Nonlinear Control*, Prentice-Hall International Editions, Prentice-Hall, 1991. URL <https://books.google.nl/books?id=HddxQgAACAAJ>.
- [34] Isidori, A., “The zero dynamics of a nonlinear system: From the origin to the latest progresses of a long successful story,” *European Journal of Control*, Vol. 19, No. 5, 2013, pp. 369–378. <https://doi.org/https://doi.org/10.1016/j.ejcon.2013.05.014>, the Path of Control.
- [35] Kumtepe, Y., Pollack, T., and Kampen, E.-J. V., *Flight Control Law Design using Hybrid Incremental Nonlinear Dynamic Inversion*, AIAA, 2022. <https://doi.org/10.2514/6.2022-1597>.
- [36] Cappuyns, T., “Handling Qualities of a Flying V Configuration,” Master’s thesis, Delft University of Technology, 2019.
- [37] Matamoros, I., and de Visser, C. C., *Incremental Nonlinear Control Allocation for a Tailless Aircraft with Innovative Control Effectors*, AIAA, 2018. <https://doi.org/10.2514/6.2018-1116>.
- [38] M., H. R., “Development of the Transport Class Model (TCM) Aircraft Simulation From a Sub-Scale Generic Transport Model (GTM) Simulation,” Tech. rep., NASA - Langley Research Center, 2011.
- [39] R., B., *Flugregelung. 2. Aufl.*, Springer Berlin, 2001.
- [40] Jean-François Magni, J. T., Samir Bennani, *Robust Flight Control - A design Challenge*, Springer Berlin Heidelberg, Berlin, Heidelberg, 1997. <https://doi.org/10.1007/bfb0113842>.
- [41] ZI-QIN WANG, P. L., and SKOGESTAD, S., “Representation of uncertain time delays in the H^∞ framework,” *International Journal of Control*, Vol. 59, No. 3, 1994, pp. 627–638. <https://doi.org/10.1080/00207179408923097>.
- [42] Moorhouse, D., Boer, W., Fielding, C., Hahn, K.-U., Hofinger, G., Magni, J.-F., and Verde, L., *Flight Control Design - Best Practices*, Canada Communication Group Inc, 2000.
- [43] MITCHELL, D. G., and HOH, R. H., “PROPOSED INCORPORATION OF MISSION-ORIENTED FLYING QUALITIES INTO MIL-STD-1797A,” Tech. rep., WRIGHT LABORATORY, 1994.
- [44] unknown, “FLYING QUALITIES OF PILOTED AIRPLANES,” Tech. rep., Department of Defense, 2004.
- [45] unknown, “FLIGHT CONTROL SYSTEMS - DESIGN, INSTALLATION AND TEST OF PILOTED AIRCRAFT, GENERAL SPECIFICATION FOR,” Tech. rep., Department of Defense, 2008.
- [46] William Bihle, J., “A handling qualities theory for precise flight path control,” Tech. rep., WRIGHT LABORATORY, 1966.
- [47] ENNS, D., BUGAJSKI, D., HENDRICK, R., and STEIN, G., “Dynamic inversion: an evolving methodology for flight control design,” *International Journal of Control*, Vol. 59, No. 1, 1994, p. 71–91. <https://doi.org/10.1080/00207179408923070>.
- [48] Tischler, M., Berger, T., Ivler, C., Mansur, H., Cheung, K., and Soong, J., *Practical methods for aircraft and rotorcraft flight control design: an optimization-based approach*, American Institute of Aeronautics and Astronautics, 2017.
- [49] Apkarian, P., and Noll, D., “The H-infinity Control Problem is Solved,” *AerospaceLab Journal*, 2017, pp. 1–11.
- [50] Balas, G., Chiang, R., Packard, A., and Safonov, M., “Robust Control Toolbox - User’s Guide,” , 2005. URL <https://www.mathworks.com>.
- [51] Young, P., “Controller design with mixed uncertainties,” *Proceedings of 1994 American Control Conference - ACC '94*, Vol. 2, 1994, pp. 2333–2337 vol.2. <https://doi.org/10.1109/ACC.1994.752496>.

- [52] Veenman, J., and Scherer, C. W., "IQC-Synthesis with General Dynamic Multipliers," *IFAC Proceedings Volumes*, Vol. 44, No. 1, 2011, pp. 4600–4605. <https://doi.org/https://doi.org/10.3182/20110828-6-IT-1002.00776>, 18th IFAC World Congress.
- [53] Veenman, J., and Scherer, C. W., "A synthesis framework for robust gain-scheduling controllers," *Automatica*, Vol. 50, No. 11, 2014, pp. 2799–2812. <https://doi.org/https://doi.org/10.1016/j.automata.2014.10.002>.
- [54] Veenman, J., Scherer, C. W., and Köroğlu, H., "Robust stability and performance analysis based on integral quadratic constraints," *European Journal of Control*, Vol. 31, 2016, pp. 1–32. <https://doi.org/https://doi.org/10.1016/j.ejcon.2016.04.004>.
- [55] Apkarian, P., and Noll, D., "Nonsmooth H^∞ Synthesis," *IEEE Transactions on Automatic Control*, Vol. 51, No. 1, 2006, pp. 71–86. <https://doi.org/10.1109/TAC.2005.860290>.
- [56] Gahinet, P., and Apkarian, P., "A linear matrix inequality approach to H^∞ control," *International Journal of Robust and Nonlinear Control*, Vol. 4, No. 4, 1994, pp. 421–448. <https://doi.org/https://doi.org/10.1002/rnc.4590040403>.
- [57] Scherer, C., Gahinet, P., and Chilali, M., "Multiobjective output-feedback control via LMI optimization," *IEEE Transactions on Automatic Control*, Vol. 42, No. 7, 1997, pp. 896–911. <https://doi.org/10.1109/9.599969>.
- [58] Apkarian, P., and Noll, D., "IQC analysis and synthesis via nonsmooth optimization," *Systems Control Letters*, Vol. 55, No. 12, 2006, pp. 971–981. <https://doi.org/https://doi.org/10.1016/j.sysconle.2006.06.008>.
- [59] Bates, D., and Postlethwaite, I., *Robust Multivariable Control of Aerospace Systems*, Control and simulation, DUP Science, 2002. URL <https://books.google.nl/books?id=luJSAAAAMAAJ>.
- [60] Roos, C., Biannic, J.-M., and Evain, H., "A new step towards the integration of probabilistic μ in the aerospace Vamp;V process," *CEAS Space Journal*, Vol. 16, No. 1, 2023, p. 59–71. <https://doi.org/10.1007/s12567-023-00487-y>.

Part II

Literature Study

*This part has been assessed for the course AE4020 Literature Study.

State-of-the-Art Research Flying V

This chapter describes the current state of the research on the Flying-V. First, a brief overview of the historical development of the Flying-V is presented in section 2.1. Thereafter, a more in-depth overview of the research related to the simulation model of the Flying-V is provided in section 2.2. Subsequently, an overview of the previous assessments of the Flying-V's eigenmodes and handling qualities is given in section 2.3. Section 2.4 provides an overview of the proposed stability & control augmentation systems for the Flying-V. This is followed by an introduction to INDI-based control laws and a review of the state-of-the-art in section 2.5. Finally, a brief summary of this chapter is provided in section 2.6.

This chapter aims to answer research question 1, which is restated hereafter.

What is the state-of-the-art research on the Flying-V?

2.1. Historical overview of the development of the Flying-V

As mentioned in the introduction, the initial design of the Flying-V was established by Benad in 2013. Initial estimates provided by Benad indicated that the Flying-V may offer a 10% higher L/D ratio and a 2% mass reduction when compared to the Airbus A350-900, which was chosen as its reference aircraft due to its similarity in size and capacity. A side-by-side schematic of the two aircraft is depicted in figure 2.3. In order to demonstrate the flight characteristics of the initial design, a radio controlled Styrofoam model was built and flown in 2014. Both non-powered glider flights and powered flights with engines mounted on the aircraft were performed, as shown in figures 2.1 & 2.2 [13].



Figure 2.1: Flight test with glider model of the Flying-V, adopted from [13]



Figure 2.2: Flight test with powered model of the Flying-V, adopted from [13]

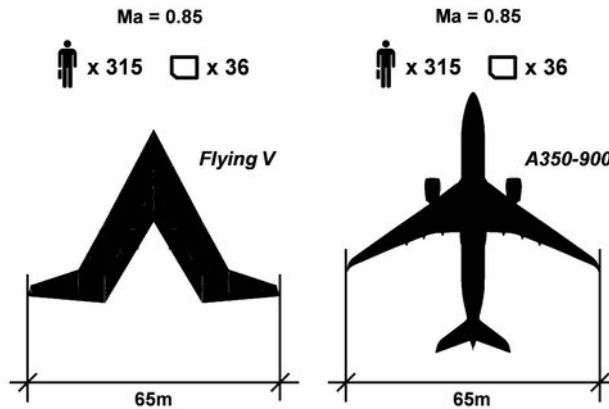


Figure 2.3: Flying V and Airbus A350-900 side by side, adopted from [13]

As previously mentioned, 2016 marked the start of a collaboration between KLM, Airbus and the TU Delft on the research of the Flying-V. In 2017, Faggiano et al. [17] studied the aerodynamic design of the Flying-V and optimized its geometry for a specific cruise condition, at Mach 0.85 and an altitude of 13km. The aerodynamically optimised design, shown in figure 2.4, was compared to the NASA Common Research Model and displayed a 25% higher L/D ratio .

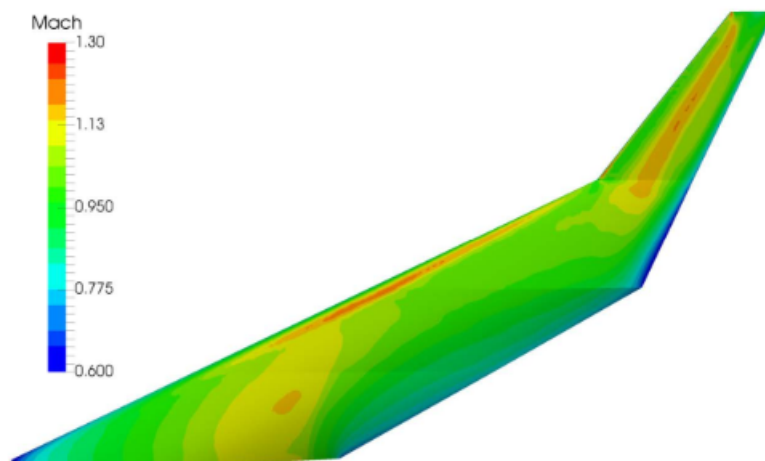


Figure 2.4: Optimized Flying-V wing shape for cruise flight with mach contours, adopted from [17]

An initial parametrization of the Flying-V's structure was carried out by van der Schaft at the Airbus Future Projects office in Hamburg [38]. Subsequently, Claeys performed a structural weight estimation, showing a 17% FEM weight reduction when compared to the reference aircraft [39]. These results were used to estimate its effect on the fuel burn of the Flying-V. It was estimated that the Flying-V offers a 20% fuel burn reduction when compared to modern twin-aisle aircraft with the same top-level aircraft requirements, technology assumptions and propulsion system. This promising figure sparked the interest of researchers and has resulted in continued research efforts, ranging from dynamics and control to cabin design.

In 2019, the design of the Flying-V was updated to allow for family design. Hillen provided a new parametrization of the aircraft enabling the stretching and shrinking of the inboard part of the wing, as shown in figure 2.5 [14].

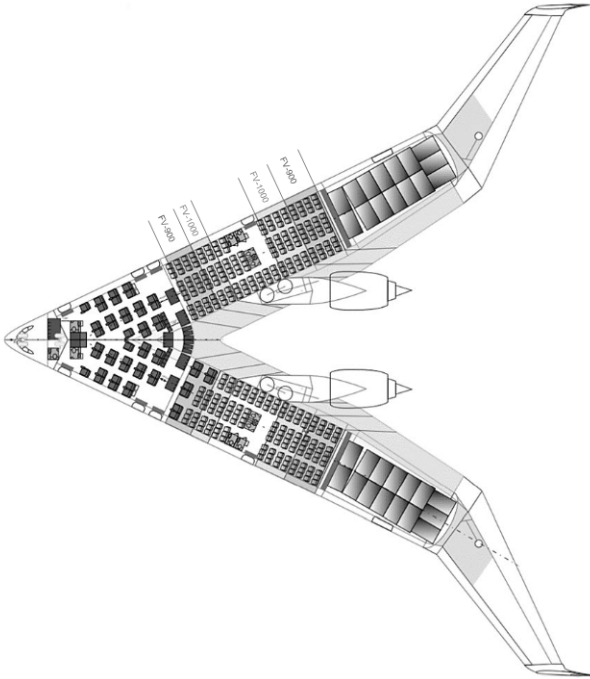


Figure 2.5: 2020 iteration of the Flying-V enabling family design, adopted from [14]

Subsequently, Oosterom and Vos performed a multidisciplinary design optimization for the design of three family members [16]. They concluded that the two smaller family members displayed a 22% and 20% fuel reduction when compared to comparable members of the A350 family, whilst maintaining commonality with the largest aircraft. The layout of the Flying-V's control surfaces can be seen in figure 2.6. Moreover, an overview of the key design parameters of the Flying-V are shown in table 2.1.

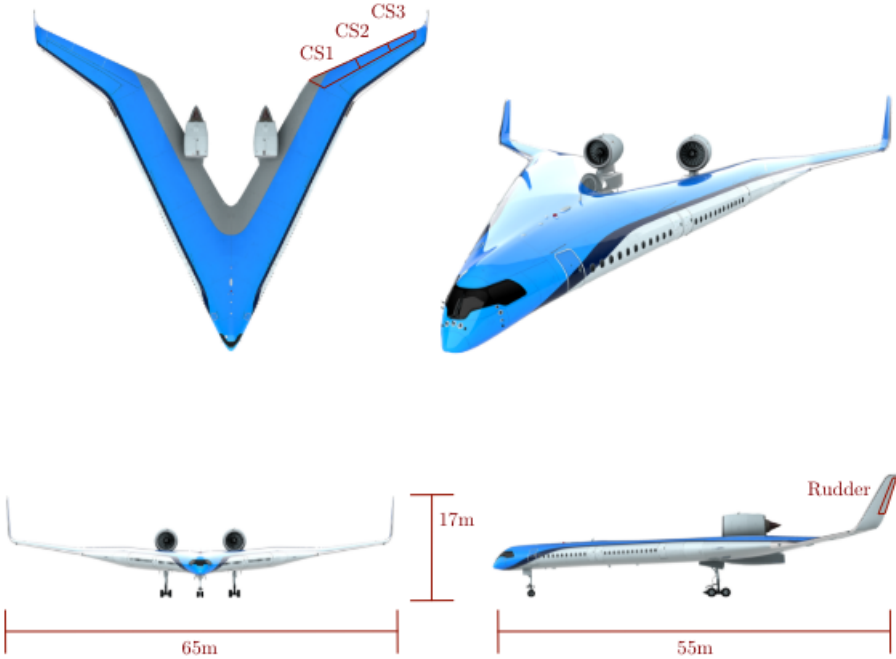


Figure 2.6: Control surface layout of the Flying-V, adopted from [12]

Table 2.1: Design parameters Flying-V, adopted from [20]

Parameter	Value	Unit
Length	55	[m]
Wingspan	65	[m]
Height	17	[m]
Pax	314	[-]
Fuel Capacity	140.000	[l]
Cargo Capacity	160	[m ³]
Design Mach number	0.85 [-]	
Cruise altitude	43.000 [ft]	

The flight tests performed by Benad in 2015 demonstrated that the Flying-V, in its form at the time, could be flown with adequate handling qualities [13]. However, the various modifications over the years warranted re-evaluation of the flight dynamics and control properties of the Flying-V. The following sections provide an overview of the research has been performed on the modelling, dynamics and control augmentation systems of the Flying-V over the years.

2.2. Simulation model of the Flying-V

The simulation model of the Flying-V consists of various subsystems that can be divided into the following categories: aircraft kinematics, aerodynamics and the flight control system (FCS). As such, this section is divided into subsections corresponding to the aforementioned categories.

2.2.1. Aircraft Kinematics & Dynamics

The simulation model of the Flying-V is based on the 6-DOF equations of motion (EOM) with the following assumptions [20].

- The aircraft is a rigid body with a constant mass.
- Flat, non-rotating Earth.
- zero wind and perfect atmosphere corresponding to ISA.
- resultant thrust lies in symmetry plane.
- gravitational acceleration is assumed to be constant.

The result force acting on the aircraft consists of gravitational forces, propulsion forces and aerodynamic forces. Moreover, it is assumed that the distributed forces can be replaced by point forces generating moments about the centre of gravity (cg) [40]. The resulting 6-DOF EOM are shown in equation 2.1.

$$\begin{bmatrix} {}^\beta \dot{\mathbf{v}} \\ {}^\beta \dot{\boldsymbol{\omega}}_{\beta/E} \end{bmatrix} = \begin{bmatrix} -{}^\beta \boldsymbol{\Omega}_{\beta/E} & 0 \\ 0 & -J^{-1}({}^\beta \boldsymbol{\Omega}_{\beta/E})J \end{bmatrix} \begin{bmatrix} {}^\beta \mathbf{v} \\ {}^\beta \boldsymbol{\omega}_{\beta/E} \end{bmatrix} + \begin{bmatrix} \frac{1}{m}({}^\beta \mathbf{F}_{grav} + {}^\beta \mathbf{F}_{aero} + {}^\beta \mathbf{F}_{thrust}) \\ J^{-1}({}^\beta \mathbf{M}_{aero} + {}^\beta \mathbf{M}_{thrust} + {}^\beta \mathbf{M}_{cg}) \end{bmatrix} \quad (2.1)$$

The states of this dynamic system are the velocity of the aircraft expressed in the body frame ${}^\beta \mathbf{v}$ and the angular velocity of the body-frame w.r.t. the earth fixed frame expressed in the body frame ${}^\beta \boldsymbol{\omega}_{\beta/E}$. ${}^\beta \boldsymbol{\Omega}_{\beta/E}$ represents the angular velocity matrix and J represents the inertia matrix. The resultant force is made up of the gravity forces, the thrust forces and the aerodynamic forces: $({}^\beta \mathbf{F}_{grav} + {}^\beta \mathbf{F}_{aero} + {}^\beta \mathbf{F}_{thrust})$. The moments are the sum of the aerodynamic moment, the thrust induced moment and the moment induced by the shift in CG: $({}^\beta \mathbf{M}_{aero} + {}^\beta \mathbf{M}_{thrust} + {}^\beta \mathbf{M}_{cg})$. A graphic representation of the different reference frames is shown in figure 2.7.

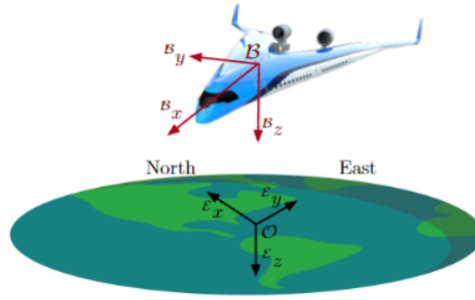


Figure 2.7: Reference frames of the Flying-V, from [21]

The relevant kinematic equations are defined as follows [40].

$$\begin{bmatrix} \dot{\phi} \\ \dot{\theta} \\ \dot{\psi} \end{bmatrix} = \begin{bmatrix} 1 & \sin \phi \tan \theta & \cos \phi \tan \theta \\ 0 & \cos \psi & -\sin \psi \\ 0 & \frac{\sin \psi}{\cos \theta} & \frac{\cos \psi}{\cos \theta} \end{bmatrix} \begin{bmatrix} p \\ q \\ r \end{bmatrix}_{\beta} \quad (2.2)$$

Where (ψ, θ, ϕ) represent the roll, pitch and yaw angles. Furthermore (p, q, r) represent the roll, pitch and yaw rates. In addition, the inertia matrix of the aircraft is defined as follows.

$$I = \begin{bmatrix} I_{xx} & -I_{xy} & -I_{xz} \\ -I_{xy} & I_{yy} & -I_{yz} \\ -I_{xz} & -I_{yz} & I_{zz} \end{bmatrix} \quad (2.3)$$

I_{xy} and I_{yz} are set to zero, as it is assumed that the Flying-V is a mass symmetrical aircraft [20]. Cappuyns estimated the inertia matrix based on the lumped mass model. The power plant and landing gear are considered as point masses. The remainder of the aircraft is split into lumped masses which are placed at half chord locations. These lumped masses are then divided over point masses equally spaced from the root to the tip of the wing. Making use of the Steiner theorem, the total moments of inertia of the aircraft around its principle axes can be determined. The results of these calculations are shown in table 2.2 [20].

Table 2.2: Moments of Inertia of the Flying-V around the principle axes, sourced from [20]

Inertia	MTOW	Empty Weight	Unit
I_{xx}	3.9641	1.2275	$[10^7 \text{ kgm}^2]$
I_{yy}	2.7619	1.0504	$[10^7 \text{ kgm}^2]$
I_{zz}	6.5822	2.1437	$[10^7 \text{ kgm}^2]$

2.2.2. Aerodynamic models

Over the years, various sources of aerodynamic data of the Flying-V have emerged. Namely, data from a Vortex Lattice Method (VLM) model, data from wind-tunnel experiments (WTE) with a scale model and finally, data from a series of flight test experiments (FTE). As a result, distinct models have been established. Later on, a combined model was constructed. The respective data sources and resulting models are discussed hereafter.

VLM model

The first aerodynamic model of the Flying-V followed from an analysis by Cappuyns in [20] and was based on the parametric geometry established earlier by Faggiano [17]. Cappuyns applied the VLM method to the parametrized model of the Flying-V with a control surface layout consisting of two elevons and one rudder, as defined by Faggiano. The geometry was then translated into a panel model that could be

used in Odilila. The output of the Odilila model contains the aerodynamic coefficients for specified Mach numbers, taking into account the taper, twist, camber, control surfaces, high lift devices and nacelles. The aerodynamic coefficients were determined with the linear set of equations stated in equation 2.4. Here, C_* refers to C_X , C_Y , C_Z , C_m , C_n and C_l . p^* , q^* and r^* are defined in equation 2.5.

$$C_* = C_{*\alpha}\alpha + C_{*\beta}\beta + C_{*p^*}p^* + C_{*q^*}q^* + C_{*r^*}r^* + C_{*\delta_1}\delta_1 + C_{*\delta_2}\delta_2 + C_{*\delta_3}\delta_3 \quad (2.4)$$

$$\begin{aligned} p^* &= p \frac{c}{V} \\ q^* &= q \frac{c}{2V} \\ r^* &= r \frac{c}{V} \end{aligned} \quad (2.5)$$

In order to validate the results of the VLM model, the obtained lift coefficient and pitching moment coefficient were compared with the results of wind tunnel tests performed by Palermo et al. [41]. It is worth stating the discrepancies between the two models used in the analysis. Primarily, the fact that the wind tunnel experiments were performed on a half-wingspan model of the aircraft without winglets. Whereas the VLM model is based on the full-scale parameterized geometry as defined by Faggiano et al. [17]. Moreover, the VLM model only has two elevons, whereas the half-wingspan model used by Palermo et al. in the wind tunnel experiments has three elevons. The aerodynamic coefficients obtained from the VLM model and those obtained from the wind tunnel experiments are shown in figure 2.8.

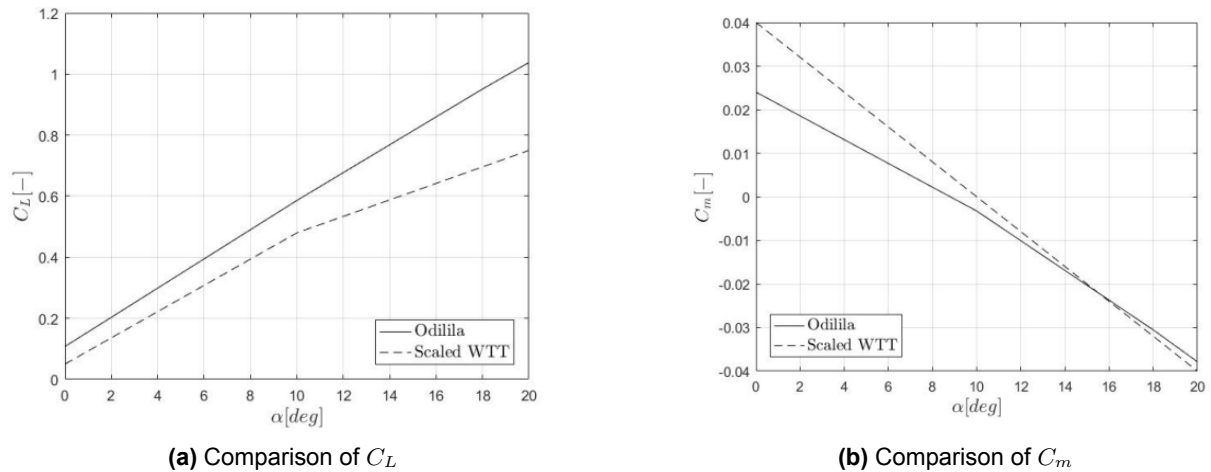


Figure 2.8: Comparison of aerodynamic coefficients from VLM model and WTT, from [20]

As seen in figure 2.8, the slope of the lift curves are similar up to an angle of attack of 10° and start to diverge at larger angles of attack. The opposite can be concluded for the moment curves, where the slopes converge for angles of attack greater than 10° . It must be stated that the wind tunnel experiments were performed with a free stream velocity of 20 m/s and a Reynolds number of $1 \cdot 10^6$, whereas the VLM model assumes a velocity of 250 m/s and a Reynolds number of $6.5 \cdot 10^6$. This difference in Reynolds number could explain the inconsistency between the two, as at a higher Reynolds number, C_l tends to be greater and C_m tends to be smaller [42].

It is worth mentioning that the VLM model has limited fidelity. The VLM model is based on linear aerodynamic data. As such, it is not capable of accurately modelling corners of the flight envelope where nonlinear effects occur. As such, deviating from the predetermined linearization points yields inaccurate estimates. Ultimately, the results of the VLM model were validated for angles of attack in the range of -5° to 15° [21]. Furthermore, frictional drag, ground effects, compressibility effects and aeroelastic effects are not taken into account [43]. In addition, the atmospheric model that was used does not include wind, wind shear and turbulence effects. In addition to that, the analysis was performed on a parameterized model that excludes the landing gear and fairing of the Flying-V, as well as additional parts present on the real aircraft that may all alter the dynamic behavior of the aircraft [20].

Cappuyns concluded that the VLM model is not capable of adequately capturing the unstable longitudinal

behavior of the Flying-V, as seen in the wind tunnel experiments performed by Palermo et al. [41]. However, Cappuyns concluded that the model is capable of accurately capturing the lateral coefficients of the Flying-V, revealing the aircraft's unstable dutch roll behavior [20].

WTE model

The geometrically scaled 4.6%, half wingspan scale-model of the Flying-V has been used in a number of wind tunnel experiments at the TU Delft Open Jet Facility. Palermo et al. and Viet et al. first studied the low speed characteristics of the Flying-V based on wind tunnel data [41, 18]. These studies led to a number of insights into the static stability characteristics of the aircraft. Subsequently, Garcia performed a number of wind tunnel experiments and performed aerodynamic model identification with a spline-based input/output model [44]. The resulting model contains the longitudinal force and moment coefficients and their derivatives w.r.t. airspeed, angle of attack and control surface deflection.

During the experiments performed by Garcia, it was observed that at higher angles of attack, vibrations occurred and the accuracy of the measurements deteriorated. As such, the experiments were repeated several times and it was ultimately concluded that the measurements are sufficiently accurate for angles of attack ranging between -10° and $+30^\circ$, speeds of roughly $12.5 - 30\text{ m/s}$ and control surface deflections between -14° and 19° . Figure 2.9 shows the regions where the aerodynamic coefficients were deemed reliable. Outside of this convex hull, unmodeled effects take place, hence no guarantee of validity can be provided [44].

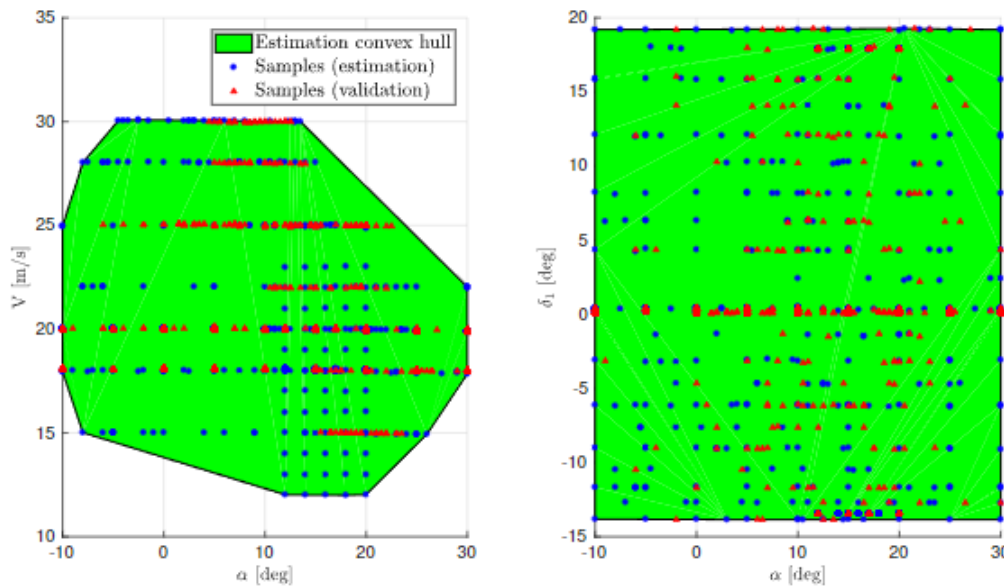


Figure 2.9: Convex estimation hulls, α versus airspeed (left), α versus elevator deflection (right), taken from [44]

A set of polynomials were used to capture the aerodynamic coefficients, these include both lateral and longitudinal lift and moment coefficients. Due to measurement uncertainty, it was concluded that the lateral force coefficient C_Y was not suitable for analysis. Hence, only C_Z , C_l and C_n were determined [44].

Flight Test Experiments

In 2020, a 4.6% sub-scale flight test model of the Flying-V was built and its maiden flight took place in the summer of 2020. Initial aerodynamic model identification was performed on the flight test data stemming from the maiden flight. A comparison of the resulting lift and drag coefficients and those obtained from the WTE model in 2019 is depicted in figure 2.11.



Figure 2.10: The TU Delft Flying-V on the runway during its maiden flight, taken from [45]

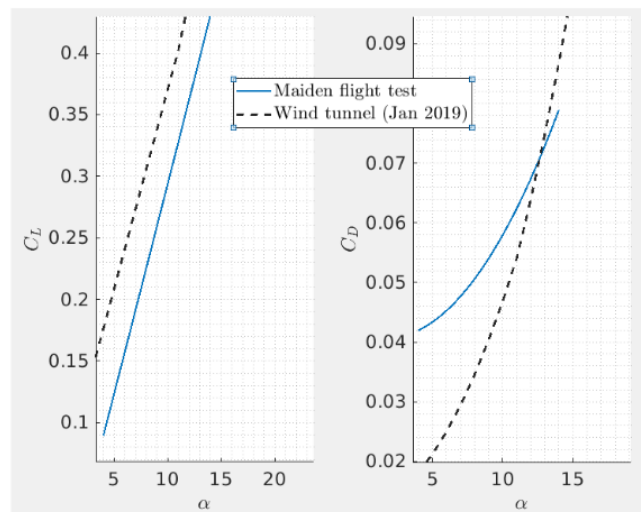


Figure 2.11: Comparison between the lift and drag coefficients obtained from the maiden flight test and those from wind tunnel tests, taken from [44]

As can be concluded from figure 2.11, the lift coefficient resulting from the flight test data displays an offset w.r.t. the WTE model. Similarly, the drag coefficients display an offset, which is likely due to induced drag from the landing gear, nacelles and pylons according to Garcia [44].

Ultimately, the model was deemed insufficiently valid for a number of reasons. First off, the model is based on flight test data of a single flight. During this flight, no specific aerodynamic system identification manoeuvres were performed. Furthermore, the data used to determine the pitching moment coefficient C_m was contaminated with noise. In addition, only small control surface deflections were applied during the flight test [21].

In the summer of 2021, a series of dedicated flight test experiments were performed. A number of longitudinal and lateral-directional maneuvers were performed to excite the aircraft dynamic modes. Subsequently, Garcia et al. [46] used the flight test data to perform aerodynamic model identification. The results, shown in figure 2.12, depict that the pitching moment coefficient from the flight test data model has a constant shift w.r.t. the wind tunnel data model. This can be explained by the additional drag induced by the landing gear, which was protracted during the test flights.

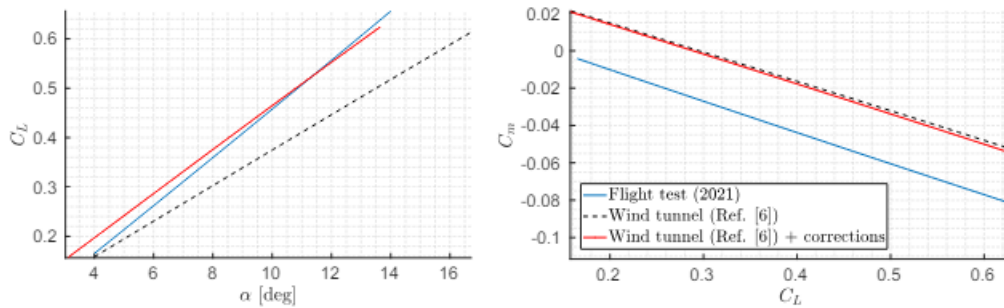


Figure 2.12: Comparison between the lift and pitching moment coefficients obtained from the test flight campaign and those from wind tunnel experiments, obtained from [46]

Combined Model

In an attempt to merge the results of the different models, Van Overeem [47] introduced the combined model. This model aims to fuse the results of the VLM model, the WTE model and the flight test experiments. Specifically, the combined model ought to capture the pitch break tendency, as well as the unstable Dutch roll during approach conditions. The model obtained from the VLM demonstrates the unstable Dutch roll behavior, yet due to its linear nature, is unable to capture the pitch break behavior. The WTE model does in fact display the pitch break behavior, yet it does not capture the unstable dutch roll. The latter due to the limited lateral-directional system identification capabilities during WTE. During the flight test experiments, the aircraft displayed unstable Dutch roll behavior, which is captured in the FTE model. As the edges of the flight envelope were not explored during the flight tests, the FTE model does not capture the pitch break behavior. These limitations justify the need for a model that captures both of these dynamic features, hence, the combined model was proposed [47].

It is worth stating the inconsistencies between the distinct models. Firstly, the VLM model was based on the full-scale aircraft whereas the WTE model is based on the 4.6% half-wingspan model. Additionally, the control surface layout of the two models vary. The full-scale aircraft possesses an inboard elevon, an outboard elevon and a rudder integrated into the winglet. Whereas the scale model possesses three elevons without winglets or rudders. The structural differences are highlighted in figure 2.13. Moreover, the aerodynamic models obtained from these two models are valid in different airspeed regimes, attributable to the size discrepancies between the two. Combining this data requires Froude scaling, which can be used to scale the airspeed of a scale model in order to capture the relative motions observed on a full-scale aircraft [48].

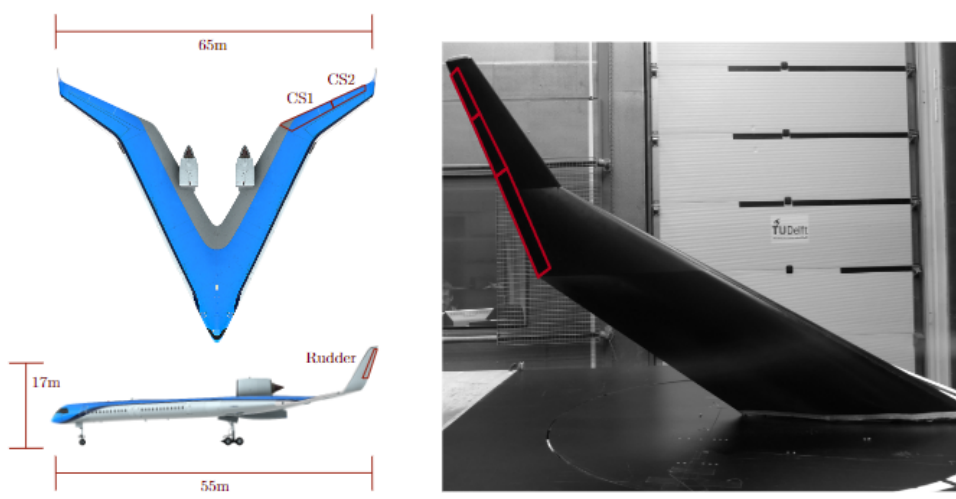


Figure 2.13: Control surface layout differences between the model used in the VLM and the 4.6 % half-wingspan model used in the WTE, obtained from [21]

Ultimately, the combined model that was established in [47] uses the VLM model as its baseline. Making use of the configuration consisting of an inboard elevon, an outboard elevon and a rudder integrated into the winglet. The elements of the WTE model that capture the pitch break behavior are added to the baseline VLM model, such that the combined model captures both the unstable Dutch roll mode and the pitch instability.

Specifically, the longitudinal coefficients that are fused together consist of the longitudinal force coefficient C_x , the directional force coefficient C_z and the pitch moment coefficient C_M . The remaining coefficients are the lateral force coefficient C_Y , the roll moment coefficient C_l and the yaw moment coefficient C_N respectively, these were obtained from the VLM model. All the coefficients were determined for an approach and cruise condition, at $Ma = 0.2$ and $Ma = 0.85$ respectively and at angles of attack ranging between -5° to 30° . A comparison between the aerodynamic coefficients of the WTE model and the VLM model is shown in figure 2.14.

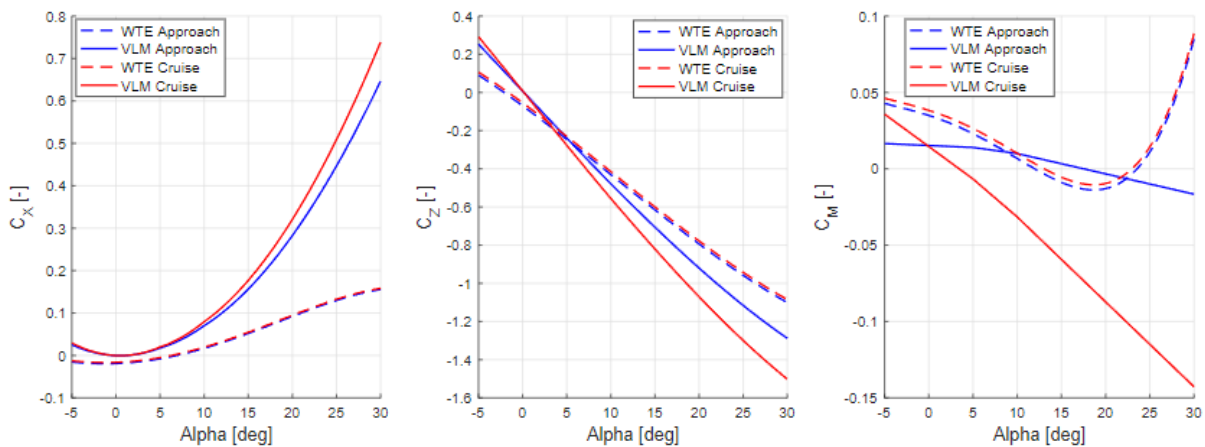


Figure 2.14: Comparison of aerodynamic coefficients from WTE model and VLM model, obtained from [21]

Due to the VLM model's inability to capture the pitch break behavior at $\alpha = 20^\circ$, Van Overeem applied spline-based interpolation to merge the two curves. As a result, the combined aerodynamic model uses the coefficients from the VLM model for angles of attack between -5° and 15° . Between 15° and 30° , the aerodynamic coefficients from the WTE model are used. The resulting aerodynamic coefficient curves are shown in figure 2.15.

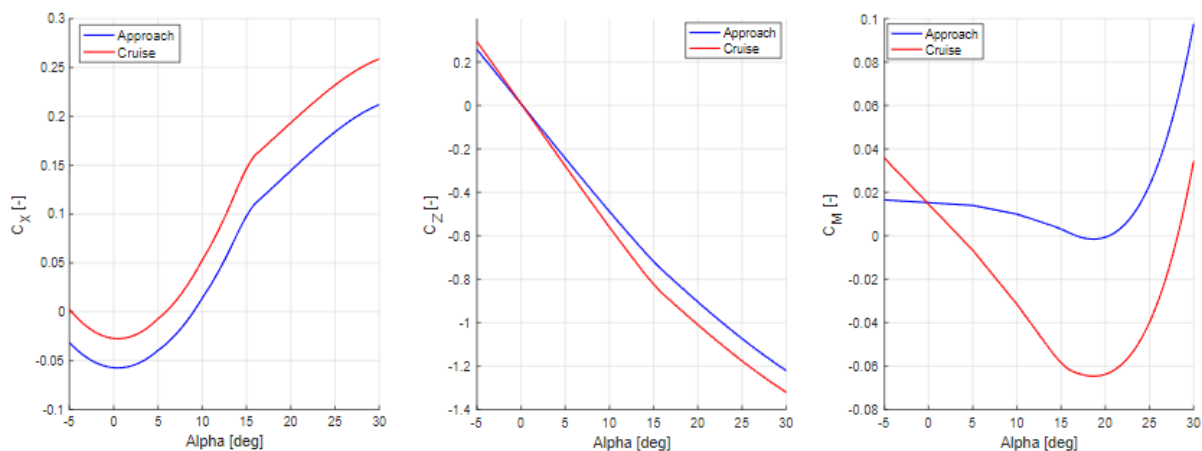


Figure 2.15: Aerodynamic coefficients of the combined model displaying pitch break tendency at $\alpha = 20^\circ$, from [21]

Several assumptions that limit the fidelity of the combined model remain. First off, the zero-lift drag of the full scale model of the Flying-V is not available. As a replacement, the zero-lift drag from the A350-900 is added to the aerodynamic model of the Flying-V [21]. In addition, it was assumed that only the angle of attack contributes to the force and moment coefficients in a non-linear manner. In reality, control surfaces are also expected to show nonlinear behavior at greater angles of attack.

Moreover, Froude scaling was used in order to fuse the VLM and the WTE model. The use of Froude scaling requires that the relative density factor and the relative moment of inertia of the sub-scale aircraft is equal to that of the full-scale aircraft, which is not the case [48]. In addition, the combined model does not account for frictional drag, as it is not possible to accurately estimate frictional drag from the WTE model due to scaling effects. To account for frictional drag, the value from the reference aircraft was added to the combined model.

The underlying assumptions, simplifications and uncertainty limit the fidelity of the combined model. However, it is currently the only model that captures both the unstable Dutch roll behavior and the pitch break behavior of the Flying-V.

Van Overeem verified the validity of aerodynamic model by comparative analysis with previously obtained results by Viet et al., Palermo et al. and Faggiano et al. [17, 18, 41]. Van Overeem deemed the model useful in the operational range depicted in table 2.3 [47].

Table 2.3: Verified operational range of the aerodynamic model, sourced from [21]

Parameter	α	β	p, q, r	$\delta_{cs1}, \delta_{cs2}, \delta_{cs3}$
Range	$[-5^\circ, 30^\circ]$	$[-20^\circ, 20^\circ]$	$[-10^\circ/s, 10^\circ/s]$	$[-25^\circ, 25^\circ]$

2.2.3. FCS hardware modelling

The fidelity of the simulation model of the Flying-V can be increased by including Flight Control System (FCS) hardware models. Van Overeem used a first order model to capture the dynamic behavior of the control surface actuators [47]. Later on, Stougie [24] opted for a second-order model, in line with the work of Matamoros [49]. Moreover, a first order engine model was employed. The second order actuator model and the thrust model used by van Overeem are shown in equation 2.6.

$$H_{act}(s) = \frac{4000}{s^2 + 140s + 4000}, \quad H_{thrust}(s) = \frac{1}{0.2s + 1} \quad (2.6)$$

The transfer function for the thrust converts the commanded thrust to actual engine thrust with an upper limit of $3.79 \cdot 10^5 N$, which is based on the maximum thrust delivered by the engines of the reference aircraft, the Rolls-Royce Trent XWB engine series [50].

The rate limits for δ_{cs1} and δ_{cs2} are $80^\circ/s$, δ_{cs3} has a rate limit of $120^\circ/s$. The position limit for δ_{cs1} and δ_{cs2} is 25° . Respectively, the position limit for δ_{cs3} is 30° , as defined by Cappuyns [20]. The actual control surface limits of the scale model were determined during flight tests and are shown in table 2.4.

Table 2.4: Control surface deflection limits of scale model, adopted from [21]

Control Surface	Max. down deflection	Max. up deflection
CS1	+18°	-25°
CS2	+25°	-25°
CS3	+25°	-25°
Rudders	+27°	-29°

In addition, Stougie introduced a model for the sensor dynamics. Moreover, discretization blocks were added to account for the digital nature of the flight control computer and the air data sensors, as shown in figure 2.16 [24].

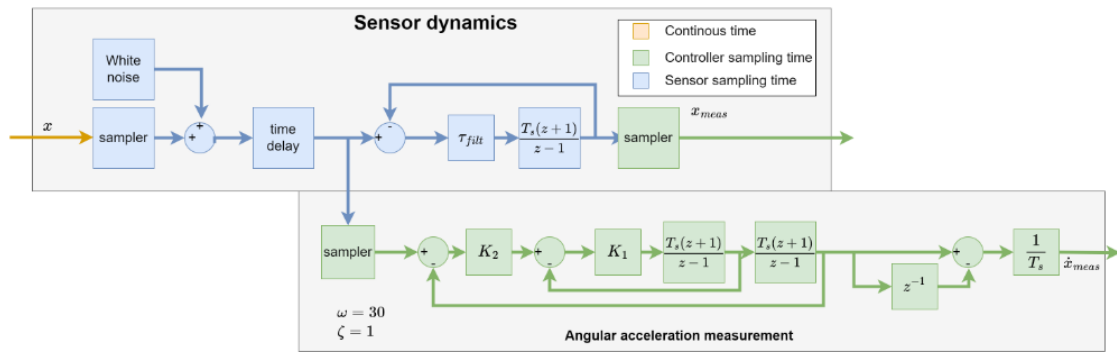


Figure 2.16: Sensor dynamics model, as seen in [24]

The baseline values for each of the sensors are depicted in table 2.5 and are based on the sensors of the Citation II PH-LAB aircraft, defined in [32]. These are based on the assumption that the air density and the control surface deflections are known at all times, free of any bias, noise or time delay.

Table 2.5: Baseline sensor values, adopted from [32]

Sensor	Sampling rate [Hz]	Time delay [s]	Noise	Bias	Filter time Constant
p, q, r [rad/s]	50	0.1	$1 \cdot 10^{-9}$	$3 \cdot 10^{-5}$	0.05
ψ, θ [rad]	50	0.1	$1 \cdot 10^{-9}$	$4 \cdot 10^{-5}$	0.05
V [m/s]	1/0.065	0.325	$1 \cdot 10^{-4}$	2.5	0.05
α, β [rad]	50	0.1	$7.5 \cdot 10^{-8}$	$3 \cdot 10^{-5}$	0.05
A_x, A_y, A_z [g]	50	0.1	$1 \cdot 10^{-5}$	$2.5 \cdot 10^{-3}$	0.05

2.3. Stability & Handling quality assessment

van Overeem performed an eigenmode analysis of the linearized equations of motion at two distinct trim points. Specifically, one approach condition and a cruise condition, the flight conditions of which are listed in table 2.6 [21]. The necessary requirements for these trim conditions follow from EASA CS25.161 and can be subdivided into longitudinal and lateral-directional requirements [51]. According to CS25.161., the longitudinal trimmability must be assessed for the least favorable centre of gravity (CG) location. As such, the combined model by van Overeem was trimmed at the aforementioned flight conditions for two separate CG locations, a forward CG location (29.372 m) and an aft CG location (31.714 m).

Table 2.6: Two flight Conditions of the Flying-V defined by van Overeem [47]

Approach Conditions	Cruise Condition
Ma= 0.2	Ma= 0.85
$\rho = 1.225 \text{ kg/m}^3$	$\rho = 0.265483 \text{ kg/m}^3$
$a_{mach} = 343 \text{ m/s}$	$a_{mach} = 295 \text{ m/s}$
mass= 210,000 kg	mass= 240,000 kg

Moreover, van Overeem constructed a trim algorithm, the resulting trim states for the earlier defined flight conditions are shown in table 2.7.

Table 2.7: Trim results seen in [47]

Flight Condition	Forward CG	Aft CG
Approach (Ma=0.2)	$u = 64.1\text{m/s}$	$u = 65.4\text{m/s}$
	$w = 24.5\text{ m/s}$	$w = 20.7\text{ m/s}$
	$\alpha = 20.9^\circ$	$\alpha = 17.5^\circ$
	$\theta = 17.9^\circ$	$\theta = 14.5^\circ$
	$\delta_{CS1}/\delta_{CS2} = 20.2^\circ$	$\delta_{CS1}/\delta_{CS2} = 3.9^\circ$
	$T = 175642.8\text{ N}$	$T = 109867.0\text{ N}$
Cruise (Ma=0.85)	$u = 248.8\text{m/s}$	$u = 249.3\text{m/s}$
	$w = 31.1\text{ m/s}$	$w = 26.8\text{ m/s}$
	$\alpha = 7.1^\circ$	$\alpha = 6.1^\circ$
	$\theta = 7.1^\circ$	$\theta = 6.1^\circ$
	$\delta_{CS1}/\delta_{CS2} = 8.0^\circ$	$\delta_{CS1}/\delta_{CS2} = 2.6^\circ$
	$T = 124199.7\text{ N}$	$T = 124377.6\text{ N}$

It can be concluded from the results in table 2.7 that moving the CG forward induces a pitch down moment, resulting in a greater elevon deflection upwards. This in turn requires an increase in lift force, which is achieved by an increase in angle of attack. Van Overeem suggests that the relatively large increase in thrust at the approach condition is mainly due to the larger increase in angle of attack than that seen at the cruise condition [47].

The trimmed model was subsequently linearized and verified by van Overeem, who compared the step response of the nonlinear model to the obtained linear model [47]. van Overeem concluded that the linear model is capable of approximating the nonlinear response for a 1° step input on the inboard elevons. Following the trim and linearization procedure, van Overeem performed an eigenmode analysis at the two flight conditions, the results of which are presented hereafter.

2.3.1. Eigenmode analysis

The eigenvalues following from the analysis performed by van Overeem are shown in figures 2.17 and 2.18. The corresponding natural frequencies and damping ratios are depicted in figure 2.19

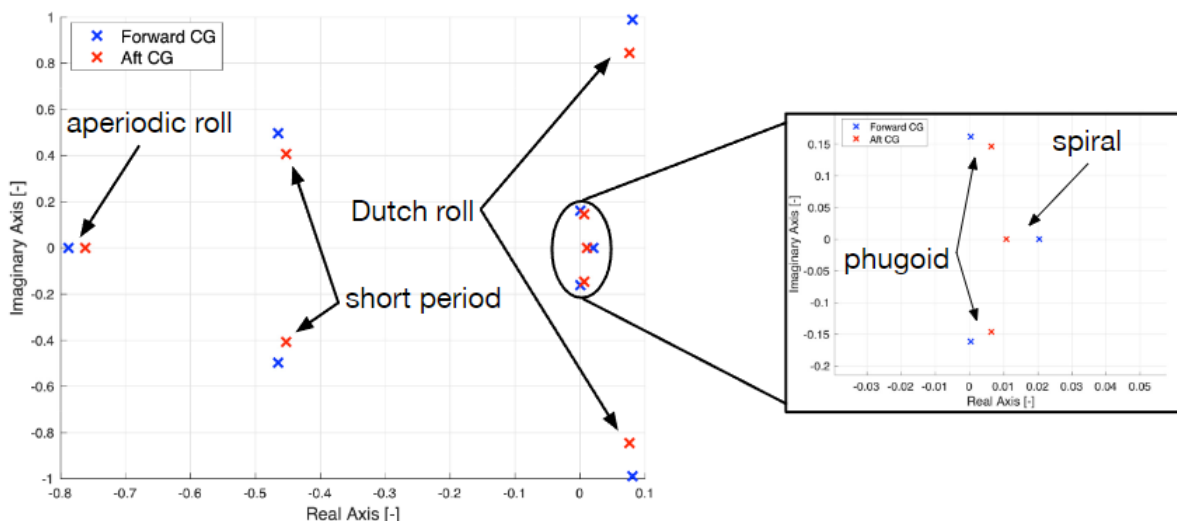


Figure 2.17: Eigenvalues of the Flying-V during approach, considering both the forward and aft CG configuration. [21]

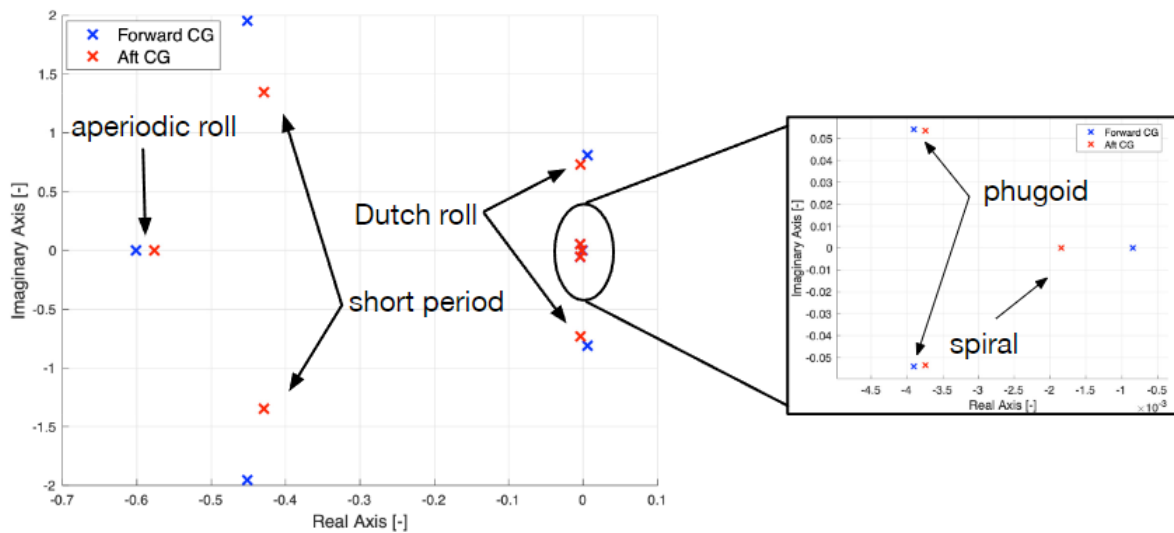


Figure 2.18: Eigenvalues of the Flying-V during cruise, considering both the forward and aft CG configuration, obtained from [21]

Eigenmodes	Approach (Ma = 0.2)				Cruise (Ma = 0.85)			
	Forward		Aft		Forward		Aft	
	ζ	ω	ζ	ω	ζ	ω	ζ	ω
Short Period	0.683	0.681	0.744	0.609	0.225	2.01	0.303	1.41
Phugoid	$-2.31 \cdot 10^{-3}$	0.161	$-4.37 \cdot 10^{-2}$	0.146	$7.19 \cdot 10^{-2}$	$5.43 \cdot 10^{-2}$	$6.97 \cdot 10^{-2}$	$5.37 \cdot 10^{-2}$
Dutch Roll	$-8.14 \cdot 10^{-2}$	0.992	$-8.97 \cdot 10^{-2}$	0.848	$-7.38 \cdot 10^{-3}$	0.811	$4.68 \cdot 10^{-3}$	0.732
Aperiodic Roll	-	-	-	-	-	-	-	-
Spiral	-	-	-	-	-	-	-	-

Figure 2.19: Damping ratios and natural frequencies of the Flying-V's eigenmodes, taken from [21]

At the approach condition, the short period mode and aperiodic roll mode are stable. Whereas the phugoid, Dutch roll mode and spiral mode are unstable.

At the cruise condition, the short period, phugoid and aperiodic roll mode are stable. Whereas the spiral mode is unstable. The Dutch roll mode is unstable at the forward CG location, yet stable at the aft CG location.

When shifting the CG aft, similar trends can be observed in both of the flight conditions. Namely, moving the CG aft results in an increased short period damping ratio and a decreased short period frequency.

Shifting the CG aft results in an increased phugoid damping ratio when it is unstable, whereas the damping ratio decreases in case the phugoid is stable. The natural frequency of the phugoid decreases when the CG is moved aft. Moreover, it can be concluded that the longitudinal stability deteriorates as the CG is moved aft. These findings are coherent with previous research on the flight dynamics and handling qualities of BWB aircraft [52].

When shifting the CG aft, the Dutch roll mode damping ratio increases at the approach condition. During the cruise condition, shifting the CG aft results in a stabilization of the Dutch roll mode. Moreover, the natural frequency of the Dutch roll mode is decreased when moving the CG aft. As such, the poles shift to the left when moving the CG aft. This suggests an increase in stability, contrary to existing literature, which show a deterioration of stability when moving the CG aft [52, 53]. Van Overeem concluded that this originates from the contribution of C_{Y_p} . The sign and magnitude of this coefficient is mainly dependant on the size and location of the winglets of the Flying-V w.r.t. the CG location. C_{Y_p} is negative for small angles of attack and becomes positive for larger angles of attack [54, 55]. As such, a shift in the CG forwards results in a decreased damping effect of the winglets, suggesting a deterioration of stability.

Moving the CG aft results in a decreased magnitude of the eigenvalues corresponding to the aperiodic roll mode and spiral mode.

The findings from the eigenmode analysis by Van Overeem is consistent with previous findings from Cappuyns [20].

2.3.2. Handling quality analysis

Following the eigenmode analysis, van Overeem assessed the Flying-V's handling qualities based on the handling requirements listed in MIL-F-8785C [56].

A summary of the assessment for the approach condition is given in table 2.8, similarly, the assessment for the cruise condition is provided in table 2.9.

Table 2.8: Flying quality assessment at approach condition, adopted from [47]

Flying quality parameters at approach (Ma=0.2)		
Mode	Forward CG	Aft CG
Short period	$\zeta_{sp} = 0.683$ (Level 1)	$\zeta_{sp} = 0.744$ (Level 1)
Phugoid	unstable, $T_{ph} = 39.0s$ (-)	unstable, $T_{ph} = 43.0s$ (-)
Dutch roll	Unstable (-)	Unstable (-)
Aperiodic roll	$T_r = 1.26$ (Level 1)	$T_r = 1.32$ (Level 1)
Spiral mode	$T_s = 42.6$ (Level 1)	$T_s = 79.4$ (Level 1)

Table 2.9: Flying quality assessment at cruise condition, adopted from [47]

Flying quality parameters at Cruise (Ma=0.85)		
Mode	Forward CG	Aft CG
Short period	$\zeta_{sp} = 0.225$ (Level 2)	$\zeta_{sp} = 0.303$ (Level 1)
Phugoid	stable, $\zeta_{ph} = 0.0719$ (Level 1)	stable, $\zeta_{ph} = 0.0697$ (Level 1)
Dutch roll	Unstable (-)	$\zeta_d = 4.68e^{-3}$, $\zeta_d\omega_d = 3.43e^{-3}$, $\omega_d = 0.732$ (Level 3)
Aperiodic roll	$T_r = 1.32$ (Level 1)	$T_r = 1.71$ (Level 2)
Spiral mode	Stable (Level 1)	Stable (Level 1)

In the tables above, the corresponding handling quality level as defined in MIL-F-8785C is listed in between brackets. If no level is provided, the corresponding value could not be assessed by the military standards.

Van Overeem also performed a handling quality analysis based on the Control Anticipation Parameter (CAP). The CAP values determined by van Overeem are listed in table 2.10. A more in depth discussion on handling quality criteria, including the CAP, is provided in chapter 4

Table 2.10: CAP parameters of the Flying-V, as seen in [47]

	Approach	Cruise
Forward CG	0.16	0.51
Aft CG	0.12	0.22

During approach, the Flying-V demonstrates Level 1 handling qualities with the forward CG configuration. Whereas it demonstrates Level 2 handling qualities with the aft CG configuration. During cruise, it shows Level 1 handling qualities at the aft CG and Level 2 handling qualities at the forward CG. Note that these findings have not been validated by piloted flight simulations.

In summary, moving the CG aft results in a lower CAP value, indicating a more sluggish response. This in turn may lead the pilot to oversteering, which can cause PIOs [57]. This behavior is consistent with research findings on other flying wings [53].

In order to stabilize the unstable eigenmodes and improve the handling qualities of the Flying-V, an active FCS can be introduced. In previous research, various stability and control augmentation solution to improve the handling qualities of the Flying-V have been proposed. These are discussed hereafter.

2.4. Stability & Control augmentation systems for the Flying-V

This section is devoted to providing an overview of the existing literature regarding stability and control augmentation systems for the Flying-V. Prior to discussing the various approaches, it is worth mentioning the overall FCS design cycle. The classical approach to flight control design often consists of a number of sequential steps. The first step involves the derivation of a nonlinear dynamic model of the aircraft. This is then followed by the trim-and-linearize routine, typically accompanied by a linear stability analysis. Subsequently, a controller architecture is typically defined and a first design is proposed. This step typically entails gain-scheduling in order to cover the aircraft's entire flight envelope. Thereafter, implementation of the control law on the nonlinear model follows and off-line simulations, followed by piloted simulations, are typically carried out. This process is often repeated to optimize the design based on predetermined criteria. This process is then repeated over the entire flight envelope of the aircraft and the resulting designs are then linked to one another through gain-scheduling. This approach is known as the *divide-and-conquer* strategy. A streamlined overview of this process is depicted in figure 2.20

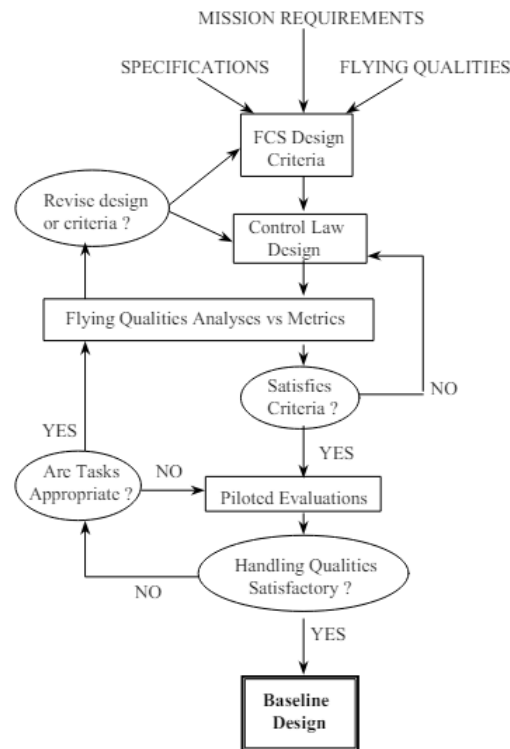


Figure 2.20: Flight control system design process, taken from [58]

This process tends to be rather time-consuming, costly and requires expertise in a wide variety of fields. All in all, this makes the task of FCS design challenging from a technical and managerial point of view [58, 59]. The authors of [59] identified that the application of advanced techniques promises a significant reduction of design time, as this would replace the divide-and-conquer approach and reduce the number of design points for which a controller needs to be designed. This is something to keep in mind when assessing the value of proposed control solutions for the Flying-V.

Torelli proposed a PID-based pitch rate Command controller to improve the controllable bandwidth and improve the handling qualities of the low-speed handling qualities of the Flying-V [60]. Torelli concluded that the controller proved effective at improving the handling qualities, yet mentioned issues with control

authority, a result of the sizing of the elevons of the Flying-V.

Joosten designed a lateral-directional SAS consisting of a roll-damper, yaw damper and a sideslip feedback system [61]. Joosten concluded that the SAS significantly improves stability, yet inevitably reducing maneuverability. The Dutch roll mode was successfully augmented to adhere to stability requirements, however none of the manoeuvrability requirements were met. Joosten also highlighted the lack of control authority and suggested further optimisation of the control allocation, although doubting that this would relieve the issue, further suggesting a resizing of the control surfaces .

Völker proposed the design of a Deep-Reinforcement Learning (DRL) based altitude controller. The proposed controller is based on a gradient method known as TD3 [62]. The designer controller demonstrated that the controller is capable of learning altitude control for the nonlinear simulation of the Flying-V in an offline environment, whilst adhering to a maximum tracking error requirement. Völker assessed the robustness of the controller by analyzing if the controller is capable of dealing with aerodynamic error, sensor noise, various reference signals an unfavourable initial flight conditions and concluded by stating that the controller is robust. This however, does not constitute a formal robustness analysis, as will be discussed in chapter 3. Therefore, no formal stability and performance guarantees can be deduced from those results.

Van Overeem [47] proposed the design of two INDI-based augmentation systems. Specifically, a SAS consisting of an INDI-based inner rate controller and a PID-based outer-loop airspeed controller. Secondly, van Overeem presents a CAS featuring an outer-loop consisting of roll angle, flight path angle and sideslip angle control, with INDI-based inner rate controllers. The proposed designs hinge on the time-scale separation principle, such that the output of the slower outer-loop serves as the reference input to the faster inner-loop. van Overeem proceeds to assess the efficacy of the proposed augmentation systems in improving the stability and handling qualities of the Flying-V during the approach condition with the forward CG configuration. The author concluded that the previously unstable dynamic modes were stabilized and that the closed-loop remains stable in the presence of up to 20% variation in the aerodynamic parameters. The effect of time delays and sensor noise on the closed-loop stability were not assessed. Although demonstrating the robustness of the proposed controllers to aerodynamic uncertainty with Monte-Carlo simulations, these observation do also not provide any formal stability and performance guarantees.

Stougie presented a controller structure consisting of an inner-loop INDI controller similar to van Overeem, with an addition of Flight Envelope Protection (FEP) [24]. As discussed previously, the Flying-V exhibits pitch-break tendencies at $\alpha > 20^\circ$. FEP can prevent the aircraft from reaching angles of attack where the pitch break becomes unrecoverable. Stougie proposes a longitudinal outer-loop controller based on the C^* criterion, whereas roll control was achieved with a Rate Command Attitude Hold (RCAH) controller. Moreover, a sideslip compensator was included. Stougie assessed the handling qualities for the selected cruise and approach conditions and suggested that the augmented aircraft exhibits Level 1 handling qualities. In addition, Stougie assessed the gain and phase margins in the presence of sensor dynamics and studied the impact of discretization effects on the handling quality level. Stougie suggested that for sufficiently fast body rate sensors, the aircraft can be tuned to Level 1 handling qualities, for as long as the time-delay in the body rate sensors is no longer than 0.04s. Moreover, Stougie concluded that the controller remained stable for sampling times smaller than 0.1s. Stougie simulated the closed-loop response for parametric aerodynamic uncertainty up to 20% and claimed that the controller is robust to model uncertainties. Stougie concludes by suggesting a number of additional effects that remain to be studied. Namely, the effect of mismatches in CG location, the impact of aeroelastic effects and time-delays on the FCC, which may severely degrade the stability and performance of INDI-based control laws.

Similar to van Overeem's conclusion on the robustness of the proposed INDI-based control system, these claims follow from empirical simulation observation and do not present formal stability guarantees. This falls in line with earlier work on INDI, such as the works of Bacon and Ostroff [63, 64]. Moreover, both Stougie and van Overeem only considered parametric uncertainty, which falls in the category of regular perturbations. As will be seen in section 2.5, INDI is most affected by singular perturbation. As such, the work of van Overeem and Stougie only provide limited insights into the robustness properties of the proposed INDI-based controllers. In the following section, a historical overview as well as a review

of the state-of-the-art on (I)NDI-based control laws is provided. Fundamental insights into the robustness properties of (I)NDI-based control laws are provided later in section 3.3.

2.5. State-of-the-art INDI

This section provides an introduction to (I)NDI as well as a review of the state-of-the-art.

2.5.1. NDI

Nonlinear Dynamic Inversion (NDI) emerged in the seventies and provides an alternative to the classical so called divide-and-conquer approach. Instead of dividing the flight envelope into various operating points, linearizing, applying linear control methods and gain scheduling, NDI aims to globally reduce the dynamics of the controlled variables to integrators. Subsequently, a closed loop system is designed that exhibits specified command responses. As such, the need for gain-scheduling is removed, whilst providing greater reusability across airframes. As well as providing flexibility for changing model and greater power to access non-standard flight regimes. These were the claims by Enns et al. [65], who believed that inversion-based control law design would eventually replace the divide-and-conquer approach. A decade later, this was confirmed by Balas in his famous 2003 survey paper [66], who identified it as the most widely applied multivariable control design technique .

NDI is based on the principle of feedback linearization and is sometimes referred to as such. NDI-based control laws consist of two parts. An inner dynamic inversion loop, transforming the channels describing the nonlinear bare airframe dynamics into a chain of integrators and an outer virtual control loop, aimed at shaping the desired dynamics. As a result, the workings of the inner loop transforms the nonlinear control problem to a linear one. In doing so, NDI presents a modular approach to flight control design, visually depicted in figure 2.21.

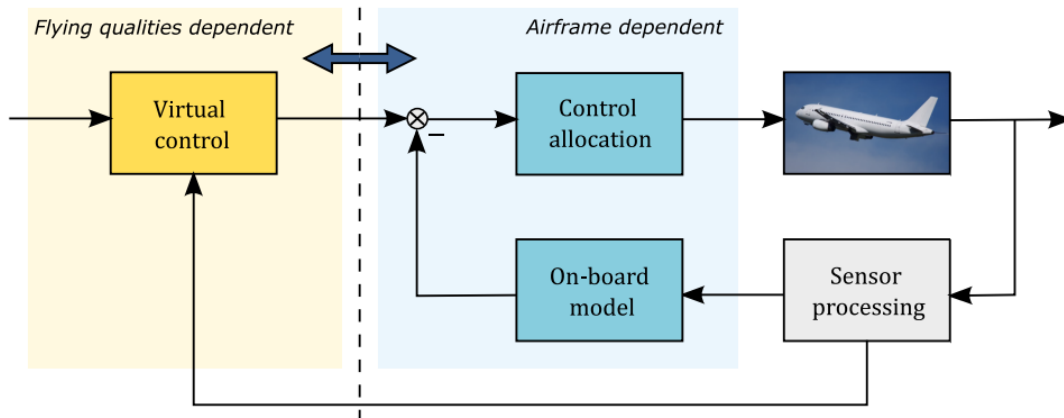


Figure 2.21: Modular structure of NDI, obtained from [35]

The formulation of the NDI control law is based on the assumption that the nonlinear flight dynamics can be described in the following manner [67].

$$\begin{aligned}\dot{\mathbf{x}} &= \mathbf{f}(\mathbf{x}) + G(\mathbf{x})\mathbf{u} \\ \mathbf{y} &= h(\mathbf{x})\end{aligned}\tag{2.7}$$

Where $\mathbf{x} \in \mathbb{R}^{n \times 1}$ represent the state vector, $\mathbf{u} \in \mathbb{R}^{m \times 1}$ represents the input vector, $\mathbf{y} \in \mathbb{R}^{m \times 1}$ represents the output vector, \mathbf{f} and h represent smooth vector fields and $G \in \mathbb{R}^{n \times m}$ is a smooth matrix. Note that the input \mathbf{u} does not explicitly appear in the output \mathbf{y} . It appears implicitly through the state variable \mathbf{x} and the nonlinear equation $h(\mathbf{x})$. To arrive at a direct relation between \mathbf{y} and \mathbf{u} , the concept of input-output linearization is required [67].

Consider again the nonlinear state equations in equation 2.7. To arrive at the NDI control law, the output

y is differentiated along its vector fields f and g . These derivatives are known as the Lie derivatives, denoted by $L_f h(x)$ and $L_g h(x)$ respectively. The number of times that y has to be differentiated to arrive at an explicit relation between y and u is known as the relative degree r . Applying the differentiation results in the following [68].

$$\dot{y} = \frac{dh(x)}{dt} = L_f h(x) + L_g h(x)u \quad (2.8)$$

if $L_g h(x) \neq 0$ for some $x = x_0$, the input transformation shown in equation 2.9 results in a linear relation between y and v , namely $\dot{y} = v$, where v is some virtual control law.

$$u = \frac{1}{L_g h(x)}(v - L_f h(x)) \quad (2.9)$$

Generalizing equation 2.8 for a system with relative degree r , one arrives at the following.

$$y^{(r)} = L_f^r h(x) + L_g L_f^{r-1} h(x)u \quad (2.10)$$

Similarly, the generalized control law for a system of degree r becomes the following.

$$u = \frac{1}{L_g L_f^{r-1} h(x)}(v - L_f^r h(x)) \quad (2.11)$$

Yielding the relation $y^{(r)} = v$. if the relative degree is equal to the system order: $r = n$, such that the output vector is equal to the state vector, this input-output linearization is called input-state linearization. In the example presented, assume that $\dot{y} = \dot{x}$, such that

$$\dot{y} = f(x) + G(x)u \quad (2.12)$$

Assuming that $G(x)$ is an invertible matrix, the control input is defined as follows.

$$u = G^{-1}(x)(v - f(x)) \quad (2.13)$$

A visual representation of the NDI control law and its relation to the virtual outer-loop control law is depicted in figure 2.22. For a more elaborate explanation of the underlying mathematical concepts of NDI, the reader is referred to the textbook on applied nonlinear control by Slotine, which provides an excellent explanation [67].

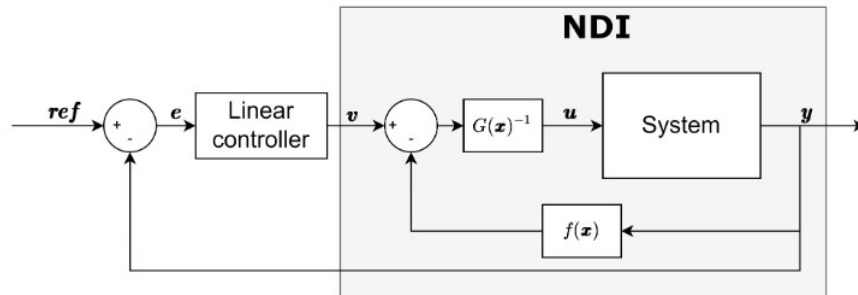


Figure 2.22: NDI control law with linear outer control loop, adopted from [34]

The applications of NDI to flight control have been numerous. Some high-profile examples include its application on the HARV, the X-38, the STOVL X-35 and the F-35 [69, 70, 71, 72]. The numerous implementations of NDI-based control laws highlights the maturity of the method. However, NDI heavily relies on the presence of an accurate on-board model (OBM) of the aerodynamics of the airframe. This is often challenging, as accurate OBMs may not always be available.

2.5.2. INDI

Incremental Nonlinear Dynamic Inversion (INDI), also known as sensor-based (SB) INDI emerged around the same time as NDI. As opposed to NDI, INDI no longer relies on an accurate model of the airframe dynamics to obtain the state derivatives. Instead, direct sensor measurements are used to obtain these. The only required model information is knowledge of the control effectiveness. SB-INDI first emerged in a 1998 paper by Smith, whom referred to it as simplified NDI [25]. Preliminary analyses demonstrated the control law's ability to perform in the presence of control effectiveness uncertainty and measurement noise. Subsequently, a series of flight tests with the VAAC Harrier were carried out, showing promising results [31]. Later, Bacon and Ostroff demonstrated the robustness properties of the control law in terms of gain and delay margins and demonstrated how INDI could be modified to mitigate the effects of measurement noise and actuator saturation [63, 64].

Literature on INDI remained sparse in the following years, up until a 2010 paper by Sieberling et al. [26], who proposed sensor-based INDI as an inexpensive yet powerful control strategy for UAVs. Moreover, the paper highlighted the robustness to parametric uncertainty, confirming the earlier findings of Smith, Bacon and Ostroff [31, 63, 64]. Sieberling et al. [26] demonstrated that the robustness to aerodynamic model uncertainty comes at the cost of an increased sensitivity to sensor delays. In the subsequent years, various studies demonstrating its capabilities in simulation emerged, such as those by Acquatella and Simplicio [27, 28].

Following these successful simulation studies, INDI was deployed on various platforms and demonstrated in flight. Initially on a quadrotor, later on a fixed-wing UAV and eventually finding its way to a CS-25 certified passenger aircraft, the PH-LAB Cessna Citation II [29, 32]. These flight tests showed promising results, such that Grondman et al. [32] claimed that INDI performed superior to conventional NDI. In the years following, INDI has seen widespread research application. Applications range from VTOL UAVs [73, 74], to fault-tolerant control of quadrotors [75, 76], to launch vehicles [77], piloted simulations of helicopters [78] and simulator motion control [79]. Moreover, various design augmentations have been proposed, which will be briefly reviewed in section 2.5.3.

The derivation of the INDI control law is similar to the NDI law, yet one starts by stating the incremental form of the system dynamics as seen in equation 2.7. Consider now, for the sake of simplicity, the following description of the state dynamics.

$$\dot{x} = f(x) + G(x)u = f(x, u) \quad (2.14)$$

The Taylor expansion of this equation around the state at time $t_0 = t - \Delta t$, where Δt represents the sampling interval, is given by the following

$$\begin{aligned} \dot{x} &\approx f(x_0, u_0) + \left. \frac{\partial f(x, u)}{\partial x} \right|_{x_0, u_0} (x - x_0) + \left. \frac{\partial f(x, u)}{\partial u} \right|_{x_0, u_0} (u - u_0) + \mathbf{R}_1 \\ &= \dot{x}_0 + F(x_0, u_0)\Delta x + G(x_0, u_0)\Delta u + \mathbf{R}_1 \end{aligned} \quad (2.15)$$

Where $\Delta x = x - x_0$, $\Delta u = u - u_0$ and \mathbf{R}_1 represents the expansion remainder.

Under the assumption that the sampling rate is high enough and that the control surface dynamics Δu happen orders of magnitude faster than the aircraft dynamics Δx , it is common practice to apply the time scale separation principle, which dictates that all state-dependant and residual terms can be omitted [26, 30, 32]. Subsequently, equation 2.15 reduces to the following.

$$\dot{x} \approx \dot{x}_0 + G(x_0, u_0)\Delta u \quad (2.16)$$

Rearranging the terms in equation 2.16 results in the incremental control law Δu , which is added to u_0 to obtain u , as shown in equation 2.17 below.

$$\begin{aligned} \Delta u &= G^{-1}(x_0)(v - \dot{x}_0) \\ u &= u_0 + \Delta u \\ &= u_0 + G^{-1}(x_0)(v - \dot{x}_0) \end{aligned} \quad (2.17)$$

As seen in equation 2.17, u is no longer directly dependant on the system dynamics $f(x)$, as is the case for its non incremental counterpart stated in equation 2.13. Instead, the INDI control law relies on the knowledge of the previous control input u_0 , the previous state x_0 , the previous state derivative \dot{x}_0 and

the control effectiveness matrix G . Note that the source of \dot{x}_0 in the case of SB-INDI are direct sensor measurements. A model-based version of INDI (MB-INDI) is also an option, these do require a model estimate of \dot{x}_0 . A typical INDI control law architecture is depicted in figure 2.23.

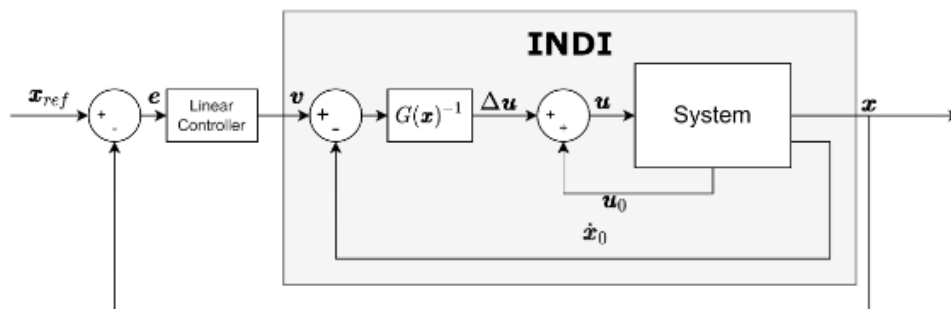


Figure 2.23: INDI control law with linear outer control loop, adopted from [34]

Grondman et al. [32] provide a comprehensive summary on some of the fundamental properties of INDI, which includes the following: INDI differs from NDI in that it requires only partial knowledge of the system dynamics, as the resulting control law only depends on the control effectiveness G . However, additional feedback signals in the form of the input measurement u_0 and the state derivative \dot{x}_0 are required. Moreover, the controller ought to be discretized with sufficiently high sampling rate. Finally, stating that synchronization between the input u_0 and the state derivative \dot{x}_0 is required, as the calculated control increment is based on a linearisation around a specific point in time. As will be seen in the section hereafter, many of the proposed design features are aimed at dealing with the implications of the aforementioned properties of INDI [32].

2.5.3. Review of the state-of-the-art

Sieberling et al. [26] propose a INDI-based controller augmented with a linear predictive filter aimed at predicting the angular accelerations. Thereby tackling the time delay issue and angular acceleration availability issue. According to Sieberling et al. the proposed solution, dubbed PINDI, results in better robust performance than regular NDI. Moreover, they emphasize the practical usability of the proposed PINDI. However, it was also observed that the PINDI controller is slightly more sensitive to model uncertainty than regular INDI. Which the authors claim stems from the assumption of an ideal response in the predictive filter design [26].

In 2016, Smeur et al. [29] propose Adaptive INDI, aimed at providing solutions for two major challenges associated with INDI, sensor and actuator delays and control effectiveness variations. The first is addressed with signal synchronization, ensuring synchronization between the angular acceleration and control surface deflection measurement and/or estimation. To deal with the latter, a LMS adaptive filter was proposed, aimed at onboard estimation of the control effectiveness. The implementation of these two solutions were successfully demonstrated in flight on a quadrotor.

Van 't Veld et al. [30] conducted a preliminary study on the stability and robustness properties of INDI in the presence of real-world effects encountered in aircraft. Subsequently, flight tests were carried out on the PH-LAB Cessna Citation II, as documented by Grondman et al. [32]. The preliminary analysis performed by Van 't Veld et al. provided a number of contributions. The authors provided an analytical stability analysis showing that a discrete time implementation of INDI with sampling times smaller than 0.02s results in large stability margins. Moreover, delay of the actuator measurements was found to degrade system stability. In addition, the effect of real-world phenomena in the form of bias, discretization, noise and time delay on an INDI-controlled aircraft was studied. It was shown that actuator measurement bias, angular rate measurement noise, angular rate measurement delay and actuator measurement delay result in significant performance degradation. The authors suggest that the observed performance degradation can be prevented in a number of ways. These include PI-control in the virtual control input

to prevent steady-state error due to actuator measurement bias, as well as a low-pass filter to reduce the noise in the angular rate measurement. Moreover, the authors suggest synchronizing the angular rate and actuator measurements to prevent oscillatory behavior. The importance of measurement synchronization was confirmed by an analytical stability analysis as well as simulations. These suggested that INDI is inherently more sensitive to additional angular rate delay compared to additional actuator delay. The authors state that this can partly be resolved by using pseudo control hedging (PCH), as identified earlier by Simplicio et al. [28]. These outcomes provide a more detailed insight into the sensitivity of INDI-based control laws to these real world phenomena.

Following the preliminary analysis by Van 't Veld et al. , the flight test campaign with the PH-LAB Cessna Citation II followed suit. The campaign marked the first successful implementation of INDI on a CS-25 class fixed-wing aircraft. For comparison, the aircraft was also flown with a classical NDI control law. Results showed that the INDI controller clearly outperformed the NDI controller. Grondman et al. [32] remarked that one area of attention is the higher noise levels in the control signal of INDI compared to NDI. Which is seen as a direct consequence of the differentiation of the angular rates, required to obtain the angular accelerations. The authors observed that the bandwidth of the filter used to obtain the derivative could not be lowered any further without seriously compromising performance. The authors conclude by stating that the development of angular accelerometers for aircraft is essential for the further development of INDI.

Keijzer et al. [73] further tested INDI and Incremental Backstepping (IBS) on the PH-LAB, making use of Angular Accelerometer (AA) feedback. The authors concluded that both of these control laws provide satisfactory performance in flight tests and that the AA feedback has a negligible effect on performance in nominal flight, whereas the authors observed that it substantially increases the robustness of the controllers to model mismatch.

Li et al. [80] propose angular acceleration estimation-based INDI (EINDI). The authors claim that this may reduce the effects of noise and time delays on the angular acceleration, therefore ensuring robustness of the system. In addition, the proposed controller incorporates PCH to prevent unwanted actuator dynamics. The proposed adaptive law combines control surface deflection and existing knowledge of the aerodynamic parameters to estimate angular accelerations. Moreover, a compensator is added to compensate for angular acceleration estimation errors caused by disturbances and model uncertainties. Note that this adaptive scheme does require additional knowledge of the aerodynamic parameters, contrary to conventional INDI. However, the authors state that the existence of the adaptive law makes it such that the aerodynamic parameters do not have to be known accurately, as the adaptive law compensates for deviations in its value. Similarly, the authors state that the adaptive law is capable of compensating for the effect of disturbances and time delays caused by the measurements. Results of simulation studies demonstrate that the proposed EINDI controller is effective at reducing the effect of model uncertainty and CG changes when compared to regular NDI. Moreover, the authors observe that the EINDI controller outperforms a conventional INDI controller in a tracking task.

Kumtepe et al. [33] present Hybrid INDI, aimed at alleviating issues associated with synchronization delays. The authors propose a complementary filter that fuses a model estimate with sensor measurements to generate an angular acceleration estimate. In doing so, the authors claim that the high-frequency dynamics are captured by the on-board model, whereas the sensor measurements accurately capture the low-to-medium frequency dynamics. To demonstrate its effectiveness, the proposed Hybrid INDI controller is tested in simulation and compared to SB-INDI. The authors demonstrate that, in the nominal case, Hybrid-INDI responds quicker than SB-INDI, as the angular acceleration measurement lags behind the model estimate, Hybrid INDI is capable of responding quicker to changes in the angular acceleration. Moreover, simulations in the presence of aerodynamic uncertainty display that the on-board model of Hybrid-INDI does not have to be very accurate for the controller to be robust against model mismatches. In addition, the robustness of Hybrid INDI against measurement delay is tested. To do so, a transport delay of 0.05s is introduced in the angular rate measurement. It is demonstrated that the performance of Hybrid INDI barely deviates from its nominal performance, whereas oscillations occur in SB-INDI. Additional simulations with increased time delay demonstrate that the SB-INDI controller is rendered unstable at 0.07s of time-delay, whereas the proposed Hybrid INDI controller becomes unstable at 0.13s of time-delay, indicating an improvement in robustness to time-delay.

Another version of Hybrid INDI is presented by Kim et al. [81]. The proposed controller makes use of additional angular acceleration augmentation. Moreover, control surface synchronization is included to increase the stability margin of the controller.

Recognizing the need for more rigorous stability and robustness insights, Wang et al. [34] provided these

based on nonlinear Lyapunov methods and perturbation theory. The authors presented nonlinear stability and performance properties of INDI as a function of sampling rates, yet the analysis was limited to exogenous disturbances and regular perturbations.

A reoccurring theme throughout the literature on INDI is its sensitivity to singular perturbations in the form of time delays, as seen in [32, 30, 33]. Wang et al. [34] briefly considered these in their analysis but left a detailed analysis as future work.

More recently, the research community has started to recognize the importance of considering singular perturbations, as seen in [82, 83, 84]. However, these studies assume that all model uncertainties and singular perturbations can be parameterized. It is well known that this is not the case for physical systems [36]. As is the case for aircraft, bare airframe dynamics are typically hard to model at high frequencies, due to unknown structural dynamics and aerodynamic effects, such as those seen on the Flying-V. Similarly, actuators often display unknown dynamics at high frequencies [85, 86]. These are by definition, unstructured (non-parametric) effects, which can be captured by norm-bounded uncertainty descriptions. As such, Pollack argues that to adequately assess the robust stability and performance characteristics of INDI-based control laws, these unstructured uncertainties must be included. Consequently, Pollack provides a systematic formal robustness analysis of INDI-based control laws in the presence of regular and singular perturbations, described by norm-bounded definitions. The analysis established by Pollack builds on the framework provided by linear multivariate control design and analysis tools. A comprehension of this framework and the tools it provides is necessary for understanding the robustness properties of INDI-based control design. As such, an introduction to this framework is provided in chapter 3. With the knowledge provided by this framework, the robustness properties of INDI are analyzed in section 3.3, which are based on the insights established by Pollack [35].

2.6. Conclusions

This chapter served to introduce the Flying-V and review previous research on the Flying-V in terms of modelling, stability analysis, handling assessment and control augmentation. Previous flight control designs on the Flying-V have made use of INDI-based control laws. Throughout the literature, sensor-based INDI has been shown to perform well in the presence of aerodynamic uncertainty. This however, comes at the cost of an increased sensitivity to sensor delays and digital effects, as demonstrated in various studies. These observations have, until fairly recently, been of empirical nature. The research community has started to recognize the significance of effect that singular perturbations, in the form of time delays and/or higher order dynamics, have on the stability of INDI-based control laws. Wang et al. [34] provided several insights into the nonlinear stability and performance properties of INDI control laws. The analysis was however limited to studying the effects of exogenous disturbances and regular perturbations. Other works have considered these perturbations in their analysis, yet assume that these regular perturbations can be parameterized, which is inherently not the case. Therefore, Pollack [35] argues that to gain a deeper understanding of the robust stability & performance properties of INDI, singular perturbations must be considered. Subsequently, Pollack provides methods that enable the robust stability & performance analysis of INDI-based control laws in the presence of both regular and singular perturbations. The proposed methods make use of the \mathcal{H}_∞ -framework, which offers tool such as μ -analysis and \mathcal{H}_∞ -synthesis. This framework builds on a strong foundation of research, offering tools to analyze and synthesize control systems in the presence of various uncertainties and performance requirements. The following chapter is dedicated to providing a brief introduction to the framework and lays the foundation for the robust stability & performance analysis of INDI-based control laws in the presence of both regular and singular perturbations, as established in [35].

This chapter aimed to answer research question 1 and its sub-questions. These are restated hereafter alongside the answer to these questions, to the extent that they have been answered in this chapter.

What is the state-of-the-art research on the Flying-V?

a) Which elements make up the simulation model of the Flying-V?

The simulation model of the Flying-V consists of a bare airframe model, made up of the 6DOF EOM containing the aerodynamic coefficients. These aerodynamic coefficients have been determined on numerous occasions, from different sources. A VLM model, a WTE model and a FTE model, moreover a combined model was generated previously, aimed at capturing all the relevant aerodynamic behavior. In addition to the bare airframe model, FCS hardware models have been proposed. A

second order actuator model has previously been proposed, as well as a first order engine model. Moreover, a sensor model was established in [24], capturing the discretizations effects.

b) **What are the stability and handling quality characteristics of the bare airframe?**

Van Overeem [47] presented an eigenmode analysis of the linearized EOM around two distinct trim conditions, a cruise condition and an approach condition. Moreover, the analysis considered two CG locations, a forward CG and an aft CG. The analysis showed that at the approach condition, the short period mode and the aperiodic roll mode are stable, whereas the phugoid, Dutch roll mode and spiral mode are unstable. At the cruise condition, the short period, phugoid and aperiodic roll mode are stable, whereas the spiral mode is unstable. The Dutch roll mode is unstable at the forward CG, yet stable at the aft CG location. Van Overeem concluded that shifting the CG aft results in the poles shifting to the left, suggesting an increase in stability. This is contrast with existing literature, which show a deterioration of stability when moving the CG aft, Van Overeem suggested that this has to do with the contribution of C_{Y_p} .

Van Overeem also performed a handling quality analysis on the Flying-V for the two conditions and the two CG configurations. The analysis suggested that most of the eigenmodes display Level 1 or 2 handling qualities, although room for improvement remains. One of the findings showed that moving the CG aft deteriorates the handling qualities from Level 1 to Level 2, following a decrease in the CAP value, indicating a more sluggish response.

c) **Which stability & control augmentations systems have been applied to the Flying-V?** To stabilize some of the unstable eigenmodes and improve the handling criteria of the Flying-V, stability and control augmentations systems can be utilized. Previous work on the Flying-V has looked at a traditional PID-based pitch-rate controller to improve the low-speed handling qualities. Moreover, a DRL based attitude controller was proposed. In addition, several INDI-based control laws have been implemented, showing promising results. Van Overeem presented two INDI-based augmentation systems, a SAS and a CAS and proceeds to conclude that the previously unstable dynamic modes during approach were stabilized. In addition, van Overeem states that the closed-loop remains stable up to 20% of uncertainty in the aerodynamic parameters.

Stougie [24] later introduced a C^* -controller with a INDI-based inner loop with the addition of FEP. Stougie assessed the the handling qualities for the cruise and approach conditions earlier defined by van Overeem [47] and suggested that for sufficiently fast body rate sensors, displaying a maximum time-delay of 0.04s, the aircraft displays Level 1 handling qualities. Moreover, Stougie assessed the stability margins in the presence of sensor dynamics. He concluded that the controllers remains stable for sampling times smaller than 0.1s. Stougie further suggested that the closed-loop system is robust up to 20% of aerodynamic uncertainty. Yet also states that the effect of various other phenomena, such as CG mismatch, aeroelastic effects and time-delays remain to be studied.

d) **What is the state-of-the-art on INDI-based flight control design?**

INDI-based control law design has been praised for its simplicity, cost effectiveness and robustness to parametric uncertainty. Various renditions of INDI have emerged over the years, such as EINDI and Hybrid INDI. These have emerged in an attempt to deal with some of the issues commonly seen in SB-INDI-based control laws. An issue with SB-INDI-based control laws is the need for accurate state derivative and input measurements. These may not always be present or may introduce time-delays. Grondman et al. [32] highlighted this issue and emphasized that the input measurement and state derivative measurement have to be synchronized in time to prevent stability and performance degradation. Van 't Veld et al. [30] concluded that additional body rate measurement delay has a greater destabilizing effect than additional actuator measurement delay.

In an attempt to alleviate issues associated with synchronization delay, Kumtepe et al. [33] proposed Hybrid INDI. Proposing a complementary filter that fuses a model-based estimate with sensor measurement to generate the angular acceleration estimate. Kumtepe et al. state that this makes it such that the high-frequency dynamics are captured by the onboard-model, whereas the low-to-medium frequency dynamics are captured by the sensor measurement. Simulations performed by Kumtepe et al. demonstrated that Hybrid-INDI outperforms regular SB-INDI. Moreover, it was demonstrated that the Hybrid-INDI controller can tolerate larger time-delays before destabilizing when compared to SB-INDI.

A reoccurring theme throughout the state-of-the-art research on INDI has been its robustness properties. Multiple studies have observed a level of robustness to aerodynamic uncertainty. Yet it has been observed that INDI-based control laws are sensitive to time-delays. These observations have

highlighted the need for more rigorous stability and robustness insights into INDI-based control laws. Wang et al. [34] were the first to establish formal nonlinear stability and performance properties of INDI-based control laws as a function of sampling rate. However, the analysis was limited to regular perturbations and exogenous disturbances. As stated, time-delays have been shown to have the greatest destabilizing effect on INDI-based control laws. Time-delay is part of the category of singular perturbations. As such, a thorough stability and robustness analysis of INDI must include singular perturbations. Wang et al. [34] briefly considered these, yet left a detailed analysis as future work. More recently, the research community has started to recognize the importance of studying the effect of singular perturbations. Yet, most of these studies assume that all model uncertainty and singular perturbations can be parameterized. It is well known that, for physical systems, these can not be parameterized. These include unknown structural dynamics and aerodynamic effects, such as those seen on the Flying-V. These are by definition unstructured (non parametric) by nature and can be captured by norm-bounded uncertainty descriptions. Pollack [35] argues that to adequately assess the stability and robustness of INDI-based control laws, these unstructured uncertainties must be included. Pollack establishes a systematic formal robustness analysis of INDI-based control law, making use of the \mathcal{H}_∞ -framework. This framework is established in the following chapter.

Robust Control methods for Flight Control applications

This chapter serves to introduce the multivariate linear control framework and the tools enabling a robust stability & performance analysis, which is provided in section 3.1. Subsequently, its application to FCS design is reviewed in section 3.2. Finally, a robust stability & analysis of INDI-based control laws is provided in section 3.3. As such, this chapter aims to answer research question 2, which is restated hereafter.

How can \mathcal{H}_∞ -control tools be used to establish robust INDI-based control system designs?

3.1. Introduction to multivariate linear control analysis

The tools that enable a robust stability & performance analysis of (I)NDI or any other feedback-based control laws are rooted in multivariate linear control analysis. In words, a control system is robust if it ensures stability and performance in the presence of mismatches between the actual system and the model of the system used to design the controller. This has not always been of utmost interest to researchers in mathematical control theory, until a revolution occurred. Such were the words of Safonov in a paper on the origins of robust control [87].

Robust control as a field of study formally emerged in the late 1970s. According to Safonov, a gap between mathematical control theorist and control engineers had emerged in the 1960s. As mathematical control theorists considered the root-locus and frequency domain methods used in engineering practice as simplistic and sought to pose feedback design as a mathematical optimization problem. These optimization formulations did however not have explicit representations of robustness in their definitions. According to Safonov, the first mathematical definition of a robust feedback problem dates back to 1963, when Horowitz recognized that plant uncertainty is the limiting factor to what can be achieved with a feedback control system [88]. This work would go on to be unnoticed by control theorists initially, this took a turn in the early seventies.

A group of researchers at MIT led by Athans attempted to apply optimization-based control methods to the design of complex multivariate feedback controllers for military aircraft and submarines [89, 90]. To the surprise of the researchers, their controllers failed. A lack of attention to robustness was identified as the leading cause in these failures. In 1976, Athans' team at MIT shifted their attention to developing methods for analyzing and optimizing the robustness of feedback control systems, seeking multivariate generalizations of Horowitz's ideas [88]. This marked the birth of robust control as a field of study and signified a paradigm shift in control theory [87].

Broadly speaking, robust control can be split into two parts, robust stability & performance analysis and robust controller synthesis. The former pertains to the analysis of the stability & performance characteristics of a closed-loop system. The latter revolves around the synthesis of a controller that adheres to certain stability & performance requirements. These two parts are complementary and typically follow a structured workflow. Skogestad et al. define the following workflow [36].

1. Determine the uncertainty set. In other words, find a mathematical representation of the model uncertainty (specifying what we know that we don't know).

2. Check Nominal Stability (NS), check the stability of the unperturbed system $G(s)$.
3. Check Robust Stability (RS), determine whether the system remains stable for all plants in the defined uncertainty set.
4. Check Robust Performance (RP), if RS is satisfied, determine whether the performance specifications are met for all plants in the uncertainty set.
5. Robust controller synthesis, if necessary, design a controller that does provide RS and RP.

According to Skogestad et al., this approach does not always guarantee optimal performance, especially if the worst-case plant rarely or never occurs. In that case, they suggest the use of other approaches, such as optimizing average performance or applying adaptive control methods [36].

The foundational tools that are used throughout robust control are presented hereafter, the majority of the conventions regarding notation and definition follow from the work of Skogestad [36], unless explicitly stated otherwise.

3.1.1. Norms and Singular values

Many of the analysis and synthesis tools in Robust Control rely on the evaluation of the norm of a signal. A signal can be evaluated according to various norms. In the context of robust control, commonly seen norms are the \mathcal{H}_2 and the \mathcal{H}_∞ norms. Consider some stable, rational system $G(s)$ that maps some input w to some output z . A question that arises is, how large can the output z become if the system G is given the input w ? To answer this question, the notion of the norm of a system is a useful one. In the context of multivariate control analysis, two commonly seen norms are the \mathcal{H}_∞ and \mathcal{H}_2 norm, where \mathcal{H} refers to the Hardy space. \mathcal{H}_∞ refers to the Hardy space of the set of transfer functions with bounded ∞ -norm, which is the set of *stable and proper* transfer functions. Similarly, \mathcal{H}_2 refers to the Hardy space of transfer functions with a bounded 2-norm (l_2 -norm), which is the set of *stable and strictly proper* transfer functions. For a comprehensive introduction to these norms and their value in the context of control system design, the reader is referred to the material provided by Mackenroth [91].

Consider some stable, *strictly proper* system $G(s)$, its \mathcal{H}_2 -norm is obtained using the Frobenius norm (using a matrix description of $G(s)$) and integrating over frequency.

$$\|G(s)\|_2 \triangleq \sqrt{\frac{1}{2\pi} \int_{-\infty}^{\infty} \text{tr}(G(j\omega)^H G(j\omega)) d\omega} \quad (3.1)$$

Analogously, by Parseval's theorem, the \mathcal{H}_2 -norm of $G(s)$ is equal to the \mathcal{H}_2 -norm of the impulse response.

$$\|G(s)\|_2 = \|g(t)\|_2 \triangleq \sqrt{\int_0^{\infty} \text{tr}(g(\tau)^T g(\tau)) d\tau} \quad (3.2)$$

It can be shown that the \mathcal{H}_2 -norm of $G(s)$ is equivalent to the 2-norm output resulting from applying unit impulses to each input, as follows.

$$\|G(s)\|_2 = \max_{w(t)=\text{unit impulses}} \|z(t)\|_2 \quad (3.3)$$

Consider now some stable, *proper* system $G(s)$, the \mathcal{H}_∞ -norm of the system is defined as the peak singular value over frequency:

$$\|G(s)\|_\infty \triangleq \max_{\omega} \bar{\sigma}(G(j\omega)) \quad (3.4)$$

A similar time-domain interpretation of the \mathcal{H}_∞ -norm exists namely, it provides a measure of the largest gain for sinusoidal inputs at any frequency. The equivalent time-domain definition is shown in equation 3.5

$$\|G(s)\|_\infty = \max_{w(t) \neq 0} \frac{\|z(t)\|_2}{\|w(t)\|_2} = \max_{\|w(t)\|_2=1} \|z(t)\|_2 \quad (3.5)$$

Analogously, equation 3.5 implies that the \mathcal{H}_∞ -norm can be interpreted as the l_2 gain by which the energy of the input signal w is amplified.

Both of these norms are used throughout control engineering, within the context of robust control design, design goals are often related to minimizing the \mathcal{H}_2 -norm or \mathcal{H}_∞ -norm of some transfer function. Skogestad summarizes the goals of these two methods elegantly as follows [36].

- Minimizing \mathcal{H}_∞ -norm : "push down peak of largest singular value". (In other words, minimizing peak gain in worst possible direction at worst possible frequency)
- Minimizing \mathcal{H}_2 -norm : "push down the whole thing". In other words, minimizing all singular values over all frequencies (average direction, average frequency)

3.1.2. Generalized interconnection structures

In the context of \mathcal{H}_∞ -control, one is typically interested in minimizing some norm of the closed loop control system. The notion of an closed-loop LFT, as introduced by Doyle [92], is a very useful one in this context. The standard closed-loop LFT interconnection structure is depicted in figure 3.1. Where $u \in \mathbb{R}^{n_u}$ is defined as the control vector, $y \in \mathbb{R}^{n_y}$ as the measured output vector, $w \in \mathbb{R}^{n_w}$ as the vector of exogenous inputs and $z \in \mathbb{R}^{n_z}$ is defined as the vector of exogenous outputs. This LFT structure is referred to as $F_l(P, K)$

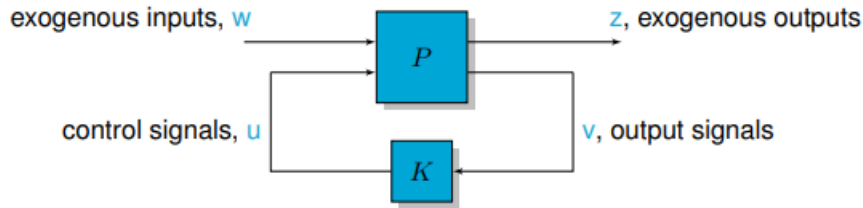


Figure 3.1: Standard closed-loop LFT interconnection, from [93]

The generalized plant P and the controller K can be described in terms of a state-space description and can be partitioned, as seen in equations 3.6 and 3.7 respectively.

$$P = \begin{cases} \dot{x} = Ax + B_1w + B_2u \\ z = C_1x + D_{11}w + D_{12}u \\ y = C_2x + D_{21}w + D_{22}u \end{cases}, \quad P(s) = \left[\begin{array}{c|cc} A & B_1 & B_2 \\ \hline C_1 & D_{11} & D_{12} \\ C_2 & D_{21} & D_{22} \end{array} \right] \quad (3.6)$$

$$K = \begin{cases} \dot{x}_K = A_Kx_K + B_Ky \\ u = C_Kx_K + D_Ky \end{cases}, \quad K(s) = \left[\begin{array}{c|c} A_K & B_K \\ \hline C_K & D_K \end{array} \right] \quad (3.7)$$

In \mathcal{H}_∞ -control, the general problem in terms of the generalized LFT structure discussed above is defined as follows.

$$\begin{aligned} & \text{Minimize } \|F_l(P, K)\|_\infty \\ & \text{Where } K \text{ stabilizes } P \\ & K \in \kappa \end{aligned} \quad (3.8)$$

In words, the \mathcal{H}_∞ -control problem is defined as: find some optimal controller $K^* \in \kappa$ that minimizes the l_2 -gain from the exogenous input signals w to the exogenous output signals z whilst rendering P internally stable. Examples of exogenous input signals are atmospheric disturbances, sensor noise and pilot inputs. Examples of exogenous output signals could be a tracking error signal or a plant input/output signal. Typically, multiple signals are to be minimized and are weighted and stacked onto one another, this will be discussed in section 3.2.

3.1.3. Uncertainty Modelling

In the context of designing a robust controller, one is interested in examining the stability and performance of the resulting control system in the presence of uncertainty. When considering model uncertainty, the dynamic behavior of a plant is no longer described by a single model but by a set of possible models. The set of possible plants is typically referred to as the uncertainty set Π , containing both the nominal plant $G(s)$ and all of the perturbed plants $G_p(s)$. Uncertainties stem from a variety of sources but can, broadly speaking, be distinguished into two main categories.

- I Parametric (real) uncertainty: The model structure, including the order of the model are known, yet some of the parameters are uncertain.

- II Dynamic (complex), typically frequency dependant, uncertainty: The model error stems from missing dynamics.

A typical source of parametric uncertainty is uncertainty in aerodynamic coefficients, which are typically not perfectly known. Dynamic uncertainty often pertains to unmodeled or neglected dynamics. These may stem from nonlinear flow effects, structural coupling or deliberate model-reduction. As such, to accurately capture the dynamic behavior of a plant, the model must include:

- i A model of the nominal plant.
- ii A model of the uncertainties.

Parametric uncertainty

Parametric uncertainty is typically represented by describing a perturbed parameter with defined upper and lower bounds. Consider a perturbed parameter α_p , the set of all possible values of α_p can be represented as:

$$\alpha_p = \bar{\alpha}(1 + r_\alpha \Delta) \quad (3.9)$$

Where $\bar{\alpha}$ represents the mean parameter value, r_α represents the relative uncertainty and Δ is any real scalar satisfying $|\Delta| \leq 1$.

Dynamic uncertainty

Dynamic uncertainty is typically described in the frequency domain. This representation leads to the notion of normalized complex perturbations of the form $\|\Delta\|_\infty \leq r$, with r being some constant. Dynamic uncertainty can be further subdivided into a number of categories, as follows.

1. Additive and inverse additive perturbations:

$$\begin{aligned} G_p(s) &= G(s) + \Delta(s) \\ G_p^{-1}(s) &= G^{-1}(s) + \Delta(s) \end{aligned} \quad (3.10)$$

2. Input and output multiplicative perturbations:

$$\begin{aligned} G_p(s) &= G(s)[I + \Delta(s)] \\ G_p(s) &= [I + \Delta(s)]G(s) \end{aligned} \quad (3.11)$$

3. Inverse input and output multiplicative perturbations:

$$\begin{aligned} G_p^{-1}(s) &= [I + \Delta(s)]G^{-1}(s) \\ G_p^{-1}(s) &= G^{-1}(s)[I + \Delta(s)] \end{aligned} \quad (3.12)$$

4. Left and Right coprime factor perturbations:

$$\begin{aligned} G_p(s) &= (\tilde{M} + \Delta_{\tilde{M}})^{-1}(\tilde{N} + \Delta_{\tilde{N}}) \\ G_p(s) &= (\tilde{N} + \Delta_{\tilde{N}})(\tilde{M} + \Delta_{\tilde{M}})^{-1} \end{aligned} \quad (3.13)$$

Additive uncertainty descriptions provide a measure of absolute error between the actual dynamics and the nominal model. Multiplicative descriptions provide a measure of relative error. Note that $\Delta(s)$ is often replaced by $W(s)\Delta(s)$, where $W(s)$ is some weighting function used to represent the spectral content of the uncertainty and $\Delta(s)$ is normalized, such that $\|\Delta(s)\|_\infty \leq 1$.

Coprime factor perturbations are based on a different concept. Namely, it hinges on the concept that a plant $P(s)$ can be expressed as a ratio of two transfer function N and M that do not have common factors (they are coprime). Subsequently, the perturbations are added to these transfer functions in the form of $\Delta_{\tilde{N}}$ and $\Delta_{\tilde{M}}$.

An advantage of the additive and/or multiplicative description is that it is rather intuitive. However, the descriptions hinge on the fact that the uncertainties $\Delta(s)$ are constrained to stable transfer matrices. This in turn implies that every model in the uncertainty set has the same number of right half plane poles as the nominal plant. Thus, these uncertainty models can not be used to describe a situation where uncertainty

drives a stable system to become unstable. In an aircraft this can occur due to CG position changes for example, as illustrated in [94]. On the contrary, coprime-factor uncertainty descriptions are capable of capturing this behavior. Moreover, Bates [94] states that coprime-factor perturbations are better suited to describe uncertainty in the vicinity of lightly damped resonant poles. The uncertainty descriptions used in this research are based on additive and multiplicative uncertainties.

For the purpose of analysis and synthesis in the presence of norm bounded uncertainty, it is typically the case that the various sources of uncertainty in a plant are lumped into a single (diagonal) uncertainty matrix, such that:

$$\Delta(s) = \begin{bmatrix} \Delta_1(s) & & \\ & \ddots & \\ & & \Delta_n(s) \end{bmatrix} \quad (3.14)$$

Note that for the SISO case, this is rather straightforward. In the case of a MIMO plant, this may not work well according to Skogestad and requires additional care [36]. Subsequently, the closed-loop description of a perturbed plant can be represented as follows

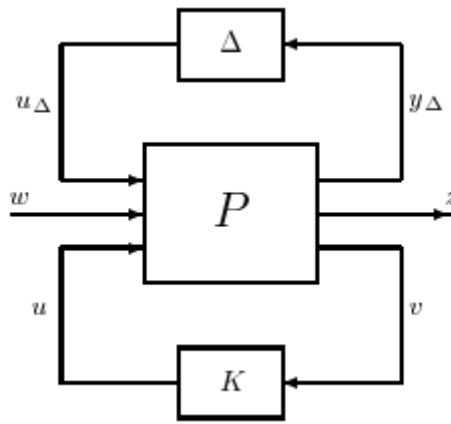


Figure 3.2: General control configuration with perturbations, from [36]

The general configuration shown in 3.2 can be further split up into the known parts of the plant N and the unknown part Δ . This is obtained by making use of the lower linear fractional transformation (LFT) of P and K , which is defined by:

$$N = F_l(P, K) \triangleq P_{11} + P_{12}K(I - P_{22}K)^{-1}P_{21} \quad (3.15)$$

This results in the so called $N\Delta$ -structure, depicted in figure 3.3.

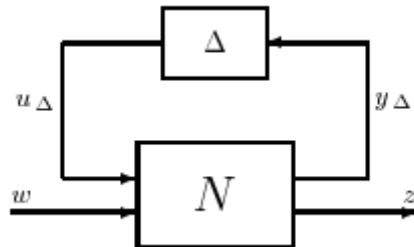


Figure 3.3: $N\Delta$ -structure, from [36]

Similarly, the closed-loop transfer function relating w to z , $z = Fw$ is related to N and Δ by an upper LFT, as seen in equation 3.16.

$$F = F_u(N, \Delta) \triangleq N_{22} + N_{21}\Delta(I - N_{11}\Delta)^{-1}N_{12} \quad (3.16)$$

To analyze the robust stability of F , as defined in equation 3.16, the system is typically rearranged into the so-called $M\Delta$ -structure, depicted in figure 3.4.

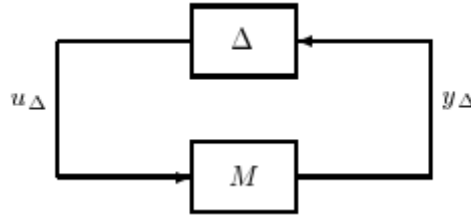


Figure 3.4: $M\Delta$ -structure, from [36]

Where $M = N_{11}$, represents the transfer function from the output to the input of the perturbation block. The various generalized interconnection structures each have their purpose in the context of robust analysis and synthesis, as will be elaborated hereafter.

3.1.4. Robust analysis & synthesis

Robust Stability & Robust Performance definitions

Once the types of uncertainty present in a control system are established, RS and RP analysis can be assessed. Making use of the closed-loop definition of the $M\Delta$ -structure as seen in figure 3.4 and applying the generalized Nyquist stability criterion (assuming M is stable), robust stability is ensured iff. the following determinant stability condition holds, for both real and/or complex perturbations [36].

$$\begin{aligned} & \text{Nyquist plot of } \det(I - M\Delta(s)) \text{ does not encircle origin, } \forall \Delta \\ & \Leftrightarrow \det(I - M\Delta(j\omega)) \neq 0, \forall \omega, \forall \Delta \\ & \Leftrightarrow \lambda_i(M\Delta) \neq 1, \forall i, \forall \omega, \forall \Delta \end{aligned} \quad (3.17)$$

If one considers the case where $\Delta(s)$ is any full complex transfer function matrix satisfying $\|\Delta\|_\infty \leq 1$, it can be shown that the RS condition reduces to.

$$RS \Leftrightarrow \bar{\sigma}(M(j\omega))\bar{\sigma}(\Delta(j\omega)) < 1, \forall \omega, \forall \Delta \quad (3.18)$$

RP is characterized by the magnitude of the transfer function from the exogenous inputs w to the exogenous outputs z . As such, the RP condition can be formulated as a RS condition on the transfer function $z = F(\Delta)w$, as seen in equation 3.16. As such, RP is guaranteed if the following holds.

$$\|F(\Delta)\|_\infty \leq 1, \forall \Delta, \|\Delta\|_\infty \leq 1 \quad (3.19)$$

The structured singular value μ

It is typically the case that uncertainty in aerospace systems is related to variations in specific, known parameters. As such, structured uncertainty descriptions are often possible [94]. Assume that all of the uncertainties can be captured in a block diagonal uncertainty matrix as follows.

$$\Delta(j\omega) = \text{diag}(\Delta_1(j\omega), \dots, \Delta_n(j\omega)), \bar{\sigma}(\Delta_i(j\omega)) \leq k \forall \omega \quad (3.20)$$

Moreover, assume that the nominal closed-loop system is stable. The following question then arises, how large can k get before the closed-loop system becomes unstable? Such that $(I - M\Delta)$ is rendered singular. Applying the small gain theorem (SGT) to this question yields conservative results [94]. Therefore, Doyle introduced the notion of the structured singular value (SSV) μ , which is formally defined as follows [95].

$$\mu_\Delta(M) \triangleq \frac{1}{\min_{\Delta \in \Delta} \{\bar{\sigma}(\Delta(j\omega)) \mid \det(I - M\Delta) = 0\}} \quad (3.21)$$

As such, the SSV is a measure for how small of an uncertainty a closed-loop system can tolerate before it becomes unstable, i.e. how robust it is. Ironically enough, Safonov introduced the notion of the

Multivariate Stability Margin k_m in the same journal as Doyle's SSV definition [96]. Where k_m is defined as the reciprocal of the SSV: $k_m(M) = \mu(M)^{-1}$, which perhaps provides a more intuitive definition of a robustness margin. The RS condition in terms of the SSV can be defined as follows.

$$\text{RS iff. } \Leftrightarrow \mu(M(j\omega)) < 1, \forall \omega \quad (3.22)$$

Similarly, the RP condition can be formulated in terms of the SSV. Ultimately, all of the nominal and robust stability & performance criteria can be formulated in terms of the $N\Delta$ -structure, as summarized in equation 3.23. These definitions are defined like those established by Skogestad et al. in [36].

$$\begin{aligned} \text{NS: } & N \text{ is internally stable} \\ \text{NP: } & \bar{\sigma}(N_{22}) = \mu_{\Delta_p} < 1, \forall \omega \text{ and NS} \\ \text{RS: } & \mu_{\Delta}(N_{11}) < 1, \forall \omega \text{ and NS} \\ \text{RP: } & \mu_{\hat{\Delta}}(N) < 1, \forall \omega, \hat{\Delta} = \begin{bmatrix} \Delta & 0 \\ 0 & \Delta_p \end{bmatrix} \text{ and NS} \end{aligned} \quad (3.23)$$

Where Δ represents a block-diagonal matrix containing the uncertainties and Δ_p is a full complex matrix representing the \mathcal{H}_∞ performance specifications.

The calculation of the SSV turns out to be a NP hard problem [97]. As such, computing the exact value of μ is practically impossible. Alternatively, upper and lower bounds on the value of μ are typically computed. The complexity of computing these bounds depends on the type of uncertainty: complex, real or mixed. In the simplest case, the case of purely complex uncertainty, Packard et al. [98] demonstrated that the lower bound $\underline{\mu}$ and upper bound $\bar{\mu}$ can be calculated as follows.

$$\begin{cases} \underline{\mu} : \mu(M) = \max_{U \in \mathcal{U}} \rho(MU) \\ \bar{\mu} : \mu(M) \leq \min_{D \in \mathcal{D}} \bar{\sigma}(DM D^{-1}) \end{cases} \quad (3.24)$$

Where \mathcal{U} is the set of all unitary matrices U with the same block-diagonal structure as Δ and \mathcal{D} is the set of matrices D that commute with Δ [94]. Fan et al. [99] provide a method for computing the upper bound of μ for mixed real and dynamic uncertainty. Various other methods have been established, including the LMI-based method proposed by Balakrishnan [100]. These outer-relaxation based methods provide conservative results according to Apkarian et al., who propose alternative inner relaxation-based techniques [101].

An alternative approach to solving the μ -problem is provided by a more general framework provided by integral quadratic constraints (IQCs) [102]. According to Pollack, the IQC framework extends the scope of μ -theory to a wider context. The IQC approach to μ -analysis is beyond the scope of this research. For an elaborate description of the use of IQCs in the context of robust control analysis & design, the reader is referred to [102, 35].

\mathcal{H}_∞ -optimal controller synthesis

As seen in equation 3.8, \mathcal{H}_∞ -control problems are concerned with the minimization of the norm on the closed-loop interconnection structure. In practice, finding an optimal solution to the \mathcal{H}_∞ problem is not required. A sub-optimal solution is computationally and theoretically simpler to obtain and suffices. If γ_{min} represents the minimum value of $\|F_l(P, K)\|_\infty$ over all stabilizing controllers K , the sub-optimal control becomes the following [36].

$$\begin{aligned} & \text{Given } \gamma > \gamma_{min}, \\ & \text{Find all stabilizing controllers } K \text{ such that: } \|F_l(P, K)\|_\infty < \gamma \\ & \text{Where } K \text{ stabilizes } P \\ & K \in \kappa \end{aligned} \quad (3.25)$$

This problem was first formally defined by Zames back in 1981, although he first recognized the problem back in the 1960s [103]. In a keystone 1989 paper, Doyle et al. [104] demonstrate that solving the \mathcal{H}_∞ -problem requires solving two algebraic Riccati equations (ARE). In 1994, Gahinet and Apkarian provide an alternative solution, reducing it to a linear matrix inequality (LMI) [105]. Several solutions to

the problem have emerged over the years [106].

The solutions provided throughout the 80s and 90s based on solving AREs and LMIs are all obtained within the full-order controller space κ_{full} , which is a convex problem [105]. As such, the obtained controller will be of the same order as the generalized plant P , which may be of very high order. This was deemed unpractical by control engineers at the time, whom preferred the use of simple control elements like PIDs, low-order filters, etc.

Finding a solution in a smaller and more practical controller space is a significantly harder problem. In the late 90s, Apkarian and Noll investigated the use of bilinear matrix inequalities (BMIs) for feedback controller synthesis and recognized it as the solution that would allow for structured controller design. The difficulty in solving the structured \mathcal{H}_∞ -problem lies in the fact that it is non-convex and non-smooth, as well as posing closed-loop stability issues.

Apkarian et al. [107] proposed a non-smooth optimization method synthesis method enabling \mathcal{H}_∞ -synthesis of structured control laws in a seminal 2006 paper. The problem now being described by the following \mathcal{H}_∞ -objective function [107].

$$\min_{\kappa} \max_{\omega \in \mathbb{R}} \bar{\sigma} \left(C(K(\kappa))(j\omega I - A(K(\kappa)))^{-1} B(K(\kappa)) + D(K(\kappa)) \right) \quad (3.26)$$

Where κ are design parameters of the structured controller. This functionality became available to the public in 2010, when it was incorporated into the Matlab function *Hinfstruct* [37]. Following the introduction of the non-smooth optimization method, various extensions followed. Including multi-objective mixed $\mathcal{H}_2/\mathcal{H}_\infty$ -synthesis [108], multidisk problems and limited frequency intervals, which are described in [106].

Robust controller synthesis

The standard (un)structured \mathcal{H}_∞ -problem definition does not consider any uncertainty in the definition of the plant P . As such, the resulting optimal controller K is only optimal for the nominal plant definition. In reality, uncertainty is omnipresent, this problem has long been recognized in the control community. Accordingly, methods for synthesizing robust controllers have emerged. These tools essentially combine μ -analysis with \mathcal{H}_∞ -synthesis and are named μ -synthesis accordingly. The arising problem is the following. Consider a plant P subject to some structured uncertainty Δ , with controller K and consider $M(P, K) = F_l(P, K)$. The optimization problem w.r.t. the RS and RP conditions summarized in equation 3.23, can be formulated as follows [109].

$$\inf_{K(s)} \sup_{\omega \in \mathbb{R}} \mu [M(P, K)(j\omega)] \quad (3.27)$$

In 1985, Doyle first proposed an iterative method to solve this problem, known as D-K iterations [110]. The procedure involves a two-step iterative approach, alternating between computing the upper bound on μ (D-step) and solving a suboptimal unstructured \mathcal{H}_∞ -problem (K-step). The starting point is the upper bound on μ as defined in equation 3.24. The goal is to find the controller that minimizes the \mathcal{H}_∞ -norm of this upper bound, such that

$$\min_K \left(\min_{D \in \mathcal{D}} \|DM(K)D^{-1}\|_\infty \right) \quad (3.28)$$

This is achieved by alternating between minimizing the norm w.r.t. either K or D, whilst holding the other fixed. To initiate the process, an initial rational stable transfer matrix $D(s)$ is chosen (typically the identity matrix). The iterations proceed as follows [36].

1. K-step, synthesize a \mathcal{H}_∞ controller for the scaled problem $\min_K \|DM(K)D^{-1}\|_\infty$ with fixed $D(s)$.
2. D-step, find $D(j\omega)$ to minimize at each frequency $\bar{\sigma}(DMD(j\omega))$ with fixed M.
3. fit the magnitude of each element of $D(j\omega)$ to a stable and minimum-phase transfer function $D(s)$ and return to step 1.

This process is continued until satisfactory performance is achieved, such that $\bar{\mu} < 1$ or until the \mathcal{H}_∞ -norm no longer decreases. Each of these steps separately are convex, joint convexity is however not guaranteed. As such, the process may converge to a local optimum and no global optimality guarantees are provided. Nonetheless, the method has often been found to work sufficiently well in practice [36]. It must be stated that the D-K iterations method makes use of a structured complex (dynamic) uncertainty description. As such, real (parametric) uncertainties are also described as complex uncertainty, which

may yield conservative results.

An alteration to the D-K iterations was proposed by Young et al. [111] in 1994 in the form of D,G-K iterations, which does consider mixed real and complex perturbations. It boils down to finding the scaling matrices D and G that minimize the upper bound of the mixed μ . The upper bound now being defined by the following expression.

$$\Gamma = \bar{\sigma} \left(\left(\frac{DM D^{-1}}{\beta} - jG \right) (I + G^2)^{-\frac{1}{2}} \right) \quad (3.29)$$

Where β is a real positive scalar. A thorough, step-by-step description of the D,G-K iteration process borrowed from [112] is shown in appendix A.

These iterative schemes belong to the category of outer-relaxation techniques. Apkarian [113] highlights the shortcoming of these techniques, raising concerns about the numerical stability and accuracy of these methods. Another issue is the size inflation in the controller order, as classical \mathcal{H}_∞ -synthesis is a full-order method, the plant order and the order of the D -scalings accumulate in the resulting controller K . Hence for practical purposes, controller order reduction is required. In 2010, Apkarian [113] proposes a mixed μ -synthesis method based on non-smooth optimization. The proposed method incorporate the D,G-scaling as specially structured controller elements. In the proposed setup, the controller and scalings are computed simultaneously as parts of a fictitious block-diagonal controller [113]. The method belongs to the category of inner-relaxation methods.

The \mathcal{H}_∞ -objective of the mixed parametric control problem can be formulated as the following semi-infinite minmax optimization problem

$$\min_{\kappa \in \mathbb{R}^n} \max_{\Delta \in \mathbf{\Delta}} \|T_{w \rightarrow z}(\Delta, K)\|_\infty \quad (3.30)$$

Where $K(\kappa)$ represents some structured control law [106]. Ultimately, the non-smooth structured controller synthesis method established earlier and the newly proposed inner-relaxation techniques were incorporated into the Matlab design tool *ystune* in 2012, which can be seen as a successor to *hinfstruct*. One of the main advantages of the nonsmooth methods is that they facilitate multi-model and multi-objective structured control design. In later works by Apkarian et al. and Aguiar et al. [101, 114], new methods for solving harder parametric robust synthesis problems are proposed. Apkarian et al. [101] presents a method based on so called *dynamic inner approximation*, which was later incorporated into Matlab's Robust Control Toolbox [37]. Aguiar et al. [114] present three relaxation approaches to the mixed parametric synthesis problem and compared these. The proposed inner-relaxation method produced the best results of of the three. Moreover, the methods were compared with classical D,G-K iterations. Aguiar et al. concluded that despite its age, D,G-K iterations performed remarkably well, though not outperforming the newly proposed methods [114]. For an elaborate overview of the different \mathcal{H}_∞ -methods proposed over the years, the reader is referred to [106].

Note that most of the software tools that have been developed over the years are embedded in the Matlab *Robust Control Toolbox* [37]. As of today, no alternative (open source) platforms offer the more advanced methods beyond basic full-order \mathcal{H}_∞ -synthesis, which is also found in the *Python Control Systems Library* [115].

3.2. Practical robust control design methods

As established in section (refer to previous section), solving the robust control problem requires an appropriate description of the respective elements P , Δ and K (in case of a structured controller). Moreover, this formulation enables the concept of multivariate transfer function shaping. This pertains to the shaping of the singular values of any of the open-loop and closed-loop transfer function contained in the \mathcal{H}_∞ -problem definition. This section provides an overview of some commonly seen methods for shaping these transfer functions and the rationale behind these methods.

Prior to discussing these different methods, it is worth stating the fundamental trade-off in MIMO feedback design. Doyle and Stein first generalized the ideas of loop-shaping to multivariate systems in their seminal 1981 paper [116]. As will be seen in some of the methods presented, closed-loop design requirements are often cast on the sensitivity S , complementary sensitivity T and the control sensitivity KS . Recall that the relation between these is given by $S + T = I$. As such, one can not constrain both S and T in the same frequency range, even if this might be desirable. Requirements on the closed-loop transfer functions might therefore be in conflict with one another. As so elegantly stated by Skogestad [36] "Feedback design is therefore a trade-off over frequency of conflicting objectives".

This might not always be problematic, as the frequency ranges over which the different design goals are important are often disjoint from one another. Classical loop-shaping is concerned with shaping the magnitude of $L = GK$, whereas MIMO design requirements are formulated in terms of closed-loop requirements. Given the relation $S = (I + L)^{-1}$, it follows that

$$\underline{\sigma}(L) - 1 \leq \frac{1}{\bar{\sigma}(S)} \leq \underline{\sigma}(L) + 1 \quad (3.31)$$

As such, several closed-loop requirements can be formulated in terms of the bounds on the singular value of the multivariate open-loop $\sigma(GK)$. The illustration in figure 3.5 provides a comprehensive summary of perhaps the central idea in (multivariate) robust feedback control, the shaping of $\bar{\sigma}(GK)$. The crossover frequency ω_c plays a crucial role, as it reflects the bandwidth of the feedback loop, which provides insight into the stability and performance characteristics of the feedback control system. The higher the bandwidth of the feedback loop, the better the robust performance, disturbance rejection and its capability of stabilizing low-frequency unstable modes. This comes at the cost of increased actuator activity, decreased stability margins and an increased sensitivity to high-frequency noise. Lowering the crossover frequency has the opposite effect.

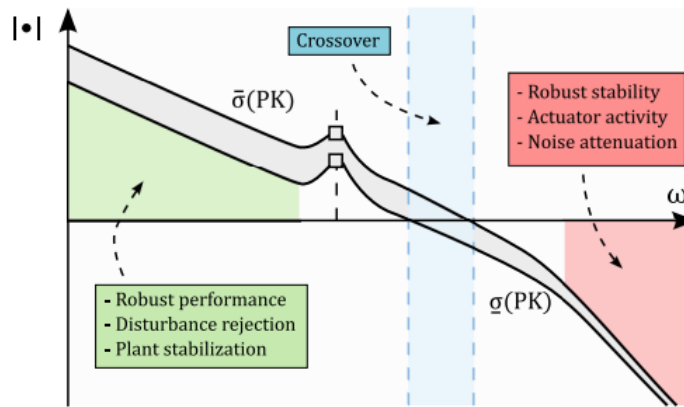


Figure 3.5: Loop shape specification, adopted from [35]

Horowitz recognized this in his 1963 work [88] and dubbed it *the fundamental costs of feedback*. This ultimately stems from a fundamental conservation law of feedback control, the *Bode Integral* [85].

$$\int_0^{\infty} \ln|S(j\omega)| d\omega = 0 \quad (3.32)$$

In words, the log of the sensitivity function integrated over frequency must be zero. This implies that increased performance (in the \mathcal{H}_∞ -sense) in one frequency range comes at the expense of performance deterioration in another range. As comically depicted by Stein in the seminal 2003 paper [85], all of the modern (multivariate) feedback control design tools are essentially complicated shovels, digging up area under the sensitivity curve from one frequency range to the other. This can be traced back to the loop-shape of $\bar{\sigma}(GK)$ and its characteristics.

3.2.1. \mathcal{H}_∞ loop-shaping

\mathcal{H}_∞ loop-shaping was first introduced by Glover and Mcfarlane in 1990 [117]. It essentially combines \mathcal{H}_∞ robust stabilization with classical loop shaping and consists of two steps. The first step entails open-loop shaping with the use of pre-and-post-compensators W_1 and W_2 , such that $G_s = W_2GW_1$. Subsequently, the resulting open-loop G_s is robustified with respect to normalized coprime factor (NCF) uncertainty using \mathcal{H}_∞ optimization. Consider the following family of perturbed plant models.

$$G_{s,p} = \{(M_s + \Delta_{M_s})^{-1}(N_s + \Delta_{N_s}) : \|\Delta_{N_s} \Delta_{M_s}\|_\infty < \epsilon\} \quad (3.33)$$

Where ϵ is the stability margin. Robust stabilization of NCF plant descriptions is concerned with maximizing the value of this ϵ . It can be shown that the maximum value of the stability margin is given by the following [36].

$$\gamma_{min} = \epsilon_{max}^{-1} = \left\{ 1 - \left\| \begin{bmatrix} N_s & M_s \end{bmatrix} \right\|_H^2 \right\}^{-\frac{1}{2}} \quad (3.34)$$

Where $\| \cdot \|_H$ represents the Hankel norm. Ultimately, robust stability of a plant perturbed with NCF is guaranteed for a controller that satisfies the following [36].

$$\left\| \begin{bmatrix} K \\ I \end{bmatrix} (I - G_s K_s)^{-1} M_s^{-1} \right\|_{\infty} \leq \gamma \quad (3.35)$$

For some $\gamma > \gamma_{min}$. Note that since there exists an explicit expression for γ_{min} , seen in equation 3.34, an explicit solution to the \mathcal{H}_{∞} problem defined in equation 3.35 can be found by solving only two AREs, avoiding the need for an additional γ -iteration step.

The challenge of \mathcal{H}_{∞} loop-shaping becomes the selection of the weights in the pre- and post-compensators. Nonetheless, its simplicity and effectiveness have been demonstrated on many occasions, such as in [118, 119]. Although the method is widely used, it remains limited to the shaping of a single transfer function, the open-loop shape. This may pose challenges if multiple design goals are presented. Skogestad et al. [36] state that for design situations with multiple performance objectives, more complex design approaches may be more appropriate.

3.2.2. Mixed-Sensitivity design

Mixed-sensitivity \mathcal{H}_{∞} -control is based on the principle of stacking various closed-loop transfer functions on top of one another and minimizing the singular value of the resulting closed-loop system. This allows the designer to impose multiple, perhaps conflicting closed-loop requirements on the controller. Shaping the output sensitivity function $S_o = (I + GK)^{-1}$ is often chosen as the first requirement. Usually, the complementary output sensitivity function $T_o = I - S_o$ and/or the controller sensitivity $K S_o$ are chosen as the additional transfer functions to be shaped.

In order to actually shape these transfer functions, weighting filters are included in the description of the plant P , as shown in figure 3.6.

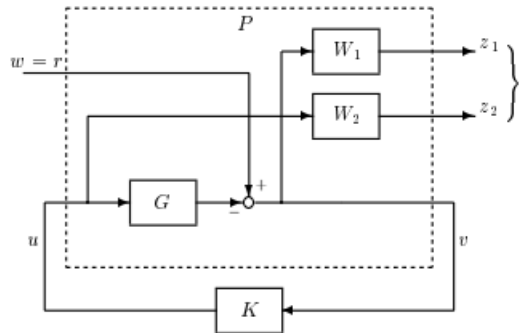


Figure 3.6: S/KS mixed-sensitivity minimization in its standard form [36]

Including the weighting filters in the plant definition results in the following definition of the \mathcal{H}_{∞} -problem.

$$\min \|F_l(P, K)\|_{\infty} = \min \left\| \begin{bmatrix} W_1(j\omega)S_o \\ W_2(j\omega)K S_o \end{bmatrix} \right\|_{\infty} \quad (3.36)$$

This can be extended to include the shaping of T_o , as follows.

$$\min \|F_l(P, K)\|_{\infty} = \min \left\| \begin{bmatrix} W_1(j\omega)S_o \\ W_2(j\omega)K S_o \\ W_3(j\omega)T_o \end{bmatrix} \right\|_{\infty} \quad (3.37)$$

Consider now the the sensitivity function S_o , which is a good indicator of closed-loop performance. One could imagine wanting to limit its peak magnitude at high frequencies to attenuate high frequency noise, such that $\|S(j\omega)\|_\infty \leq M$. Where M is some upper bound on the peak magnitude. this can be captured by an upper bound on the magnitude of S_o [36]. Such that:

$$\begin{aligned} |S(j\omega)| &< 1/W_1(j\omega), \forall \omega \\ \Leftrightarrow |W_1(j\omega)S_o(j\omega)| &< 1, \forall \omega \\ \Leftrightarrow \|W_1(j\omega)S_o(j\omega)\|_\infty &< 1 \end{aligned} \quad (3.38)$$

Naturally, it arises that in order to achieve a desired closed-loop shape for S_o , $W_1(j\omega)$ can be shaped such that its inverse represents the desired shape of S_o . This concept extends to choosing the shaping filters of the mixed sensitivity problem, as seen in equation 3.37. As such, the mixed sensitivity \mathcal{H}_∞ -problem formulation boils down to the following [36].

$$\|N\|_\infty = \max_{\omega} \bar{\sigma}(N(j\omega)) < 1, \quad N = \begin{bmatrix} W_1(j\omega)S_o \\ W_2(j\omega)KS_o \\ W_3(j\omega)T_o \end{bmatrix} \quad (3.39)$$

The \mathcal{H}_∞ -optimal controller is then obtained by solving the following problem [36].

$$\min_K \|N(K)\|_\infty \quad (3.40)$$

The rationale behind shaping the weighting filters, and therefore the sensitivity functions, can be summarized as follows.

- Shaping S_o , S_o is defined as the transfer function relating the output disturbance d_o to the output y . In order to provide good disturbance attenuation, S_o is desired to be small at low frequencies. Moreover, a minimum bandwidth frequency ω_b of the loop-shape L is typically desired to ensure adequate performance. In addition, the peak magnitude S_o at high frequencies ought to be limited. As such, W_1 is shaped such that its inverse resembles the desired shape of S_o . A common choice for W_1 is a lag-lead filter [36].
- Shaping KS_o , KS_o represents the transfer function from the output disturbance d_o to the control signal u . The low-frequency gain of KS_o is solemnly determined by the plant itself. Typically, one is interested in limiting the bandwidth of controller, to reduce high frequency noise amplification at the plant input and to prevent actuator rate saturation and associated wear-and-tear of the actuators. Moreover, high frequency roll-off is desired. As such, W_2 is often chosen to be a high-pass filter, such that its inverse resembles a low-pass filter. The crossover frequency of the filter is often set to the bandwidth of the actuator.
- Shaping T_o , T_o represents the complementary sensitivity, which is the transfer function relating the reference input r to the output y . To ensure adequate reference tracking, provide noise attenuation and improve robustness to output multiplicative uncertainties, T_o is desired to be large at low frequencies and roll-off at high frequencies. As such W_3 is typically chosen to resemble a high-pass filter.

Note that the relationship between the sensitivity and the complementary sensitivity function $S_o + T_o = I$ hints at the fundamental trade-off in feedback design stated earlier. As such, the weighting filters provide a set of design knobs that allow the designer to strike a balance between RS and RP. It must be emphasized that the weighting functions ought to be stable transfer functions to ensure feasibility of Doyle's algorithm [36]. As such, the proposed low or high-pass filter shapes are often augmented to lead-lag filters to prevent improper transfer functions. A discussion on the choice of the weighting filters is provided in [120]. Variations of the $S/KS/T$ mixed-sensitivity design are ubiquitously seen in application [121, 122, 123].

It is often the case that the filter parameters are chosen by the designer and tweaked by hand. This can lead to sub-optimal choices for the weighting filters. Alternatively, more elaborate, optimized weighting filters could be selected. Kumar et al. [124] propose a genetic algorithm, Zhang et al. [125] propose a Quantum genetic algorithm. These methods are however computationally expensive and require significant design effort. Thus, their application might be of value for fine-tuning of the weighting functions

but are not of interest in initial design stages, hence beyond the scope of this research. Another recently applied method is so called co-design, which sets the weighting filter parameters as individual gains to be tuned in the optimization [126].

3.2.3. Shaping additional transfer functions

Consider the following general two degree-of-freedom control system.

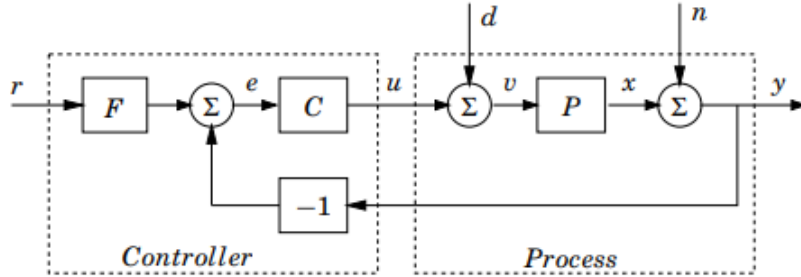


Figure 3.7: General two-DOF control system, taken from [127]

Looking at the feedback control system in figure 3.7, six unique transfer functions between the external inputs r , d and n and the signals of interest x , y and u can be deduced. These are known as the *Gang of Six* and are defined in equation 3.41. Note that the naming convention for the transfer functions presented in equation 3.41 is slightly different from that seen in figure 3.7. Specifically, C is replaced by K and P is replaced by G . This is done to keep consistent with the naming convention seen in [36].

$$\begin{aligned} S_o &= \frac{I}{I + GK} & T_o &= \frac{GK}{I + GK} & T_o F &= \frac{GKF}{I + GK} \\ S_o G &= \frac{G}{I + GK} & KS_o &= \frac{K}{I + GK} & KS_o F &= \frac{KF}{I + GK} \end{aligned} \quad (3.41)$$

The transfer functions in the first column provide information on how the output y responds to disturbances at the plant output (S_o) and input ($S_o G$). The second columns represents the transfer functions relating the output y to the reference r : T_o and the control signal u to the reference: KS_o . The same holds true for the last column, in case a feed-forward term is included. If $F = 1$, the system has pure feedback and the system is fully characterized by the transfer functions in the first two columns. These are then often referred to as the *Gang of Four* [127]. Having established these fundamental relations, it makes sense as to why one would be interested in shaping these in the context of robust control design.

Accordingly, extensions of mixed sensitivity design are seen in the literature, commonly seen approaches are the four-block method and the so-called signal based approach [91, 128]. The four-block method pertains to the filtering of the *Gang of Four*. This is achieved by applying input filters to the reference signal and the input disturbance W_r and W_{d_i} respectively. As such, the resulting closed-loop system is formulated as follows [91].

$$F_l(P, K) = \begin{bmatrix} W_1 S_o W_r & W_1 S_o G W_{d_i} \\ W_2 K S_o W_r & W_2 K S_o G W_{d_i} \end{bmatrix} \quad (3.42)$$

Where W_1 and W_2 represent the output weighting filters, as defined earlier. The input filters W_r and W_{d_i} should reflect the spectral content of the exogenous inputs. According to Belletti et al. [129] this information is not often available and the weights are often chosen by hand. However, within the context of flight control design, educated choices can be made. A form of input disturbance on an aircraft is wind turbulence. As such, a commonly seen choice for the input disturbance filter W_{d_i} is the Dryden wind gust model [86, 130, 35]. Similarly, the reference filter W_r can be chosen such that it reflects the spectral input of the pilot, based on McRuer's pilot model for instance [131].

The four-block method can be seen as special case of a more general approach known as signal-based \mathcal{H}_∞ -control. In this approach, the emphasis is on defining exogenous signals affecting the control system

these same issues [137, 85, 138]. These effects are inherently unstructured and lend themselves well to norm-bounded uncertainty descriptions [36].

Up until a fairly recent publication by Pollack et al. [135], no formal robustness analysis of INDI-based control laws under mixed uncertainty has been presented. In contrast with NDI, which has seen elaborate robustness assessments [139, 140, 141].

3.3.2. Robustness properties of INDI under mixed uncertainty

As mentioned, Pollack was the first to provide analytical stability and performance robustness properties of INDI-based control laws in the presence of mixed perturbations [35]. Prior to assessing the actual robustness properties, Pollack highlights the importance of recognizing the various elements that come together to provide the robustness of (I)NDI control laws. Namely, the following [35].

- **Virtual control design**, limiting the virtual control crossover frequency and using e.g. PI-control in the virtual control loop affects overall CL robustness.
- **Inversion strategy**, choosing either MB-INDI or SB-INDI results in fundamentally different robustness properties.
- **Feedback linearization procedure**, feedback is used to linearize the plant, this has implications on the robustness.
- **Control allocation**, different combinations of active control effectors leads to different closed-loop characteristics.

The fact that the robustness properties of (I)NDI-based control laws are a product of these different elements highlights that one should not view the robustness of any given inversion law in isolation. Pollack proceeds to establish the fundamental robustness characteristics of MB and SB-INDI control laws based on insights from nonlinear and linear state-space formulations. The most important insights are provided hereafter [35].

Consider some MIMO, input-affine, non-linear system Σ , its output dynamics can be described as follows.

$$\Sigma = \begin{cases} \dot{x} &= f(x) + G(x)u \\ y &= h(x) \end{cases} \quad (3.43)$$

Where $x \in \mathbb{R}^n$ represents the state vector, $u \in \mathbb{R}^m$ the input vector, $y \in \mathbb{R}^m$ the observation vector and f , G and h represent smooth mappings. Writing the system relative degree as: $\rho = [\rho_1, \dots, \rho_m]^T$, the output dynamics can be described by the following.

$$\mathbf{y}^{(\rho)} = \begin{bmatrix} \mathcal{L}_f^{\rho_1} h_1(x) \\ \vdots \\ \mathcal{L}_f^{\rho_m} h_m(x) \end{bmatrix} + \begin{bmatrix} \mathcal{L}_{g_1} \mathcal{L}_f^{\rho_1-1} h_1(x) h_1(x) & \dots & \mathcal{L}_{g_m} \mathcal{L}_f^{\rho_1-1} h_1(x) \\ \vdots & \ddots & \vdots \\ \mathcal{L}_{g_1} \mathcal{L}_f^{\rho_m-1} h_m(x) & \dots & \mathcal{L}_{g_m} \mathcal{L}_f^{\rho_m-1} h_m(x) \end{bmatrix} = \boldsymbol{\alpha}(x) + \boldsymbol{\mathcal{B}}(x)u \quad (3.44)$$

Where $\mathcal{L}_f^k h_i(x)$ and $\mathcal{L}_{g_i} \mathcal{L}_f^k h_i(x)$ represent repeated Lie derivatives of h_i along the vector fields f and g_i . g_i being a column vector of the matrix G . The INDI control laws is then defined as follows.

$$\mathbf{u} = \mathbf{u}_0 + \hat{\mathcal{B}}^{-1}(x_0)[\boldsymbol{\nu} - \mathbf{y}_0^{(\rho)}] \quad (3.45)$$

Consider now the perturbed output dynamics, as shown in equation 3.46.

$$\mathbf{y}^{(\rho)} = [\hat{\boldsymbol{\alpha}}(x) + \boldsymbol{\xi}(x)] + [\hat{\boldsymbol{\mathcal{B}}}(x) + \boldsymbol{\Xi}(x)]u \quad (3.46)$$

Where $\boldsymbol{\xi}$ and $\boldsymbol{\Xi}$ represent additive regular perturbations. These do not change the order of the system and represent known or unknown variations w.r.t. model representations embedded into the INDI law and are assumed to be bounded. The system input is now modelled as the control law output perturbed by an uncertain causal, linear mapping $\boldsymbol{\Delta}$. This perturbation represents unmodelled or neglected dynamics existing in cascade with the nonlinear system formulated in equation 3.43. This could represent higher-order dynamics in the actuators or neglected high-order structural modes. Consider now the following description of the system input and output at t_0

$$\mathbf{u}_0 = (\mathbf{I} + \boldsymbol{\Delta}_1)u \quad (3.47)$$

$$\mathbf{y}_0^{(\rho)} = (\mathbf{I} + \boldsymbol{\Delta}_2)\mathbf{y}^{(\rho)} \quad (3.48)$$

Where Δ_i again represent causal, linear mappings. It follows that the INDI control law output is now described by the following.

$$u = (I + \Delta_1)u + \hat{\mathcal{B}}^{-1}(x)[\nu - (I + \Delta_2)y^{(\rho)}] \quad (3.49)$$

This formulation of control output enables the robustness analysis of SB-INDI in the presence of linear perturbations. Moreover, it enables direct analysis of the synchronization effect, which is known to cause problem in incremental control laws [29, 74, 30]. The synchronization effect significantly influences the closed-loop dynamics and arises when there is a difference in the arrival times of the output derivative and input feedback signals.

Using the formulation of u seen in equation 3.49, the closed-loop output dynamics can be explicitly formulated as follows.

$$\begin{aligned} y^{(\rho)} &= \nu + \mathcal{S}(x, \Delta_1, \Delta_2)^{-1} [\mathcal{D}_1(x, \Delta_1)(\nu - [\hat{\alpha} + \xi(x)]) - \Delta_2\nu] \\ &\triangleq \nu + \epsilon_{INDI}(x, \nu, \Delta_1, \Delta_2) \end{aligned} \quad (3.50)$$

Where $\mathcal{S}(x, \Delta_1, \Delta_2)$ and $\mathcal{D}_1(x, \Delta_1)$ are defined as follows.

$$\begin{aligned} \mathcal{S}(x, \Delta_1, \Delta_2) &\triangleq I - \mathcal{D}_1(x, \Delta_1) + \Delta_2 \\ \mathcal{D}_1(x, \Delta_1) &\triangleq \hat{\mathcal{B}}(x)\Delta_1(\hat{\mathcal{B}}(x) + \Xi(x))^{-1} \end{aligned} \quad (3.51)$$

These results highlight that if u and y^ρ can be measured accurately, the closed-loop system will be robust against regular perturbations in the output dynamics [135].

Moreover, if the \mathcal{L}_2 -gain of the perturbations Δ_i is expressed as γ_i , the upper bound on the \mathcal{L}_2 -gain of the residual ϵ_{INDI} is given by

$$\begin{aligned} \|\epsilon_{INDI}\|_2 &= \left\| \mathcal{S}(x, \Delta_1, \Delta_2)^{-1} [\mathcal{D}(x, \Delta_1)(\nu - [\hat{\alpha}(x) + \xi(x)]) - \Delta_2\nu] \right\|_2 \\ &\leq \gamma_{S_i} \left(\gamma_1 \left\| \hat{\mathcal{B}}(x)(\hat{\mathcal{B}}(x) + \Xi(x))^{-1}(\nu - [\hat{\alpha}(x) + \xi(x)]) \right\|_2 + \gamma_2 \|\nu\|_2 \right) \end{aligned} \quad (3.52)$$

Where γ_{S_i} represents an upper bound on the \mathcal{L}_2 -gain of the inverse mapping $\mathcal{S}(x, \Delta_1, \Delta_2)^{-1}$. From the result in equation 3.52, it can be concluded that the upper bound on $\|\epsilon_{INDI}\| \rightarrow 0$ as $\gamma_i \rightarrow 0$, independent of $\xi(x)$ and $\Xi(x)$. In reality, actuator dynamics and finite sampling times make it such that $\gamma_i \geq 1$

This demonstrates that the robustness of SB-INDI stems mostly from the quality of the sensor measurements and less on the accuracy of the on-board model. Moreover, the inverse mapping \mathcal{S}^{-1} needs to be bounded for ϵ_{INDI} to remain bounded at any given state x . This limits the permissible perturbation dynamics for which the control loop remains stabilizable. This is a direct consequence of the synchronization effect. For example, if $\Delta_1 \rightarrow 0$, ϵ_{INDI} will grow unbounded if $\Delta_2 \rightarrow -I$. Pollack highlights that this is contrary to (model-based) NDI, for which upper bounds on the inversion residual can always be found, given that certain assumptions hold [35].

Pollack proceeds to provide a design solution, namely, ensure that $\mathcal{D}(x, \Delta_1) = \Delta_2$, such that $\mathcal{S} = I$ holds. This implies that the inversion residual can be expressed as follows.

$$\epsilon_{INDI}(x, \Delta_2) = -\Delta_2[\hat{\alpha}(x) + \xi(x)] \quad (3.53)$$

Pollack refers to this strategy as the *matching strategy*, it lies in accordance with design strategies seen earlier in [30, 29, 32]. Pollack emphasizes that this strategy is only feasible when the control effectiveness and the singular perturbation dynamics are completely known. This approach does not guarantee a nonzero inversion residual for a nonzero Δ_2 . However, the norm of the residual will be small if Δ_2 is small within the operating time-scale of Σ , which aligns with the time-scale separation principle.

Pollack demonstrates that the matching strategy is indeed successful at improving the robustness properties of SB-IDI. Although it comes at the cost of a larger inversion residual. Consequently, Pollack analyses the inversion residual for a hybrid INDI set up with a complementary filter, as seen in [33] for example, and demonstrates that the residual reduces to the following.

$$\epsilon_{HB}(x, \Delta_2) = -\Delta_2\xi(x) \quad (3.54)$$

Additional insight into the stability and robustness properties of INDI are provided by looking the linear state-space representation of the closed-loop dynamics in the following normal form.

$$\Sigma : \begin{cases} \dot{\zeta} = R\zeta + T\eta + Bu \\ \dot{\eta} = P\zeta + Q\eta \\ y = R\zeta \end{cases} \quad (3.55)$$

Pollack establishes an interconnection framework that enables the evaluation of the linear robustness properties of INDI-based control laws. In turn enabling the use norm-based robustness analysis tools (μ -analysis), as introduced in chapter 3.

Omitting a number of intermediary steps, Pollack arrives at a state-space representation of the dynamics of the inverse map $\mathcal{S}(x, \Delta_1, \Delta_2)^{-1}$ and verifies its boundedness in two special cases. One being the case where only strictly proper dynamics are present in the feedback path, the other assessing the impact of discretization effects as a result of the digital implementation of the controller. Either way, the stability of the synchronization dynamics can be directly assessed by verifying if the A matrix of the synchronization dynamics A_{S_i} adheres to the Hurwitz criterion [135]. That is, if the eigenmodes of \mathcal{S}^{-1} lay sufficiently far away from the eigenmodes of Σ , which is a valid claim under the assumption of the time-scale separation principle.

In summary, INDI displays a level of robustness to regular perturbations. However, the inversion residual may become unbounded for certain combinations of singular perturbations, resulting in a loss of robust stability. This is a direct result of the synchronization effect. The application of additional augmentation strategies to the feedback signals may improve the robustness properties of INDI, as concluded in [135]. Moreover, the interconnection framework established by Pollack enables the application of norm-based analysis and design tools for INDI-based control systems.

3.4. Multi-loop robust design of (I)NDI-based control laws

An obvious objective for flight control law design is the improvement of handling qualities. As discussed previously, the (I)NDI framework provides great benefit over the classical *divide-and-conquer* approach in terms of gain scheduling and modularity. However, a drawback of the standard (I)NDI approach is that it provides no robustness guarantees. In contrast, formal robust control design tools, such as \mathcal{H}_∞ -loop shaping, \mathcal{H}_∞ -mixed sensitivity design and μ -synthesis do provide these guarantees when applied to the classical *divide-and-conquer* techniques. As such, robust outer-loop designs for INDI-control laws have been extensively studied [86, 65, 139], to name a few. Similarly, robust outer-loop synthesis combined with inner loop SB-INDI and hybrid-INDI has garnered some research attention. Including \mathcal{H}_∞ mixed-sensitivity design, seen in [142] and multi-objective optimization approaches, such as those seen in [32, 81, 143]. However, these studies do not optimize for the inner inversion-loop itself. Therefore, the robustness characteristics arising from these design strategies are inherited from the selected inversion strategy itself [35].

As such, Pollack provides a multi-loop synthesis strategy enabling the design of explicit model-following (I)NDI control systems with adequate robust stability and performance in the presence of mixed parametric and dynamic uncertainty. Pollack establishes a structured \mathcal{H}_∞ synthesis algorithm to optimize all of the design parameters and demonstrates the approach for MB, SB and hybrid inversion strategies. The method is demonstrated in the context of a C^* model-following CAS design for the short-period approximation of a Boeing 747. Moreover, Pollack provides a robustness analysis based on the IQC framework and assesses the robust performance against LTI and LTV (linear time-varying) uncertainties [35]. The consideration of LTV uncertainties and the use of the IQC framework is beyond the scope of this research.

The INDI-based explicit model-following (EMF) control system interconnection used by Pollack is shown in figure 3.9. This interconnection structure serves as an example for the approach that will be applied to the Flying-V.

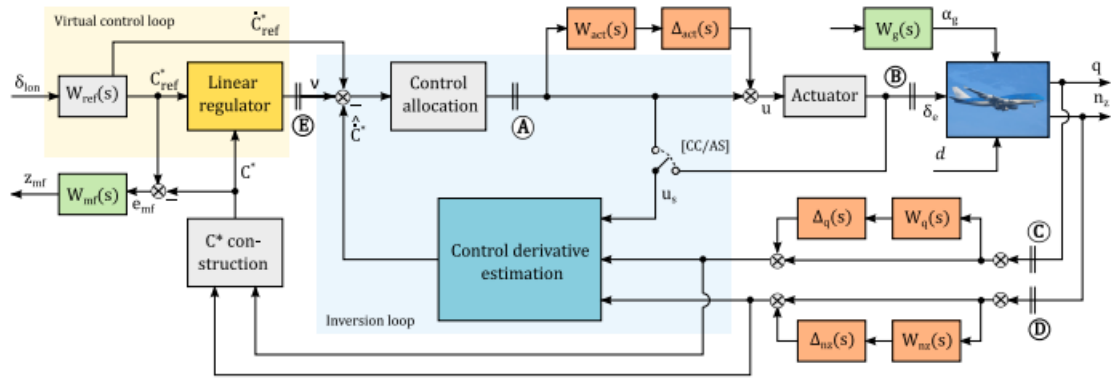


Figure 3.9: INDI-based EMF control system interconnection structure, from [35]

3.5. Conclusions

This chapter served to provide an introduction to the \mathcal{H}_∞ -framework enabling analysis and design of robust control control systems. A theoretical background was provided, alongside some practical design tools and insights into the machinery behind the tools. In addition, the established framework was applied to assess the robustness properties of INDI-based control laws. Finally, a multi-loop approach to robust INDI-based control law design was presented. The latter will serve as the design strategy of choice for the control system presented in the later stages of this research.

This chapter addressed research question 2 and portions of research question 4. The research questions are restated below, along with the degree to which they have been addressed.

How can \mathcal{H}_∞ -based tools be used to establish robust INDI-based control system designs?

a) How is the \mathcal{H}_∞ framework defined?

The \mathcal{H}_∞ -framework is a norm-based descriptions of transfer function. Technically, it refers to the Hardy space of the set of transfer functions with a bounded ∞ -norm. In terms of transfer functions, it is defined as the peak singular value over frequency. Subsequently, \mathcal{H}_∞ -control tools are often concerned with the minimization of the largest singular value over frequency. Specifically, one is often interested in the minimization of the \mathcal{H}_∞ -norm of some closed-loop system. To enable this, the framework makes use of the so called generalized plant description, which can be formulated in terms of the LFT of the plant and the controller $N = F_l(P, K)$.

This generalized description also facilitates the incorporation of uncertainties. Various forms of uncertainty descriptions exist, these can be captured in a uncertainty matrix Δ . As such, a closed-loop system containing uncertainty can be described by the LFT of the plant-controller interconnection and the uncertainty matrix: $M = F_l(\Delta, N)$. Subsequently, this description can be used to perform a robustness analysis of the closed-loop system.

A natural question that arises is: *How much uncertainty can a closed-loop system tolerate before it becomes unstable?* This question can be answered by looking at the structured singular value (SSV or μ). This boils down to finding the smallest uncertainty that renders the determinant of the closed-loop system singular. Moreover, necessary and sufficient conditions for robust stability and robust performance can be described using the SSV.

Computing the SSV turns out to be a NP-hard problem. In practice, bounds on the value of μ are instead computed, which lie sufficiently close to the actual value. Over the years, various algorithms that calculate the bounds on μ have been established. These can be divided into outer-relaxation techniques and inner-relaxation techniques. According to some. outer-relaxation techniques provide conservative results.

Solving the \mathcal{H}_∞ -optimal control problem involves finding all stabilizing controller K , such that $\|F_l(P, K)\|_\infty < \gamma$, where $\gamma > \gamma_{min}$. This corresponds to a sub-optimal solution which is sufficiently close to the optimal solution and easier to obtain, theoretically and computationally. The problem was first formally defined by Zames [103] back in 1981, ever since, many solutions to the problem have emerged. Doyle et al. [104] first identified that solving the problem requires solving two AREs.

Later on, alternative, LMI-based solutions emerged [105, 106]. The ARE and LMI-based solutions are all found in the full controller space κ_{full} , which is a convex problem. The resulting (sub)-optimal controllers will be of the same order of the generalized plant P . Finding a solution in a smaller and more practical controller space is a much more difficult problem, as this is a non-convex and non-smooth problem. In the late 90s, BMI-based solutions emerged, these methods would ultimately hold the key to solving the structured \mathcal{H}_∞ -problem. In a seminal 2006 paper, Apkarian et al. [107] present a non-smooth optimization based method that facilitates structured \mathcal{H}_∞ -optimal controller synthesis. This approach has since been refined [106].

The standard \mathcal{H}_∞ -optimal control problem does not take into account any uncertainty. In reality, uncertainty is omnipresent. Methods for synthesizing \mathcal{H}_∞ -optimal controllers in the presence of uncertainty have emerged over the years. These tools effectively combine μ -analysis with \mathcal{H}_∞ -synthesis and are known as μ -synthesis tools. The first solution to this problem was provided in Doyle in 1985 [110] and is known as DK-iterations. This is an iterative approach that alternates between computing the upper bound on μ and solving an unstructured \mathcal{H}_∞ -problem. Each of these steps separately are convex, yet joint convexity is not guaranteed. As such, global optimality is not guaranteed, although the method has been seen to work well in practice [36]. D-K iterations only considers dynamic uncertainty, this may yield conservative results in the presence of parametric uncertainty. An alteration to D-K iterations is provided by DG-K iterations, introduced by Young et al. [111], which does consider both real and dynamic uncertainty. One issue with these techniques is that they make use of classical \mathcal{H}_∞ -synthesis, resulting in full-order controllers. In 2010, Apkarian et al. [113] proposed a non-smooth method for mixed μ -synthesis based on inner-relaxation techniques. One of the main advantages of these non-smooth methods is the ability to handle multi-model and multi-objective control design. Later alterations to the method proposed in [113] are seen in [114, 101]. These tools have been included in the Matlab Robust Control toolboxTM [37].

Practical tools for designing robust control systems include \mathcal{H}_∞ loop-shaping, mixed sensitivity design and signal-based \mathcal{H}_∞ -control. The first is concerned with the shaping of the open-loop with pre-and-post-compensators. The latter two methods are concerned with the shaping of closed-loop functions. A typical starting point is the shaping of a combination of the closed-loop sensitivity functions S , KS and T . These are shaped with weighting filters, such that the solution to the \mathcal{H}_∞ -problem definition minimizes the product of the sensitivity functions and their respective weighting filters. This can be extended to include a variety of signals and weighting filters and is referred to as signal-based \mathcal{H}_∞ -control. This approach allows one to specify the spectral content of individual signals and facilitates the minimization of distinct signals. Including a model following error, an approach often seen in flight control [133, 134].

Note that \mathcal{H}_∞ -problems often present a trade-off between conflicting objectives. The weighting filters therefore provide the designer with tuning knobs, allowing the designer to strike a balance between robust stability and robust performance.

b) How can \mathcal{H}_∞ -based tools be applied to flight control system design?

As mentioned, practical methods for \mathcal{H}_∞ -control allow the designer to shape the closed-loop functions with a set of weighting filters. These weighting filters can be placed at inputs and outputs. As such, these can represent the spectral content of an input or represent a desired spectral output of a given closed-loop function. In the context of flight control system design, a commonly seen choice for a disturbance input filter is the Dryden wind gust model [132, 35, 130]. Similarly, the reference input can be chosen such that it reflects the spectral content of the pilot's input, based on McRuer's pilot model for instance [57].

Minimizing a model-following error is a common choice in flight control system design. This is achieved by constraining the model-following error $e = y - y_{ref}$, where $y_{ref} = G_{ref}r$ by some weighting filter W_e . G_{ref} reflects some desired response, a good choice for G_{ref} for pitch-axis control is some desired short-period response as seen in MIL-STD-1797A [132]. Examples of this approach are seen in [133, 134, 35]. As such, by choosing appropriate weighting filters, the response of the close-loop system can be shaped. As well as achieving the desired robust stability and performance characteristics.

c) What are the robustness properties of (I)NDI based control laws?

Pollack was the first to provide analytical stability and performance and robustness properties of INDI-based control laws in the presence of mixed uncertainty [35]. The insights provided in [35] are based on the linear state-space formulation of INDI, which enables one to view INDI-based control

laws through the lens of the \mathcal{H}_∞ -framework. Prior to establishing these fundamental insights, Pollack highlights the fact that robustness properties of any given (I)NDI-based control law is a product of a number of factors. As such, robustness of any given inversion law should never be viewed in isolation.

One of the key findings is that the robustness of SB-INDI stems from the quality of the sensor measurements and less on the accuracy of the onboard-model. Pollack states that the inversion residual ϵ_{INDI} may grow to be unbounded for certain combinations of singular perturbations, as a direct consequence of the synchronization effect. This is in contrast to NDI, for which upper-bounds on the inversion residual can always be found. In order to prevent the inversion residual from becoming unbounded, Pollack provides a design solution known as the *Matching strategy*, which has been shown to improve the robustness properties of SB-INDI.

In addition, Pollack provides a multi-loop \mathcal{H}_∞ -synthesis strategy, allowing one to design robust sensor-based, model-based or hybrid-INDI controllers.

In addition, research question 4 and its sub-questions has been touched upon, these are restated hereafter.

How can \mathcal{H}_∞ tools be applied to INDI-based flight control law design to improve the longitudinal handling qualities of the Flying-V?

- a) **How can the design criteria be included in the formulation of a structured \mathcal{H}_∞ synthesis problem?** As briefly touched upon, design criteria in the form of weighting filters can be included in a \mathcal{H}_∞ -synthesis problem. This allows the designer to strike a balance between different design objectives. These design criteria can be expressed as desired spectral content of output signals. The specific design criteria that might be of interested are discussed in chapter 4.
- b) **How can INDI-based control systems be included in the formulation of a structured \mathcal{H}_∞ synthesis problem?** As seen in section (refer to section 3.4), INDI-based control laws can be incorporated into a closed-loop interconnection structure that enables structured \mathcal{H}_∞ -synthesis. An example of such an interconnection structure is shown in figure 3.9.
- c) **What are the robust stability & performance characteristics of robust INDI-based control systems on the Flying-V?** A general perspective on the robustness properties of INDI-based control systems was provided. However, as stated in the beginning of section 3.3.2, the robustness of any (I)NDI-based control law is the product of a variety of design choices. Therefore, no concluding remarks about the robustness characteristics of any specific INDI-based control systems for the Flying-V can be made yet.

4

Longitudinal Handling Quality, Performance & Stability Criteria for the Flying V

The previous chapters were dedicated to the introduction of the Flying-V, the introduction of (I)NDI-based control laws, the norm-based \mathcal{H}_∞ -framework and robustness properties of INDI-based control law design. However, looking at figure 2.20, one could argue that establishing adequate design criteria should precede the choice for any particular control law design. As such, this chapter is aimed at answering research question 3, which is restated hereafter.

Which longitudinal handling quality, stability and performance criteria must the Flying-V satisfy

In [137], the authors distinguish between the following three categories of criteria.

- I Flying Qualities
- II Stability Criteria
- III Performance Criteria

Note that these categories are not completely disjoint from another, yet this distinction is useful. This chapter serves to introduce these criteria, describe their assessment and explore their integration into FCS design.

4.1. Flying Quality requirements

Cook defines the handling quality of an aircraft as the degree of adequacy of the short term dynamic response to control inputs when performing a certain flight task [144]. An aircraft must exhibit adequate control authority to maintain steady, levelled flight. Moreover, it must be capable of safely maneuvering from one steady state to another. In addition, stick forces experienced by the pilot must be within acceptable limits [145]. Several criteria for handling qualities have been defined by various authorities. These can be divided into civil standards, like those provided by EASA or the FAA, and military standards. The requirements stated by civil authorities are often not very specific and therefore not directly applicable during the aircraft design process. This is highlighted by Wahler [146], who discusses one of the lateral-directional handling quality specifications from EASA CS-25.181 [51]. In summary, the requirements states that the aircraft must be stable and controllable by an average pilot. No further definition of these terms are provided, nor are any quantitative measures. This example illustrates the ambiguity of these definitions.

In contrast, military handling quality standards are much more thoroughly defined and typically, far more demanding. According to Cook, using military requirements to assess an aircraft's capabilities will ensure that the aircraft meets civil requirements [144]. The military standards that were previously chosen to assess the Flying-V's handling qualities follow from MIL-STD-1797A [132]. The standards provided in MIL-STD-1797A make use of a classification based on aircraft-type. In accordance with this classification, the Flying-V classifies as a Class III aircraft (large, heavy, low-to-medium manoeuvrability aircraft, MTOM

> 30.000 kg). Moreover, these standards draw a distinction between different flight phases, as shown in table 4.1.

Table 4.1: Flight phase categories, adopted from [144]

Flight Phase Category	Flight Phase
A	Air-to-air combat Ground attack Weapon delivery/launch Reconnaissance In-flight refuel (receiver) Terrain Following Maritime search Aerobatics Close formation flying
B	Climb Cruise Loiter in-flight refuel (tanker) Descent Aerial Delivery
C	Take off Approach Overshoot Landing

Note that not all of these flight phases are relevant to the Flying-V, the relevant phases are printed in bold. Further elaboration of this classification can be found in [144]. In order to assess an aircraft's ability to complete a desired flight task, handling quality levels can be used. These indicate the level of pilot workload experienced during the execution of said task. The handling quality levels, as defined by Cook [144], are depicted in figure 4.1.

- Level 1** Flying qualities clearly adequate for the mission flight phase.
- Level 2** Flying qualities adequate to accomplish the mission flight phase, but with an increase in pilot workload and, or, degradation in mission effectiveness.
- Level 3** Degraded flying qualities, but such that the aircraft can be controlled, inadequate mission effectiveness and high, or, limiting, pilot workload.

Figure 4.1: Levels of handling qualities, as defined in [144]

Note that for each of the flight phase categories shown in table 4.1, both longitudinal and lateral-direction handling qualities can be assessed based on the classification shown in figure 4.1. Assessing and improving the lateral-directional handling qualities is beyond the scope of this research. Hence, a thorough overview of the lateral-directional handling quality criteria is omitted.

It is important to distinguish between the modes of assessment for these handling quality criteria. WL-TR-94-3162 uses the following distinction for establishing handling quality levels [86].

1. **Predicted Levels**, based on the assessment of defined flying qualities parameters.
2. **Assigned Levels**, based on piloted assessments following flight test maneuvers.

The predicted level assessment is based on the comparison of the aircraft's determined handling quality parameters with the quantitative values of the specific criteria. The assigned handling quality level follows

from the piloted assessment of a set of well-defined flight test maneuvers with a team of at least 3 pilots [86]. The predicted level assessment is based on a set of parameters which together, are expected to accurately reflect handling qualities. This might not necessarily be the case, as the set of flying quality parameters might not fully capture the actual handling qualities experienced by the pilot. As such, predicted and assigned levels may be in conflict. Similarly, the set flight test maneuvers may not be comprehensive enough to represent all mission maneuvers in every part of the flight envelope that the aircraft may encounter. According to WL-TR-94-3161, [86], the two must be compared to provide a maximum likelihood of an accurate assessment of the handling quality level. As this research is confined to the use of simulations, all handling quality level assessments provided hereafter belong to the category of *Predicted Levels*.

4.1.1. Lower-order equivalent system

The longitudinal dynamics of an aircraft are characterised by the short period mode and the Phugoid mode. Depending on the bare airframe dynamics of an aircraft and possibly, control system complexity, the actual closed-loop response may be of high order. MIL-STD-1797A [132] states that the use of lower-order equivalent systems (LOES) makes it possible to extend the application of well-established boundaries from classical aircraft data, as seen in MIL-F-8785C [56], to higher-order systems. Specifically, pitch axis boundaries established on the model parameters of the pitch attitude transfer function shown in equation 4.1, which represents a linearized, reduced-order model of the actual pitch response of an aircraft [132].

$$\frac{\theta(s)}{\delta(s)} = \frac{M_\delta(1/T_{\theta_1})(1/T_{\theta_2})e^{-\tau\theta s}}{(s^2 + 2\zeta_{ph}\omega_{ph} + \omega_{ph}^2)(s^2 + 2\zeta_{sp}\omega_{sp} + \omega_{sp}^2)} \quad (4.1)$$

Typically, the phugoid and the short-period mode lay sufficiently far away from one another such that these can be considered separately. MIL-STD-17917A states that these are often separated by at least a factor of 10. Judging by the findings of the eigenvalue analysis seen in section 2.3.1, this is indeed the case for the Flying-v. Accordingly, the transfer function can be further reduced into two distinct transfer functions.

- Phugoid Mode:

$$\left(\frac{\theta(s)}{\delta(s)}\right)_{ph} = \frac{M_\delta Z_w(1/T_{\theta_1})}{M_\alpha(s^2 + 2\zeta_{ph}\omega_{ph} + \omega_{ph}^2)} \quad (4.2)$$

- Short Period:

$$\left(\frac{\theta(s)}{\delta(s)}\right)_{sp} = \frac{M_\delta(1/T_{\theta_2})e^{-\tau\theta s}}{s(s^2 + 2\zeta_{sp}\omega_{sp} + \omega_{sp}^2)} \quad (4.3)$$

Accordingly, the handling quality requirements in [132] are split into short period requirements and phugoid requirements. The Phugoid handling requirements follow from [56] and are rather concise, these comprise of the following requirements on the Phugoid damping ratio ζ_{ph} .

Table 4.2: Phugoid damping requirements from [56]

Classification	Value
Level 1	equivalent $\zeta_{ph} > 0.04$
Level 2	equivalent $\zeta_{ph} > 0$
Level 3	$T_2 \geq 55s$

Where the equivalent phugoid damping ratio ζ_{ph} is to be determined from the LOES response seen in equation 4.1. Note that for the Level 3 requirement, the time to double amplitude T_2 is to be checked from the time-response of the actual aircraft. Although [132] states that this is seldom necessary, as higher levels are often met.

The short period handling quality requirements are much more elaborate, as a result of its importance. MIL-STD-1797A provides six alternative requirements, yet provide no guidance on when to use which requirement. This is one of the main critiques on MIL-STD-1797A presented in [86]. To that extent, WL-TR-94-3162 [86] provides an extensive discussion on the use of the different requirements, ultimately providing a roadmap for the use of short-term pitch response criteria. The six alternatives, alongside

small statements on their use case, are shown in figure 4.2, followed by the roadmap depicted in figure 4.3. Accordingly, the CAP, Dropback and Bandwidth criteria are introduced hereafter. For an elaborate discussion on these criteria, their applicability and limitations, the reader is referred to [86].

<p>1. CAP or MIL-F-8785C Criteria ("Preferred Form")</p> <ul style="list-style-type: none"> - Developed for Conventional "Classical" Airplanes - Difficult or Impossible to Apply for Unusual Modes and attitude Augmentation - Data Bases for Highly-Augmented Aircraft (Neal-Smith, LAHOS) Are in Conflict With the Requirements
<p>2. $\omega_{sp}T_{\theta_2}$, ζ_{sp}, τ_{θ} Criteria</p> <ul style="list-style-type: none"> - Closely Related to CAP, Same Observations Apply
<p>3. Transient Peak Ratio, Rise Time, Time Delay Criteria</p> <ul style="list-style-type: none"> - Applicable Only to Speed-Constrained Response for Rate Systems - Specify Pitch Rate Only, Not Flight Path - May Be Incorrect Since Limits Were Based on Mapping CAP (a Flight Path/Attitude Requirement) into Attitude-Only Limits - Time-Domain Criteria Are Highly Subject to Interpretation
<p>4. Bandwidth, Phase Delay</p> <ul style="list-style-type: none"> - Specify Attitude Only (Requires an Additional Flight Path Requirement) - In Combination With Dropback, More Effective in Specifying Flying Qualities Than Any Other Criteria - Only Criteria That Are Applicable to All Response-Types
<p>5. Pilot-in-the-Loop Criteria (Neal-Smith)</p> <ul style="list-style-type: none"> - Application Requires Extensive Closed-Loop Analysis That is Impossible for a Specification - Applicable to Attitude Response (Not Flight Path) for Rate and Conventional Response-Types Only - Proper Application Specifies Unrealistic Closed-Loop Pilot/Vehicle Operations (Low Closed-Loop Resonance and High Phase Margins) That Are Counter to Actual Piloted Operations (e.g., Ref. 3) - Continued Use as a Criterion Will Require Considerable Refinements
<p>6. Dropback and Nichols Chart Boundaries</p> <ul style="list-style-type: none"> - Not Actually "Criteria" — i.e., No Levels, No bases for Comparison, No Data Correlations to Indicate Effectiveness of Methods - Phase-Rate is Closely Related to Phase Delay in Bandwidth - Dropback Has Shown Sufficient Promise to Include it as a Supplement to Bandwidth and CAP for Rate Response-Types

Figure 4.2: Alternative short-term pitch response criteria seen in WL-TR-94-3162 [86]

RESPONSE-TYPE	SPECIFICATION AND DESIGN CRITERIA	CRITERIA FOR DESIGN GUIDANCE ONLY	CRITERIA NOT APPLICABLE
Conventional	Bandwidth (or CAP) Plus Dropback	$\omega_{sp}T_{\theta_2}$, Neal-Smith Gibson Nichols-Chart Boundaries	TPR
Rate or RCAH	Bandwidth Plus Dropback	CAP $\omega_{sp}T_{\theta_2}$, Neal-Smith Gibson Nichols-Chart Boundaries TPR	None
Attitude-Augmented (including ACAH and GCGH)	Bandwidth	None	Dropback CAP, $\omega_{sp}T_{\theta_2}$, Neal-Smith Gibson Nichols-Chart Boundaries

Figure 4.3: Road map for the use of alternative short-term pitch response criteria [86]

4.1.2. CAP criterion

The control anticipation parameter (CAP) was introduced by Bihrlé in 1966 [147]. Bihrlé argued that in order for a pilot to make precise adjustments to the flight path, the pilot must be able to anticipate the ultimate response of the aircraft. As such, the CAP is defined as the amount of instantaneous pitch acceleration \dot{q} per unit of steady state normal acceleration n_{ss} following a step control input. Assuming that the short period pitch response can be captured by the LOES shown in equation 4.3, Bihrlé arrives at the following approximation of the CAP

$$CAP = \frac{\dot{q}}{\Delta n_{z_{ss}}} \approx \frac{\omega_{sp}^2 W}{L_\alpha} \approx \frac{\omega_{sp}^2}{(n/\alpha)} \quad (4.4)$$

Where $L_\alpha \approx \frac{1}{T_{\theta_2}}$

Where W is the weight of the aircraft and n/α represents the normal acceleration per radian angle of attack. The value of the CAP can be interpreted as follows, if the CAP value is high, the aircraft's response is quicker than anticipated by the pilot, resulting in under-steer. Conversely, if the CAP value is low, the aircraft's response is experienced as sluggish, resulting in over-steer by the pilot [144].

Note that for aircraft with more modes than the classical short period and phugoid mode, the response must be reduced to a LOES of the form seen in equation 4.1 before the CAP can be assessed. The boundaries of the CAP levels for category B flight phases are shown in figure 4.4.

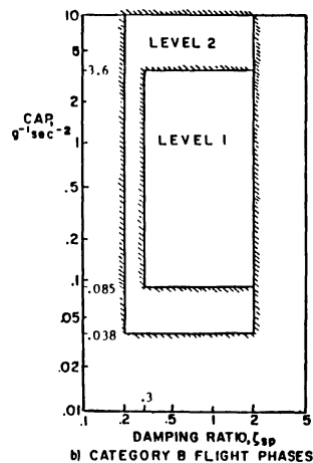


Figure 4.4: CAP boundaries for category B flight phases, from [86]

4.1.3. Dropback criterion

The Dropback criterion was first introduced by Gibson [148] and is defined as a measure of the mid-frequency response to attitude changes. It is evaluated based on a time-response plot of the pitch attitude dropback and pitch rate overshoot. According to [86], excessive Dropback results in pilot complaints on the abruptness of the aircraft and a lack of precision in pitch control. Complaints often also heard about aircraft with excessive pitch attitude bandwidth [86].

WL-TR-94-3162 presents a slightly altered definition of the Dropback defined by Gibson. For a detailed explanation of the rationale behind this alteration, the reader is referred to [86]. Mitchell et al. [86] emphasize the physical significance of the Dropback criterion. For conventional and rate response-types, the Dropback parameters are closely related to the classical short-period parameters. In the absence of high-frequency dynamics or time-delays, the Dropback is directly related to the numerator zero $1/T_{\theta_2}$, seen in equation 4.3. Moreover, Mitchell et al. concluded that increasing bandwidth results in decreasing Dropback. The definition used [86] is shown in figure 4.5.

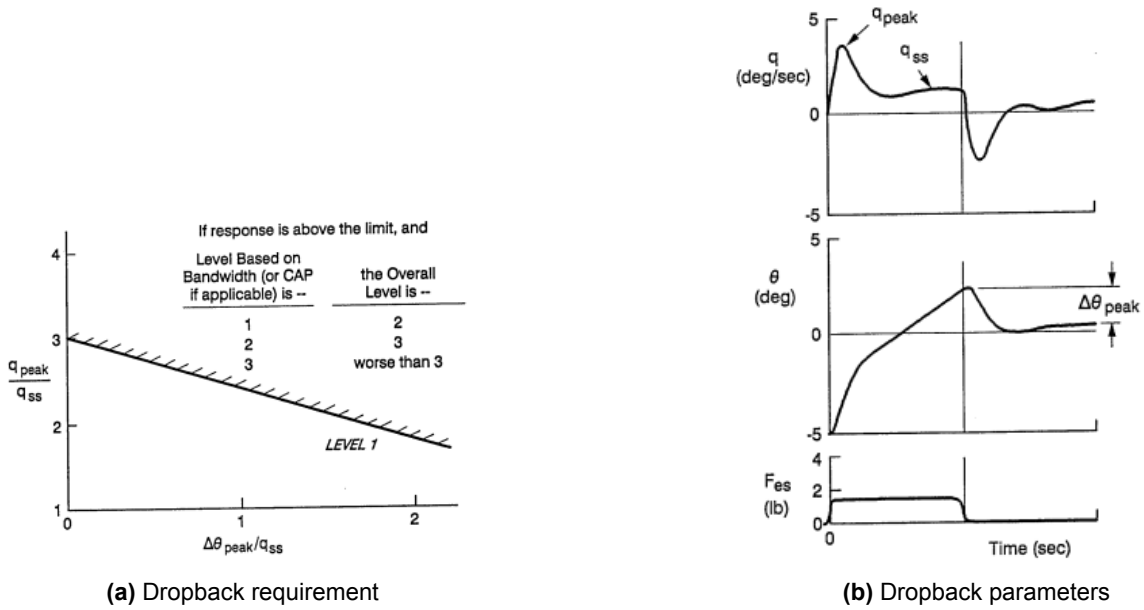


Figure 4.5: Dropback Criterion from [86]

Stougie [24] presents an INDI-based pitch-rate controller for the Flying-V that demonstrates Level 1 handling qualities according to the Dropback criterion.

4.1.4. Bandwidth criterion

MIL-STD-1797A states that a measure of the handling qualities of an aircraft is its stability margin when operated in a closed-loop compensatory task [132]. The maximum frequency at which such a tracking task can be carried out without threatening stability, is defined as the bandwidth ω_{BW} . Numerically, it is defined as the highest frequency at which $PM \geq 45^\circ$ and $GM \geq 6 \text{ dB}$ are both met. This pertains to the pilot’s ability to double his/her gain or add delay without causing instability. The value of the bandwidth is determined by the lesser of the phase crossover $\omega_{BW_{phase}}$ and the gain crossover $\omega_{BW_{gain}}$ [132]. Moreover, MIL-STD-1797A highlights that adequate closed-loop tracking is not only a function of the bandwidth, but also of the shape of the phase curve at frequencies above ω_{BW} . Phase roll-off can be represented by a time-delay, accordingly. The phase-delay parameter τ_p is estimated by the following relation [132].

$$\tau_p = \frac{\Delta\Phi_{2x} \omega_{180}}{57.3(2x \omega_{180})} \tag{4.5}$$

Where $\Delta\Phi_{2x}$ is the phase difference between the phase at twice ω_{180} and at ω_{180} . The corresponding pitch attitude bandwidth criteria is depicted in figure 4.6.

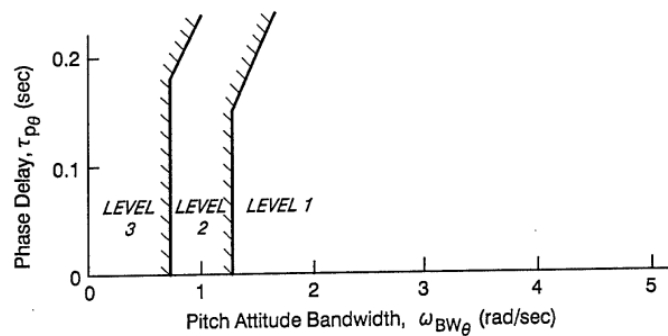


Figure 4.6: Bandwidth criteria from [132]

4.2. Stability requirements

In addition to handling quality criteria, stability requirements are typically enforced. These are, one could argue, the most important requirements in FCS design and an essential part of the FCS clearance process. Historically, stability margins were assessed by the classical SISO gain and phase margins. With the increased interest in multivariate control laws, equivalent MIMO stability margins have been established. Both of these are discussed hereafter.

4.2.1. Eigenvalue analysis

The first assessments of stability follows from a linear eigenvalue analysis. The eigenvalue specification dictates that all poles of the system must be in the left-half plane. For piloted systems, this requirement may be relaxed by the user if the unstable poles are easily compensated by the pilot [149].

4.2.2. Stability Margins

AS94900 formulates stability requirements in terms of the classical broken-loop gain (GM) and phase margins (PM). For the analysis, the loop is to be broken at the actuator, such that there is one broken-loop response per control axis. Moreover, it dictates that the stability margin requirements, shown in figure 4.7, must be maintained at the most adverse c.g., mass distribution and external storage configuration throughout the entire flight envelope [150].

Air speed Mode Frequency Hz	Below V_{oMIN}	V_{oMIN} to V_{oMAX}	At Limit Airspeed (V_L)	At $1.15 V_L$
$f_M < 0.06$	GM= 6 dB (No Phase Requirement Below V_{oMIN})	GM = ± 4.5 PM = ± 30	GM = ± 3.0 PM = ± 20	GM=0 PM=0 (Stable at Nominal Phase and Gain)
$0.06 \leq f_M < \text{First Aero-elastic Mode}$		GM = ± 6.0 PM = ± 45	GM = ± 4.5 PM = ± 30	
$f_M > \text{First Aero-Elastic Mode}$		GM = ± 8.0 PM = ± 60	GM = ± 6.0 PM = ± 45	

Figure 4.7: Gain and phase margin requirements from [150]

Where $V_{O_{min}}$ and $V_{O_{max}}$ represent the minimum and maximum operating speed. Over the range of frequencies associated with the rigid-body dynamics (0.06 Hz up to the first aeroelastic mode frequency) and the standard operational flight envelope ($V_{O_{min}}$ to $V_{O_{max}}$), the standard stability margins are used: $\pm 45^\circ$ of PM and ± 6 dB of GM. Moreover, AS94900 states that sensitivity or uncertainty analyses must be performed with 20% uncertainty in key stability derivatives and that the aforementioned margins shall not degrade by more than 50% in the presence of that uncertainty (during nominal flight conditions and at frequencies below the structural modes) [150].

Note how the margin requirements increase as the mode frequency exceeds the first aeroelastic mode, as uncertainty typically increases with frequency.

An extension to multivariate stability margins is presented in [151]. the multivariate stability margins are obtained from the loop transfer matrix L , breaking all loops simultaneously. Lavretsky et al. [151] define the return difference matrix (RDM) as $T_{rdm}(s) = I + L$ and the stability robustness matrix (SRM) as $T_{srm}(s) = I + L^{-1}$. The RDM pertains to purely additive uncertainty, the SRM provides a robustness test for multiplicative uncertainty. Subsequently, the gain and phase margins are determined from the singular values of the RDM and SRM, dubbed α_0 and β_0 respectively. The margins are defined as follows:

$$\begin{aligned}
 GM_{rtm} &= \frac{1}{1 \pm \alpha_0} & PM_{rtm} &= \pm 2 \sin^{-1} \left(\frac{\alpha_0}{2} \right) \\
 GM_{srm} &= [1 - \beta_0, 1 + \beta_0] & PM_{srm} &= \pm 2 \sin^{-1} \left(\frac{\beta_0}{2} \right)
 \end{aligned} \tag{4.6}$$

Finally, Lavretsky and Wise [151] define the combined multivariate stability (MV) margins as the union of the separate margins defined in equation 4.6, such that.

$$GM_{mv} = GM_{rdm} \cup GM_{srm}, PM_{mv} = PM_{rdm} \cup PM_{srm} \quad (4.7)$$

This analysis method considers the worst possible combination of gain and phase uncertainty. It has been suggested by some that margins based on the singular value are very conservative [149]. Tischler et al. [149] recommend checking the multivariate margins against the following requirements.

$$\begin{aligned} |GM_{mv}| &\geq 3 \text{ dB} \\ |PM_{mv}| &\geq 22.5^\circ \end{aligned} \quad (4.8)$$

4.2.3. Nichols Margins

An alternative stability margin requirement is that of the Nichols exclusion zone. The Nichols margins define robust stability margins as exclusion zones on the broken-loop gain-phase response plot [59]. Nichols margins essentially provide insight into the robustness of the system to *simultaneous* gain and phase variations, this is fundamentally different from the classical margins, which only consider one or the other. As a result, a system that may meet the classical stability margin requirements seen in figure 4.7, may fail the Nichols criteria. According to Tischler et al. [149], the Nichols margin requirements are more common in European aircraft programs, such as in the Eurofighter program [152]. For a thorough elaboration on the Nichols margins, the reader is referred to [149, 59, 153].

4.2.4. μ -based assessment of stability requirements

In the context of LTI systems, finding the robustness margin boils down to finding the maximal size of uncertainty at which closed-loop stability and performance is guaranteed. As defined in section 3.1.4, the robustness margin is defined as the inverse of the maximal SSV (μ) over frequency. Roos et al. [154] propose an algorithm capable of calculating guaranteed stability margins based on the upper bound of μ : $k_{max} = 1/\beta_{max}$. Moreover, they present a straight-forward approach to assessing the eigenvalue criterion and the stability margin criterion through μ -analysis. For an in-depth overview of these methods, the reader is referred to [154, 155].

4.3. Performance requirements

WL-TR-96-3099 [137] states that performance criteria are often expressed as time domain objectives, response statistics or frequency domain requirements. As such, performance analyses typically include three modes of analysis.

- I Time domain simulations
- II Covariance analyses
- III Frequency domain analyses

The first two methods make use of time-traces, whereas the latter is obviously a *frequency domain* method.

4.3.1. Time-domain performance metrics

Time-domain based performance requirements come in the form of requirements on various metrics, including overshoot and steady-state error. These values are assessed from the response to step inputs. Typically, linear simulations are performed first, followed by nonlinear simulations. At small inputs, these should demonstrate similar responses. Given larger inputs, it can be expected that these diverge, as the system deviates from an equilibrium condition. This highlights a key advantage of time-based performance requirements and assessments. As these can also be assessed based on nonlinear response data, making it possible to include nonlinearities, discontinuities and FCS logic in the model [137]. According to Tischler et al. [149], this is especially useful when trying to determine the maximum excursions or structural loads during high levels of turbulence, where actuator saturation might occur.

However, deterministic time-domain simulations alone provide a limited view on real life performance, as individual simulations pertain to a single model. In reality, model uncertainty is present and performance has to be guaranteed over a large set of models. To that extent, Monte Carlo simulations can be used. Subsequently, the defined performance characteristics can be assessed, arriving at a more realistic view

of reality. Typically, this is done by sampling random values of the stochastic components of a control system, such as noise and disturbances, and assessing the root mean square error (RMSE) of the responses. For a sufficiently large number of simulations, the outcomes offer a good reflection of reality, given that the magnitude of the stochastic variations are known. Note however that these simulations do not provide any guarantees on the performance.

4.3.2. Frequency-domain performance metrics

Tischler et al. [149] highlight two performance metrics that are of utmost interest. Actuator activity, in the form of an actuator RMS specification and the crossover frequency ω_c . The actuator RMS being proportional to the area under the power spectral density (PSD) curve of the transfer function from the pilot input δ_{stick} to the actuator position δ_{act} .

The broken-loop crossover frequency ω_c , as discussed in section 3.2, is probably the most significant design characteristic of a feedback control system. The minimum desired crossover frequency is dictated by the need for stabilization of low-frequency unstable modes, disturbance rejection, model-following and robust performance in the presence of uncertainty. Tischler et al. provide an overview on how each of these requirements affect the minimum value of the desired crossover frequency in the nominal case [149]. According to Berger et al. [156], rules of thumbs such as those provided in [149], company history or trade-off studies are good ways to determine the minimum desired crossover frequency. Note that the crossover frequency is highly airframe specific and that many factors influence the choice of an adequate crossover frequency. Accordingly, the crossover frequency is often a user-defined specification. Although Tischler et al. [149] provide a rough estimate of the crossover frequency for a typical fixed wing aircraft, $\omega_c \approx 3 \text{ rad/s}$.

Another way to incorporate performance requirements is through the use of weighting filters on signals in the closed-loop plant definition, as seen in chapter 3. This enables the expression of various closed-loop performance objectives, including disturbance rejection requirements, model matching requirements and control input limitations. These are ultimately included in the definition of the closed-loop transfer matrix, such that

$$\bar{\sigma}(M(\Delta, j\omega)) < W_{perf}(\omega), \text{ for all } \omega \quad (4.9)$$

Where W_{perf} represents some performance specification weight. Guaranteeing that this performance specification is met boils to assessing the condition for the nominal system $\Delta = 0$ as well as for the perturbed system $\Delta \in \Delta$, where Δ represents the uncertainty set. In other words, performing a robust performance analysis. The power of formulating performance requirements in terms of closed-loop constraints, is that robust performance verification is easily performed and provides guarantees. As such, no extensive Monte Carlo simulations are required. In addition, performance requirements are defined a-priori and are included in the synthesis problem. As opposed to merely being defined as design objectives that have to be assessed after the fact.

4.4. Conclusions

This chapter served to several introduce handling quality, stability and performance requirements. In doing so, research question 3 and its sub questions were tackled. These are restated below, along with the answers to these questions, to the extent that they have been addressed in this chapter.

Which longitudinal handling quality, stability and performance criteria must the Flying-V satisfy?

- a) **Which requirements are useful for assessing the Flying-V's longitudinal handling qualities?**
MIL-STD-1797A provides six alternative requirements that can be used to assess the short-period handling qualities of an aircraft [132]. Although no guidance on when to use which requirement is provided. In an attempt to clarify this, WL-TR-3162 provides an extensive discussion on the the use of the different requirements and provides a road map for their applicability [86]. The most important ones include the CAP criterion, the Dropback criterion and the bandwidth criterion. An issue with the CAP criterion is that it requires a LOES fit for aircraft with a higher-order response. Such a LOES fit may not always yield an accurate representation of the aircraft's actual response. In contrast, the Dropback and the bandwidth criterion can always be directly assessed.
Using multiple criteria may provide a better view of the handling qualities of an aircraft. It must be stated that any handling quality level classification remains a *predicted handling quality level* until

piloted assessments confirm the predicted level. Nonetheless, the predicted levels serve as an initial indication and can be used as a design guidance tool.

b) Which stability requirements must the FCS on the Flying-V adhere to?

Stability requirements are an essential part of the FCS clearance process. Typically, the first assessment of stability comes in the form of an eigenvalue analysis. This requires that all eigenvalues lay in the left-half plane. This requirement may be relaxed for piloted systems, given that the unstable eigenmode can be easily compensated by the pilot.

Next, stability margin analyses are typically performed. These are typically based on the stability margin requirements originating from AS94900 [150]. Which state that between the minimum and maximum operating speed of the aircraft and at frequencies up to the first aeroelastic mode of the aircraft, the margins must be at least: $\pm 45^\circ$ of PM and ± 6 dB of GM. Moreover, it states that sensitivity or uncertainty analyses must be performed with 20% uncertainty in key stability derivatives and that the aforementioned margins shall not degrade by more than 50%. These represent SISO margins.

An extension to multivariate stability margins, based on singular values, is provided in [151]. Some suggest that singular value based stability margins are very conservative [149]. Tischler et al. [149] suggest checking the multivariate stability margins against margin requirements half the size of the classical SISO margins.

An alternative stability margin requirement is the Nichols exclusion zone, which essentially provides insight into the robustness of a system to simultaneous gain and phase variations, in contrast to the classical margins. As such, an aircraft that may adhere to the classical margins, may fail the Nichols margin requirement.

For LTI systems, finding the closed-loop robustness margins boils down to finding the maximum uncertainty at which closed-loop stability and performance is guaranteed. This in turn boils down to finding the inverse of the SSV. Roos et al. [154] provide a method for calculating guaranteed stability margins based on the upper bound of the SSV. Moreover, they provide an approach to assessing the eigenvalue criterion and the stability margin criteria through μ -analysis.

c) Which performance metrics does the Flying-V have to adhere to and how can these be incorporated into design requirements?

Performance requirements can be captured in different ways. These include time-domain requirements, requirements on output statistics and frequency-domain based requirements. Assessing the adherence to these requirements therefore also requires different methods. Deterministic time-domain simulations, Monte Carlo simulations and Frequency domain analyses.

Within the context of this research, it makes sense to define frequency-based performance requirements. Having obtained a frequency-domain, norm-based description of INDI-based control laws, these requirements can be included in the controller synthesis problem. These include disturbance rejection requirements, model matching requirements and control input limitations. Checking the adherence to these requirements becomes a matter of performing a robust performance (RP) analysis. A drawback of this approach is its inability to capture nonlinear requirements, such as actuator saturation limits. Nonetheless, checking the requirements is straightforward and provides robust performance guarantees.

*This part has been assessed for the course AE4020 Literature Study.

Part III

Preliminary Analysis

*This part has been assessed for the course AE4020 Literature Study.

Preliminary Analysis

The previous chapters served to introduce the Flying-V, (I)NDI, \mathcal{H}_∞ -based control design tools and a number of design criteria. In this chapter, a preliminary design of a FCS that incorporates some of the aforementioned design criteria is presented. Specifically, the preliminary analysis revolves around the design of a robust pitch-rate controller for the short-period approximation of the Flying-V's longitudinal dynamics. The goal of this preliminary analysis is to get acquainted with \mathcal{H}_∞ -design tools, as well as μ -analysis. In doing so, this sets the foundation for the design of robust INDI-based control systems, to be presented in the final work.

This chapter is structured as follows. First off, the short period approximation of the Flying-V's longitudinal dynamics is presented. Next, the main design requirement is stated. This is followed by the controller synthesis problem formulation. Finally, the results of the design methodology are presented and discussed.

5.1. Short-period model of the Flying-V

As mentioned, this preliminary analysis focuses merely on the short-period approximation of the longitudinal dynamics of the Flying-V. The longitudinal dynamics of an aircraft consist of two disjoint dominant modes. The Phugoid mode and the short period mode. The short period dynamics are thus obtained by omitting the terms in the longitudinal EOM corresponding to the phugoid mode, as seen in equation 5.1.

$$\begin{bmatrix} \dot{u} \\ \dot{w} \\ \dot{q} \\ \dot{\theta} \end{bmatrix} = \begin{bmatrix} x_u & x_w & x_q & x_\theta \\ z_u & z_w & z_q & z_\theta \\ m_u & m_w & m_q & m_\theta \\ 0 & 0 & 1 & 0 \end{bmatrix} \begin{bmatrix} u \\ w \\ q \\ \theta \end{bmatrix} + \begin{bmatrix} x_\eta \\ z_\eta \\ m_\eta \\ 0 \end{bmatrix} \eta \quad (5.1)$$

The short period oscillation is captured by studying the behavior of pitch rate q and the angle of attack α , whilst assuming constant longitudinal velocity $u = 0$. Moreover, it is assumed that the EOM are captured in the aircraft wind axes and that the aircraft is initially in steady, levelled flight. It can be assumed that $\theta_e = \alpha_e = 0$ and $U_e = V_0$, moreover, $z_\theta = m_\theta = 0$. Thus equation 5.1 reduces to the following.

$$\begin{bmatrix} \dot{w} \\ \dot{q} \end{bmatrix} = \begin{bmatrix} z_w & z_q \\ m_w & m_q \end{bmatrix} \begin{bmatrix} w \\ q \end{bmatrix} + \begin{bmatrix} z_\eta \\ m_\eta \end{bmatrix} \eta \quad (5.2)$$

Additionally, using the approximation $\alpha \approx \frac{w}{u_0}$, defining the corresponding elements of the A matrix appropriately and substituting η by the elevator deflection δ_e , the short period mode can be approximated by the following set of equations [144].

$$\begin{aligned} \begin{bmatrix} \dot{\alpha} \\ \dot{q} \end{bmatrix} &= \begin{bmatrix} \frac{z_\alpha}{u_0} & 1 \\ m_\alpha + \frac{m_{\dot{\alpha}} z_\alpha}{u_0} & m_q + m_{\dot{\alpha}} \end{bmatrix} \begin{bmatrix} \alpha \\ q \end{bmatrix} + \begin{bmatrix} \frac{z_{\delta_e}}{u_0} \\ m_{\delta_e} + \frac{m_{\dot{\alpha}} z_{\delta_e}}{u_0} \end{bmatrix} \delta_e \\ &= A_{sp} \begin{bmatrix} \alpha \\ q \end{bmatrix} + B_{sp} \delta_e \end{aligned} \quad (5.3)$$

Prior to linearizing the EOM and isolating the states corresponding to the short period mode, the aircraft is trimmed around a given condition. This has been done by adopting the trim routine formulated in [21].

For the sake of this preliminary analysis, the scope is limited to the analysis of a single flight condition. Namely, this work is centered around a cruise condition at $Ma = 0.85$, an altitude of $H = 13 \text{ km}$ and a target velocity of $V_{target} = 300 \text{ m/s}$.

This results in the linear set of equations depicted in equation 5.3. Note that for the sake of convenience, the elevators are lumped together to form one single elevator, corresponding to a single control input δ_e . The resulting transfer function is shown in equation 5.4. The natural frequency ω_{sp} and damping ratio ζ_{sp} corresponding to the short period approximation are shown in table 5.1. A comparison of the step response for the original nonlinear EOM, the linearized longitudinal EOM as seen in equation 5.1 and the short period approximation is shown in figure 5.1.

$$\frac{q(s)}{\delta(s)} = \frac{1.899s + 0.5362}{s^2 + 0.7007s + 1.664} \quad (5.4)$$

Pole locations	ζ_{sp}	ω_{sp} (rad/s)
$-0.35 \pm 1.24i$	0.272	1.29

Table 5.1: Short period poles, damping and natural frequency

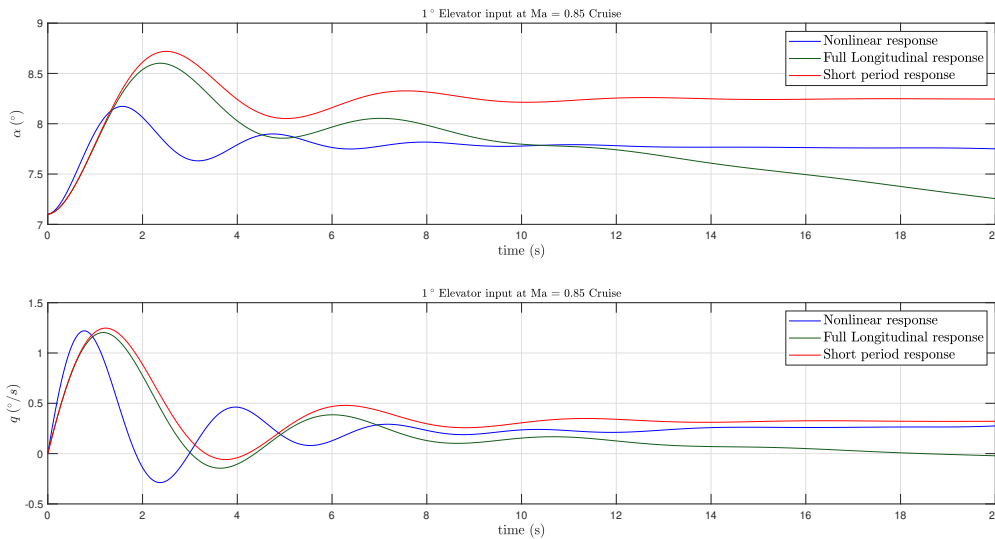


Figure 5.1: Comparison of responses to 1° elevator step input

As is visible in table 5.1, the short period approximation displays two complex, stable poles. Which is also clearly reflected in the step responses, seen in figure 5.1. These results are in line with earlier work [21]. The analysis is centered around a simulation model consisting of the short period dynamics and the elevator dynamics, which are modelled as seen in equation 2.6. The modelling & simulations are performed in Matlab R2023b [157].

5.2. Design Requirements

The handling quality requirements that the short-period mode of the Flying-V is to adhere to originate from MIL-STD-1797A. Specifically, adherence to the the CAP criteria is adopted as the primary design objective. Table 5.2 shows the short-period damping ratio ζ_{sp} of the Flying-V during the cruise condition, which meets Level 2 handling qualities.

Eigenmode	Value Flying-V	requirements
Short Period	$\zeta_{sp} = 0.2729$	Level 1: $0.3 < \zeta_{sp} < 2.0$ Level 2: $0.2 < \zeta_{sp} < 2.0$ Level 3: $\zeta_{sp} > 0.1$

Table 5.2: Short period handling quality requirements during cruise

The requirement in MIL-STD-1797A states that the equivalent pitch rate response to stick input should be of the form depicted in equation 5.5 over a frequency range of 0.1 to 10 radians per second:

$$\frac{q_{ref}(s)}{\delta_{stick}(s)} = \frac{K_q(T_{\theta_2}s + 1)}{s^2 + 2\zeta_{sp}\omega_{sp}s + \omega_{sp}^2} \quad (5.5)$$

Moreover, the CAP parameter is to fall within the regions depicted in figure 5.2 depending on the desired flying quality level. The Flying-V is considered a class III type aircraft and during cruise, is considered to be in flight phase B. The CAP parameter is to be estimated from the equivalent-system parameters $1/T_{\theta_2}$ and ω_{sp} , as shown in equation 5.6.

$$CAP = \frac{\omega_{sp}^2}{n_\alpha} = \frac{g\omega_{sp}^2 T_{\theta_2}}{V} \quad (5.6)$$

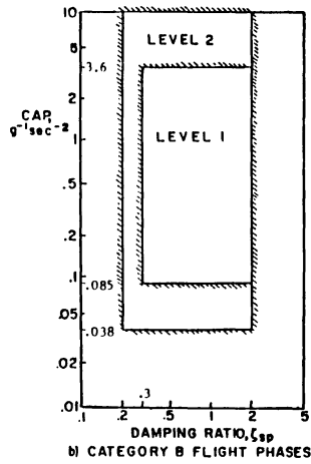


Figure 5.2: Short period dynamic requirements for category B flight phases

n_α is known as the gust-or load-factor sensitivity of the aircraft. As can be seen in figure 5.2, the desired values for the damping ratio and the CAP value are within the following ranges $0.3 \leq \zeta_{des} \leq 2.0$ and $0.085 \leq CAP \leq 3.6$ [132]. The desired closed-loop response is formed with the choice of values stated in table 5.3 and serves as the main design objective for the controller.

Desired parameter values
$CAP_d = 0.4$
$\zeta_d = 1.5$
$\omega_d = 3.0$
$T_{\theta_2}^d = \frac{CAP_d V}{g\omega_{sp}^2}$
$K_q^d = \frac{\omega_d^2}{\omega_{sp}^2} K_q^{ba}$

Table 5.3: Short period design parameters for preliminary analysis, based on MIL-STD-1797A [132]

These values yield a transfer function displaying Level 1 qualities that also possesses favorable time-response characteristics. The step-response of the desired transfer function is depicted in figure 5.3, alongside the step response of the bare air-frame dynamics.

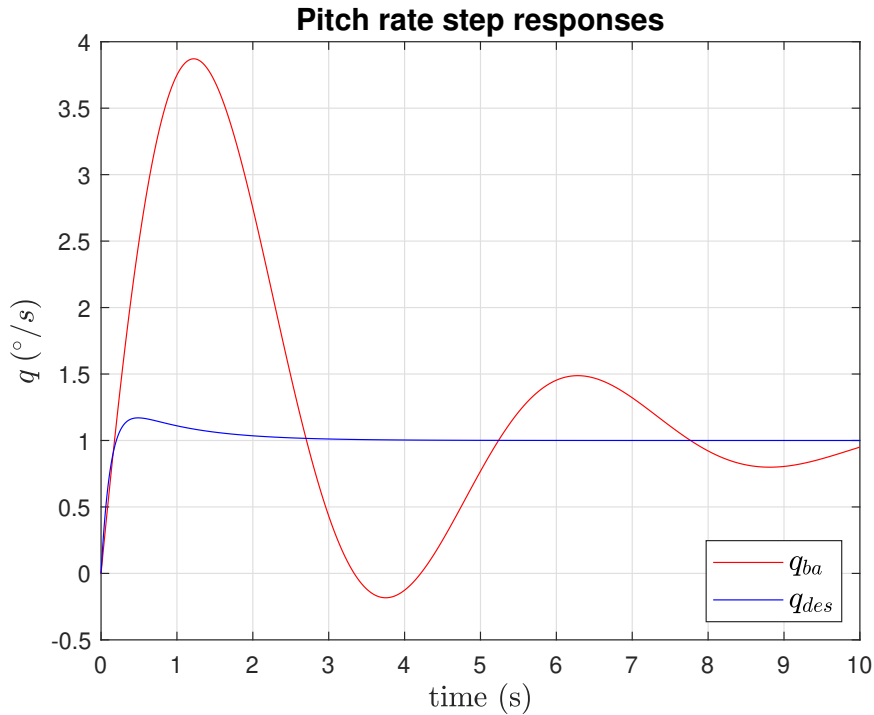


Figure 5.3: Desired pitch rate response alongside bare air-frame response

5.3. Controller Synthesis

5.3.1. Closed-loop problem formulation

Next to the desired closed-loop time-domain response, a variety of additional frequency-domain constraints have been set. These constraints are formulated in terms of closed-loop constraints and included in the \mathcal{H}_∞ -control problem. The proposed designs includes the four-block approach, as mentioned in section 3.2.3. The closed-loop definition of the four-block problem, as seen earlier in equation 3.42, is defined as follows.

$$\min_K \left\| \begin{pmatrix} W_1 S_o W_r & W_1 S_o G W_d \\ W_2 K S_o W_r & W_2 K S_o G W_d \end{pmatrix} \right\|_\infty \quad (5.7)$$

Considering both input and output disturbances, d_i , d_o as well as noise n and a reference input r , the transfer functions from each of these signals to the error e , control signal u and output y are provided in table 5.4.

Table 5.4: Non-weighted transfer functions

Outputs	Inputs			
	r	d_i	d_o	n
e	S	$-SG$	$-S$	$-S$
y	T	SG	S	$-T$
u	KS	$-KSG$	$-KS$	$-KS$

Shaping of these transfer functions is done with the design of the filters. Where W_r and W_d represent pre-filters of respectively the reference signal r and the input disturbance signal d_i . These were set as

scalar values and found to result in adequate closed-loop performance, similar to the approach in [128], where $W_r = 1$ and $W_d = 0.01$. A more elaborate approach would be to shape the pre-filters to reflect the frequency content of the exogenous input signals. For the reference signal, this would reflect the frequency content of the pilot stick input. Respectively, the disturbance pre-filter can be chosen to reflect the frequency content of input disturbances, such as gusts, an example of the use of a Dryden gust model is seen in [158].

The choice of the output weights W_1 and W_2 follows the rhetoric explained in section 3.2.2. Accordingly, W_1 is shaped as a low-pass lead-lag filter and W_2 is shaped like a high-pass lead-lag filter to ensure sufficient input and output disturbance attenuation, noise attenuation, steady-state tracking performance and to limit control effort. These are defined as follows.

$$\begin{aligned} W_1(s) &= \frac{1.413s + 2.993e^{-5}}{s + 2.993} \\ W_2(s) &= \frac{0.01s + 140}{s + 0.0014} \end{aligned} \quad (5.8)$$

In addition to the closed-loop transfer functions associated with the four-block description, an additional closed-loop transfer function is included in the design. Specifically, a model-matching error is included in the design. The model-matching error is defined as the desired output q_{des} minus the actual output q . Where the desired output in this case follows from the transfer function $G_{ref}(s)$ describing the pitch-rate response shown in figure 5.3, following from the parameters listed in table 5.3. As such, the exogenous output describing the model matching error is described as follows.

$$z_{te}(s) = (\delta_{stick}(s)G_{ref}(s) - q(s))W_{te}(s) \quad (5.9)$$

Where $W_{te}(s)$ represents the output filter for the model-matching error, with the following transfer function.

$$W_{te}(s) = \frac{3}{s + 0.015} + \frac{1}{30} \quad (5.10)$$

Where the parameters of $W_{te}(s)$ were chosen such that it enforces a upper bound on the steady-state tracking error of 0.005, a high-frequency error bound of 30 and a gain crossover frequency of 3 rad/s. Accordingly, the transfer functions that map the input signals r and d_i to the model-matching tracking error are referred to as $T_{r \rightarrow te}(s)$ and $T_{d_i \rightarrow te}(s)$.

The overall closed-loop norm that needs to be minimized consists of the transfer function from the exogenous inputs w to the exogenous outputs z , which reduces to the following.

$$\min_K \left\| \begin{pmatrix} r \\ d_i \end{pmatrix} \rightarrow \begin{pmatrix} z_1 \\ z_2 \\ z_{te} \end{pmatrix} \right\|_{\infty} \quad (5.11)$$

5.3.2. Uncertainty description

Uncertainty is introduced in two forms. Namely, in the form of real parametric uncertainty and complex dynamic uncertainty. The former is present as modelling uncertainty in the aerodynamic coefficients m_{α} and m_{δ} , with a deviation from their nominal values of $\pm 75\%$ and $\pm 25\%$ respectively.

Dynamic uncertainty is introduced in the form of multiplicative input uncertainty in the actuator model and the bare airframe model. These serve as lumped representations of higher-order, unmodeled dynamics and are introduced in the input channels of the actuator and bare airframe models as follows.

$$\begin{aligned} G_{act}^{\Delta}(s) &= G_{act}(s)(1 + \Delta_{act}(s)W_{act}(s)) \\ G_{ba}^{\Delta}(s) &= G_{ba}(s)(1 + \Delta_{ba}(s)W_{ba}(s)) \end{aligned} \quad (5.12)$$

Where $w_{act}(s)$ and $w_{ba}(s)$ represent the uncertainty weights, these are defined as follows.

$$W_{act}(s) = W_{ba}(s) = K_0 \frac{\tau_{lag} s + \tau_{lead}}{\tau_{lead} s + \tau_{lag}} \quad (5.13)$$

With $K_0 = 0.1$, $\tau_{lag} = 5$ and $\tau_{lead} = 100$. These weights enforce an upper bound of 10% model error at steady-state which grows beyond 100% model error at frequencies larger than 50 rad/s.

5.3.3. Closed-loop interconnection structure

Having established the closed-loop constraints and the uncertainty structures, the synthesis of a full-order controller is rather straightforward. Using the Matlab function *Musyn* from the *Robust Control Toolbox*TM [37], a full-order μ -optimal controller for the given closed-loop problem formulation is obtained. The closed-loop interconnection structure is depicted in the figure below.

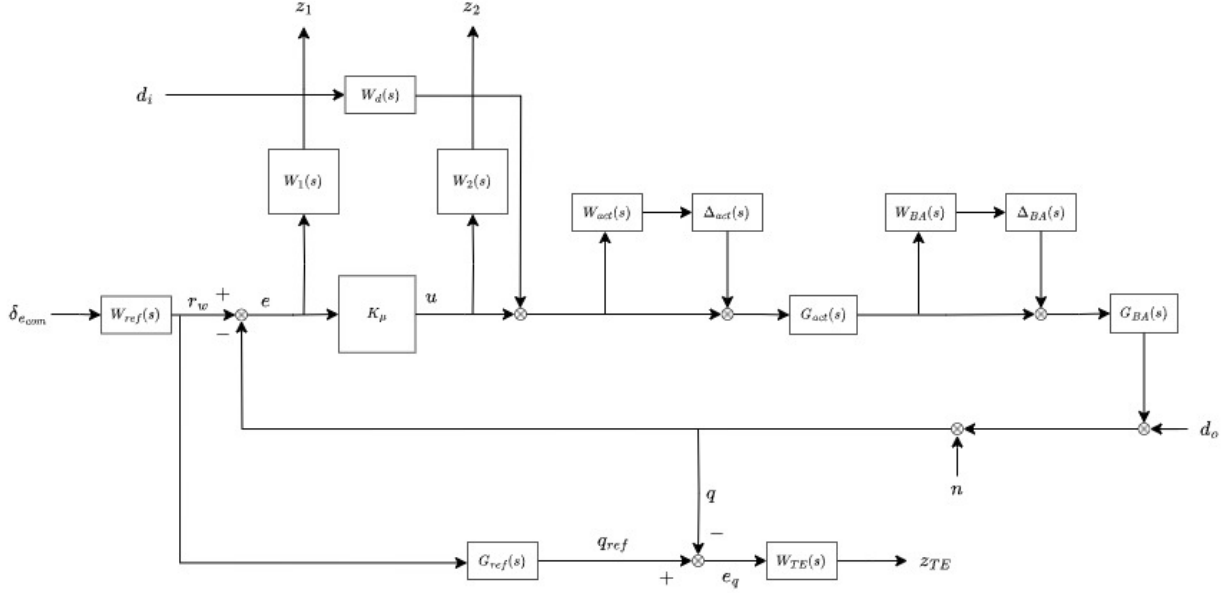


Figure 5.4: Control system interconnection structure with unstructured μ -controller

Note that for the synthesis of the controller K_μ , the controller is left out of interconnection shown above. The remaining parts make up the generalized plant P . The closed-loop norm to minimize, as shown in equation 5.11 is explicitly stated in equation 5.14 below.

$$\min_K \left\| \begin{pmatrix} W_1 S_o W_r & -W_1 S_o G W_d \\ W_2 K S_o W_r & -W_2 K S_o G W_d \\ W_{te} T_{r \rightarrow te} W_r & -W_{te} T_{d_i \rightarrow te} W_d \end{pmatrix} \right\|_\infty \quad (5.14)$$

5.4. Results

This section describes the results of the synthesized controller. First off, a frequency-domain analysis of the relevant closed-loop transfer functions is presented. This is followed by a classical stability margin analysis alongside a disk-based stability margin analysis. Next, a more elaborate robust stability & performance analysis is presented in the form of μ -analysis. Finally, linear simulations alongside an assessment of the CAP criterion and the Gibson criteria is presented.

5.4.1. Closed-loop transfer function analysis

The frequency domain analysis is based on the closed-loop transfer functions as described before. Figure 5.5 depicts the closed-loop transfer functions from each of the exogenous inputs w to each of the exogenous outputs z . Note that the transfer function from the input disturbance d_i to the model tracking error e_q is not shown, as it is equivalent to $S_o G$.

The cyan coloured lines represent the closed-loop transfer functions of 20 random realizations of the perturbed plant. The dark blue line represents the nominal closed-loop transfer function. The inverse weighting filters, acting as the enforced bound on the respective transfer function, are depicted in red.

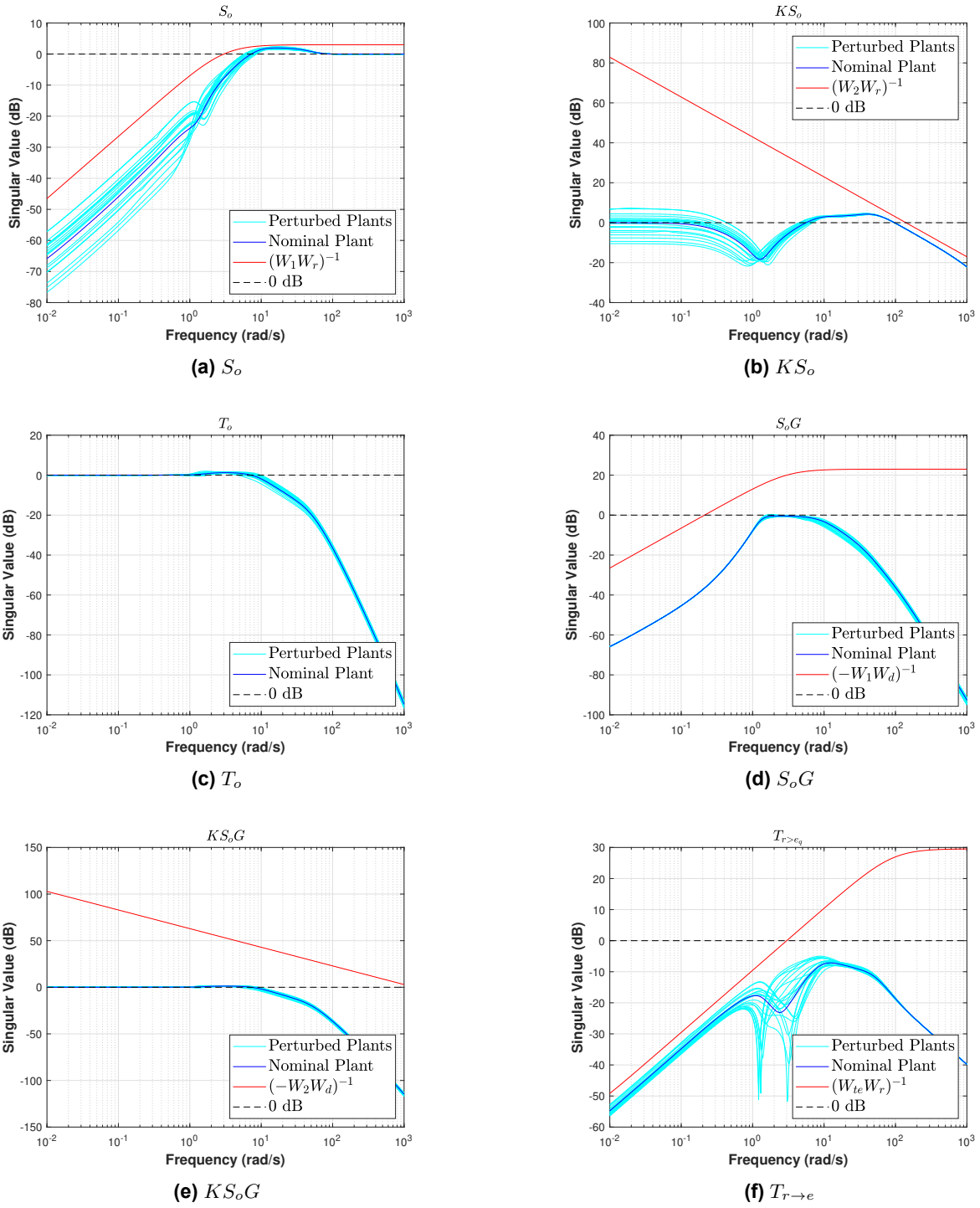


Figure 5.5: Closed-loop transfer functions

As can be seen, the resulting closed-loop transfer functions obey the enforced upper bounds. S_o and S_oG are limited at low frequencies, demonstrating sufficient disturbance attenuation at those frequencies. Looking at the control sensitivity KS_o , it remains close to unity in the low-frequency range. Whereas it shows a slight dip at around 10^0 rad/s, before increasing to values greater than unity until meeting the upper-bound at around 10^2 rad/s and rolling off thereafter. This is a result of the choice of the bandwidth of S_o . Choosing to speed up the dynamics, in other words, shifting S_o to the right, will also result in KS_o being shifted to the right. This cannot be done free of the charge, as one runs into the limits of the actuator bandwidth. Another peculiarity of the control sensitivity of the sampled systems is the DC-gain. For the controller synthesis, the plant was scaled by the inverse of the DC-gain of the nominal plant. Resulting in a control sensitivity function with unitary DC-gain for the nominal plant. However, as the DC-gain of the perturbed plants is slightly different, the resulting DC gain of the perturbed controller sensitivities is not equal to 1.

Looking at transfer function associated with the model-matching error $T_{r \rightarrow e}$, at low to mid frequencies it is sufficiently small, indicating good reference model-tracking capabilities. This favorable reference-model tracking behavior comes at the cost of increased control effort in this frequency range, as can be seen in KS_o , highlighting the trade-off between the two.

5.4.2. Classical & disk-based stability margins Analysis

An initial judgement of the stability of a given controller is typically provided by a classical gain and phase margin analysis. In addition to a classical analysis, a disk-based assessment was performed. The disk-based stability margins as a function of frequency are shown in figure 5.6. Moreover, table 5.5 shows a side-by-side comparison of the classical and disk-based margins for both the nominal and the worst case perturbed closed-loop system.

MIL-DTL-94090E states that the gain and phase margin must be at least 6 dB and 45° respectively [150]. As listed in table 5.5, the nominal aircraft model adheres to these criteria for both of the margin analysis methods. However, it is clear that the worst-case model does not meet these requirements. Moreover, looking at figure 5.6, it can be concluded that the discrepancy in margins between the nominal and worst-case plant are most pronounced between 1 to 5 rad/s. Suggesting that the plant has an increased sensitivity to uncertainty in this frequency range. This is confirmed by the value of S_oG within this region, as seen in figure 5.5.

	Classical		Disk-based	
	Gain (dB)	Phase ($^\circ$)	Gain (dB)	Phase ($^\circ$)
Nominal plant	27.73	57.04	10.13	55.38
Worst case	-3.41	20.88	2.18	14.22

Table 5.5: Classical and disk-based stability margins

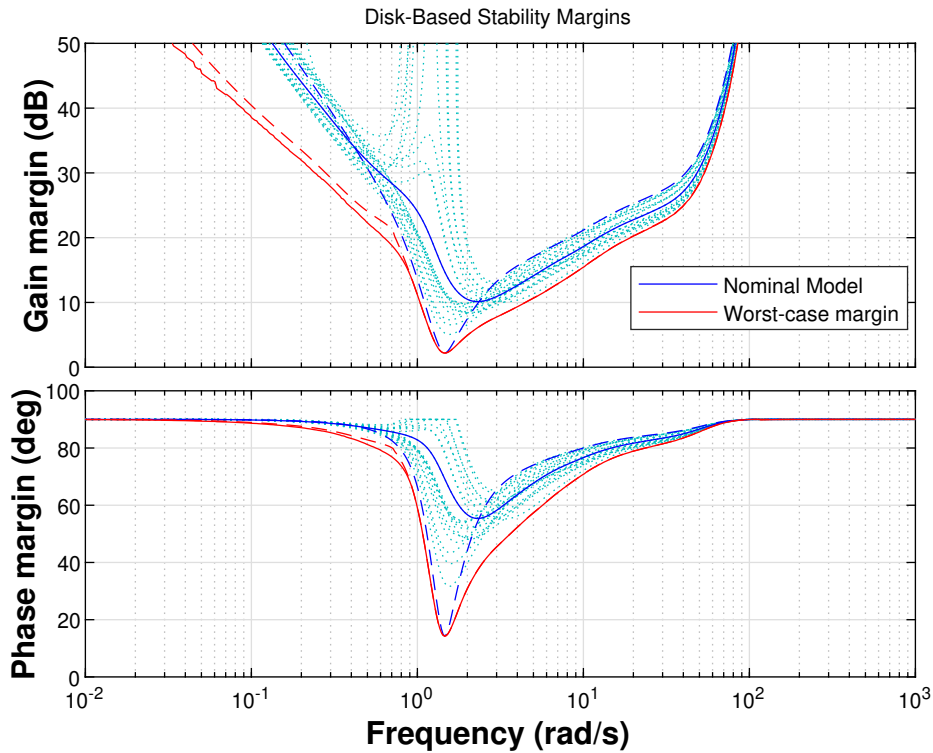


Figure 5.6: Disk-based stability margins of closed-loop system

5.4.3. Robust stability & performance analysis (μ -analysis)

Aside from a disk-based margin analysis, a more elaborate μ -analysis was performed on the resulting closed-loop systems. This is split up into a robust stability analysis and a robust performance analysis. The breakdown of the robust stability assessment is seen in figure 5.7, the robust performance measure μ_{RP} is depicted in figure 5.8.

The results of the robust stability analysis show that the closed-loop remains stable for the entire uncertainty set, corresponding to a singular value $\mu_{RS} < 1$. Moreover, from figure 5.7, it can be concluded that up until 5 rad/s , robust stability is most impacted by parametric uncertainty δ . Above that frequency, dynamic uncertainty dominates the robust stability measure. Moreover, the peak in μ_{RS} between 1-5 rad/s verifies the finding of the disk-based stability analysis, showing an increased sensitivity in this frequency range.

The nominal performance of the closed-loop system is guaranteed, as $\mu_{NP} < 1$. Moreover, looking at the robust performance measure μ_{RP} in figure 5.8, it can be concluded that performance is also guaranteed over the entire uncertainty set, as $\mu_{RP} < 1$. The degradation in robust performance is dominated by the uncertainty in m_α and m_δ , similar to the degradation in robust stability.

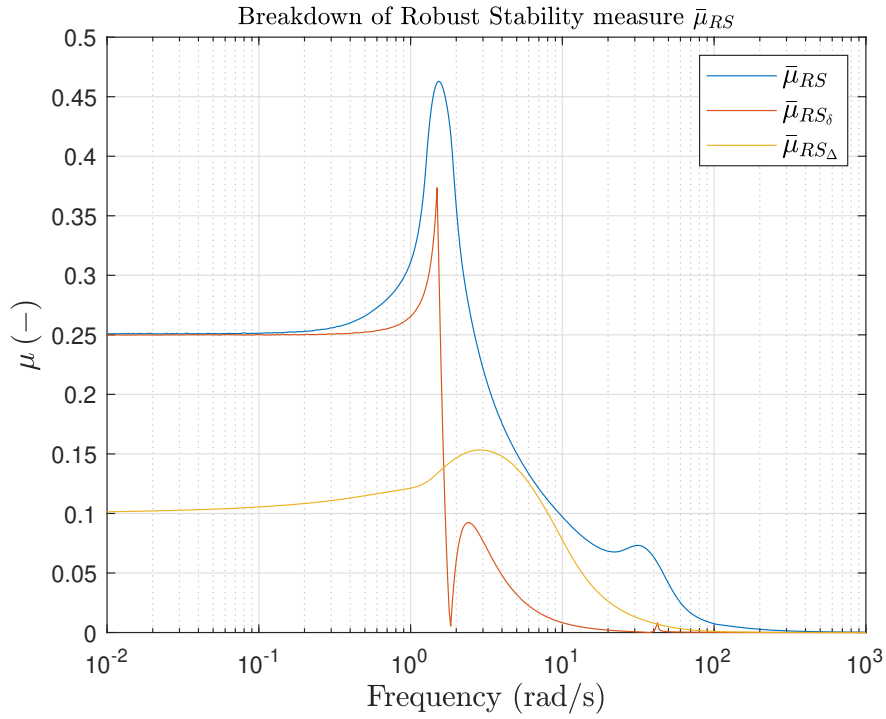


Figure 5.7: Robust Stability breakdown

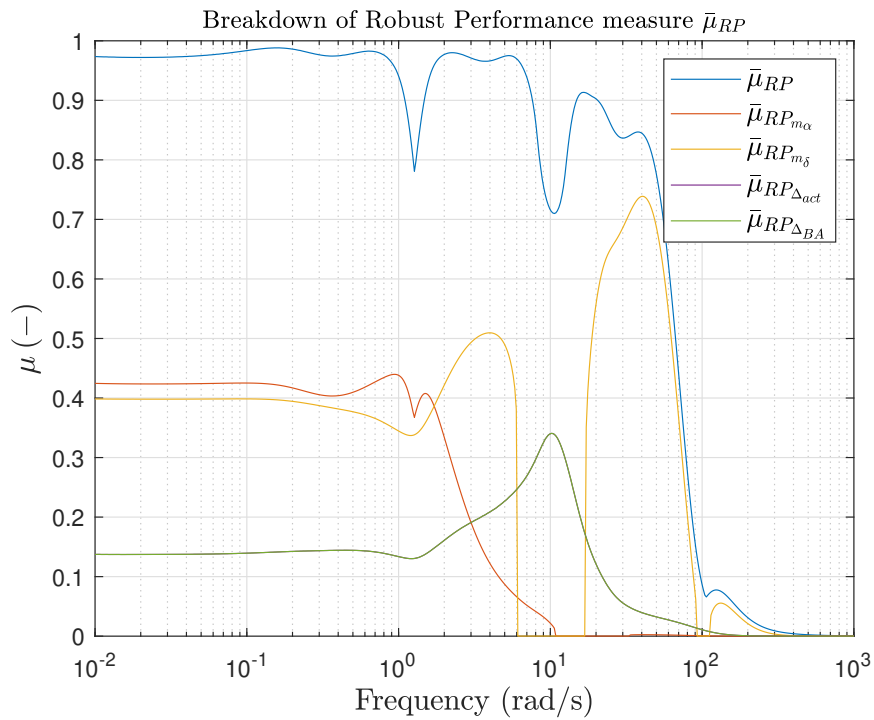


Figure 5.8: Robust Performance breakdown

5.4.4. Linear simulations

In order to verify the time-domain performance of the resulting controller, linear simulations were performed. Figure 5.9 depicts the response to a $1^\circ/s$ pitch rate reference signal. The red line represents the desired closed-loop response, following from the parameters stated in table 5.3. Note that the shaded area around the response of the nominal system represents the upper and lower bounds of the step responses of the perturbed plant, for which 20 random samples were taken. The resulting control surface activity is depicted in figures 5.10 and 5.11.

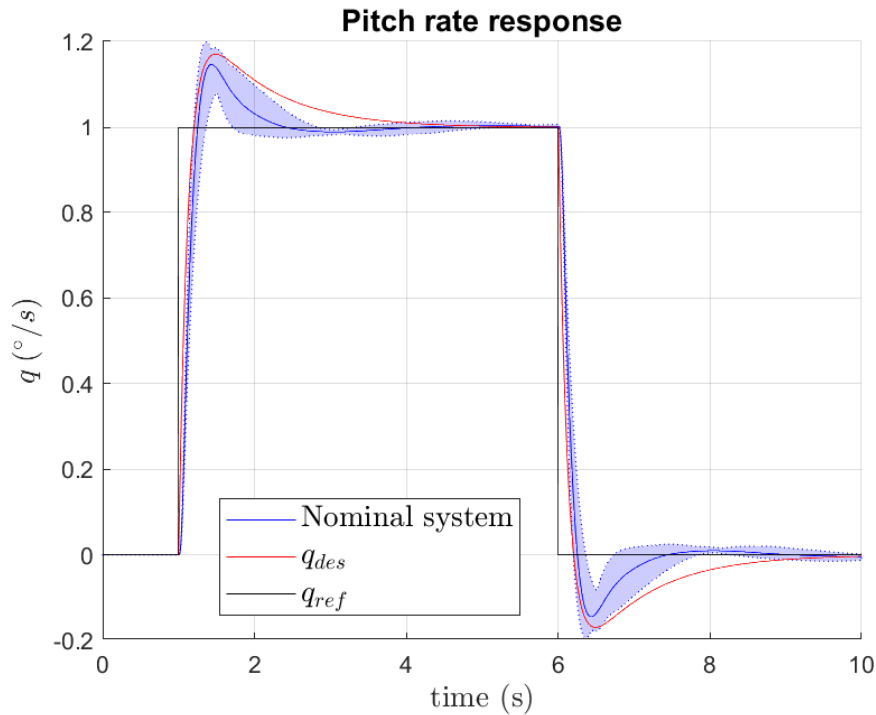


Figure 5.9: Pitch rate response of unstructured controller

Judging from the step-response depicted in figure 5.9, the closed-loop system tracks the desired pitch rate response q_{ref} sufficiently well. The mean RMSE between the perturbed systems and the desired pitch rate response is equal to $RMSE_{mean} = 1.1 \cdot 10^{-3}$ ($^\circ/s$). However, the closed-loop response seems to fall between the stick input and the desired response. This is likely to be as a consequence of the choice of the weighting filters. Altering the weights of W_{ref} or W_{te} could bias the closed-loop system to either follow the stick input more closely or track the reference model more precisely.

Judging by figure 5.10, the elevator deflections show a large spread amongst samples of the perturbed plant. This is likely due to the uncertainty in the control effectiveness parameter m_δ , warranting greater control surface deflection. This could be an issue at larger pitch rate demands or greater uncertainty levels, as the elevator deflections are limited to $\pm 25^\circ$. Hence, actuator saturation could be reached.

The elevator deflection rate, as shown in figure 5.11, shows large jumps, as expected. Nonetheless, the rates fall within the rate limits of the Flying-V's actuators, amounting to ± 80 ($^\circ/s$).

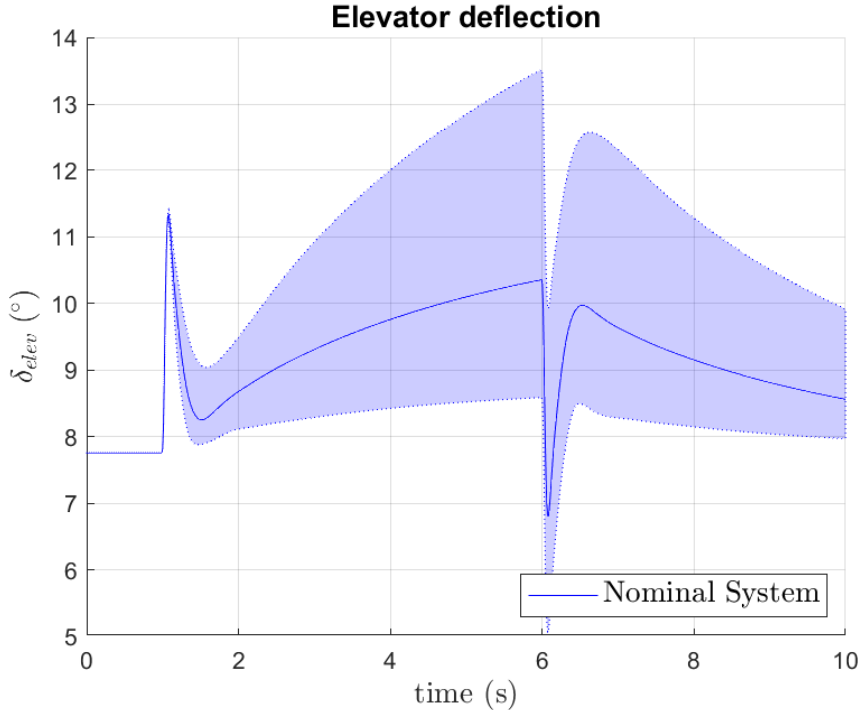


Figure 5.10: Elevator deflection

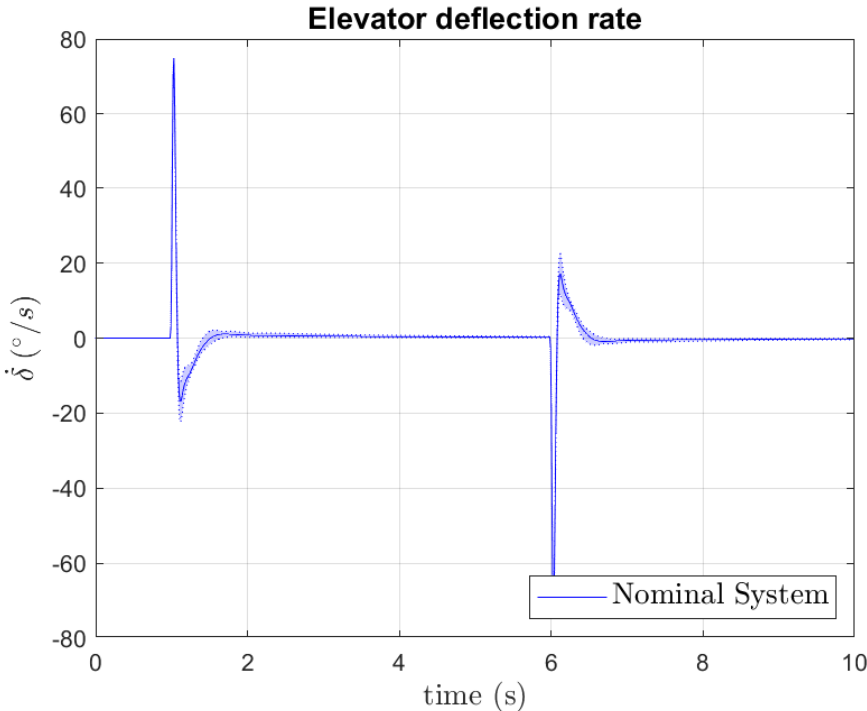


Figure 5.11: Elevator deflection rate

5.4.5. Handling quality assessment

As stated, a main design requirement for the closed-loop system was the adherence to the CAP criteria. Figure 5.12 shows the assessment of the CAP criteria for 20 random realizations of the perturbed plant, alongside the boundaries of the CAP criteria. Note that the closed-loop response is of high-order, therefore a Low-Order Equivalent System (LOES) is fit to the higher-order system, making it possible to evaluate the the CAP value.

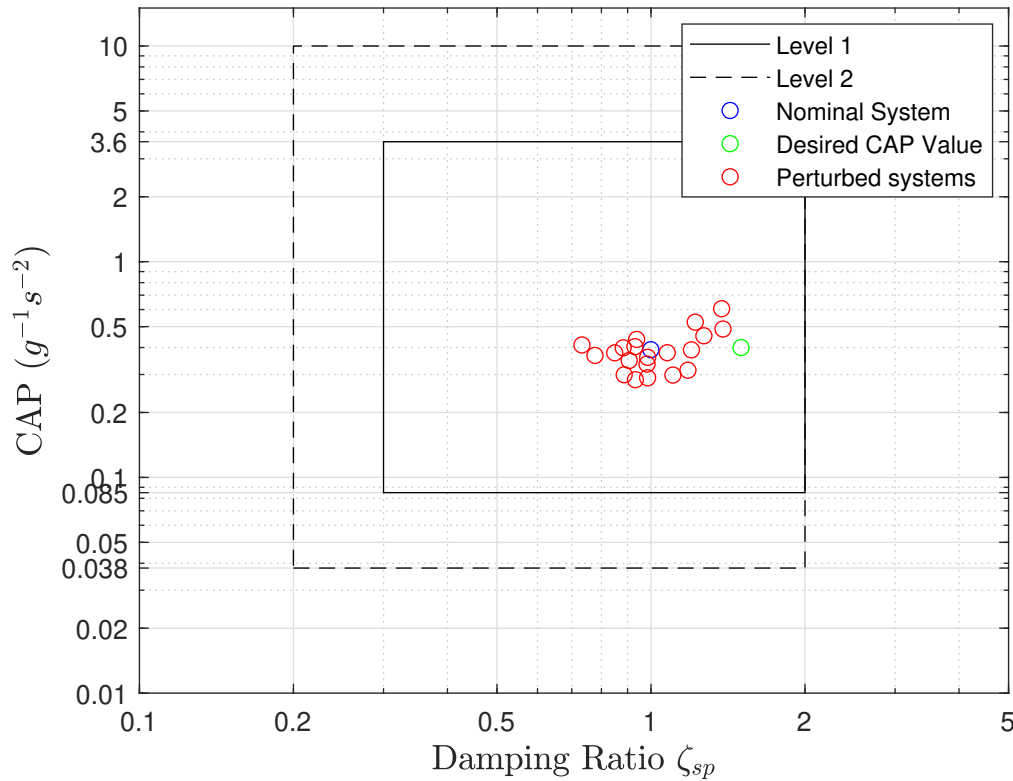


Figure 5.12: CAP criteria assessment

It can be concluded that the closed-loop system adheres to the CAP criteria for all the plants in the uncertainty set, thereby guaranteeing Level 1 handling qualities.

The Gibson criteria were not explicitly stated as design requirements. Nonetheless, these are assessed to allow for a comparison with earlier work seen in [24]. Specifically, the Gibson drop-back criteria and the flight path angle delay criteria were evaluated.

For the nominal closed-loop system, the resulting values are shown in table 5.6. A visual representation of the values for 20 random realizations of the perturbed plants are shown in figure 5.13.

	μ -controller
$\frac{q_{max}}{q_{ss}}$ (-)	1.143
$\frac{DB}{q_{ss}}$ (-)	0.065
t_γ (s)	1.906

Table 5.6: Gibson criteria values of the nominal closed-loop system

Looking at figure 5.13, it can be concluded that all of the sampled closed-loop systems adhere to the Gibson Dropback criteria. However, adherence to the flight path angle delay criterion can not be guaranteed. As seen in table 5.6, the nominal value of the flight path angle delay $t_\gamma = 1.906$ s, does not

adhere to Gibson’s suggestion of $t_\gamma < 1.5\text{ s}$ and $t_\gamma < 1.0\text{ s}$ for precision tracking tasks. Moreover, the perturbed plants show a wide spread in the value of t_γ , which is highlighted in figure 5.14. As can be seen, the flight path angle response differs greatly between samples. Some show minimal delay, whereas others respond very slowly and even display non-minimum phase behavior, in line with findings in [24]. Judging by the values seen in table 5.6, the results of the μ -controller are comparable to those of a PID-controller and INDI-based controller presented in [24].

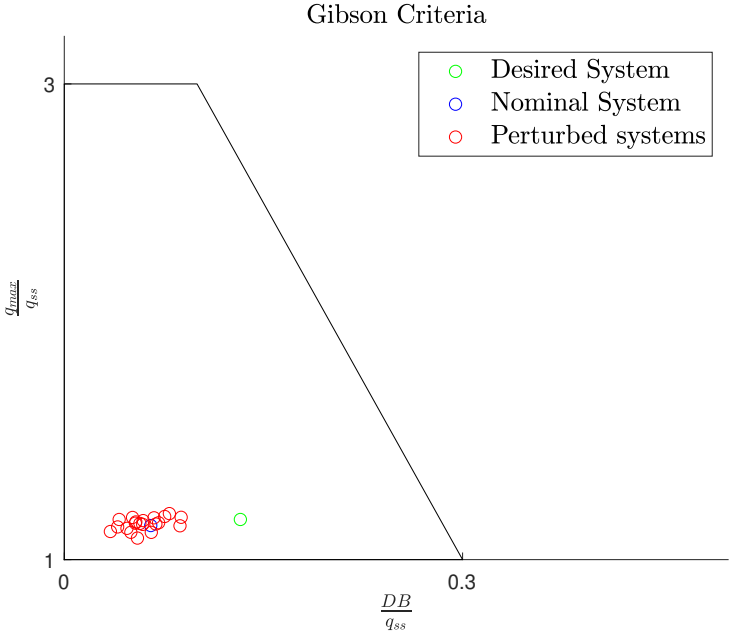


Figure 5.13: Gibson drop-back criterion assessment

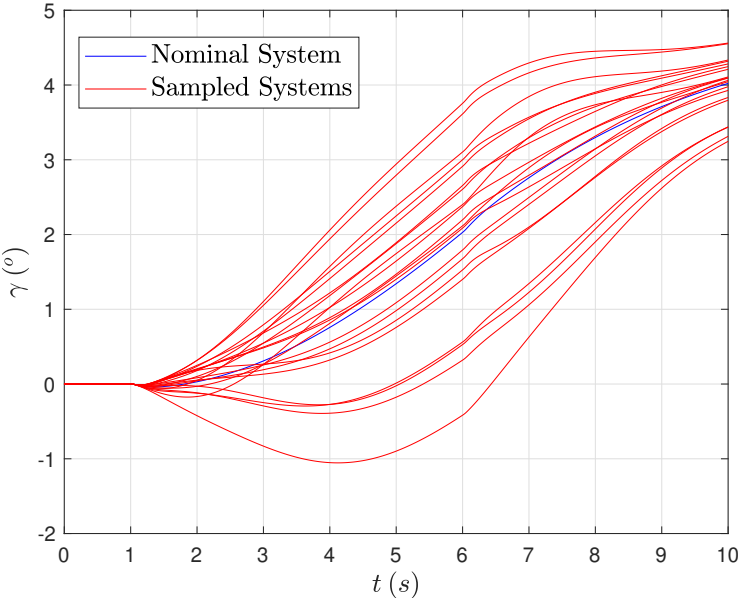


Figure 5.14: Flight Path angle simulation

Part IV

Closure

Conclusions

The goal of this research was to assess the capability of \mathcal{H}_∞ -control tools to improve the robustness of INDI-based flight control for the Flying-V. In an attempt to achieve the research objective, a number of research questions and sub-questions were established. These are restated hereafter, alongside brief answers to these question, for more elaborate answers on research questions 1-3, the reader is referred to the conclusion sections of the respective chapters in part III.

Research Question 1

What is the state-of-the-art research on the Flying-V?

1. Which elements make up the simulation model of the Flying-V?

The latest simulation model of the Flying-V consists of a number of subsystems. In essence, it revolves around a aerodynamic model that combines various aerodynamic data sources. Namely, the combined model consists of aerodynamic data from VLM simulations, WTE data and Flight test data. In addition to an aerodynamic model, FCS hardware model have been proposed in the form of discrete sensor models, a second-order actuator model and a first order engine model.

2. What are the stability and handling quality characteristics of the bare airframe?

Previous assessments of the Flying-V's eigenmodes were based on the linearized EOM at two distinct flight conditions with two distinct CG configurations. Namely, at a cruise condition and an approach condition with an aft and a forward CG configuration. It was concluded in previous research that at the approach condition, the short period mode and the aperiodic roll mode are stable, whereas the phugoid, the Dutch roll mode and the spiral mode are unstable. At the cruise condition, the short period, phugoid and aperiodic roll mode were all found to be stable. Whereas the spiral mode is unstable. The Dutch roll mode is unstable at the forward CG, yet stable with the aft CG configuration. It was concluded in previous research that shifting the CG aft results in the Dutch roll mode poles shifting to the left in the complex plane, suggesting an increase in stability, contrary to existing literature, which shows deteriorated stability when shifting the CG aft. It was suggested that this is a result of the contribution of C_{Y_p} .

3. Which stability & control augmentations systems have been applied to the Flying-V?

Previous work on the Flying-V includes a conventional PID-based pitch-rate augmentation system to improve the low-speed handling qualities of the Flying-V. Moreover, a DRL based attitude controller has been proposed. In addition, several INDI-based control laws have been implemented, showing promising results. Van Overeem presented two INDI-based augmentation systems, a SAS and a CAS. Van Overeem concludes that the previously unstable dynamic modes could be stabilized by the proposed augmentation systems. Moreover, van Overeem stated that the closed-loop system remains stable for up to 20% uncertainty in the aerodynamic parameters [47].

Stougie [24] later introduced a C^* -controller with a INDI-based inner-loop. Moreover, Stougie introduced a form of flight envelope protection. Stougie assessed the handling qualities for the cruise and approach conditions earlier defined van Overeem [47] and concluded that for sufficiently fast body rate sensors, with time-delays up to 0.04s, the aircraft displays Level 1 handling qualities. In addition, Stougie assessed the stability margins in the presence of sensor dynamics. It was concluded

that the proposed control system remains stable for sampling times smaller than 0.1s. Moreover, it was suggested that the closed-loop system remains stable up to 20% of aerodynamic uncertainty. Stougie also mentioned that the effect of various other phenomena, such as CG mismatch, aeroelastic effects and time-delays remained to be studied.

4. What is the state-of-the-art on INDI-based flight control design?

INDI has been praised for its simplicity, cost effectiveness and robustness to parametric uncertainty. Since its emergence in the early 2000s, various renditions have emerged. These include EINDI, and hybrid INDI, which have emerged in an attempt to alleviate some of the issues commonly seen in the application of standard sensor-based INDI-based control laws. An issue with the use of sensor-based INDI is the need for accurate state derivative and input measurements, which may not always be present or may introduce time-delays. Early work by Bacon and Ostroff had already provided insight into how these practical challenges could be overcome and proposed a filter-based actuator compensation strategy to reduce the impact of sensor noise [159]. Later on, researchers at DLR also recognized this and emphasized the necessity for appropriate filter design to ensure proper functioning of sensor-based INDI in practice [35]. Specifically, they observed that the challenges presented by time-delays could be overcome through *signal synchronization*, which has since become widespread practice in the design of sensor-based INDI control laws and was first conceptualized and coined in [160]. This facilitated a successful demonstration of sensor-based INDI on a fixed-wing FASER UAV in 2013 [160]. In 2016, the concept was first formalized by Smeur et al. [29], whom performed subsequent in-flight experiments using a quadrotor UAV [29, 161]. Later on, in-flight demonstrations of INDI on a CS-25 certified passenger aircraft jointly owned by the Delft University of Technology and NLR, the PH-LAB Cessna Citation II, were performed. Prior to these demonstrations, Van 't Veld carried out a preliminary analysis on the foreseen implementation challenges [30]. The impact of exogenous disturbances, controller sampling rates, aerodynamic model mismatches, measurement noise and time-delays were studied. Moreover, it was concluded that additional body rate measurement delay has a greater destabilizing effect than additional actuator measurement delay. In addition, it was demonstrated that the synchronization strategy proposed by Smeur et al. [29] was an effective strategy on the PH-LAB as well. This eventually resulted in a number of in-flight demonstrations on the PH-LAB in 2018.

In an attempt to alleviate the issues associated with synchronization delay, Kumtepe et al. [33] and Kim et al. [81] have proposed variations of Hybrid INDI. Hybrid INDI fuses the model-based and sensor-based approaches in an attempt to establish an inversion strategy that is more balanced from a robustness perspective. Kumtepe proposed a Hybrid INDI approach based on complementary filtering and demonstrated that the proposed control law retains good performance in the presence of model mismatches and measurement delays, to an extent that exceeds sensor-based INDI. Demonstrating that the hybrid INDI approach can tolerate larger time-delays before destabilizing when compared to sensor-based INDI [33].

A reoccurring theme throughout the research on INDI has been its robustness properties. Multiple studies have observed a level of robustness to aerodynamic uncertainty. Yet it has been observed that INDI-based control laws are sensitive to time-delays. These observations have highlighted the need for greater insight into the stability and robustness properties of INDI-based control laws. Wang et al. [34] were the first to establish formal nonlinear stability and performance properties of INDI-based control laws as a function of sampling rate. However, the analysis was limited to regular perturbations and exogenous disturbances. As stated, time-delays have been shown to have the greatest destabilizing effect on INDI-based control laws. Time-delay is part of the category of singular perturbations. As such, a thorough stability and robustness analysis of INDI must include singular perturbations. Wang et al. [34] briefly considered these, yet left a detailed analysis as future work. More recently, the research community has started to recognize the importance of studying the effect of singular perturbations. Yet, most of these studies assume that all model uncertainty and singular perturbations can be parameterized. It is well known that, for physical systems, these can not be parameterized. Singular perturbations include unknown structural dynamics and aerodynamic effects, such as those seen on the Flying-V. These are by definition unstructured (non parametric) by nature and can be captured by norm-bounded uncertainty descriptions. Pollack [35] argues that to adequately assess the stability and robustness of INDI-based control laws, these unstructured uncertainties must be included. To that extent, Pollack established a systematic formal robustness analysis of INDI-based control law, making use of the \mathcal{H}_∞ -framework.

Research Question 2

How can \mathcal{H}_∞ tools be used to establish robust flight control systems?

1. How is the \mathcal{H}_∞ framework defined?

The \mathcal{H}_∞ -framework is a norm-based descriptions of transfer function. Technically, it refers to the Hardy space of the set of transfer functions with a bounded ∞ -norm. In terms of transfer functions, it is defined as the peak singular value over frequency. Subsequently, \mathcal{H}_∞ -control tools are often concerned with the minimization of the largest singular value over frequency. Specifically, one is often interested in the minimization of the \mathcal{H}_∞ -norm of some closed-loop system. To enable this, the framework makes use of the so called generalized plant description, which can be formulated in terms of the LFT of the plant and the controller $N = F_l(P, K)$.

This generalized description also facilitates the incorporation of uncertainties. Various forms of uncertainty descriptions exist, these can be captured in a uncertainty matrix Δ . As such, a closed-loop system containing uncertainty can be described by the LFT of the plant-controller interconnection and the uncertainty matrix: $M = F_l(\Delta, N)$. Subsequently, this description can be used to perform a robustness analysis of the closed-loop system.

A natural question that arises is: *How much uncertainty can a closed-loop system tolerate before it becomes unstable?* This question can be answered by looking at the structured singular value (SSV or μ). This boils down to finding the smallest uncertainty that renders the determinant of the closed-loop system singular. Moreover, necessary and sufficient conditions for robust stability and robust performance can be described using the SSV.

Computing the SSV turns out to be a NP-hard problem. In practice, bounds on the value of μ are instead computed, which lie sufficiently close to the actual value. Over the years, various algorithms that calculate the bounds on μ have been established. These can be divided into outer-relaxation techniques and inner-relaxation techniques. According to some, outer-relaxation techniques provide conservative results.

Solving the \mathcal{H}_∞ -optimal control problem involves finding all stabilizing controller K , such that $\|F_l(P, K)\|_\infty < \gamma$, where $\gamma > \gamma_{min}$. This corresponds to a sub-optimal solution which is sufficiently close to the optimal solution and easier to obtain, theoretically and computationally. The problem was first formally defined by Zames [103] back in 1981, ever since, many solutions to the problem have emerged. Doyle et al. [104] first identified that solving the problem requires solving two AREs. Later on, alternative, LMI-based solutions emerged [105, 106]. The ARE and LMI-based solutions are all found in the full controller space κ_{full} , which is a convex problem. The resulting (sub)-optimal controllers will be of the same order of the generalized plant P . Finding a solution in a smaller and more practical controller space is a much more difficult problem, as this is a non-convex and non-smooth problem. In the late 90s, BMI-based solutions emerged, these methods would ultimately hold the key to solving the structured \mathcal{H}_∞ -problem. In a seminal 2006 paper, Apkarian et al. [107] present a non-smooth optimization based method that facilitates structured \mathcal{H}_∞ -optimal controller synthesis. This approach has since been refined [106].

The standard \mathcal{H}_∞ -optimal control problem does not explicitly take into account uncertainty, although robustness to uncertainty is certainly one of the major consideration in \mathcal{H}_∞ -based control. Methods for synthesizing \mathcal{H}_∞ -optimal controllers in the presence of structured uncertainty have emerged over the years. These tools effectively combine μ -analysis with \mathcal{H}_∞ -synthesis and are known as μ -synthesis tools. There are no methods of computing the globally optimal, general feedback controller in the μ framework. However, various approaches to μ -synthesis have emerged. The first of these is the so called DK-iterations, which can be traced back to early 80s [116, 95, 162, 110]. This is an iterative approach that alternates between computing the upper bound on μ and solving an unstructured \mathcal{H}_∞ -problem. Each of these steps separately are convex, yet joint convexity is not guaranteed. As such, global optimality is not guaranteed, although the method has been seen to work well in practice [36]. D-K iterations only considers dynamic uncertainty. This may yield conservative results in the presence of parametric uncertainty. An alteration to D-K iterations is provided by DG-K iterations, introduced by Young et al. [111], which does consider both real and dynamic uncertainty. One issue with these techniques is that they make use of classical \mathcal{H}_∞ -synthesis, resulting in possibly very high order controllers. In 2010, Apkarian et al. [113] proposed a non-smooth

method for mixed μ -synthesis based on inner-relaxation techniques. One of the main advantages of these non-smooth methods is the ability to handle multi-model and multi-objective control design. Later alterations to the method proposed in [113] are seen in [114, 101]. These tools have been included in the Matlab Robust Control toolboxTM [37]

2. How can \mathcal{H}_∞ -based tools be applied to flight control system design?

Practical tools for designing robust control systems include \mathcal{H}_∞ loop-shaping, mixed sensitivity design and signal-based \mathcal{H}_∞ -control. The first is concerned with the shaping of the open-loop with pre-and-post-compensators. The latter two methods are concerned with the shaping of closed-loop functions. A typical starting point is the shaping of a combination of the closed-loop sensitivity functions S , KS and T . These are shaped with weighting filters, such that the solution to the \mathcal{H}_∞ -problem definition minimizes the product of the sensitivity functions and their respective weighting filters. This can be extended to include a variety of signals and weighting filters and is referred to as signal-based \mathcal{H}_∞ -control. This approach allows one to specify the spectral content of individual signals and facilitates the minimization of distinct signals. In the context of flight control system design, a common design goal is to minimize some model-following error. This can be achieved by constraining a model-following error $e = y - y_{ref}$, where $y_{ref} = G_{ref}r$, which is penalized by some weighting filter W_{MF} . A common choice for G_{ref} in the context of pitch-axis control is a desired short-period response, as seen in MIL-STD-1797A [132]. Examples of this approach are seen in [133, 134, 35]. In addition to shaping the desired transfer functions, external disturbances can be shaped as well. In the context of flight control system design, one form of disturbance that enters the bare airframe is wind disturbance. This can be represented by a disturbance input filter, a commonly seen choice is that of the Dryden wind gust model [132, 35, 130]. Similarly, the reference input could be filtered such that it reflects the spectral content of the pilot's input on the stick, based on McRuer's pilot model for instance [57].

Note that \mathcal{H}_∞ -problems often present a trade-off between conflicting objectives. The weighting filters therefore provide the designer with tuning knobs, allowing the designer to strike a balance between robust stability and robust performance.

3. What are the robustness properties of (I)NDI based control laws? Many of the earlier observations on the robustness of INDI have been purely empirical by nature. Wang et al. [34] first established formal nonlinear stability and performance properties of INDI-based control laws in the presence of regular perturbations based on Lyapunov methods and nonlinear perturbation theory. The authors prove that INDI offers greater robustness to regular perturbations than NDI, which is confirmed with numerical simulations. The analysis by Wang et al. was however limited to regular perturbations. As stated earlier, an analysis including both regular and singular perturbations is required, these have been considered, in [83, 82] for example. Yet these studies accept that all model uncertainty and singular perturbations can be parameterized. It is well known that for physical systems, this is inherently not the case. Moreover, these can be accurately represented by norm-bounded descriptions [112, 36]. To that extent, Pollack [35] argued that in order to assess the robustness of INDI-based flight control laws, these singular values must be considered.

Pollack first established analytical stability and performance and robustness properties of INDI-based control laws in the presence of mixed uncertainty [35]. The insights provided in [35] are based on the linear state-space formulation of INDI, which enables the use of the \mathcal{H}_∞ -framework. Prior to establishing these fundamental insights, Pollack highlights the fact that robustness properties of any given (I)NDI-based control law is a product of a number of factors. As such, robustness of any given inversion law should never be viewed in isolation.

Moreover, it is stated that the inversion residual ϵ_{INDI} , associated with imperfect inversion, may grow to be unbounded for certain combinations of singular perturbations, as a direct consequence of the synchronization effect. This is in contrast to NDI, for which upper-bounds on the inversion residual can always be found. In order to prevent the inversion residual from becoming unbounded, Pollack provides a design solution known as the *Matching strategy*, which has been shown to improve the robustness properties of SB-INDI.

In addition, Pollack provides a multi-loop \mathcal{H}_∞ -synthesis strategy, enabling the synthesis of robust inversion-based control systems.

Research Question 3

Which longitudinal handling quality, stability and performance criteria must the Flying-V satisfy?

1. **Which requirements are useful for assessing the Flying-V's longitudinal handling qualities?**
 MIL-STD-1797A provides six alternative requirements that can be used to assess the short-period handling qualities of an aircraft [132]. Although no guidance on when to use which requirement is provided. In an attempt to clarify this, WL-TR-3162 provides an extensive discussion on the use of the different requirements and provides a road map for their applicability [86]. The most important ones include the CAP criterion, the Dropback criterion and the bandwidth criterion. An issue with the CAP criterion is that it requires a LOES fit for aircraft with a higher-order response. Such a LOES fit may not always yield an accurate representation of the aircraft's actual response. In contrast, the Dropback and the bandwidth criterion can always be directly assessed. Using multiple criteria may provide a better view of the handling qualities of an aircraft. It must be stated that any handling quality level classification remains a *predicted handling quality level* until piloted assessments confirm the predicted level. Nonetheless, the predicted levels serve as an initial indication and can be used as a valuable design guidance tool.
2. **Which stability requirements must the FCS on the Flying-V adhere to?**
 Stability requirements are an essential part of the FCS clearance process. Typically, the first assessment of stability comes in the form of an eigenvalue analysis. This requires that all eigenvalues lay in the left-half plane. This requirement may be relaxed for piloted systems, given that the unstable eigenmode can be easily compensated by the pilot.
 Next, stability margin analyses are typically performed. These are typically based on the stability margin requirements originating from AS94900 [150]. Which state that between the minimum and maximum operating speed of the aircraft and at frequencies up to the first aeroelastic mode of the aircraft, the margins must be at least: $\pm 45^\circ$ of PM and ± 6 dB of GM. Moreover, it states that sensitivity or uncertainty analyses must be performed with 20% uncertainty in key stability derivatives and that the aforementioned margins shall not degrade by more than 50%. These represent SISO margins.
 An extension to multivariate stability margins, based on singular values, is provided in [151]. Some suggest that singular value based stability margins are very conservative [149]. Tischler et al. [149] suggest checking the multivariate stability margins against margin requirements half the size of the classical SISO margins.
 An alternative stability margin requirement is the Nichols exclusion zone, which essentially provides insight into the robustness of a system to simultaneous gain and phase variations, in contrast to the classical margins. As such, an aircraft that may adhere to the classical margins, may fail the Nichols margin requirement.
 For LTI systems, finding the closed-loop robustness margins boils down to finding the maximum uncertainty at which closed-loop stability and performance is guaranteed. This in turn boils down to finding the inverse of the SSV. Roos et al. [154] provide a method for calculating guaranteed stability margins based on the upper bound of the SSV. Moreover, they provide an approach to assessing the eigenvalue criterion and the stability margin criteria through μ -analysis.
3. **Which performance metrics does the Flying-V have to adhere to and how can these be incorporated into design requirements?**
 Performance requirements can be captured in different ways. These include time-domain requirements, requirements on output statistics and frequency-domain based requirements. Assessing the adherence to these requirements therefore also requires different methods. Deterministic time-domain simulations, Monte Carlo simulations and Frequency domain analyses.
 Within the context of this research, it makes sense to define frequency-based performance requirements. Having obtained a frequency-domain, norm-based description of IDI-based control laws, these requirements can be included in the controller synthesis problem. These include disturbance rejection requirements, model matching requirements and control input limitations. Checking the adherence to these requirements becomes a matter of performing a robust performance (RP) analysis. A drawback of this approach is its inability to capture nonlinear requirements, such as actuator saturation limits. Nonetheless, checking the requirements is straightforward and provides robust

performance guarantees.

Research Question 4

How can \mathcal{H}_∞ tools be applied to INDI-based flight control law design to improve the longitudinal handling qualities of the Flying-V?

1. How can the design criteria be included in the formulation of a structured \mathcal{H}_∞ -synthesis problem?

Design criteria can be included in the classical \mathcal{H}_∞ -synthesis problem formulation in the form of weighting filters, an example of this is provided in I. The problem formulation presented in I contains a performance requirement in the form of an Explicit Model-Following (EMF) design. Moreover, uncertainty weighting filters are included. Together, these form the robust stability and performance bounds of the specific design case. An issue with this approach in the context of classical mixed μ -synthesis, is that the robust performance and robust stability requirements can not be enforced separately. This goes back to the fundamental machinery of \mathcal{H}_∞ -control methods. Which aim to push one closed-loop formulation down over the entire frequency range, as stated in chapter 3. This may result in robust performance being achieved, yet robust stability not necessarily being preserved. To circumvent this shortcoming, alterations to the classical μ -synthesis tools have been proposed, such as those in [35, 163, 114]. These alterations enable the formulation of robust multi disk margin requirements, an extension necessary to guarantee robust stability when applying μ -synthesis tools.

2. How can INDI-based control systems be included in the formulation of a structured \mathcal{H}_∞ -synthesis problem?

As INDI is inherently nonlinear and can not directly be included in the formulation of a linear \mathcal{H}_∞ -synthesis problem, its linear counterpart is required, IDI. Effectively, the obtained IDI control law can be formulated in terms of a structured controller. Subsequently, the structured controller can be connected to the generalized linear plant P with the use of LFTs, ultimately establishing the structured closed-loop system. This description can subsequently be used in commercially available software packages such as the MATLAB TM Robust Control Toolbox [37], to establish robust control designs. It must be stated that the resulting controller is designed for the LTI plant formulation. To enable the design for a wider flight envelope, multiple LTI based controllers could be synthesized, effectively employing a form of gain-scheduling. Alternatively, robust controllers could be designed for LTV descriptions of the bare airframe dynamics and LTV uncertainties. Such an approach is presented in [35], this approach extends the problem to consider a class of nonlinear uncertainty.

It must be emphasized that the actual nonlinear description of any plant can not directly be included in the \mathcal{H}_∞ -framework, as it is linear by nature. As such, the use of \mathcal{H}_∞ -synthesis tools requires LTI descriptions. A more elaborate description is provided by LPV representations of the nonlinear dynamics. However, robust control design for LPV systems requires the use of more complex IQC-based synthesis tools, such as those presented in [164, 165, 166]. Additionally, the IQC framework allows for LTV uncertainties.

3. What are the robust stability & performance characteristics of robust IDI-based control systems on the Flying-V?

As seen in part I, the robust stability and performance characteristics of the various inversion architectures differ inherently. This is best understood when looking at the loop-shape at the plant input L_i and the breakdown of μ_{RS} and μ_{RS} . These demonstrate the fundamental trade-off between robust stability and robust performance in inversion based design (and feedback design in general). In part I, various inversion-based designs were synthesized. Including the standard model-based approach, a sensor-based design and multiple hybrid designs. It was observed that the best achievable robust performance is achieved when the robustness functionality of both the inner-loop and the outer-loop is leveraged. This can be done by employing a multi-loop synthesis approach. It was shown that the hybrid architecture achieves the greatest robust stability and performance, it does so by fully leveraging the added design flexibility offered by the multi-loop approach. To that extent, the hybrid approach offers the designer the greatest amount of freedom to establish robust inversion-based control designs. The choice of inversion strategy is of course, highly dependent

on the availability of the different resources. That is, the sensor-based approach requires sensor measurements, whereas the model-based approach requires an (accurate) model and the hybrid approach requires a bit of both. If both are available, the hybrid approach achieves the greatest robust stability and performance, as it effectively balances the two. Hence, if possible, hybrid INDI is preferred. A breakdown of the robust performance μ_{RP} showed that the individual contributions of the various modeled uncertainties show similar trends in all of the inversion schemes. Although it could be observed that dynamic actuator uncertainty is more significant in the standard MB approach, due to the lack of feedback in the inner loop.

Closing remarks and outlook

NDI and INDI have become well established methods in the flight control community for reasons mentioned earlier. More so, its widespread popularity seems to stem from its modularity, transparency and elimination of nonlinear dynamics. This makes it relatively easy to understand, hence making it an attractive approach for engineers, including those less familiar with advanced control methods. This can be viewed in the context of the flight control law design cycle, as shown in figure 2.20. The FCS design cycle often concerns various disciplines, bare airframe modeling and control law design are often handled by different teams in an organization. Subsequently, the design process is often held up by iterative dependencies of the different disciplines. Think of control engineers awaiting a new bare airframe model from the modeling department before being able to proceed with control law design. The modular nature of (I)NDI offers an alternative design cycle, one where modeling and control design can happen in parallel, offering a reduction in the time required for a single design iteration. This makes it such that the control engineer is left with the task of establishing an adequately robust design with the necessary outer-loop feedback design, which in turn depends on the inversion strategy. To that extent, the use of \mathcal{H}_∞ -synthesis offer the control engineer an extra means to an end. In the author's opinion, this is where the power of these tools lie. As the choice for either model-based, sensor-based or even hybrid-based (I)NDI is often not merely a choice of the control engineer, but one that relies on the overall aircraft design. As such, the control engineer ought to aim for a robust control design, regardless of the underlying control law architecture. \mathcal{H}_∞ -tools offer exactly that. Therefore, the use of \mathcal{H}_∞ -tools is a powerful, general tool that can be utilized throughout the entire FCS design process, regardless of specific design choices and uncertainties. As the Flying-V is still in its design phases, thus subject to design changes and substantial design uncertainty, it is advised that \mathcal{H}_∞ -tools remain utilized in the future, regardless of the specific control law choice.

Recommendations

This chapter provides a brief overview of the primary recommendations for the future continuation of this research project. As this research covered multiple domains, the recommendations are best divided into these subdomains. Consider the following division:

1. The Flying-V
2. The Flight control law clearance process
3. Inversion-based control law design
4. The use of \mathcal{H}_∞ -tools in inversion-based flight control design.

Following this subdivision, the following sections contain the recommendations for each of these.

7.1. The Flying-V

It must be stated that the following recommendations regarding the Flying-V come from the flight control engineering perspective, as such, these must be seen in that context. The Flying-V is still in its developmental stages, which means that a lot of design uncertainty remains. Although various models have been established, a lot of uncertainty in the bare airframe model still remains. As such, it is suggested that continued research on the Flying-V's aerodynamics is required. Moreover, well trimmed models of the Flying-V's dynamics have to be established, as this has been a source of ambiguity within the Flying-V research group. This is currently being tackled, although better standards have to be agreed upon and established. This becomes especially important when aiming to use \mathcal{H}_∞ -control tools, as these tools rely heavily on well trimmed linear models of the plant that is to be controlled. This is of less concern for INDI-based designs, yet still, establishing well trimmed linear models is a fundamental step in the flight control law design process that should not be overlooked.

7.2. The flight control law clearance process

As seen in figure 2.20, the flight control system design process is an iterative process consisting of numerous steps. Prior to control law design, a set of mission requirements, design specifications and flying qualities have to be established. It has been observed that a rigorous establishment of the aforementioned is lacking for the Flying-V, instead control law design has been prioritized. It could be argued that for the overall development of the Flying-V project as a whole, these must be studied and established first. An issue that comes to mind is the adequate choice of the desired flying qualities. As discussed in chapter 4, ambiguity around the adequate choice of handling criteria exists. The majority of the MIL-SPEC documents stem from decades ago and were established for aircraft with conventional shapes, control surface layouts and response types. Therefore, it is recommended that more elaborate and appropriate flying qualities are established for the Flying-V. Similarly, stability assessments based on the classical stability margins are not sufficient for coupled, highly augmented, MIMO flight control systems. Therefore, more adequate stability margin requirements are needed, an issue that was discussed many years ago in [167]. Therefore, it is recommended that the flight control law clearance process is to be well studied and understood before establishing advanced flight control designs. This may not be the "flashiest" part of flight control law design, yet it remains invaluable, especially within the context of an ongoing research project such as the Flying-V.

7.3. Inversion-based control law design

Various inversion schemes were considered in this research and their robustness properties were assessed in the presence of both regular and singular perturbations, based on their linear equivalents. In the author's opinion, the control engineer must be aware of the robustness implications of the specific inversion-based control law architecture. These implications are best understood when keeping in mind the "fundamental costs of feedback", as defined by Horowitz [88]. Moreover, the flight control engineer ought to be aware of the physical constraints posed by the aircraft and its constituent parts. This includes bandwidth constraints but also control law architecture constraints, which are in part imposed by the (in)availability of models and/or sensor measurements. These should guide the control law choice and its robustness implications should be understood by the control engineer.

7.4. The use of \mathcal{H}_∞ -tools in inversion-based flight control design.

The use of \mathcal{H}_∞ design tools have been shown to aid in the design of robust inversion-based flight control systems. Specifically, it has been shown that these can aid in reaching robust performance goals. In this research specifically, classical mixed μ -synthesis was applied. An issue with the use of this approach is the fact that robust stability and robust performance can not be defined as a multi-tiered set of design objectives. As such, the resulting controllers may improve robust performance, yet sacrifice robust stability. To that extent, augmentations to the classical μ -synthesis have been proposed, such as those in [35, 114, 163]. It is recommended that these tools are explored if a μ -synthesis based approach to inversion-based control design is considered.

Aside from the discussion about the use of various μ -based tools for the synthesis of robust control design, its utility could be questioned in the first place. Although μ -analysis provides great insight into the specific robust stability and performance characteristics of a given closed-loop system, the use of μ -synthesis tools can be rather tedious. In the authors experience, the synthesis outcomes are highly dependent on the combination of uncertainty weighting filters, plant description and synthesis settings. From a practical perspective, this is perhaps not very desirable. Ultimately, the goal of the μ -synthesis machinery is to establish a design with adequate robust stability and performance. This is ultimately reflected in the shape of the loop-transfer function at the plant input (L_i). As such, simpler tools, such as \mathcal{H}_∞ -loop shaping, might be capable of yielding very similar results in terms of robustness, without the need for explicit uncertainty descriptions. This is however a design trade-off, as on the other hand μ -based tools provide machinery that is capable of establishing optimal or slightly suboptimal designs. In the context of inversion-based control design, these tools have their place. Specifically, these tools are best capable of utilizing the multi-loop architecture to achieve the greatest robust stability and performance.

Bibliography

- [1] Frederico Afonso, Martin Sohst, Carlos M.A. Diogo, Simão S. Rodrigues, Ana Ferreira, Inês Ribeiro, Ricardo Marques, Francisco F.C. Rego, Abdolrasoul Sohoul, Joana Portugal-Pereira, Hugo Policarpo, Bruno Soares, Bruna Ferreira, Edgar C. Fernandes, Fernando Lau, and Afzal Suleman. "Strategies towards a more sustainable aviation: A systematic review". In: *Progress in Aerospace Sciences* 137 (2023), p. 100878. DOI: <https://doi.org/10.1016/j.paerosci.2022.100878>.
- [2] A. Abbas, J. de Vicente, and E. Valero. "Aerodynamic technologies to improve aircraft performance". In: *Aerospace Science and Technology* 28.1 (2013), pp. 100–132. DOI: <https://doi.org/10.1016/j.ast.2012.10.008>. URL: <https://www.sciencedirect.com/science/article/pii/S1270963812001587>.
- [3] R. Storck. *Flying Wings: die historische Entwicklung der Schwanzlosen- und Nurflügelflugzeuge der Welt*. Bernard and Graefe, 2003. URL: <https://books.google.nl/books?id=iPUfAQAAIAAJ>.
- [4] E Torenbeek. *Advanced Aircraft Design - Conceptual Design, Analysis and Optimization of Subsonic Civil Airplanes*. English. John Wiley and Sons, 2013.
- [5] R. H. Liebeck, M. A. Page, and B. K. Rawdon. "Blended-Wing-Body Subsonic Commercial Transport". In: *AIAA Paper 98-0438* (1998).
- [6] R. H. Liebeck. "Design of the Blended Wing Body Subsonic Transport". In: *Journal of Aircraft* 41.1 (2004), pp. 10–25. DOI: 10.2514/1.9084.
- [7] Paul Okonkwo and Howard Smith. "Review of evolving trends in blended wing body aircraft design". In: *Progress in Aerospace Sciences* 82 (Feb. 2016). DOI: 10.1016/j.paerosci.2015.12.002.
- [8] Zhenli CHEN, Minghui ZHANG, Yingchun CHEN, Weimin SANG, Zhaoguang TAN, Dong LI, and Binqian ZHANG. "Assessment on critical technologies for conceptual design of blended-wing-body civil aircraft". In: *Chinese Journal of Aeronautics* 32.8 (2019), pp. 1797–1827. DOI: <https://doi.org/10.1016/j.cja.2019.06.006>.
- [9] R. Martinez-Val. "Flying Wings. A New Paradigm for Civil Aviation?" In: *Acta Polytechnica* 47 (Jan. 2007). DOI: 10.14311/914.
- [10] J Benad and R Vos. "Design of a Flying V Subsonic Transport". English. In: *ICAS 2022*. 2022.
- [11] F.J. Palacin R. Martinez-Val P.J. Perez. "Optimising transport flying wings". In: *25th International Congress of the Aeronautical Sciences (ICAS)*. 2006.
- [12] Delft University of Technology. *Flying-V*. <https://www.tudelft.nl/lr/flying-v> [Accessed: 25-02-2024]. 2024.
- [13] J. Benad. "The Flying V - A new Aircraft Configuration for Commercial Passenger Transport". English. In: *Deutscher Luft- und Raumfahrtkongress 2015, Rostock ; Conference date: 22-09-2015 Through 24-09-2015*. 2015, pp. 1–8. DOI: 10.25967/370094.
- [14] Hillen M. "Parametrisation of the Flying-V Outer Mould Line." MA thesis. Delft University of Technology, 2020.
- [15] Robert Liebeck. "Blended Wing Body Design Challenges". In: *AIAA International Air and Space Symposium and Exposition: The Next 100 Years*. AIAA, 2003. DOI: 10.2514/6.2003-2659. eprint: <https://arc.aiaa.org/doi/pdf/10.2514/6.2003-2659>.
- [16] Wilco Oosterom and Roelof Vos. "Conceptual Design of a Flying-V Aircraft Family". In: *AIAA AVIATION 2022 Forum*. AIAA, 2022. DOI: 10.2514/6.2022-3200. eprint: <https://arc.aiaa.org/doi/pdf/10.2514/6.2022-3200>.

- [17] Francesco Faggiano, Roelof Vos, Max Baan, and Reinier van Dijk. "Aerodynamic Design of a Flying V Aircraft". English. In: *17th AIAA Aviation Technology, Integration, and Operations Conference*. 17th AIAA Aviation Technology, Integration, and Operations Conference ; Conference date: 05-06-2017 Through 09-06-2017. United States: American Institute of Aeronautics and Astronautics Inc. (AIAA), 2017. DOI: 10.2514/6.2017-3589.
- [18] Viet R. "Analysis of the flight characteristics of a highly swept cranked flying wing by means of an experimental test". MA thesis. Delft University of Technology, 2019.
- [19] J. Benad. "Development of a numerical flow channel with the Lattice Boltzmann method and application to highly swept wings at high angles of attack". PhD thesis. TU Berlin, 2022.
- [20] Thibaut Cappuyns. "Handling Qualities of a Flying V Configuration". MA thesis. Delft University of Technology, 2019.
- [21] Simon van Overeem, Xuerui Wang, and Erik-Jan Van Kampen. "Handling Quality Improvements for the Flying-V Aircraft using Incremental Nonlinear Dynamic Inversion". In: *AIAA SCITECH 2023 Forum*. AIAA, 2023. DOI: 10.2514/6.2023-0105. eprint: <https://arc.aiaa.org/doi/pdf/10.2514/6.2023-0105>.
- [22] G. Vugts, O. Stroosma, Roelof Vos, and Max Mulder. "Simulator Evaluation of Flightpath-oriented Control Allocation for the Flying-V". English. In: *AIAA SciTech Forum 2023*. AIAA SCITECH 2023 Forum ; Conference date: 23-01-2023 Through 27-01-2023. 2023. DOI: 10.2514/6.2023-2508.
- [23] Sjoerd Joosten, Olaf Stroosma, Roelof Vos, and Max Mulder. "Simulator Assessment of the Lateral-Directional Handling Qualities of the Flying-V". In: *AIAA SCITECH 2023 Forum*. AIAA, 2023. DOI: 10.2514/6.2023-0906. eprint: <https://arc.aiaa.org/doi/pdf/10.2514/6.2023-0906>.
- [24] Jurian Stougie, Tijmen Pollack, and Erik-Jan Van Kampen. "Incremental Nonlinear Dynamic Inversion control with Flight Envelope Protection for the Flying-V". In: *AIAA SCITECH 2024 Forum*. AIAA, 2024. DOI: 10.2514/6.2024-2565.
- [25] P. Smith. "A simplified approach to nonlinear dynamic inversion based flight control". In: *23rd Atmospheric Flight Mechanics Conference*. AIAA, 1998. DOI: 10.2514/6.1998-4461. eprint: <https://arc.aiaa.org/doi/pdf/10.2514/6.1998-4461>.
- [26] S. Sieberling, Q. P. Chu, and J. A. Mulder. "Robust Flight Control Using Incremental Nonlinear Dynamic Inversion and Angular Acceleration Prediction". In: *Journal of Guidance, Control, and Dynamics* 33.6 (2010), pp. 1732–1742. DOI: 10.2514/1.49978. eprint: <https://doi.org/10.2514/1.49978>.
- [27] Paul Acquatella, Wouter Falkena, Erik-Jan van Kampen, and Q. Ping Chu. "Robust Nonlinear Spacecraft Attitude Control using Incremental Nonlinear Dynamic Inversion." In: *AIAA Guidance, Navigation, and Control Conference*. AIAA, 2022. DOI: 10.2514/6.2012-4623. eprint: <https://arc.aiaa.org/doi/pdf/10.2514/6.2012-4623>.
- [28] P. Simplício, M.D. Pavel, E. van Kampen, and Q.P. Chu. "An acceleration measurements-based approach for helicopter nonlinear flight control using Incremental Nonlinear Dynamic Inversion". In: *Control Engineering Practice* 21.8 (2013), pp. 1065–1077. DOI: <https://doi.org/10.1016/j.conengprac.2013.03.009>.
- [29] Ewoud J. J. Smeur, Qiping Chu, and Guido C. H. E. de Croon. "Adaptive Incremental Nonlinear Dynamic Inversion for Attitude Control of Micro Air Vehicles". In: *Journal of Guidance, Control, and Dynamics* 39.3 (2016), pp. 450–461. DOI: 10.2514/1.G001490.
- [30] Ronald van 't Veld, Erik-Jan Van Kampen, and Q Ping Chu. "Stability and Robustness Analysis and Improvements for Incremental Nonlinear Dynamic Inversion Control". In: *2018 AIAA Guidance, Navigation, and Control Conference*. AIAA, 2018. DOI: 10.2514/6.2018-1127. eprint: <https://arc.aiaa.org/doi/pdf/10.2514/6.2018-1127>.
- [31] Phill Smith and Andrew Berry. "Flight test experience of a non-linear dynamic inversion control law on the VAAC Harrier". In: *Atmospheric Flight Mechanics Conference*. 2000. DOI: 10.2514/6.2000-3914. eprint: <https://arc.aiaa.org/doi/pdf/10.2514/6.2000-3914>.

- [32] Fabian Grondman, Gertjan H.N. Looye, Richard O. Kuchar, Q. Ping Chu, and Erik Jan van Kampen. "Design and flight testing of incremental nonlinear dynamic inversion based control laws for a passenger aircraft". English. In: *AIAA Guidance, Navigation, and Control*. AIAA Guidance, Navigation, and Control Conference, 2018 ; Conference date: 08-01-2018 Through 12-01-2018. United States: American Institute of Aeronautics and Astronautics Inc. (AIAA), Jan. 2018. DOI: 10.2514/6.2018-0385.
- [33] Yagiz Kumtepe, Tijmen Pollack, and Erik-Jan Van Kampen. "Flight Control Law Design using Hybrid Incremental Nonlinear Dynamic Inversion". In: *AIAA SCITECH 2022 Forum*. AIAA, 2022. DOI: 10.2514/6.2022-1597. eprint: <https://arc.aiaa.org/doi/pdf/10.2514/6.2022-1597>.
- [34] Xuerui Wang, Erik-Jan van Kampen, Qiping Chu, and Peng Lu. "Stability Analysis for Incremental Nonlinear Dynamic Inversion Control". In: *Journal of Guidance, Control, and Dynamics* 42.5 (May 2019), pp. 1116–1129. DOI: 10.2514/1.g003791.
- [35] T.S.C. Pollack. "Advances in Dynamic Inversion-based Flight Control Law Design: Multivariable Analysis and Synthesis of Robust and Multi-Objective Design Solutions". English. PhD thesis. Delft University of Technology, 2024. DOI: 10.4233/uuid:28617ba0-461d-48ef-8437-de2aa41034ea.
- [36] Sigurd Skogestad and I Postlethwaite. "Multivariable Feedback Control: Analysis and Design". In: vol. 2. John Wiley and Sons, Jan. 2005.
- [37] Gary Balas, Richard Chiang, Andy Packard, and Michael Safonov. *Robust Control Toolbox - User's Guide*. Natick, Massachusetts, United States, 2005. URL: <https://www.mathworks.com>.
- [38] Luuk van der Schaft. "Development, Model Generation and Analysis of a Flying V Structure Concept". MA thesis. Delft University of Technology, 2017. URL: <https://api.semanticscholar.org/CorpusID:117228916>.
- [39] Mathias Claeys. "Flying V and Reference Aircraft Structural Analysis and Mass Comparison". MA thesis. Delft University of Technology, 2018. URL: <https://api.semanticscholar.org/CorpusID:70176031>.
- [40] Peter H. Zipfel. *Modeling and Simulation of Aerospace Vehicle Dynamics, Third Edition*. Reston, Virginia: American Institute of Aeronautics and Astronautics, Inc., 2014. DOI: 10.2514/4.102509.
- [41] Marco Palermo and Roelof Vos. "Experimental Aerodynamic Analysis of a 4.6%-Scale Flying-V Subsonic Transport". In: *AIAA Scitech 2020 Forum*. AIAA, 2020. DOI: 10.2514/6.2020-2228. eprint: <https://arc.aiaa.org/doi/pdf/10.2514/6.2020-2228>.
- [42] T.A. Talay. *Introduction to the Aerodynamics of Flight. NASA SP 367*. Vol. 367. Provided by the SAO/NASA Astrophysics Data System. NASA, 1975. URL: <https://ui.adsabs.harvard.edu/abs/1975NASSP.367.....T>.
- [43] Thomas Lambert, Norizham Abdul Razak, and Grigorios Dimitriadis. "Vortex Lattice Simulations of Attached and Separated Flows around Flapping Wings". In: *Aerospace* 4.2 (2017). DOI: 10.3390/aerospace4020022.
- [44] Alberto Ruiz Garcia, Roelof Vos, and Coen de Visser. "Aerodynamic model identification of the flying V from wind tunnel data". English. In: *AIAA AVIATION 2020 FORUM*. AIAA AVIATION 2020 FORUM ; Conference date: 15-06-2020 Through 19-06-2020. United States: American Institute of Aeronautics and Astronautics Inc. (AIAA), 2020. DOI: 10.2514/6.2020-2739.
- [45] J Benad. *The Flying V*. <https://www.jbenad.com/flyingv>. Accessed: 01-02-2022.
- [46] Alberto Ruiz Garcia, Malcom Brown, Daniel Atherstone, Nando v. Arnhem, and Roelof Vos. "Aerodynamic Model Identification of the Flying V from Sub-Scale Flight Test Data". In: *AIAA SCITECH 2022 Forum*. 2022. DOI: 10.2514/6.2022-0713. eprint: <https://arc.aiaa.org/doi/pdf/10.2514/6.2022-0713>.
- [47] Simon van Overeem. "Modelling, Control, and Handling Quality Analysis of the Flying-V". MA thesis. Delft University of Technology, 2022.

- [48] Gavin K. Ananda, Moiz Vahora, Or D. Dantsker, and Michael S. Selig. "Design Methodology for a Dynamically-Scaled General Aviation Aircraft". In: *35th AIAA Applied Aerodynamics Conference*. AIAA, 2017. DOI: 10.2514/6.2017-4077. eprint: <https://arc.aiaa.org/doi/pdf/10.2514/6.2017-4077>.
- [49] Ismael Matamoros and Coen C. de Visser. "Incremental Nonlinear Control Allocation for a Tailless Aircraft with Innovative Control Effectors". In: *2018 AIAA Guidance, Navigation, and Control Conference*. AIAA, 2018. DOI: 10.2514/6.2018-1116. eprint: <https://arc.aiaa.org/doi/pdf/10.2514/6.2018-1116>.
- [50] Rolls-Royce Deutschland Ltd and Co KG. *TYPE-CERTIFICATE DATA SHEET Trent XWB series engines*. Tech. rep. EASA, 2022.
- [51] unknown. *on certification specifications, including airworthiness codes and acceptable means of compliance, for large aeroplanes (« CS-25 »)*. Tech. rep. EASA, 2003.
- [52] H.V. De Castro. "Flying and handling qualities of a fly-by-wire blended-wing-body civil transport aircraft". PhD thesis. Cranfield University, 2003.
- [53] Yasim J. Hasan, Jana Schwithal, Till Pfeiffer, Carsten M. Liersch, and Gertjan Looye. "Handling Qualities Assessment of a Blended Wing Body Configuration Under Uncertainty Considerations". In: *Deutscher Luft- und Raumfahrtkongress, 2017*. Sept. 2017.
- [54] R.D. Finck. *USAF STABILITY AND CONTROL DATCOM*. Tech. rep. McDonnell Douglas Corporation, 1978.
- [55] Thomas A. Toll and M. J. Queijo. *Approximate Relations and Charts for Low-Speed stability derivatives of swept wings*. Tech. rep. Langley Memorial Aeronautical Laboratory, 1948.
- [56] unknown. *MIL-F-8785C FLYING QUALITIES OF PILOTED AIRPLANES*. Tech. rep. Department of Defense, 1980.
- [57] D.T. McRuer. *Pilot-Induced Oscillations and Human Dynamic Behavior*. NASA contractor report. NASA, 1995. URL: <https://books.google.nl/books?id=0F81AQAIAAJ>.
- [58] D.J. Moorhouse, W. Boer, C. Fielding, K.-U Hahn, G. Hofinger, J.-F Magni, and Leopoldo Verde. *Flight Control Design - Best Practices*. Canada Communication Group Inc, Jan. 2000.
- [59] Jan Terlouw Jean-François Magni Samir Bennani. *Robust Flight Control - A design Challenge*. Berlin, Heidelberg: Springer Berlin Heidelberg, 1997. DOI: 10.1007/bfb0113842.
- [60] Riccardo Torelli, Olaf Stroosma, Roelof Vos, and Max Mulder. "Piloted Simulator Evaluation of Low-Speed Handling Qualities of the Flying-V". In: *AIAA SCITECH 2023 Forum*. AIAA, 2023. DOI: 10.2514/6.2023-0907. eprint: <https://arc.aiaa.org/doi/pdf/10.2514/6.2023-0907>.
- [61] Sjoerd Joosten. "Piloted Assessment of the Lateral-Directional Handling Qualities of the Flying-V". MA thesis. Delft University of Technology, 2022.
- [62] Willem Völker. "Reinforcement Learning for Flight Control of the Flying V". MA thesis. Delft University of Technology, 2022.
- [63] Barton Bacon and Aaron Ostroff. "Reconfigurable flight control using nonlinear dynamic inversion with a special accelerometer implementation". In: *AIAA Guidance, Navigation, and Control Conference and Exhibit*. AIAA, 2000. DOI: 10.2514/6.2000-4565. eprint: <https://arc.aiaa.org/doi/pdf/10.2514/6.2000-4565>.
- [64] Barton Bacon, Aaron Ostroff, and Suresh Joshi. "Reconfigurable NDI controller using inertial sensor failure detection and isolation". In: *Aerospace and Electronic Systems, IEEE Transactions on* 37 (Nov. 2001), pp. 1373–1383. DOI: 10.1109/7.976972.
- [65] DALE ENNS, DAN BUGAJSKI, RUSS HENDRICK, and GUNTER STEIN. "Dynamic inversion: an evolving methodology for flight control design". In: *International Journal of Control* 59.1 (1994), pp. 71–91. DOI: 10.1080/00207179408923070.

- [66] Gary J. Balas. "Flight Control Law Design: An Industry Perspective". In: *European Journal of Control* 9.2 (2003), pp. 207–226. DOI: <https://doi.org/10.3166/ejc.9.207-226>.
- [67] J.J.E. Slotine and W. Li. *Applied Nonlinear Control*. Prentice-Hall International Editions. Prentice-Hall, 1991. URL: <https://books.google.nl/books?id=HddxQgAACAAJ>.
- [68] C.C. de Visser and Erik-Jan van Kampen. Lecture notes AE4311 - Nonlinear and Adaptive Flight Control.
- [69] DANIEL BUGAJSKI, DALE ENNS, and MICHAEL ELGERSMA. "A dynamic inversion based control law with application to the high angle-of-attack research vehicle". In: *Guidance, Navigation and Control Conference*. 1990. DOI: 10.2514/6.1990-3407. eprint: <https://arc.aiaa.org/doi/pdf/10.2514/6.1990-3407>.
- [70] John Valasek, Daigoro Ito, and Donald Ward. "Robust dynamic inversion controller design and analysis for the X-38". In: *AIAA Guidance, Navigation, and Control Conference and Exhibit*. 2001. DOI: 10.2514/6.2001-4380. eprint: <https://arc.aiaa.org/doi/pdf/10.2514/6.2001-4380>.
- [71] Greg Walker and Dave Allen. "X-35B STOVL Flight Control Law Design and Flying Qualities". In: *2002 Biennial International Powered Lift Conference and Exhibit*. 2002. DOI: 10.2514/6.2002-6018. eprint: <https://arc.aiaa.org/doi/pdf/10.2514/6.2002-6018>.
- [72] Dan Canin. "F-35 High Angle of Attack Flight Control Development and Flight Test Results". In: *AIAA Aviation 2019 Forum*. 2019. DOI: 10.2514/6.2019-3227. eprint: <https://arc.aiaa.org/doi/pdf/10.2514/6.2019-3227>.
- [73] Twan Keijzer, Gertjan Looye, Q Ping Chu, and Erik-Jan Van Kampen. "Design and Flight Testing of Incremental Backstepping based Control Laws with Angular Accelerometer Feedback". In: *AIAA Scitech 2019 Forum*. AIAA, 2019. DOI: 10.2514/6.2019-0129. eprint: <https://arc.aiaa.org/doi/pdf/10.2514/6.2019-0129>.
- [74] Wim Ekeren, Gertjan Looye, Richard Kuchar, Q.P. Chu, and Erik-Jan Van Kampen. "Design, Implementation and Flight-Tests of Incremental Nonlinear Flight Control Methods". In: *AIAA 2018-0384*. Jan. 2018. DOI: 10.2514/6.2018-0384.
- [75] Sihao Sun, Leon Sijbers, Xuerui Wang, and Coen de Visser. "High-Speed Flight of Quadrotor Despite Loss of Single Rotor". In: *IEEE Robotics and Automation Letters* 3.4 (2018), pp. 3201–3207. DOI: 10.1109/LRA.2018.2851028.
- [76] Sihao Sun, Xuerui Wang, Qiping Chu, and Coen de Visser. "Incremental Nonlinear Fault-Tolerant Control of a Quadrotor With Complete Loss of Two Opposing Rotors". In: *IEEE Transactions on Robotics* 37.1 (2021), pp. 116–130. DOI: 10.1109/TR0.2020.3010626.
- [77] Erwin Mooij. "Robust Control of a Conventional Aeroelastic Launch Vehicle". In: *AIAA Scitech 2020 Forum*. 2020. DOI: 10.2514/6.2020-1103. eprint: <https://arc.aiaa.org/doi/pdf/10.2514/6.2020-1103>.
- [78] Marilena D. Pavel, Perumal Shanthakumaran, Qiping Chu, Olaf Stroosma, Mike Wolfe, and Harm Cazemier. "Incremental Nonlinear Dynamic Inversion for the Apache AH-64 Helicopter Control". In: *Journal of the American Helicopter Society* 65.2 (2020), pp. 1–16. DOI: 10.4050/jahs.65.022006.
- [79] Yingzhi Huang, Daan M. Pool, Olaf Stroosma, and Qiping Chu. "Long-Stroke Hydraulic Robot Motion Control With Incremental Nonlinear Dynamic Inversion". In: *IEEE/ASME Transactions on Mechatronics* 24.1 (2019), pp. 304–314. DOI: 10.1109/TMECH.2019.2891358.
- [80] Yu Li, Xiaoxiong Liu, Peng Lu, Qizhi He, Ruichen Ming, and Weiguo Zhang. "Angular acceleration estimation-based incremental nonlinear dynamic inversion for robust flight control". In: *Control Engineering Practice* 117 (2021), p. 104938. DOI: <https://doi.org/10.1016/j.conengprac.2021.104938>.
- [81] Chong-Sup Kim, Chang-Ho Ji, Gi-Oak Koh, and Byoung Soo Kim. "Stability Margin and Structural Coupling Analysis of a Hybrid INDI Control for the Fighter Aircraft". In: *International Journal of Aeronautical and Space Sciences* 22.5 (2021), pp. 1154–1169. DOI: 10.1007/s42405-021-00394-8.

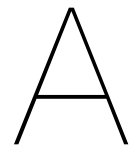
- [82] Rafael A. Cordeiro, Apolo S. Marton, José R. Azinheira, José R. H. Carvalho, and Alexandra Moutinho. "Increased Robustness to Delay in Incremental Controllers Using Input Scaling Gain". In: *IEEE Transactions on Aerospace and Electronic Systems* 58.2 (2022), pp. 1199–1210. DOI: 10.1109/TAES.2021.3123215.
- [83] Yingzhi Huang, Ye Zhang, Daan M. Pool, Olaf Stroosma, and Qiping Chu. "Time-Delay Margin and Robustness of Incremental Nonlinear Dynamic Inversion Control". In: *Journal of Guidance, Control, and Dynamics* 45.2 (2022), pp. 394–404. DOI: 10.2514/1.G006024. eprint: <https://doi.org/10.2514/1.G006024>.
- [84] Jing Chang, Roeland De Breuker, and Xuerui Wang. "Discrete-time Design and Stability Analysis for Nonlinear Incremental Fault-tolerant Flight Control". In: *AIAA SCITECH 2022 Forum*. AIAA, 2022. DOI: 10.2514/6.2022-2034. eprint: <https://arc.aiaa.org/doi/pdf/10.2514/6.2022-2034>.
- [85] G. Stein. "Respect the unstable". In: *IEEE Control Systems Magazine* 23.4 (2003), pp. 12–25. DOI: 10.1109/MCS.2003.1213600.
- [86] DAVID G. MITCHELL and ROGER H. HOH. *PROPOSED INCORPORATION OF MISSION-ORIENTED FLYING QUALITIES INTO MIL-STD-1797A*. Tech. rep. WRIGHT LABORATORY, 1994.
- [87] Michael G. Safonov. "Origins of robust control: Early history and future speculations". In: *Annual Reviews in Control* 36.2 (2012), pp. 173–181. DOI: <https://doi.org/10.1016/j.arcontrol.2012.09.001>.
- [88] Isaac M. Horowitz. *Synthesis of Feedback Systems*. Academic Press, 1963.
- [89] M. Athans, D. Castanon, K. Dunn, C. Greene, Wing Lee, N. Sandell, and A. Willsky. "The stochastic control of the F-8C aircraft using a multiple model adaptive control (MMAC) method—Part I: Equilibrium flight". In: *IEEE Transactions on Automatic Control* 22.5 (1977), pp. 768–780. DOI: 10.1109/TAC.1977.1101599.
- [90] Jr. Nils R. Sandell. *Recent Developments in the Robustness theory of Multivariable Systems*. Tech. rep. MIT Lab for Information and Decision Systems, 1979.
- [91] Uwe Mackenroth. *Robust Control Systems*. Berlin, Heidelberg: Springer Berlin Heidelberg, 2004. DOI: 10.1007/978-3-662-09775-5.
- [92] J. Doyle, A. Packard, and K. Zhou. "Review of LFTs, LMIs, and μ ". In: *Proceedings of the 30th IEEE Conference on Decision and Control*. 1991, 1227–1232 vol.2. DOI: 10.1109/CDC.1991.261572.
- [93] J.W. Van Wingerden. *Lecture Slides SC42145*. 2023.
- [94] D. Bates and I. Postlethwaite. *Robust Multivariable Control of Aerospace Systems*. Control and simulation. DUP Science, 2002. URL: <https://books.google.nl/books?id=luJSAAAAMAAJ>.
- [95] John Doyle. "Analysis of feedback systems with structured uncertainties". In: *IEE Proceedings D Control Theory and Applications* 129.6 (1982), p. 242. DOI: 10.1049/ip-d.1982.0053.
- [96] M.G. Safonov. "Stability margins of diagonally perturbed multivariable feedback systems". In: *IEE Proceedings D Control Theory and Applications* 129.6 (1982), p. 251. DOI: 10.1049/ip-d.1982.0054.
- [97] Richard Braatz, Peter Young, John Doyle, and Manfred Morari. "Computational Complexity of SSV Calculation". In: *IEEE Transactions on Automatic Control - IEEE TRANS AUTOMAT CONTR* 39 (July 1993), pp. 1682–1683. DOI: 10.1109/9.284879.
- [98] A. Packard and J. Doyle. "The complex structured singular value". In: *Automatica* 29.1 (1993), pp. 71–109. DOI: [https://doi.org/10.1016/0005-1098\(93\)90175-S](https://doi.org/10.1016/0005-1098(93)90175-S).
- [99] M.K.H. Fan, A.L. Tits, and J.C. Doyle. "Robustness in the presence of mixed parametric uncertainty and unmodeled dynamics". In: *IEEE Transactions on Automatic Control* 36.1 (1991), pp. 25–38. DOI: 10.1109/9.62265.

- [100] V. Balakrishnan. "Linear matrix inequalities in robustness analysis with multipliers". In: *Systems Control Letters* 25.4 (1995), pp. 265–272. DOI: [https://doi.org/10.1016/0167-6911\(94\)00087-C](https://doi.org/10.1016/0167-6911(94)00087-C).
- [101] Pierre Apkarian, Minh Ngoc Dao, and Dominikus Noll. "Parametric Robust Structured Control Design". In: *IEEE Transactions on Automatic Control* 60.7 (2015), pp. 1857–1869. DOI: 10.1109/TAC.2015.2396644.
- [102] Joost Veenman, Carsten W. Scherer, and Hakan Koroğlu. "Robust stability and performance analysis based on integral quadratic constraints". In: *European Journal of Control* 31 (2016), pp. 1–32. DOI: <https://doi.org/10.1016/j.ejcon.2016.04.004>.
- [103] G. Zames. "Feedback and optimal sensitivity: Model reference transformations, multiplicative seminorms, and approximate inverses". In: *IEEE Transactions on Automatic Control* 26.2 (1981), pp. 301–320. DOI: 10.1109/TAC.1981.1102603.
- [104] John Doyle, Keith Glover, P. Khargonekar, and Bruce Francis. "State Space Solution to Standard H-2 and H-infinity Control Problem". In: *Automatic Control, IEEE Transactions on* 34 (Sept. 1989), pp. 831–847. DOI: 10.1109/9.29425.
- [105] Pascal Gahinet and Pierre Apkarian. "A linear matrix inequality approach to H ∞ control". In: *International Journal of Robust and Nonlinear Control* 4.4 (1994), pp. 421–448. DOI: <https://doi.org/10.1002/rnc.4590040403>. eprint: <https://onlinelibrary.wiley.com/doi/pdf/10.1002/rnc.4590040403>.
- [106] Pierre Apkarian and Dominikus Noll. "The H-infinity Control Problem is Solved". In: *AerospaceLab Journal* (Nov. 2017), pp. 1–11.
- [107] P. Apkarian and D. Noll. "Nonsmooth H ∞ Synthesis". In: *IEEE Transactions on Automatic Control* 51.1 (2006), pp. 71–86. DOI: 10.1109/TAC.2005.860290.
- [108] Pierre Apkarian, Dominikus Noll, and Aude Rondepierre. "Mixed H $_2$ /H ∞ control via nonsmooth optimization". In: *Proceedings of the 48th IEEE Conference on Decision and Control (CDC) held jointly with 2009 28th Chinese Control Conference*. 2009, pp. 6460–6465. DOI: 10.1109/CDC.2009.5400165.
- [109] Da-Wei Gu, Petko H. Petkov, and Mihail M Konstantinov. *Robust Control Design with MATLAB®*. London: Springer London, 2013. DOI: 10.1007/978-1-4471-4682-7.
- [110] John C. Doyle. "Structured uncertainty in control system design". In: *1985 24th IEEE Conference on Decision and Control*. 1985, pp. 260–265. DOI: 10.1109/CDC.1985.268842.
- [111] P.M. Young. "Controller design with mixed uncertainties". In: *Proceedings of 1994 American Control Conference - ACC '94*. Vol. 2. 1994, 2333–2337 vol.2. DOI: 10.1109/ACC.1994.752496.
- [112] K. Zhou, J.C. Doyle, and K. Glover. *Robust and Optimal Control*. Feher/Prentice Hall Digital and Prentice Hall, 1996. URL: <https://books.google.nl/books?id=RPS0QgAACAAJ>.
- [113] Pierre Apkarian. "Nonsmooth μ -synthesis". In: *International Journal of Robust and Nonlinear Control* 21.13 (2010), pp. 1493–1508. DOI: 10.1002/rnc.1644.
- [114] Raquel Stella da Silva de Aguiar, Pierre Apkarian, and Dominikus Noll. "Structured Robust Control Against Mixed Uncertainty". In: *IEEE Transactions on Control Systems Technology* 26.5 (2018), pp. 1771–1781. DOI: 10.1109/TCST.2017.2723864.
- [115] Sawyer Fuller, Ben Greiner, Jason Moore, Richard Murray, René van Paassen, and Rory Yorke. "The Python Control Systems Library (python-control)". In: *2021 60th IEEE Conference on Decision and Control (CDC)*. 2021, pp. 4875–4881. DOI: 10.1109/CDC45484.2021.9683368.
- [116] J. Doyle and G. Stein. "Multivariable feedback design: Concepts for a classical/modern synthesis". In: *IEEE Transactions on Automatic Control* 26.1 (1981), pp. 4–16. DOI: 10.1109/TAC.1981.1102555.
- [117] Duncan C. McFarlane and Keith Glover. *Robust Controller Design Using Normalized Coprime Factor Plant Descriptions*, 990. Berlin/Heidelberg: Springer-Verlag, 1990. DOI: 10.1007/bfb0043199.

- [118] R.A. Hyde and K. Glover. "Development of a Robust Flight Control Law for a VSTOL Aircraft". In: *IFAC Proceedings Volumes* 25.22 (1992). 12th IFAC Symposium on Automatic Control in Aerospace 1992, Ottobrun, Germany, 7-11 September, pp. 97–102. DOI: [https://doi.org/10.1016/S1474-6670\(17\)49639-X](https://doi.org/10.1016/S1474-6670(17)49639-X).
- [119] Ian Postlethwaite, Emmanuel Prempain, Ercument Turkoglu, Matthew Turner, Karena Ellis, and Arthur Gubbels. "Design and flight testing of various H^∞ controllers for the Bell 205 helicopter". In: *Control Engineering Practice* 13 (Mar. 2005), pp. 383–398. DOI: [10.1016/j.conengprac.2003.12.008](https://doi.org/10.1016/j.conengprac.2003.12.008).
- [120] Gjerrit Meinsma. "Unstable and nonproper weights in H-infinity control". In: *Automatica* 31.11 (1995), pp. 1655–1658. DOI: [https://doi.org/10.1016/0005-1098\(95\)00086-C](https://doi.org/10.1016/0005-1098(95)00086-C).
- [121] Camille Pirat, Finn Ankersen, Roger Walker, and Volker Gass. "H-infinity and -Synthesis for Nanosatellites Rendezvous and Docking". In: *IEEE Transactions on Control Systems Technology* PP (Feb. 2019), pp. 1–8. DOI: [10.1109/TCST.2019.2892923](https://doi.org/10.1109/TCST.2019.2892923).
- [122] Sike Ma, Min Wu, Luefeng Chen, Chengda Lu, and Weihua Cao. "Robust mixed-sensitivity H-infinity control of weight on bit in geological drilling process with parameter uncertainty". In: *Journal of the Franklin Institute* 358.13 (2021), pp. 6433–6461. DOI: <https://doi.org/10.1016/j.jfranklin.2021.06.005>.
- [123] Xingcheng Zhao, Meini Yuan, Pengyun Cheng, Le Xin, and Leibin Yao. "Robust H-infinity /S-plane Controller of Longitudinal Control for UAVs". In: *IEEE Access* 7 (2019), pp. 91367–91374. DOI: [10.1109/ACCESS.2019.2927000](https://doi.org/10.1109/ACCESS.2019.2927000).
- [124] Parvesh Kumar and Shiv Narayan. "Optimal design of robust FOPID for the aircraft pitch control system using multi-objective GA". In: *2016 IEEE Students' Conference on Electrical, Electronics and Computer Science (SCEECS)*. 2016, pp. 1–6. DOI: [10.1109/SCEECS.2016.7509267](https://doi.org/10.1109/SCEECS.2016.7509267).
- [125] Shaojie Zhang and Qingkai Meng. "An anti-windup INDI fault-tolerant control scheme for flying wing aircraft with actuator faults". In: *ISA Transactions* 93 (2019), pp. 172–179. DOI: <https://doi.org/10.1016/j.isatra.2019.02.037>.
- [126] Carlos Alcolea Pérez, Spilios Theodoulis, Florian Sève, and Laurent Goerig. "Automatic weighting filter tuning for robust flight control law design". In: *IFAC-PapersOnLine* 55.16 (2022). 18th IFAC Workshop on Control Applications of Optimization CAO 2022, pp. 400–405. DOI: <https://doi.org/10.1016/j.ifacol.2022.09.057>.
- [127] Karl Johan Aström. *Control System Design, Lecture notes for ME 155A*. 2002.
- [128] Yu Huang, Timo Pe, Andrey P. Popov, Herbert Werner, and Frank Thielecke. "Control of a two-load-path Trimmable Horizontal Stabilizer Actuator of an aircraft — Comparison of H-infinity design approaches". In: *49th IEEE Conference on Decision and Control (CDC)*. 2010, pp. 4863–4868. DOI: [10.1109/CDC.2010.5716948](https://doi.org/10.1109/CDC.2010.5716948).
- [129] Jose Pablo Belletti Araque, Alessandro Zavoli, Domenico Trotta, and Guido De Matteis. "Genetic Algorithm Based Parameter Tuning for Robust Control of Launch Vehicle in Atmospheric Flight". In: *IEEE Access* PP (July 2021), pp. 1–1. DOI: [10.1109/ACCESS.2021.3099006](https://doi.org/10.1109/ACCESS.2021.3099006).
- [130] Pierre Apkarian. "Tuning controllers against multiple design requirements". In: *Proceedings of the American Control Conference*. June 2013, pp. 3888–3893. DOI: [10.1109/ACC.2013.6580433](https://doi.org/10.1109/ACC.2013.6580433).
- [131] D.T. McRuer and H.R. Jex. "A Review of Quasi-Linear Pilot Models". In: *IEEE Transactions on Human Factors in Electronics* HFE-8.3 (1967), pp. 231–249. DOI: [10.1109/THFE.1967.234304](https://doi.org/10.1109/THFE.1967.234304).
- [132] unknown. *FLYING QUALITIES OF PILOTED AIRPLANES*. Tech. rep. Department of Defense, 2004.
- [133] Florian Sève, Spilios Theodoulis, Philippe Wernert, Michel Zasadzinski, and Mohamed Boutayeb. "Pitch/Yaw Channels Control Design for a 155mm Projectile with Rotating Canards, using a H-infinity Loop-Shaping Design Procedure". In: *AIAA Guidance, Navigation, and Control Conference*. AIAA, 2014. DOI: [10.2514/6.2014-1474](https://doi.org/10.2514/6.2014-1474). eprint: <https://arc.aiaa.org/doi/pdf/10.2514/6.2014-1474>.

- [134] Florian Seve, Spilios Theodoulis, and Philippe Wernert. "Gain-scheduled H-infinity loop-shaping autopilot design for spin-stabilized canard-guided projectiles". In: *Aerospace Lab* 13 (2017), pp. 1–24. DOI: 10.12762/2017.AL13-03.
- [135] Tijmen Pollack and Erik-Jan van Kampen. "Robust Stability and Performance Analysis of Incremental Dynamic-Inversion-Based Flight Control Laws". In: *Journal of Guidance, Control, and Dynamics* 46.9 (2023), pp. 1785–1798. DOI: 10.2514/1.G006576. eprint: <https://doi.org/10.2514/1.G006576>.
- [136] Tijmen Pollack, Gertjan Looye, and Frans Van der Linden. "Design and flight testing of flight control laws integrating incremental nonlinear dynamic inversion and servo current control". In: *AIAA Scitech 2019 Forum*. AIAA, 2019. DOI: 10.2514/6.2019-0130. eprint: <https://arc.aiaa.org/doi/pdf/10.2514/6.2019-0130>.
- [137] Unknown. *Application of Multivariable Control Theory to Aircraft Control Laws - Multivariable Control Design Guidelines*. Tech. rep. Honeywell Technology Center, Lockheed Martin Skunk Works. Lockheed Martin Tactical Aircraft Systems, 1996.
- [138] B. Stevens, F. Lewis, and E. Johnson. "Aircraft Control and Simulation: Dynamics, Controls Design, and Autonomous Systems". In: Wiley, 2015. Chap. 2 and 6.
- [139] GARY BALAS, WILLIAM GARRARD, and JAKOB REINER. "Robust dynamic inversion control laws for aircraft control". In: *Guidance, Navigation and Control Conference*. AIAA, 1992. DOI: 10.2514/6.1992-4329. eprint: <https://arc.aiaa.org/doi/pdf/10.2514/6.1992-4329>.
- [140] R.J. Adams and S.S. Banda. "Robust flight control design using dynamic inversion and structured singular value synthesis". In: *IEEE Transactions on Control Systems Technology* 1.2 (1993), pp. 80–92. DOI: 10.1109/87.238401.
- [141] Evgeny Kolesnikov. "NDI-Based Flight Control Law Design". In: *AIAA Guidance, Navigation, and Control Conference and Exhibit*. 2005. DOI: 10.2514/6.2005-5977. eprint: <https://arc.aiaa.org/doi/pdf/10.2514/6.2005-5977>.
- [142] Sofiane Pineau, Spilios Theodoulis, Michel Zasadzinski, and Mohamed Boutayeb. "Terminal Phase Nonlinear Attitude Autopilot Design For Dual-Spin Guided Projectiles". In: *Proceedings of the 2022 CEAS EuroGNC conference*. CEAS-GNC-2022-073. Berlin, Germany, May 2022.
- [143] Anthony Gong, Ronald K. Hess, and Mark Tischler. "Deterministic Reconfiguration of Flight Control Systems for Multirotor UAV Package Delivery". In: *Proceedings of the Vertical Flight Society 77th Annual Forum* (2021). URL: <https://api.semanticscholar.org/CorpusID:250042525>.
- [144] Michael V. Cook. *Flight Dynamics Principles*. Elsevier, 2007. DOI: 10.1016/b978-0-7506-6927-6.x5000-4.
- [145] Jan Roskam. *Airplane Design VII: Determination of Stability, Control and Performance Characteristics: FAR and Military Requirements, Volume 1*. DARcorporation, 1985.
- [146] Nicolas Wahler. *The Impact of Control Allocation on Optimal Control Surface Positioning and Sizing: A comparative study for a PrandtlPlane*. 2021.
- [147] Jr. William Bihle. *A handling qualities theory for precise flight path control*. Tech. rep. WRIGHT LABORATORY, 1966.
- [148] J.C. Gibson. *The definition, understanding and design of aircraft handling qualities*. Tech. rep. Delft University of Technology, 1995.
- [149] M.B. Tischler, T. Berger, C.M. Ivler, H. Mansur, K.K. Cheung, and J.Y. Soong. *Practical methods for aircraft and rotorcraft flight control design: an optimization-based approach*. American Institute of Aeronautics and Astronautics, 2017.
- [150] unknown. *FLIGHT CONTROL SYSTEMS - DESIGN, INSTALLATION AND TEST OF PILOTED AIRCRAFT, GENERAL SPECIFICATION FOR*. Tech. rep. Department of Defense, 2008.
- [151] Eugene Lavretsky and Kevin A. Wise. *Robust and Adaptive Control*. Cham: Springer International Publishing, 2024. DOI: 10.1007/978-3-031-38314-4.

- [152] Nikolaus Moritz and Robert Osterhuber. “Three-Stage Gradient-Based Optimization Scheme in Design of Feedback Gains Within Eurofighter Primary Control Laws”. In: *AIAA Guidance, Navigation, and Control Conference and Exhibit*. American Institute of Aeronautics and Astronautics, 2006. DOI: 10.2514/6.2006-6311. eprint: <https://arc.aiaa.org/doi/pdf/10.2514/6.2006-6311>.
- [153] D Bates, Ridwan Kureemun, and I Postlethwaite. “Quantifying the robustness of flight control systems using Nichols exclusion regions and the structured singular value”. In: *Proceedings of The Institution of Mechanical Engineers Part I-journal of Systems and Control Engineering - PROC INST MECH ENG I-J SYST C* 215 (Sept. 2001), pp. 625–638. DOI: 10.1243/0959651011541355.
- [154] Clément Roos and Jean-Marc BIANNIC. “Application of mu-Analysis Techniques to Clearance”. In: vol. 416. Springer, Jan. 2012, pp. 221–232. DOI: 10.1007/978-3-642-22627-4_12.
- [155] Declan G. Bates and Ian Postlethwaite. “The Structured Singular Value and μ -Analysis”. In: *Advanced Techniques for Clearance of Flight Control Laws*. Ed. by Christopher Fielding, Andras Varga, Samir Bennani, and Michiel Selier. Berlin, Heidelberg: Springer Berlin Heidelberg, 2002, pp. 37–55. DOI: 10.1007/3-540-45864-6_3.
- [156] Tom Berger, Mark Tischler, Steven G. Hagerott, Dagfinn Gangsaas, and Nomaan Saeed. “Longitudinal Control Law Design and Handling Qualities Optimization for a Business Jet Flight Control System”. In: *AIAA Atmospheric Flight Mechanics Conference*. AIAA, 2012. DOI: 10.2514/6.2012-4503. eprint: <https://arc.aiaa.org/doi/pdf/10.2514/6.2012-4503>.
- [157] The MathWorks Inc. *MATLAB version: 23.2 (R2023b)*. Natick, Massachusetts, United States, 2023. URL: <https://www.mathworks.com>.
- [158] Pierre Apkarian, Pascal Gahinet, and Craig Buhr. “Multi-model, multi-objective tuning of fixed-structure controllers”. In: *2014 European Control Conference (ECC)*. 2014, pp. 856–861. DOI: 10.1109/ECC.2014.6862200.
- [159] A.J. Ostroff and B.J. Bacon. “Enhanced NDI strategies for reconfigurable flight control”. In: *Proceedings of the 2002 American Control Conference (IEEE Cat. No.CH37301)*. Vol. 5. 2002, 3631–3636 vol.5. DOI: 10.1109/ACC.2002.1024492.
- [160] VLaar. C. “Incremental Nonlinear Dynamic Inversion Flight Control”. MA thesis. Delft University of Technology, 2014.
- [161] E.J.J. Smeur, G.C.H.E. de Croon, and Q. Chu. “Cascaded incremental nonlinear dynamic inversion for MAV disturbance rejection”. In: *Control Engineering Practice* 73 (Apr. 2018), pp. 79–90. DOI: 10.1016/j.conengprac.2018.01.003.
- [162] John C. Doyle. “Synthesis of robust controllers and filters”. In: *The 22nd IEEE Conference on Decision and Control*. 1983, pp. 109–114. DOI: 10.1109/CDC.1983.269806.
- [163] Bálint Patartics, György Lipták, Tamás Luspáy, Peter Seiler, Béla Takarics, and Bálint Vanek. “Application of Structured Robust Synthesis for Flexible Aircraft Flutter Suppression”. In: *IEEE Transactions on Control Systems Technology* 30.1 (2022), pp. 311–325. DOI: 10.1109/TCST.2021.3066096.
- [164] Joost Veenman and Carsten W. Scherer. “IQC-Synthesis with General Dynamic Multipliers”. In: *IFAC Proceedings Volumes* 44.1 (2011). 18th IFAC World Congress, pp. 4600–4605. DOI: <https://doi.org/10.3182/20110828-6-IT-1002.00776>.
- [165] Joost Veenman and Carsten W. Scherer. “A synthesis framework for robust gain-scheduling controllers”. In: *Automatica* 50.11 (2014), pp. 2799–2812. DOI: <https://doi.org/10.1016/j.automatica.2014.10.002>.
- [166] Mark C. Palframan, J. Micah Fry, and Mazen Farhood. “Robustness Analysis of Flight Controllers for Fixed-Wing Unmanned Aircraft Systems Using Integral Quadratic Constraints”. In: *IEEE Transactions on Control Systems Technology* 27.1 (2019), pp. 86–102. DOI: 10.1109/TCST.2017.2766598.
- [167] C Fielding, A Varga, S Bennani, and M Selier. *Advanced Techniques for Clearance of Flight Control Laws*. Springer, 2002.



D,G-K iterations

Consider again the generalized closed-loop description seen in figure 3.1. Making use of the robust performance condition stated in 3.23. The robust controller synthesis problem can be formulated as follows. Find a stabilizing controller K , such that:

$$\min_K \sup_{\omega} (F_l(P, K)) \leq \beta \quad (\text{A.1})$$

It can be shown that if there are frequency dependant scaling matrices $D_{\omega} \in \mathcal{D}$ and $G_{\omega} \in \mathcal{G}$ such that:

$$\sup_{\omega} \bar{\sigma} \left[\left(\frac{D_{\omega} \mathcal{F}_l(P(j\omega), K(j\omega)) D_{\omega}^{-1}}{\beta} - jG_{\omega} \right) (I + G_{\omega}^2)^{-\frac{1}{2}} \right] \leq 1, \quad \forall \omega. \quad (\text{A.2})$$

Then, a mixed μ -synthesis procedure in the form of D,G-K iterations can be formulated as follows [112].

D, G - K Iteration:

1. Let K be a stabilizing controller. Find initial estimates of the scaling matrices $D_{\omega} \in \mathcal{D}$, $G_{\omega} \in \mathcal{G}$ and a scalar $\beta_1 > 0$ such that

$$\sup_{\omega} \bar{\sigma} \left[\left(\frac{D_{\omega} \mathcal{F}_l(P(j\omega), K(j\omega)) D_{\omega}^{-1}}{\beta_1} - jG_{\omega} \right) (I + G_{\omega}^2)^{-\frac{1}{2}} \right] \leq 1, \quad \forall \omega.$$

Obviously, one may start with $D_{\omega} = I$, $G_{\omega} = 0$, and a large $\beta_1 > 0$.

2. Fit the frequency response matrices D_{ω} and jG_{ω} with $D(s)$ and $G(s)$ so that

$$D(j\omega) \approx D_{\omega}, \quad G(j\omega) \approx jG_{\omega}, \quad \forall \omega.$$

Then for $s = j\omega$

$$\begin{aligned} & \sup_{\omega} \bar{\sigma} \left[\left(\frac{D_{\omega} \mathcal{F}_l(P(j\omega), K(j\omega)) D_{\omega}^{-1}}{\beta_1} - jG_{\omega} \right) (I + G_{\omega}^2)^{-\frac{1}{2}} \right] \\ & \approx \sup_{\omega} \bar{\sigma} \left[\left(\frac{D(s) \mathcal{F}_l(P(s), K(s)) D(s)^{-1}}{\beta_1} - G(s) \right) (I + G^*(s)G(s))^{-\frac{1}{2}} \right]. \end{aligned}$$

3. Let $D(s)$ be factorized as

$$D(s) = D_{\text{ap}}(s)D_{\text{min}}(s), \quad D_{\text{ap}}^*(s)D_{\text{ap}}(s) = I, \quad D_{\text{min}}(s), \quad D_{\text{min}}^{-1}(s) \in \mathcal{H}_{\infty}.$$

That is, D_{ap} is an all-pass and D_{min} is a stable and minimum phase transfer matrix. Find a normalized right coprime factorization

$$D_{\text{ap}}^{-1}(s)G(s)D_{\text{ap}}(s) = G_N G_M^{-1}, \quad G_N, G_M \in \mathcal{H}_{\infty}$$

such that

$$G_N^* G_M + G_M^* G_N = I.$$

Then

$$G_M^{-1} D_{\text{ap}}^{-1} (I + G^* G)^{-1} D_{\text{ap}} (G_M^*)^{-1} = I$$

and, for each frequency $s = j\omega$, we have

$$\begin{aligned} & \bar{\sigma} \left[\left(\frac{D(s)\mathcal{F}_\ell(P(s), K(s))}{\beta_1} D(s)^{-1} - G(s) \right) (I + G^*(s)G(s))^{-\frac{1}{2}} \right] \\ &= \bar{\sigma} \left[\left(\frac{D_{\min}\mathcal{F}_\ell(P, K) D_{\min}^{-1}}{\beta_1} - D_{\text{ap}}^{-1} G D_{\text{ap}} \right) (D_{\text{ap}}^* (I + G^* G) D_{\text{ap}})^{-\frac{1}{2}} \right]. \end{aligned}$$

4. Define

$$P_a = \begin{bmatrix} D_{\min}(s) & I \\ P(s) & D_{\min}^{-1}(s)G_M(s) \\ I & -\beta_1 \begin{bmatrix} G_N \\ 0 \end{bmatrix} \end{bmatrix}$$

and find a controller K_{new} minimizing $\|\mathcal{F}_\ell(P_a, K)\|_\infty$.

5. Compute a new β_1 as

$$\beta_1 = \sup_{\omega} \bar{\sigma} \inf_{\hat{D}_\omega \in \mathcal{D}, \hat{G}_\omega \in \mathcal{G}} \{\beta(\omega) : \Gamma \leq 1\}$$

where

$$\Gamma := \bar{\sigma} \left[\left(\frac{\hat{D}_\omega \mathcal{F}_\ell(P, K_{\text{new}}) \hat{D}_\omega^{-1}}{\beta(\omega)} - j\hat{G}_\omega \right) (I + \hat{G}_\omega^2)^{-\frac{1}{2}} \right].$$

6. Find \hat{D}_ω and \hat{G}_ω such that

$$\inf_{\hat{D}_\omega \in \mathcal{D}, \hat{G}_\omega \in \mathcal{G}} \bar{\sigma} \left[\left(\frac{\hat{D}_\omega \mathcal{F}_\ell(P, K_{\text{new}}) \hat{D}_\omega^{-1}}{\beta_1} - j\hat{G}_\omega \right) (I + \hat{G}_\omega^2)^{-\frac{1}{2}} \right] = 1.$$

7. Compare the new scaling matrices \hat{D}_ω and \hat{G}_ω with the previous estimates D_ω and G_ω . Stop if they are close, else replace D_ω , G_ω , and K with \hat{D}_ω , \hat{G}_ω , and K_{new} , respectively, and go back to step (2).